TECHNICAL REVIEW

NO. 86

Special issue on
"Robotics and Sensing Products and Machine Tools"

October 2018

New Policy Using Natural Energy Products
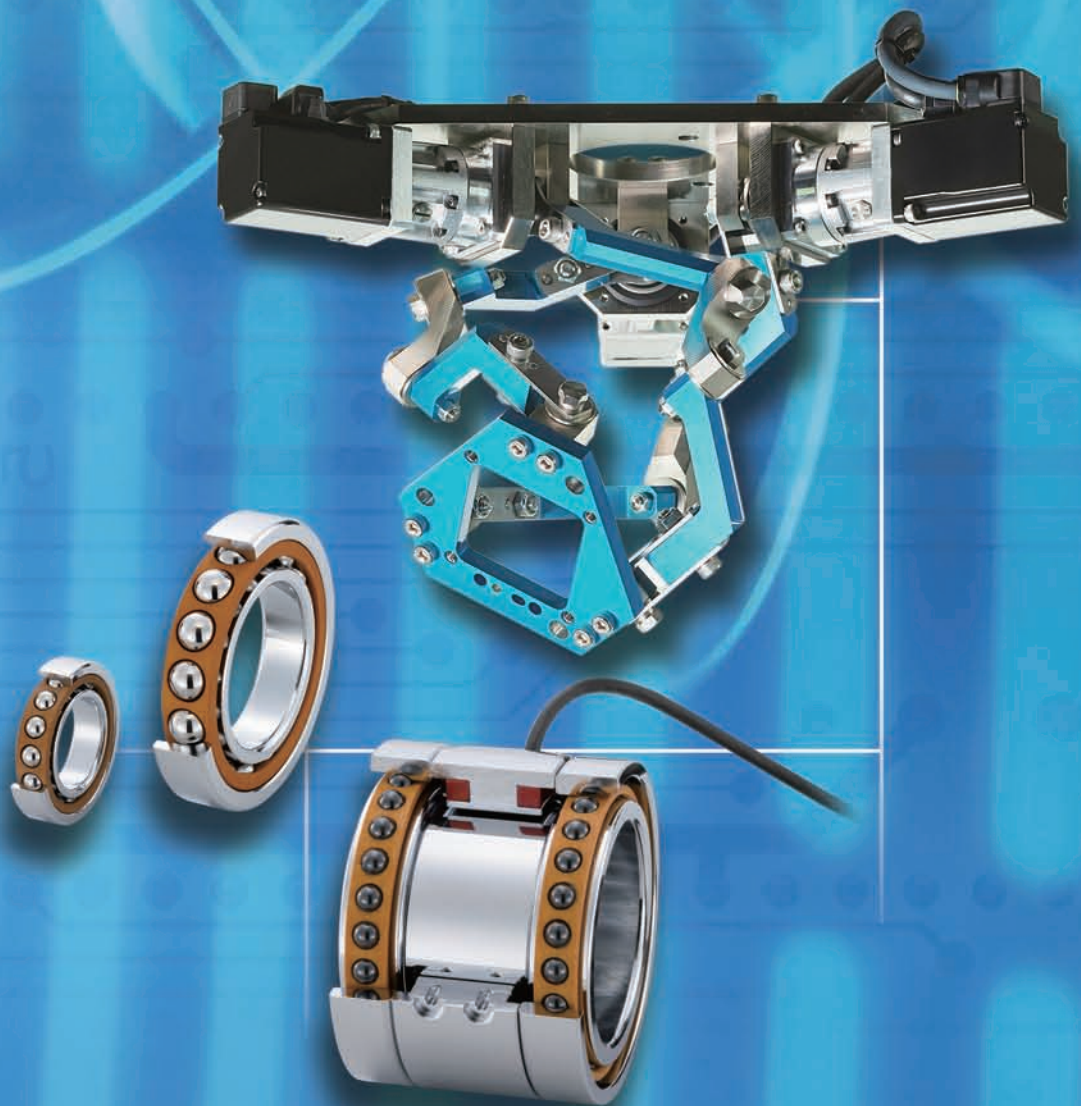
NTN Corp. marked its 100th anniversary in March 2018 and started the New Medium-term Management Plan called "DRIVE **NTN**100" in April 2018. As we promote various policies aiming for sustainable growth in the next 100 years, we conduct business development in new areas. We do so by leveraging our collective strength in R&D, production technology and distribution, which we have been developing over the years. In the area of natural energy, we have started the manufacturing and distribution of small wind turbines and micro hydro turbines utilizing our highly efficient and quiet blades.

The small wind turbine, "**NTN** Hybrid Street Light", which generates electricity from the wind and solar power, can supply electric power when and where the commercial electric power cannot be used such as in disasters or areas where such power is not supplied. **NTN** Corp. has donated its "**NTN** Hybrid Street Light" to five regions in Japan, so far, for promoting renewable energy and helping those regions with disaster and crime prevention.

We also started "Joint Research for Creating Mechanisms Regarding Disaster Prevention Monitoring and Tourism through Use of IT" with the National University Corporation Osaka University (hereafter, Osaka University) and its associated organizations as a new initiative. This joint research will integrate the "Disaster Relief Map" developed by Osaka University with "Mimamori Robokun III" Wi-Fi communication infrastructure. This is equipped with a monitoring camera and adopts the

▲ Experimental unit using **NTN** Hybrid Street Light

"**NTN** Hybrid Street Light" as the framework and independent power supply for the experimental unit. The new initiative is working on various experiments aimed at creating an information network for disaster prevention and disaster support, monitoring elderly citizens and children, and building information infrastructure for tourism.

The "**NTN** micro hydro turbine," which is a small hydroelectric generator with a unique blade shape, is able to efficiently convert water flow energy to electric power with simple installation into irrigation channels. Different from the conventional

▲ NTN micro hydro turbines placed in series in the same conduit

hydro power generators which use the difference in water levels, it does not require expensive foundation work to create the difference in water levels, which results in significant cost reduction. Furthermore, it allows serial/parallel installation of multiple units into the same water channel for obtaining desirable output based on the number of units installed. We have also launched distribution of "Grid Connectable **NTN** Micro Hydro Turbine" this year, which allows generated electric power to be sold to the grid.

NTN will promote proposals for locally produced and consumed energy by leveraging new policies using these natural energy products, and contribute to the local communities through realization of low-carbon society and safe/secure urban development.

NTN®

TECHNICAL REVIEW

No.86

Special Issue;
Robotics and Sensing Products
and Machine Tools

NTN TECHNICAL REVIEW No.86

CONTENTS

A Message for the special issue on "Robotics and Sensing Products and Machine Tool"

Yoshinori TERASAKA
Managing Director

As the population of productive age decreases in all sectors, creating a major social problem, measures against labor shortage due to the upcoming accelerated aging population and dwindling birthrate are strongly required. The market for collaborative robots is expected to grow, as these robots are able to work in a variety of manufacturing sites such as handling, assembly and testing on behalf of the workers. On the other hand, with the labor shortage as a backdrop, the demand for additional monitoring capabilities in industrial machinery is increasing, and approaches for further advancing unmanned or reduced manpower operations by leveraging the widespread adoption of IoT and sensing technology are actively being discussed.

NTN has developed a compact and high-speed appearance inspection device combining its wrist joint module "i-WRIST" with a unique link mechanism and camera as a solution to the issue of labor shortage and quality improvement in manufacturing operations. **NTN** is promoting this device as one approach toward new business development.

In addition, bearings, which are **NTN**'s platform product and are used in rotational components of all kinds of machinery, are also expected to have higher functionality, acting as the machine element for data collection by including sensing capability with various embedded sensors. **NTN** is engaged in the joint research and technology development with Osaka University for allowing trend control and damage prevention during bearing operation by integrating multi-function sensors in the bearings.

At the 29th Japan International Machine Tool Fair (JIMTOF2018) held from Nov. 1 to Nov. 6 with the theme of "CONNECT by technology for the future," we are publishing a special issue of Technical Review No. 86 "Robotics, Sensing Products and Machine Tools." In this issue, we discuss the technical trends and features of one of our platform products, industrial robot bearings, which utilize **NTN**'s base technologies including materials, heat treatment and tribology. The issue also introduces newly developed products such as sensor integrated bearing units for machine tool spindles, machine tool main spindle bearings with air cooling spacer for grease lubrication for high speed operation, and angular contact ball bearings for high-speed and heavy-cutting machine tools.

NTN marked its 100th anniversary in March 2018. We began a new three-year mid-term management plan "DRIVE **NTN**100" in April 2018 to accelerate our business structure transformation for our next 100 years. Under our philosophy of "We shall contribute to international society through creating new technology and developing new products (For New Technology Network: Networking the World With New Technology)," we will promote the research and technology development that will support the next 100 years by strengthening our unique competitive platform businesses, creating new businesses, and leveraging our core competence which targets sustainable growth of economic society.

[Contribution]

Strategic Vision for Smart Machining Tool and Measuring Instrument

Yasuhiro TAKAYA
Professor, Department of Mechanical Engineering,
Graduate School of Engineering, Osaka University

Establishment of the innovation driven manufacturing, which enables new value creation such as customized products and innovative products with services, is expected in the age of non-equilibrium and strategy. The holistic measurement based on integrating different measurement principles and multi-scale data fusion as well as smart in-process and on-machine measurement technologies will play an important role in the predictive control type manufacturing system. The connected smart in-process and on-machine measurement systems that give self-recognition ability to the manufacturing system is also the key technology in Industry 4.0 to establish the innovation driven manufacturing.

1. Introduction

The paradigm shift of the socio-economic structure from a "society of equilibrium" to a "society of non-equilibrium" which proliferates and penetrates on a global scale and its challenges can be interpreted as the transition from the "age of tactics" to "age of strategy" as shown in **Fig. 1**. With the change of the new value system and socio-economic environment, such as a sustainable society, environmental considerations, and global standards, manufacturing is also changing. Its status is termed the change from "linear society/age of railway" to "non-linear society/age of great voyage."[1] Attention is paid to the unpredictable destination (market) and the process of getting there, rather than the foreseeable and predictable destination (product), and focus is placed on fundamental thoughts (strategy) rather than the pursuit of higher added value through improvement and enhancement (tactics). Along with these trends, the challenges that cannot be solved by extending the conventional approaches are increasing. The pace of holistic transformation in many fields from science to society and economy is steady and fast, even more accelerated in recent years. This paper will identify the potential power of strategic measurement as one of the above trends which drives the manufacturing transformation, namely, the 4th Industrial Revolution, and explore the future development of the predictive production system and smart machining/measurement.

2. Innovation driven manufacturing

In the efficiency driven manufacturing of the "equilibrium/age of strategy," focus was given to the strategy to achieve addition of higher product value through high precision and efficient production systems and the tactics to realize it. The tactics were to rapidly promote a highly developed production system. Therefore, efforts were made to breakdown the manufacturing technology into elemental technology (production tools) such as machining technology, measurement technology, and production technology (CAD/CAE/CAM/CAT) that compose of production systems and solve challenges of each element. That resulted in a significant outcome. As such, the role of measurement technology was weighed heavily as one of the production tools (measurement=testing) in **Fig. 2** and used as a tactic for achieving the objectives given to the "thing" (product) such as high quality, low cost, and short delivery time. When the manufacturing process was in the "equilibrium state" for a prolonged time, "measurement in manufacturing" as a production tool played a satisfactory role.

Alternatively, in the innovation driven manufacturing of "non-equilibrium/age of strategy," strategy is weighed more heavily than tactics. Strategy in this case is new value creation, such as customized manufacturing, creation of innovative products, and the associated services in addition to the new approach of high value addition. As the tactics to respond to the strategy change over time, achieving predictive
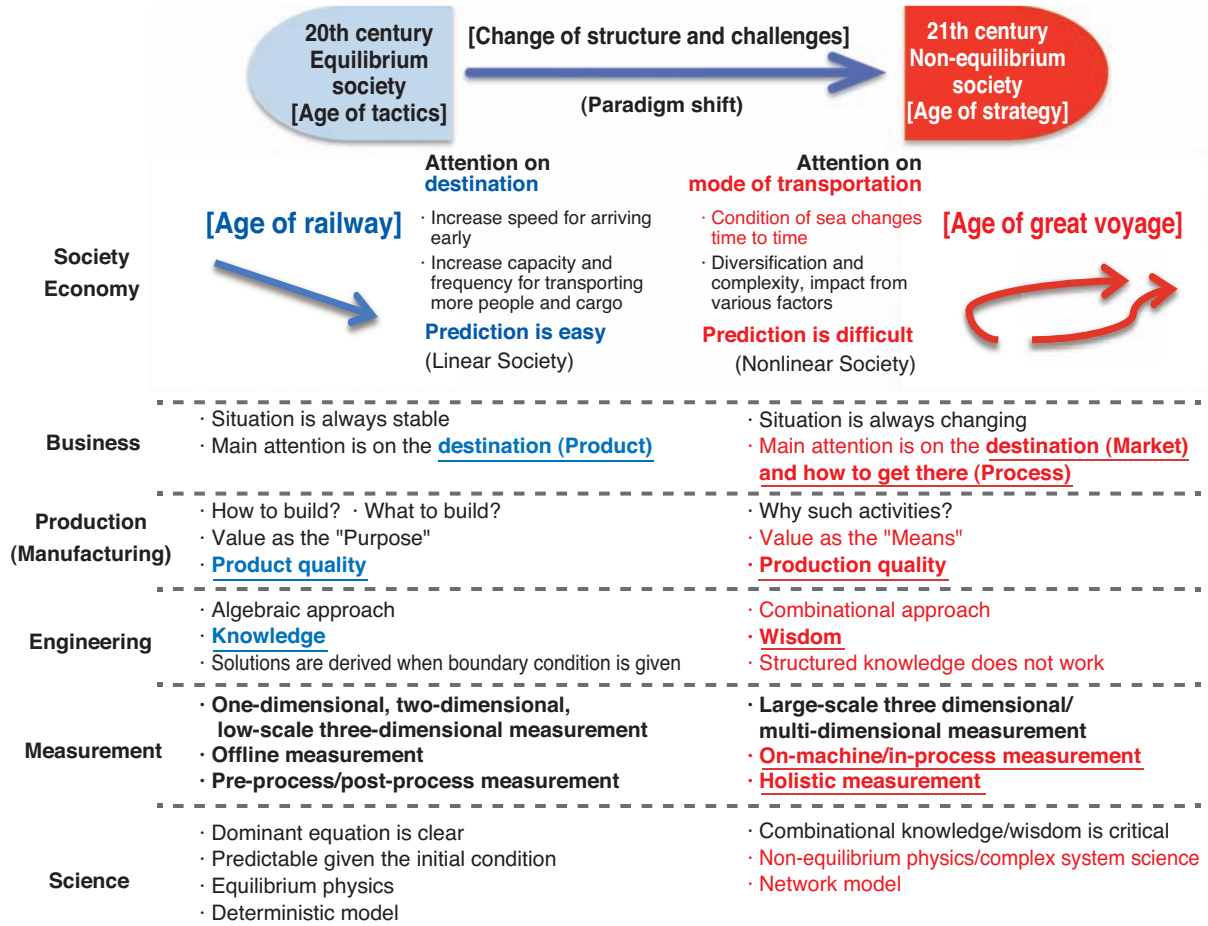
Fig. 1 Railway era to the age of discovery
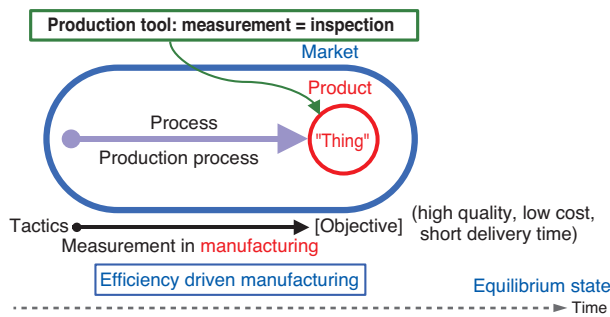
Fig. 2 Equilibrium era: Measurement technology as production tools

the manufacturing process is transitioned to a "non-equilibrium state," the measurement, which is the source of information (resource), is required to make innovative progress as a strategic tool for "measurement for 'event' creation."
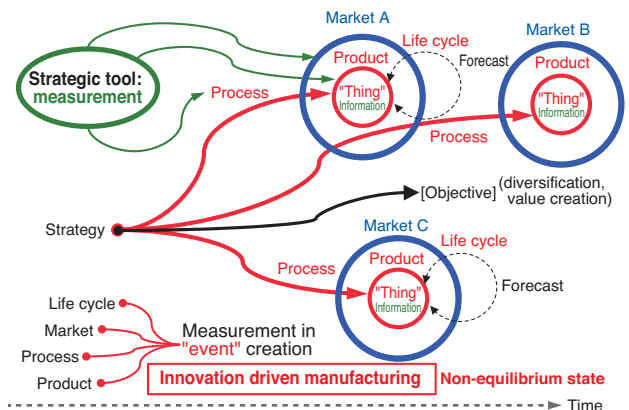
Fig. 3 The age of non-equilibrium: Measurement technology as strategic tools

production systems is necessary. Therefore, the role of the measurement technology is significantly different from the past, in addition to applying a predictive production system, as shown in **Fig. 3**. The measurement technology will be required to assume the strategy itself for achieving the diversified objectives that are heavily engaged with the entire "event" processing, such as market, product, and process throughout the "things" (product), and their life cycle, tightly connected to information. Today, when

3. Concept of new production quality

3.1 Evaluation of machining accuracy and process capacity

Taniguchi predicted that the machining limit of precision machining technology would reach $0.1 \mu m$ in 2000, in his 1983 paper. [2] The progress of mechanical machining technology has been significant and it is now reaching the area of general machining limits. The machining process is a general technology involving many elements, such as machine tools, workpieces, working conditions, working environment, and products. The machining error is caused by the influence of various factors, such as positioning accuracy and thermal displacement of machine tools, geometric accuracy and wear property of tools, material and hardness of workpieces, machining conditions, such as dry machining and processing skill set, working environment, such as temperature and vibration, and high precision and complexity of products. Based on the law of error propagation, accuracy of the entire machining process cannot be improved by compensating unstable factors by stable factors. That is, if there is even one unstable factor in the machining process, the overall accuracy is decreased, as it is determined by that factor.

Machining accuracy can be tackled separately between precision and accuracy. In addition, machining requires capability to satisfy the standard size and allowance. **Fig. 4** shows how to evaluate the machining accuracy and process capacity. If the upper and lower limits of the machining specification are LSL and USL, respectively, and the allowance is T, then when the average machining value (machining size, etc.) is the midpoint value of T and the standard deviation is σ, the limit machining accuracy p and machining capability index C_{pk} or C_p are calculated by the evaluation equation indicated in **Fig. 4**,

respectively. For example, when $C_p \geqq 1.33$, 99.1% of workpieces fall within the allowance of 1/1.33=0.75.

Machining accuracy (error) cannot be directly "observed." Therefore, it is necessary to understand how to "visualize" it through the "window of measurement." **Fig. 5** [3] shows how the machining capability index is evaluated depending on the magnitude of "uncertainty" [4] of measurement. When the allowance is T, LSL and USL shows the lower and upper limits of the machining specification, respectively. For simplicity, assume the average machining value (e.g. machining size) to be the center value of T and the standard deviation that shows the machining variance to be σ. For example, if the true machining capability index C_p (or C_{pk}) = 1.33, then C_p is observed through the "uncertain window of measurement", and when the machining capability is evaluated with the uncertainty $U = 0.1\ T$ (**Fig. 5 (a)**), then C_p (C_{pk}) is evaluated as 1.24. Alternatively, when the uncertainty $U = 0.2T$ (**Fig. 5 (b)**), C_p (C_{pk}) = 1.04 and it is evaluated as the lower machining capability. It also reveals that the entire uncertainty U', which includes the uncertainty of measurement, is larger than σ. Therefore, the magnitude of uncertainty as the index to show that the reliability of measurement determines the reliability against assurance of machining accuracy. The uncertainty of measurement is an important index for highly efficient machining processes based on the evaluation of machining capability. In order to assure high precision/high accuracy machining by the strategic measurement "to create value," it is necessary to use measurements with higher reliability (lower uncertainty). As seen above, improvement of process capability is required by reducing machining errors from the machining process, that is, bias errors and variation errors from the absolute values, for improving the machining accuracy. To do so, it is most effective to examine all

Probabilistic density (frequency)

Allowance T

Allowable machining error ε

ε

Average μ

Bias error d

Variation error σ

σ

Machining accuracy limit p : $p=d+\sigma$

Size value X

LSL Standard size USL

*Errors from the machining process include bias errors and variation errors. The following value is evaluated to determine if the machine tool has machining capability to satisfy required accuracy of parts.

【 Process capability index C_{pk} 】

$$C_{pk} = min\left[\frac{USL-\mu}{3\sigma}, \frac{\mu-LSL}{3\sigma}\right]$$

*When average, μ, is the center value of T

$$C_p = \frac{USL-LSL}{6\sigma} = \frac{T}{6\sigma}$$

（*LSL: Lower Specification Limit, USL: Upper Specification Limit）
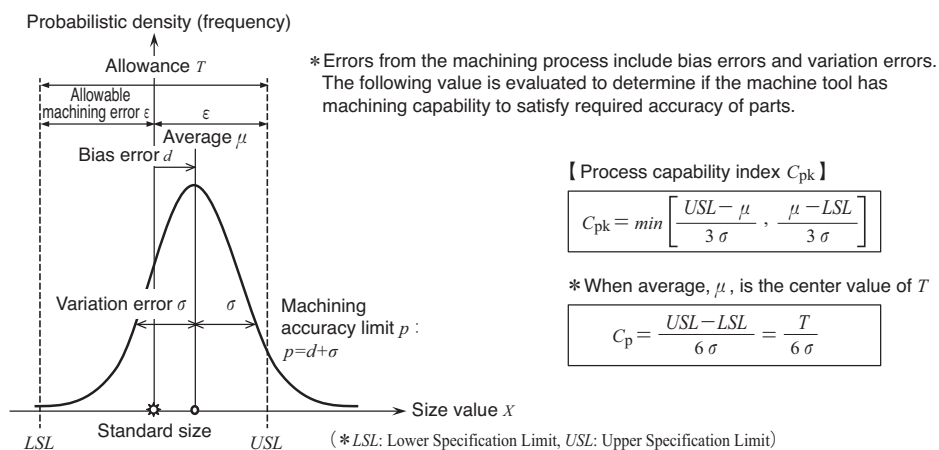
Fig. 4 Process capability index (C_{pk}, C_p) for evaluating the machining accuracy
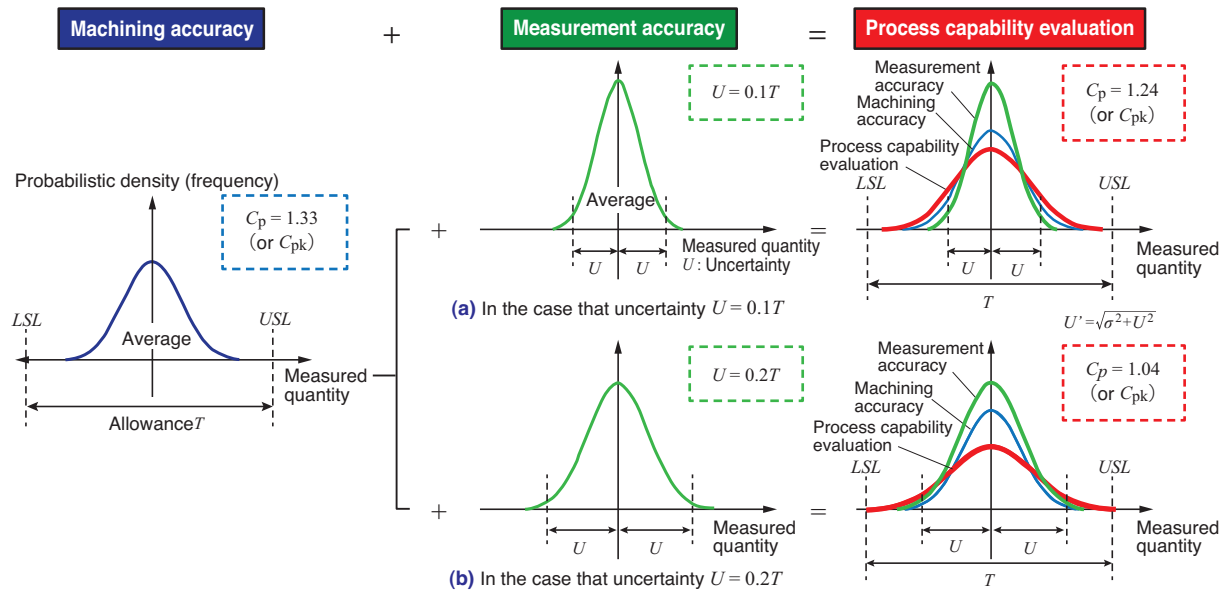
Fig. 5 Importance of measurement uncertainty to evaluate process capability index
(Reconfigured and summarized reference [3] Weckenmann et al., Precision Engineering (2000))

the elements of the entire machining process considering all the factors in the machining process as subject to measurement and apply improvement to the most unstable factor.

3.2 From product (quality) to production quality

Machining accuracy is determined by the complex superposition of machining errors that vary with various unpredictable factors, such as the properties of the machine tools and workpieces, machining environment, and machining procedures. The accidental errors included in the machining errors cannot be corrected, as their cause cannot be determined. However, they can be estimated with repetitive measurements and, therefore, it is effective in mass production, where the same machining is repeated for the same components (many probabilistic trials). Machining accuracy can be considered as the statistically fluctuated quantity, that is, probabilistically variable quantity. Therefore, the conventional quality control approach used in mass production of the efficiency-driven manufacturing is based on the machining accuracy evaluation of the statistical model.

On the other hand, together with the increase of demand of energy related facilities such as power generation turbines and customized products, the demand for aircraft parts is increasing globally, in recent years as shown in **Fig. 6** [5]. Domestic production of large precision parts which require rigorous quality control is also increasing. For small-lot or one-unit production or customized production where new quality control concepts and strategic machining measurements as the base for production

system are required, not only products but the process will also drastically change, along with the aging process of individual products in their life cycle and change of strategy. In these cases, careful consideration is required for applying quality control based on the conventional statistical concept as the systematic error in machining errors change in the environment where variation of temperature and aging of machines cause change in accuracy. In addition, when the number of units for machining is very small and the process tends to change, verification of appropriateness of the statistical assumptions shown in **Fig. 4** will be difficult.

Therefore, the concept of production quality is being proposed [6], as a new production control and quality control approach, as shown in **Fig. 7**, which can be applied to small-lot or one-unit production, or customized production solving the challenges of the conventional statistical process control approach. This approach emphasizes quality/function assurance focused on the process as the basic concept by "informatizing every process of manufacturing", not only geometric quantity of workpieces as the index to measure the quality. It establishes production quality control by defining innovative and integrated production quality that uses enormous amount of data (industrial big data), designing an entire product life cycle from production logistics to maintenance based on such definition, introducing new management / control methods for big data with advanced technology to achieve them. The technological innovation required for that includes product testing technology, machining monitoring technology, and

multi-sensor data integration technology, as shown in **Fig. 7 (a)** to **(h)**. This technology, in other words, implies that the in-process/on-machine measurement technology encompassing a broad range of elements that directly determine machining accuracy, such as tools, machine tools, machining environment, and machining/measurement operation, is critical. In addition, it is expected that small-lot production and customized production or one-unit production will increase in the "non-equilibrium/age of strategy," where the adopted strategy is to generate new value by creating innovative products. Therefore, production quality control based on in-process/on-machine measurement is indispensable, which is also the key technology for achieving predictive production system.
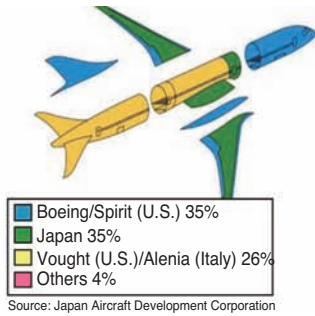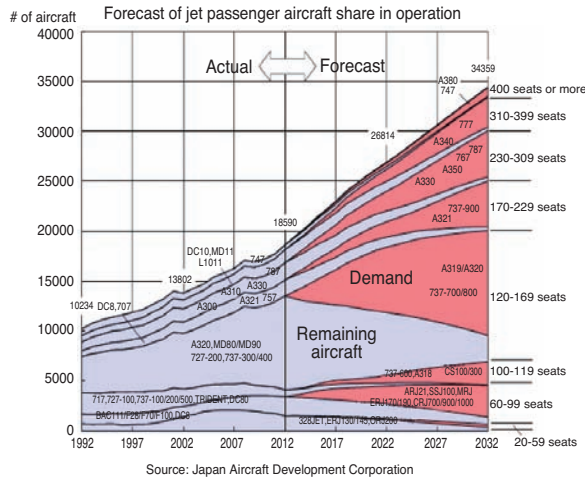

(a) Joint development of Boeing 787
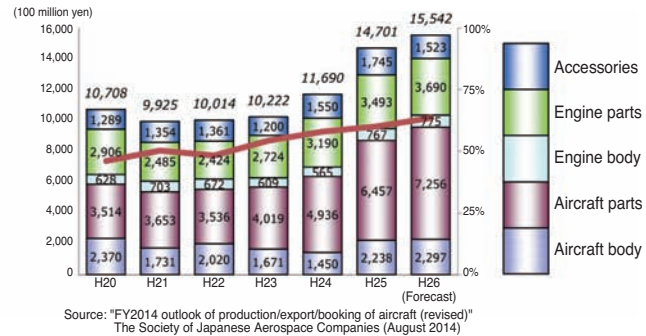
(b) Historical trend of aircraft production volume

(c) Forecast of jet passenger aircraft share in operation

Fig. 6 Increasing demand for high-precision parts in aerospace industry

【Concept of conventional quality control】	【Concept of new production quality】
(1) Mass production (2) Statistical process control (3) Yield management	(1) Small batch, Customized, or even one-of-a-kind products） (2) New paradigm beyond six sigma approach (3) Zero defect manufacturing

（＊ICT: Information and Communication Technology）

【Key elements of comprehensive production quality control】			
Innovative and integrated quality	Production logistics and maintenance design	Management and control methods	Advanced technological enablers

【Technological innovation required for establishing production quality】	
(a) Product inspection technology	(e) E-maintenance technology
(b) Process monitoring technology	(f) Product traceability technology
(c) Multi-sensor data fusion technology	(g) Production monitoring technology
(d) Learning techniques and cognitive computing methods	(h) ICT and digital manufacturing technology

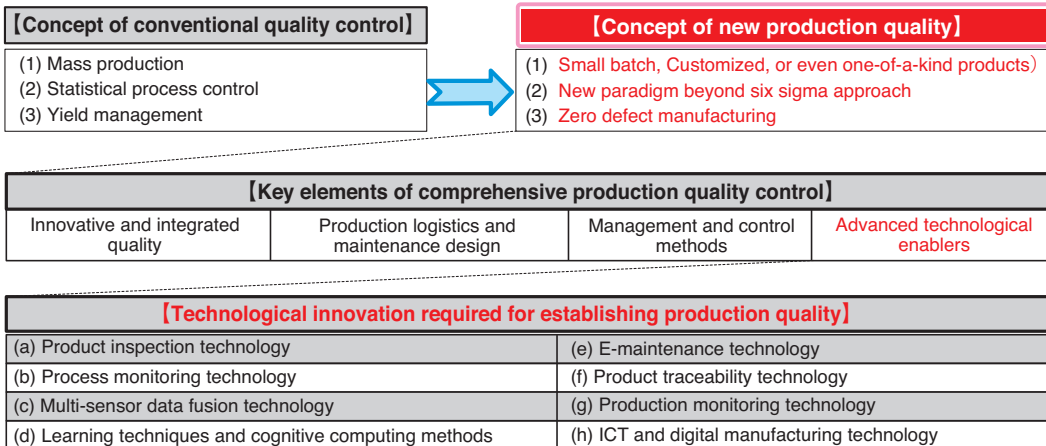(Reconfigured and summarized reference 7) Colledani et al. CIRP annals (2014))

Fig. 7 Fundamental scheme of production quality control and the required innovative technologies to establish it

4. Production quality control by holistic measurement

4.1 Current status of in-process/on-machine measurement

The role of the machining measurement for production control is "informatization" of manufacturing. In the advanced production system using diversified and vast production information, machining measurement plays an important role as the key information source on the products and machining states. The most essential purpose of machining measurement is production control, production automation, and test automation. In-process/on-machine measurement is the most efficient and effective machining measurement technology engaged directly in monitoring and controlling of machining. With the machine tools with reproducibility, the machining errors that vary over time during machining operation due to factors such as deformation and displacement of machine due to change in temperature, thermal expansion and deflection of tools, and wear may be evaluated and corrected by re-machining.

Recently, machine tools with in-process/on-machine measurement capability are being commercialized and the importance of their role is increasing. These trends are driven by diversified purposes of the measurement. In-process/on-machine measurement plays a central role for production/quality control as well. **Fig. 8** shows the fundamental measurement properties required in in-process/on-machine measurement technology and the unique properties

and relationship between machining factors across machine tools, workpieces, and machining environment and in-process/on-machine measurement. Of particular importance as a fundamental measurement property is accuracy and precision. For example, consideration for questions such as if accuracy and precision for evaluating tolerance range as the base for process capability are satisfactory and if absolute measurement is required due to machining bias errors is critical. In addition, the in-process measurement evaluation is affected by dynamic characteristics such as transient response and frequency response. Furthermore, properties specific to in-process/on-machine measurement are also required. These include environment factors required for installing measurement devices to machine tools and hardware/software factors. For example, in the case of on-machine 3D profile measurement using an optical comparator, vibration property, compactness, and switching process are required. The advantage of in-process/on-machine measurement is not limited to improvement and stabilization of machining accuracy but extended to higher efficiency of machining/measurement setup. As such, the scope of measurement extends from workpieces to machining state in space and time domain realizing "visualization of machining process" by quantifying machining factors.

The machining error, which value is constantly maintained during the repetitive machining operation, provides the same effect not influencing the accidental error. Therefore, it provides a constant bias to the
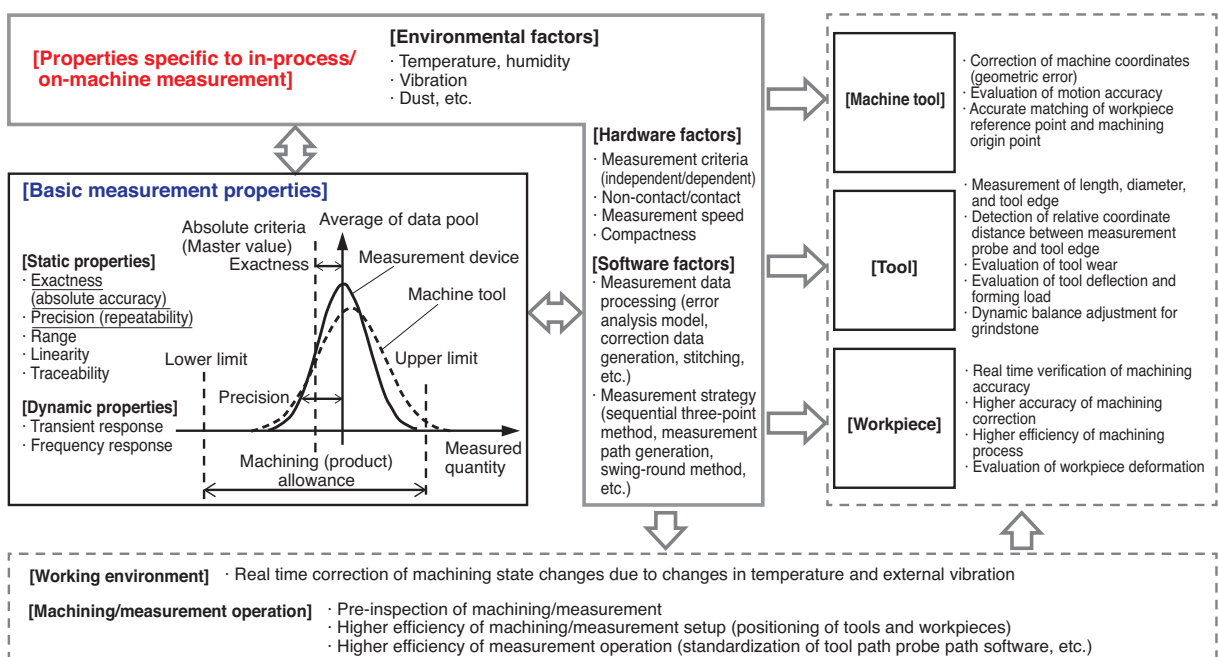

Fig. 8 Fundamental properties of measuring technology in machining process and roles of on-machine measurement

machining accuracy. In general, evaluation of systematic error which cannot be found in these repetitive measurements is difficult and often its existence cannot be detected. However, if the factor for systematic error is predetermined and its magnitude is known, it can be eliminated with correction. Therefore, a smart machine tool which can determine the factors of machining errors in real time with multiple in-process/on-machine measurements is an important concept as an elemental technology of the production system in conventional efficiency driven manufacturing. The basic concept of the smart machine tool that holistically provides machining process monitoring, recognition, and prediction using multiple sensors was presented around 1993 by Moriwaki [7]. Since then, active research and development has been conducted on in-process/on-machine measurement and machining control aimed at application to practical systems, resulting in increased development in application fields such as advanced sensors for tool condition monitoring (TCM), signal processing methods, decision making strategy, etc. These trends of research activities on the challenges of in-process/on-machine measurement indicate that attention is paid to the solution of individual challenges for each element of tools/workpieces/machine tools which are the main elements of the machining process, and the challenges in the boundary area from interaction of

these elements. In other words, adaptation to advanced and complex requirements of high-speed, multi-functional, and intelligence is sought after in addition to higher accuracy of machining processes, from the viewpoint of practical application of in-process/on-machine measurement to the real system. As the complexity of machining process increases, interaction of tools, workpieces, and machine tools has become more complex and the challenges of in-process/on-machine measurement in the boundary area have also become multifaceted and advanced.

Areas subject to in-process/on-machine measurement are expanding from geometric quantity to state quantity and the challenges are not only multifaceted, but expanding with advanced multi-axis/multi-tasking machine tools and intelligent machining process. In addition, the requirement of further improvement of accuracy for ultra-precision machining is expanding into new dimensions, such as 3D free curve profile, micro complex profile, and nano-surface pattern, which are required for commercialization of advanced functional parts. **Fig. 9** summarizes positioning and scope of in-process/on-machine measurement technology in the on-machine system with tools, workpieces, and machine tools as its key elements. It indicates the boundary areas of each element and relation among measurement technology and breaks down the time-variant phenomena into short, medium, and long period and marks their
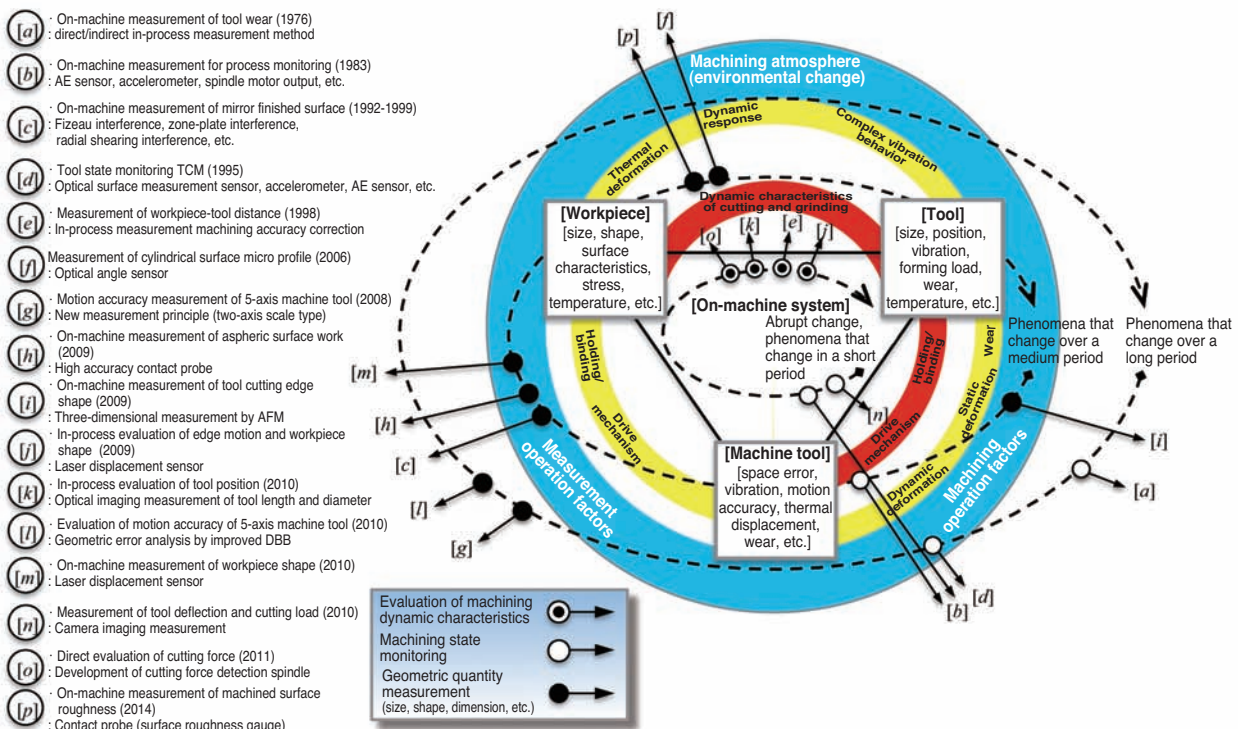

Fig. 9 Spreading roles of on-machine measuring technologies in machining process

positioning in the respective time scale. The relation of in-process/on-machine measurements is indicated by ring bands connecting two elements and a ring band circling three elements. The former indicates interaction of the elements, and the latter indicates a complex interaction area where three elements are involved. In addition, the outer ring band that encloses the entire diagram indicates machining atmosphere and manual operation. The purpose of measurement is classified into evaluation of machining dynamic characteristics, machining state monitoring, and measurement of geometric quantity, such as size, shape, and displacement, with R&D examples shown chronologically from [a] to [p]. For example, in the case of [a], on-machine measurement of tool wear (1976) is positioned as the on-machine measurement technology with the purpose of monitoring machining state that changes over time in the boundary area between tools and machine tools. Also, the in-process/on-machine measurement technology that corresponds to the solution to challenges other than the interaction between elements are only indicated with factors as the challenges to be solved in the future.

4.2 New in-process/on-machine measurement strategy

As the basic concept of new in-process/on-machine measurement by multiple sensors, an example of high functional measurement information is shown in **Fig.10** by "multi-sensor fusion" and "multi-sensor cooperation". In the manufacturing process of large precision parts, a strategy for proper installation and placement of in-process/on-machine measurement system on the machine tools at the manufacturing sites is required.

Therefore, a machining monitoring system [8) 9)] and on-machine dimensional measurement systems are built and installed on the machine tools based on the concept of "multi-sensor fusion" and "multi-sensor cooperation," respectively.

Fig. 10 (a) shows the concept of multi-sensor fusion on-machine measurement for machining state monitoring. By conducting state estimations combining feature amounts from multiple sensors, characteristics of different physical amounts can be used to improve the detecting capability of machining monitoring. In the machining process that requires long time, measurement information (physical amount varied over time) obtained from the respective sensors is integrated in real time. Use of advanced signal processing to detect feature amounts that correlate with abnormality based on the time-frequency analysis provides adaptive threshold management in machining monitoring. Its high adaptability to environment and abnormality symptom detection capability reduces the risks related to production quality, such as chattering and tool failure, which is the most important measurement strategy for achieving a zero-defect process. In addition, in the future it is expected to both maintain production quality and improve process capability by integrating estimation methods and machining monitoring information considering multiple analysis technologies and uncertainty, such as cutting phenomenon, cutter path, tool/workpiece shapes, and by optimizing machining conditions based on the process model.

Fig. 10 (b) shows the concept of multi-sensor cooperation on-machine measurement for high precision measurement of geometric quantity. Higher accuracy of measurement is pursued by optimizing
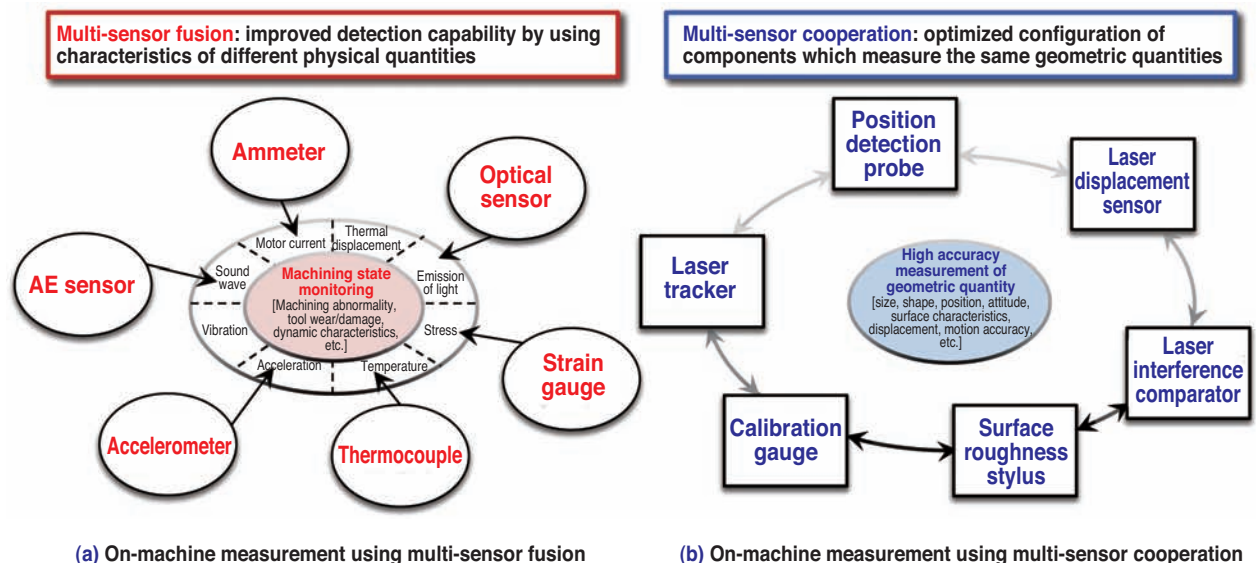

(a) On-machine measurement using multi-sensor fusion

(b) On-machine measurement using multi-sensor cooperation

Fig. 10 The smart on-machine measurement system using multi-sensor fusion and cooperation

and allocating respective roles for multiple components with the purpose of measuring the same geometric quantity (e.g. size, shape, attitude, and position) based on their measurement elements. The example of on-machine dimensional measurement systems integrated with the large CNC lathe for machining large precision parts consists of laser interferometer, laser tracker, tough trigger probe, and block gauge to realize high precision, multi-sensor cooperation for on-machine measurement providing absolute length calibration.

In the case of the machining process of steam turbine rotors, the operation of moving the work from machine tools to the measurement system was difficult and on-machine measurement was manually conducted using large micrometers, etc. Therefore, the problem was that it involved many measurement processes, resulting in increased uncertainty. To solve this problem and achieve efficiency of the manufacturing process and machining quality assurance, a high precision on-machine measurement system was developed. **Fig. 11** shows an example of on-machine measurement system for large structural parts by "multi-sensor cooperation" targeting steam turbine rotors (max. length of 10m or more, diameter of 1m or more, and dimensional tolerance of 0.1mm or less) of large CNC lathes. It shows configuration of the system which conducts absolute measurement of wheel position and axis diameter of the steam turbine rotor of the large CNC lathe by probing measurement method [10]. An inline length measuring system using laser tracker is introduced as the external coordinate system and a wireless touch trigger probe is implemented on the tool carriage. In addition, as the parts and machine elements are both affected by shrinkage and expansion (about 0.1mm of impact per 1m if the rotor temperature changes from 20˚C to 10˚C), a calibration method of absolute length is implemented using a block gauge to correct bias errors.
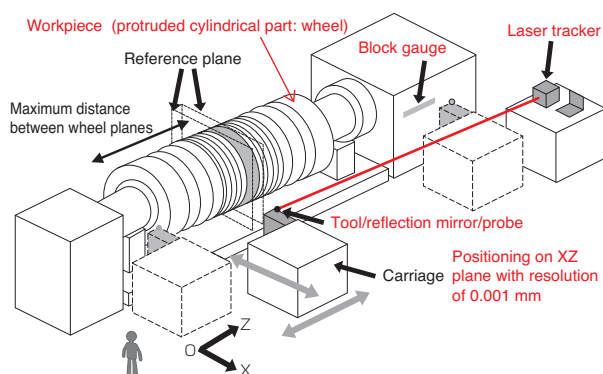

Fig. 11 The developed on-machine measuring system for a steam turbine rotor on CNC turning machine

4.3 Concept of holistic measurement

For the predictive production system, which is the foundation for innovation driven manufacturing, development of smart in-process/on-machine measurement as the strategic tool for machining measurement technology innovation is required to realize production quality control. As its foundation, the measurement strategy is to realize "informatization of every process related to manufacturing" by developing high degree of "multi-sensor fusion" and "multi-sensor cooperation," and with holistic measurement [11] based on integration of different measurement principles and multi-scale data fusion. For realizing holistic measurement, new theory for evaluating uncertainty, new comprehensive measurement principle to encompass the calibration technology, and conventional measurement principle and broader research regarding the compatibility among them are required.

As a specific example, a basic concept of intelligent multi-sensor coordinate measuring machine (CMM) is presented [12]. The holistic measurement uses new measurement technology, such as multi-sensor CMM with metrology X-ray CT (volumetric measurement). With the advancement of measured data fusion technology by integrating CAD/CAE/CAM/CAT data, this builds the foundation for advanced production quality control while different measurement systems become connected with each other through the Internet. The new strategic machining measurement which extends the concept of this measurement fusion technology to in-process/on-machine measurement is the smart in-process/on-machine measurement that realizes environment adaptive measurement with such properties as real-time, wide range, and multi-point simultaneity. As shown in **Fig. 12**, the optical non-contact measurement technology in a broad sense, including X-ray, is making rapid progress and technology that can measure surface micro-profile, 3D profile, and 3D internal structure has already been developed. Metrology X-ray CT technology in particular is making significant progress and its incorporation into inline processes and applications for assembly process inspection are being proposed [13]. When building multi-sensor CMM using these measurement technologies, 3D measurement data fusion technology is required for measurement integration of micro-profiles to complex large 3D profiles and volumetric measurement data. Efforts for developing measurement fusion technology [14] is already in progress. However, some technical challenges still remain, specifically related to multi-scale data fusion, such as measurement data quality including uncertainty, standard and calibration
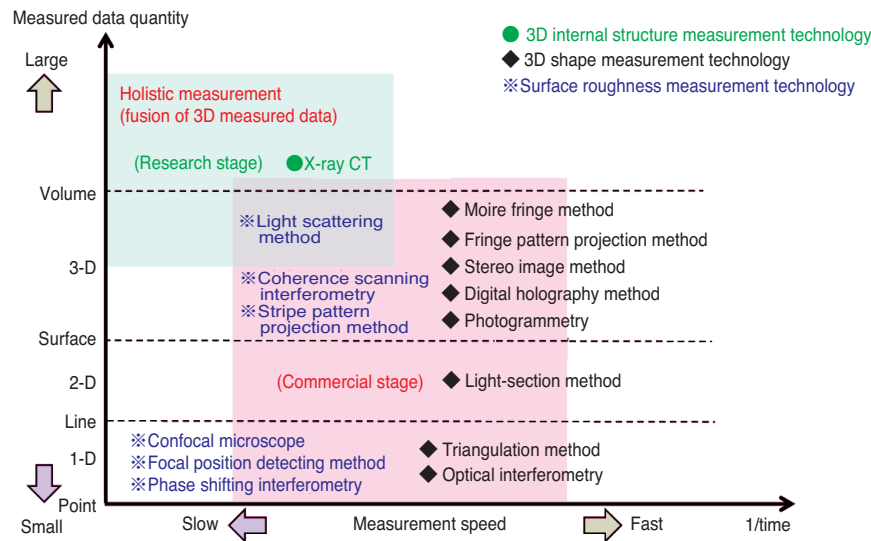
Fig. 12 Rapid progress in three dimensional measurement technologies for industrial measurement

methods, the basic quantity of measurement such as one-dimensional length and displacement, and two-dimensional surface micro profile with different angles and scale.

5. Outlook and challenges of smart machining/measurement machines

5.1 The 4th Industrial Revolution and predictive production system

The 4th Industrial Revolution is a disruptive transformation unlike the previous industrial revolutions, as significant innovation is expected not only in the manufacturing process but also across the entire product life cycle due to the rapid technological innovation in information technology, as evidenced by the promotion of Industry 4.0 in Germany and Industrial Internet in the U.S. The ultimate objective of the 4th Industrial Revolution is achievement of a new predictive production system based on the total optimization and efficiency of the manufacturing process, development of predictive maintenance, etc. That is, creation of new value by innovative products that fill the gap of "invisible value" and shift from mass production to complete customized production (one-unit production). In the manufacturing process with completely different mechanisms from the past, production quality has better adaptability than the quality control approach used in mass production. Furthermore, the basic concept of the 4th Industrial Revolution requires intelligence with autonomy (e.g. self-recognition, self-maintenance, and self-prediction) as its core property to the members of the manufacturing system (e.g. products and individual

manufacturing facilities). The key is to build predictive production systems with self-recognition capability. Internet of Things (IoT) which converts everything to data and connects them to the Internet through sensor technology, smaller and faster processors, and adoption of cloud technology, industrial big data which is collected by IoT, and cyber physical system (CPS) which use them will play the central role as the mechanism for such intelligence [15]. In addition, the measurement technology, which plays the role of information resources, is required to undergo transformation as a strategy tool. Particularly, smart in-process/on-machine measurement technology is an important and high-quality source of production information together with controllers and network systems, and requires technology innovation as a strategy tool, such as self-recognition and self-prediction embedded in the measurement systems.

5.2 Smart in-process/on-machine measurement network

The approach of intelligent machine tools by on-machine measurement using multiple sensors is a concept for standalone machine tools. Its objective is to increase efficiency of individual machining/measurement systems with knowledge base and incorporation into the machines. Therefore, it remains in the scope of efficiency driven manufacturing. On the other hand, innovation driven manufacturing requires intelligent environment adaptive in-process/on-machine measurement, i.e. open and intelligent machine tools through integration with smart in-process/on-machine measurement. Configuration of multi-sensor fusion and multi-sensor cooperation

based on holistic measurement changes in real time according to measured content (information on measurement environment, measurement condition, measured amount, subject of measurement, machining condition, required accuracy, allowance, uncertainty, etc.) to achieve advanced prediction. Its mechanism is based on the network of smart in-process/on-machine measurement connected in virtual space, as shown in **Fig. 13**. That is, the measurement content and measurement information are shared among intelligent machine tools connected to IoT, to drive predictive production systems which control production quality. The smart in-process/on-machine measurement is required to have the capability to sufficiently satisfy conditions of its measurement information such as amount, speed, diversification, and reliability. Capabilities such as self-recognition, self-maintenance, and self-prediction are obtained by CPS.

6. Summary

The most recent "2017 White Paper on Manufacturing Industries" [16] reports the initiatives and measures that the manufacturing industry in Japan is taking for the 4th Industrial Revolution. The white paper mentions that the value of virtual data from activities on the Internet is predominantly dependent on the "quantity" of data which is already dominated by the U.S. IT companies. However, the value of the real data collected by sensors in real life activities, such as operational data of the factory facilities, is potentially dependent on the "quality" of data and the companies in the manufacturing industry may be able to take a leading role depending on the future course of action. In fact, the survey results regarding data collection of the production process in **Fig. 14** indicates the trend that

the activities of "visualizing" operational states across the machines in the individual process, production line, the entire production process, traceability management, collection of production process data from overseas factories, etc. are all increasing. Therefore, it is considered that smart in-process/on-machine measurement will be increasingly important as a high-quality information source. In addition, solutions using recent digital technology are considered to be the "engineering chain" and "supply chain" indicated in **Fig. 15**. which also shows the mechanism to make those chains more efficient by quickly feeding back the smart in-process/on-machine measurement data. In contrast, the requirements for smart in-process/on-machine measurement, such as improvement of reliability and quality on the measurement data, are becoming higher and higher, as the data is more integrated, complex, and significantly larger.

Fig. 16. indicates the transition of machining measurement technology up to the 4th Industrial Revolution and transformation to the strategic machining measurement, as the foundation of production quality control. Machining measurement technology has been playing a role in element technology for production systems that satisfy the requirements of automation of inspection, production control, automation of production, etc. In that process, it underwent a series of revolutionary improvements in measurement capability, such as improvements in measurement accuracy and speed, higher sophistication from one dimensional to two dimensional, etc. However, the measurement technology required for the 4th Industrial Revolution is not an extension of conventional technology, but a fundamental transformation. That is, the predictive production system that takes advantage of IoT, industrial big data, and CPS based on real time holistic measurement
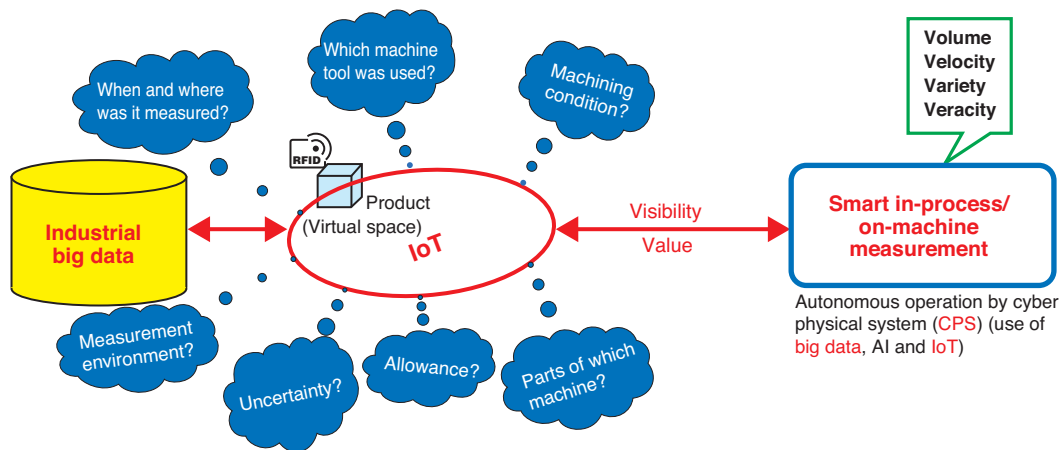
＊RFID (Radio Frequency IDentifier); IC tag

Fig. 13 Connecting data of smart in-process/on-machine measurement in cyber physical space

that uses intelligent in-process/on-machine measurement is considered to achieve the ultimate production quality control with self-recognition of the intelligent production elements.
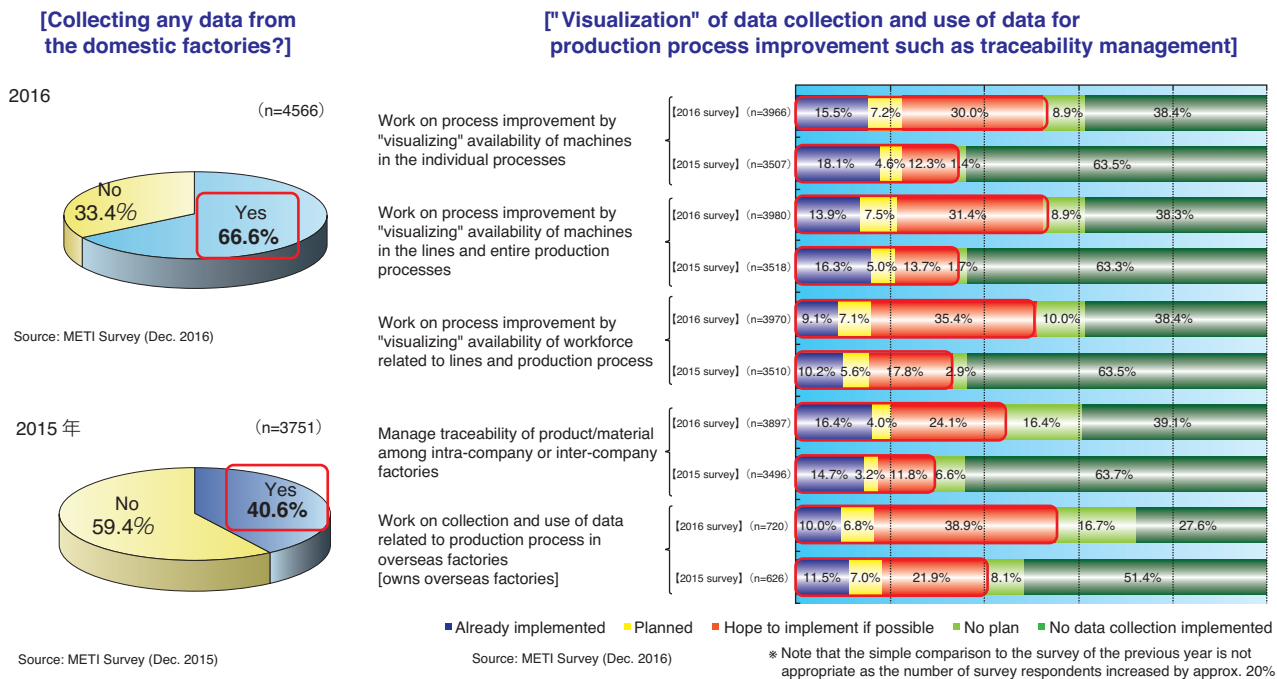
[Collecting any data from the domestic factories?]

2016   （n=4566）

No 33.4%   Yes **66.6%**

Source: METI Survey (Dec. 2016)

2015 年   （n=3751）

No 59.4%   Yes **40.6%**

Source: METI Survey (Dec. 2015)

["Visualization" of data collection and use of data for production process improvement such as traceability management]

Work on process improvement by "visualizing" availability of machines in the individual processes
- 【2016 survey】（n=3966） 15.5% | 7.2% | 30.0% | 8.9% | 38.4%
- 【2015 survey】（n=3507） 18.1% | 4.6% | 12.3% | 1.4% | 63.5%

Work on process improvement by "visualizing" availability of machines in the lines and entire production processes
- 【2016 survey】（n=3980） 13.9% | 7.5% | 31.4% | 8.9% | 38.3%
- 【2015 survey】（n=3518） 16.3% | 5.0% | 13.7% | 1.7% | 63.3%

Work on process improvement by "visualizing" availability of workforce related to lines and production process
- 【2016 survey】（n=3970） 9.1% | 7.1% | 35.4% | 10.0% | 38.4%
- 【2015 survey】（n=3510） 10.2% | 5.6% | 17.8% | 2.9% | 63.5%

Manage traceability of product/material among intra-company or inter-company factories
- 【2016 survey】（n=3897） 16.4% | 4.0% | 24.1% | 16.4% | 39.1%
- 【2015 survey】（n=3496） 14.7% | 3.2% | 11.8% | 6.6% | 63.7%

Work on collection and use of data related to production process in overseas factories [owns overseas factories]
- 【2016 survey】（n=720） 10.0% | 6.8% | 38.9% | 16.7% | 27.6%
- 【2015 survey】（n=626） 11.5% | 7.0% | 21.9% | 8.1% | 51.4%

■Already implemented ■Planned ■Hope to implement if possible ■No plan ■No data collection implemented

Source: METI Survey (Dec. 2016)

※ Note that the simple comparison to the survey of the previous year is not appropriate as the number of survey respondents increased by approx. 20%

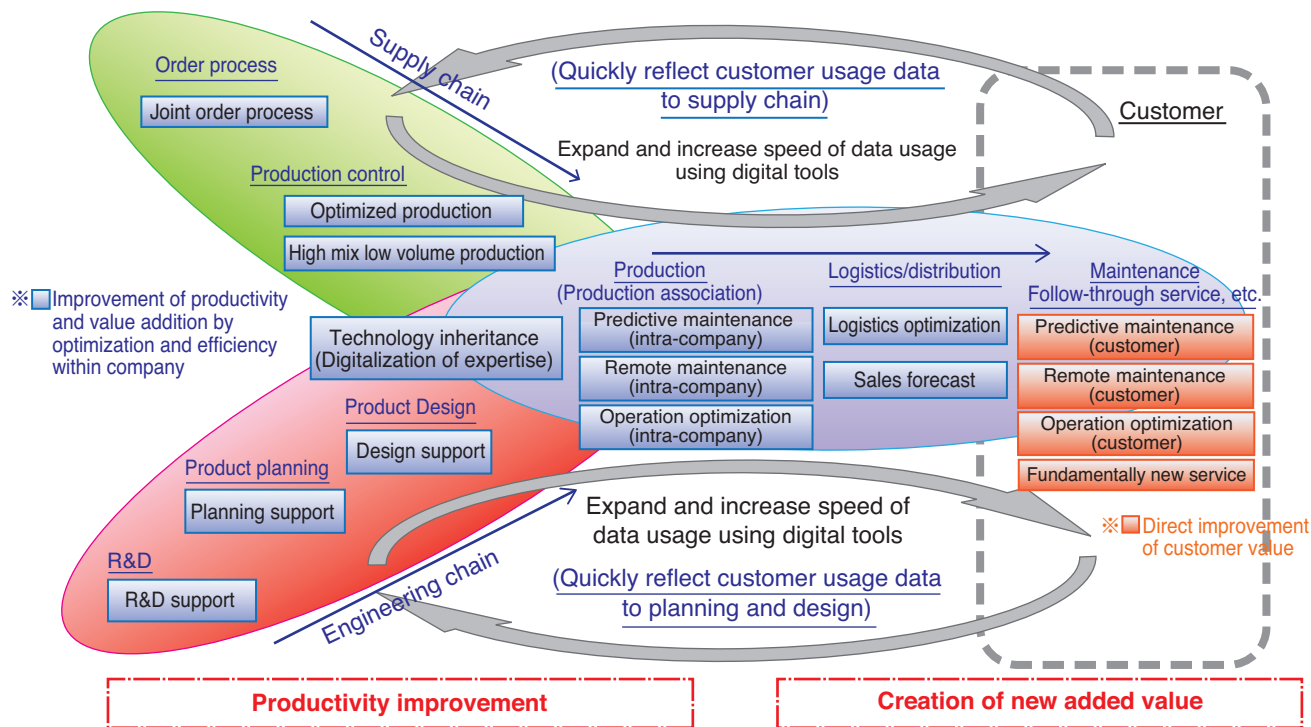**Fig. 14** Research results on data collection of production process

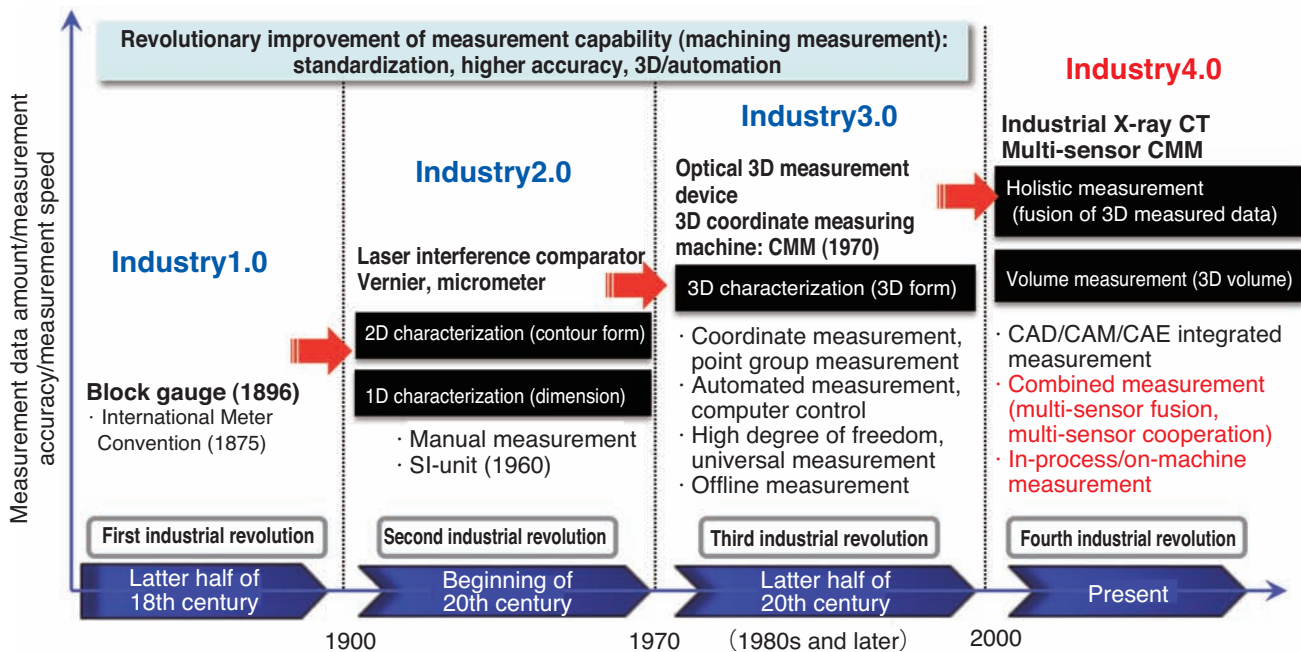**Fig. 15** Effective utilization of IOT in Industry 4.0

Fig. 16 Revolution of strategic measurement technology in production inspired by Industry 4.0

References

1) Shuichi Fukuda, "On Value Creation" Maruzen, 2005

2) Taniguchi, N., Current Status in, and Future Trends of, Ultraprecision Machining and Ultrafine Materials Processing, Annals of CIRP, Vol. 32/2, 1983), 2.

3) A. Weckenmann, M. Rinnagl, "Acceptance of processes: do we need decision rules?", Precision Engineering, Vol.24, (2000), 264-269.

4) International Organization for Standardization, "Guide to Expression of Uncertainty of Measurement", JCGM 100, (2008).

5) Ministry of Economy, Trade and Industry, Ministry of Health, Labor and Welfare, Ministry of Education, Culture, Sports, Science and Technology, 2015 White Paper on Manufacturing Industries Overview; FY2014 Promotion measures of core manufacturing technology (Overview), (2015)

6) Marcello Colledani, Tullio Tolio, Anath Fischer, Benoit Iung, Gisela, Lanza, Robert Schmitt, Józef Váncza, Design and management of manufacturing systems for production quality, CIRP Annals - Manufacturing Technology, Vol.63/2, (2014), 773-796.

7) Byrne G, Dornfeld D, Inasaki I, Ketteler G, König W, Teti R, Tool Condition Monitoring (TCM) — The Status of Research and Industrial Application, Annals of CIRP, Vol. 44/2, (1995), 541–567.

8) Masahiro Uekita, Yasuhiro Takaya, Tool condition monitoring for from milling of large parts by combining spindle motor current and acoustic emission signals, International Journal of Advanced Manufacturing Technology, Vol.89, Combined 1-4, (2017), 65-75.

9) Masahiro Uekita, Yasuhiro Takaya, Tool condition monitoring technique for deep-hole drilling of large components based on chatter identification in time–frequency domain, Measurement, Vol.103, (2017), 199-207.

10) Masahiro Uekita, Yasuhiro Takaya, On-machine dimensional measurement of large parts by compensating for volumetric errors of machine tools, Precision Engineering, 43, (2016), 200-210.

11) A. Weckenmann, THE ROLE OF METROLOGY IN THE EXCHANGE OF GOODS AND IN THE DEVELOPMENT OF MANUFACTURING TECHNOLOGIES, Proceedings of the10th International Symposium on Measurement and Quality Control 2010, (2010), 1-4.

12) A. Weckenmann, X. Jiang, K. –D. Sommer, U. Neuschaefer-Rube, J. Seewig, L. Shaw, T. Estler, Multisensor Data Fusion in Dimensional Metrology, CIRP Annals - Manufacturing Technology, Vol.58/2, (2009), 701-721.

13) L. De Chiffre, S. Carmignato, J.-P. Kruth, R. Schmitt, A. Weckenmann, Industrial applications of computed tomography, CIRP Annals - Manufacturing Technology, Vol.63/2, (2014), 655-677.

14) A. Weckenmann, X. Jiang, K. –D. Sommer, U. Neuschaefer-Rube, J. Seewig, L. Shaw, T. Estler, Multisensor Data Fusion in Dimensional Metrology, Annals of the CIRP, Vol.58/2, to be published, 2009.

15) Jay Lee, "Industrial big data; challenges of manufacturing industry toward Industry 4.0", Nikkan Kogyo Shimbun, Ltd., 2016

16) Ministry of Economy, Trade and Industry, Ministry of Health, Labor and Welfare, Ministry of Education, Culture, Sports, Science and Technology, 2017 White Paper on Manufacturing Industries Overview; FY2016 Promotion measures of core manufacturing technology (Overview), (2017)

<Author biography>
Yasuhiro TAKAYA
Professor, Doctor (Engineering), Department of Mechanical Engineering,
Graduate School of Engineering, Osaka University

March, 1992	Engineering Doctor, Doctor Course Completed, Precision Engineering Department, Graduate School of Engineering, Hokkaido University
April, 1992 - June, 1995	Assistant, Industrial Mechanical Engineering, School of Engineering, Osaka University
July, 1995 - June, 1997	Instructor, Industrial Mechanical Engineering, School of Engineering, Osaka University
July, 1997 - March, 2006	Assistant Professor, Department of Mechanical System Engineering, Graduate School of Engineering, Osaka University
April, 2006 - present	Professor, Department of Mechanical Engineering, Graduate School of Engineering, Osaka University

[Specialty]
 Precision machining measurement, optical applied nano-measurement, optical applied nano/micro machining

[Academic society and committee affiliations]
 The Japan Society for Precision Engineering: Intelligent Nano-Measure Expert Committee Chair
 The Japan Society of Mechanical Engineers: Fellow, 1st Planning Committee Chair, Manufacturing and Machine Tool Division
 The Japan Society for Abrasive Technology
 The International Academy for Production Engineering (CIRP): Fellow
 International Measurement Confederation (IMEKO): TC14 Chair
 The Japan Society for Die and Mould Technology: Director (Vice President)
 Mitsutoyo Association for Science and Technology (MAST): Advisor and many others

[Perspective]

Rolling Bearing and IoT – NTN's Approach to IoT -

Masaki EGAMI

With advancement of IoT, big data collected from various types of equipment are utilized to improve service and productivity, to reduce opportunity loss by providing appropriate maintenance and so on.   Rolling bearings are integrated and used in many familiar applications such as transportation vehicles, electrical products, and industrial machinery.   Therefore, rolling bearings are considered as one of the most suitable data collecting elements. This report introduces **NTN**'s approaches to IoT and future prospects, focusing on sensing technologies related to rolling bearings.

1. Introduction

Recently, as Germany and the U.S. promote Industry 4.0 and the Industrial Internet, respectively, the Internet of Things (IoT) is being rapidly adopted. Also, in Japan, Society 5.0 is being proposed and promoted under the leadership of the government which describes the "Super-smart society" as the society of the future [1-2]. With IoT, data is collected from any device and analyzed as big data. Initially, the focus was placed on improvement of productivity in manufacturing and reduction of lost opportunity by optimizing maintenance. However, they are now planned to be used in various fields including improving quality of life.

Rolling bearings are used in all kinds of machines, including transportation vehicles such as automobiles, rolling stock, aircraft, industrial machinery such as construction machinery, machine tools, robots, information/office equipment such as computers and printers, electrical appliances such as refrigerators, air conditioners and washing machines. The bearings are used as mechanical elements to support various rotational operations.

NTN developed rolling bearing units with embedded rotation sensors in early 1990s for industrial machinery. **NTN** continued to develop new technology for applications in industrial fields such as robotics, with enhancement of resolution of rotation sensors to

40 times compared with conventional products and development of a sensing system that enables detection of absolute angles.

With regard to the detection of abnormal operation of machinery by vibration, **NTN** started evaluating vibration acceleration. **NTN** recently moved to more sophisticated abnormality detection using artificial intelligence (AI) such as machine learning.

We also developed "Wind Doctor™" as the Condition Monitoring System (CMS) for wind turbines in 2012 as the abnormality diagnostic system for equipment, which is used with domestic power generation facilities for reduction of downtime.

In this article, we introduce this technology as our initiative related to IoT at **NTN**, and describe our vision for the future. Some of the technology and products introduced in this article are also detailed in different papers, so please excuse us for possible duplication.

2. NTN's rotation detection technology and application products

2.1. Rolling bearing with rotational sensor

Optical and magnetic sensors are generally used for detection of rotation, depending on the application. An optical sensor has the advantage of high detection sensibility; however, it is costlier and more susceptible to adverse environments such as dirt. Therefore, **NTN** has been dedicated to the application of magnetic

---

*Senior Executive Officer, R&D

sensing systems to consider the environments where rolling bearings are used. We implemented volume production of "bearings with rotational sensors" which can detect both rotation speed and direction by installing multipole (N/S poles) magnetized rings and magnetic sensor IC facing each other in rolling bearings [3-4] **Fig. 1** shows an example of bearings with rotational sensors for industrial machinery, used for detecting rotational speed and direction of drive motor for forklifts. There are other products which are made into a unit for detecting rotational angle of hydraulic shovel booms [5].

Fig. 2 shows a hub bearing with a magnetic ring for detecting rotation of anti-lock brake system (ABS) for automobiles. The magnetized ring is integrated with the bearing seal. The material is rubber with magnetic particles. Rotation is detected by placing a magnetic sensor IC against this magnetized ring. This system is produced by **NTN-SNR** under the name "Active Sensor Bearing (ASB®)" and widely used globally as the de facto standard for automotive ABS, even today.

2.2. High resolution rotational sensor

NTN-SNR developed high resolution rotational sensor with 40 times higher resolution than the conventional product for detecting rotation, using the magnetized ring described in 2.1 [6]. The sensor structure and the measurement principle are shown in **Fig. 3**. This sensor can detect small angles of less than the polarity gap width by dedicated IC, which integrates multiple magnetic sensor elements and signal processing circuits. An example of combination of this sensor and rolling bearing is shown in **Fig. 4**.

This sensing system was adopted by Light Detection and Ranging (Lidar) used for detecting obstacles around vehicles in automotive driving support systems, which is in the process of practical application. This system detects obstacles by detecting laser light reflected by obstacles by scanning laser light with a mirror. This sensing system is integrated in the rotating mechanism of the mirror, contributing to the implementation of accurate angle control.

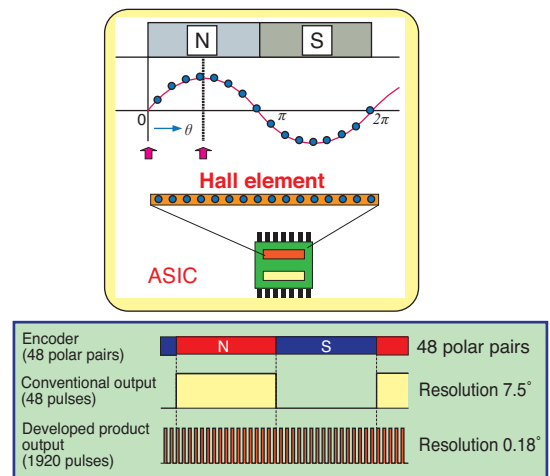An example of detection of tire rotation in an actual

Fig. 1 Rolling bearing with rotational sensor

Fig. 2 Hub bearing with magnetic encoder

Fig. 3 Sensing element for high resolution rotational sensor

Commercialized for rotating mirror detection of Lidar

Fig. 4 Ball bearing with high resolution rotational sensor

vehicle by integrating this system into the ABS sensing part of the vehicle is shown in **Fig. 5** [7]. The graph also shows the conventional ABS sensor signal. It reveals that the tire rotation at the start of vehicle is detected more in detail by the system, in the time zone indicated on the left axis. As autonomous driving is expected to grow in the future, precise measurement of road surface and tire rotation is required and therefore, application of this sensing system is expected.
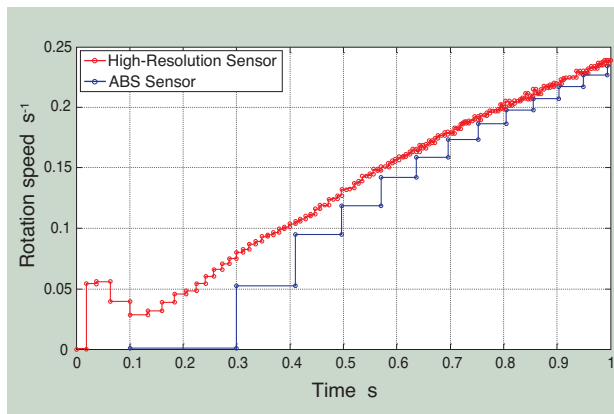

Fig. 5 Rotational signal when staring a vehicle

2.3 Absolute angle sensing by multi-track magnetic ring

NTN developed "multi-track magnetic rings" which can detect the absolute angle of rotational shaft with high resolution and precision by combining the dedicated magnetic sensor IC with the magnetic rotational sensor technology it has developed so far [8]. The ring is made of annular core metal with unvulcanized rubber material vulcanized on the metal, forming two magnetic tracks on the rubber magnetic material.

Fig. 6 shows an example of radial magnetized type. As shown in **Fig. 6 (b)**, magnetic poles of different number are magnetized in each of the two tracks at even intervals with difference in phase. From the difference of phases between the two magnetized patterns, the angle position is accurately calculated (Vernier principle) to detect the absolute position in a 360-degree range. This is described in more detail in a different article.

The multi-track magnetic ring can be designed in low profile and compact size, and cables can be included internally as it has a hollow structure. It is expected that these magnetic rings can be used for angle or torque detection of joints in collaborative robots which are expected to be quickly put into practical use **(Fig. 7)** .

(a) Outlook　　　**(b)** Magnetization pattern
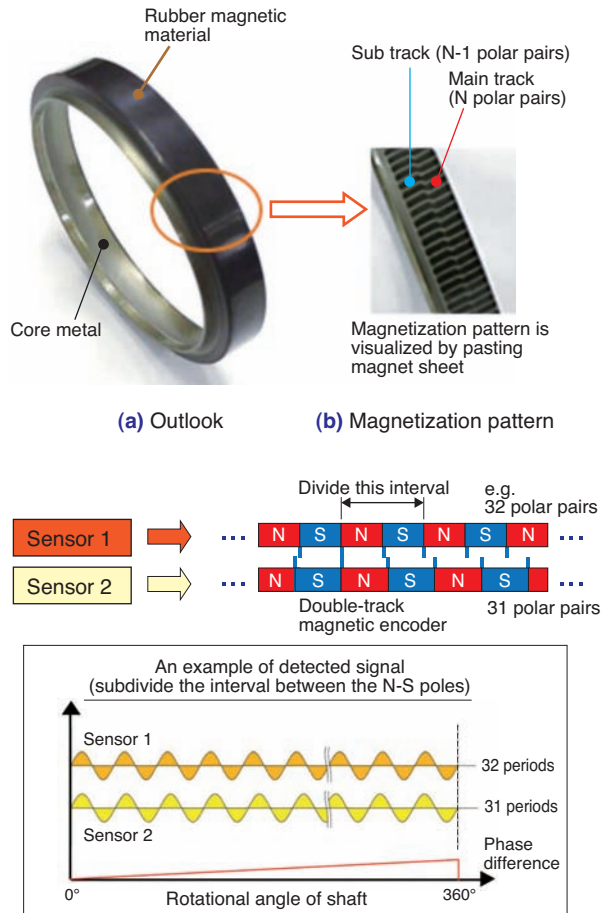
(C) Principle for detecting absolute angles (e.g.: 32-31 polar pairs)

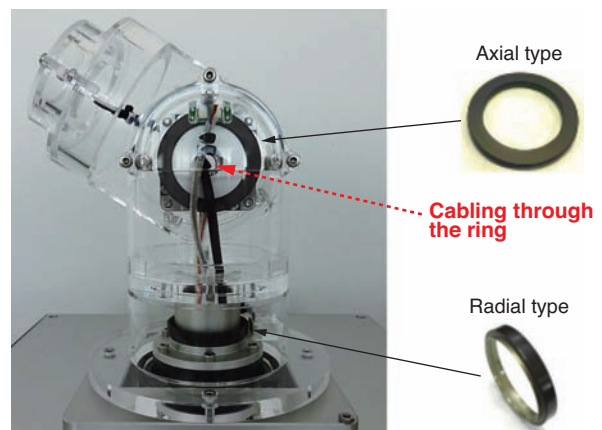**Fig. 6** Multi track magnetic ring — Radial type

Fig. 7 Multi track magnetic ring installed in joint of robot

3. Rolling bearing abnormality detection technology

Operation status monitoring is required, including surrounding machine parts in the areas where high reliability and safety are required for large equipment such as power plants, plant facilities and rolling stock. Sensors are integrated in the bearings or journal boxes for sensing vibration of the rotation shaft, rotational speed, temperature, etc. Predictive safety function is used for early warning of potential failure, by estimating the source of vibration from the detected rotational speed and vibration frequency and detecting the symptoms of increase in vibration.

The current typical abnormality detection methods of rolling bearings are evaluation of effective values of vibration acceleration and use of acoustic emission (AE) [9]. **Fig. 8** shows a transition of vibration acceleration from normal status to breakdown of rolling bearings [10]. When the bearing is in normal status (stage I), the vibration acceleration around the bearing is at a low level and increases when the bearing is damaged (stage II). When the damage reaches a certain size, the vibration acceleration remains at the same level for a while (stage III). When the damage further increases, the vibration acceleration increases (stage IV), then it abruptly increases to functional breakdown.
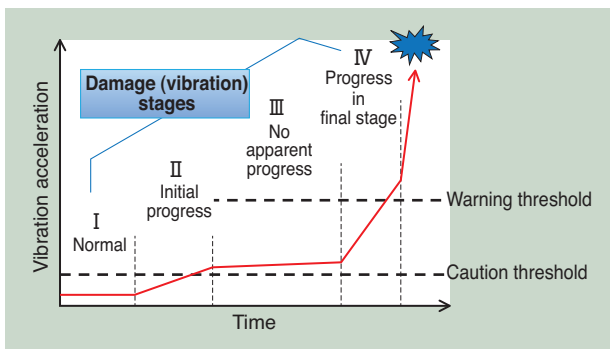
Fig. 8 Vibration transition of rolling bearing with damage growth

Fig. 8 shows a simple model to set a threshold to the effective value of vibration acceleration and issue caution and warning signals. However, in the conventional method, the threshold should be sufficiently larger than the initial background vibration to eliminate impact of temporary increase of vibration and noise. There are cases where significant damage is already given when the effective value of the signal is large enough. In these cases, the time given until the functional breakdown may be very short depending on the speed of damage progress, which causes adverse

effects on the maintenance plan.

Therefore, **NTN** is working on the damage detection of bearings for large wind turbine by participating in NEDO's project together with University of Tokyo and National Institute of Advanced Industrial Science and Technology (AIST), for improving abnormality diagnosis. In this project, we have measured and collected data on vibration installing **NTN**'s condition monitoring system "Wind Doctor ™" on wind turbines in various locations in Japan, under the leadership of the University of Tokyo. We are analyzing signals detected by ordinary monitoring in order to find further early symptoms using AI developed by AIST. **Fig. 9** shows cases of earlier detection of abnormality compared with the conventional methods by applying AI developed by **NTN** under advice of AIST.

Not only wind turbines, but many applications where damage on bearings can cause social loss. If early damage or its symptoms can be detected and the time until breakdown can be estimated, planned maintenance can be conducted to avoid reduction of the availability to a minimum. Currently, **NTN** is developing AI to predict progress of damage through **NTN** Next Generation Research Alliance Laboratory established within Osaka University in September 2017.
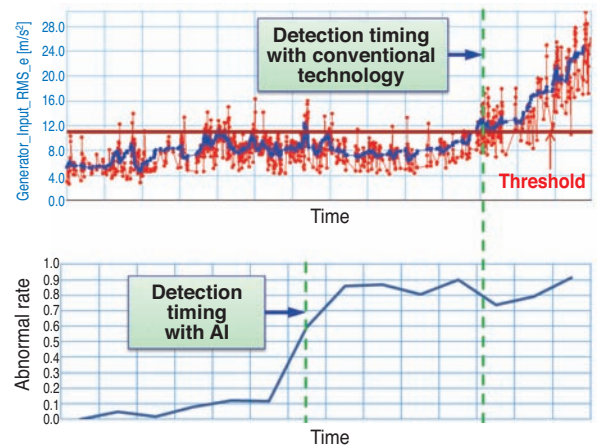

Fig. 9 Example of early detection of failure by utilizing AI

4. Introduction of NTN's initiatives for IoT

4.1. Condition monitoring system (CMS) for wind turbines

NTN developed "Wind Doctor ™" in 2012, as a condition monitoring system to help wind turbines improve their availability [11] and is actively promoting it in Japan. Various measurement sensors and data collection devices are included in the nacelle of the wind turbines (**Fig. 10**).
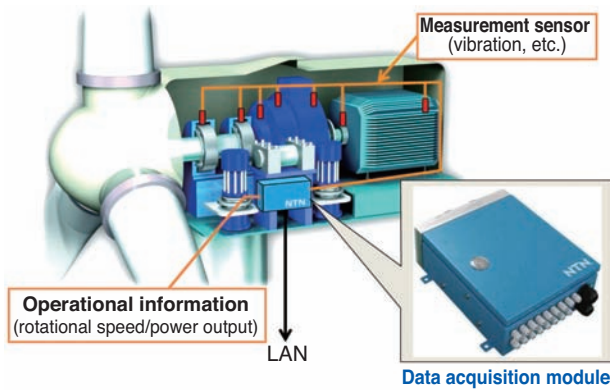
Fig. 10 Installation equipment of "Wind Doctor TM" in wind turbine nacelle

Fig. 11 shows the system configuration of "Wind Doctor TM" The collected data are recorded on the dedicated server on the Internet and through signal processing and trend analysis, system abnormality and damage detection results are notified. As mentioned in Section 3, we will improve the diagnosis capability by applying abnormality detection algorithms using AI and advance the entire system to achieve more in-depth planned maintenance (**Fig. 12**).

(1) Sensor within wind turbine + (2) Data acquisition module + (3) Dedicated server + (4) Analysis/diagnosis

(1) Attach approx. 10 sensors to main bearing, gearbox and generator
(2) Measure sensor signals with data acquisition module every two hours
(3) Send and store data to dedicated server through the Internet
(4) Diagnose abnormality by analyzing the data

Fig. 11 Components of "Wind Doctor TM" system

STEP 1
Present state

STEP 2

STEP 3

AI

(5) **Advanced preventive maintenance (2)**
Higher accuracy/early detection/ labor saving unmanned operation through introduction of AI technology

(3) **Advanced preventive maintenance (1)**
High accuracy/early detection

(2) **Data acquisition**
Trend management
Preventive maintenance

(4) **Deployment to other fields**
Rolling stock, machine tools, etc.

(1) **Sale of modules**

Fig. 12 Future image of **NTN**'s CMS

4.2 Natural energy and IoT

NTN established the Green Energy Products Division in 2016 to work on business development of small power generation systems. It also started distribution of **NTN** Hybrid Street Light which use two types of natural energy of wind and solar light, and **NTN** micro hydro turbines (micro hydro turbine). "Green Power Park" in Advanced Technology R&D Center in Kuwana-city of Mie Prefecture was established as a part of this initiative (**Fig. 13**) [12]. In the Park, 3 **NTN** vertical axis wind turbines, one **NTN** micro hydro turbine and 3 **NTN** Hybrid Street Light, which were developed by **NTN**, are installed providing energy generated by them to electric vehicles (EV) and vegetable factories (green power farms), introducing energy circulating models. The IoT room (Monitoring and Control Center) located in the site is monitoring information on "power generation, storage and consumption." **NTN** is also working on the development of energy management system pursuing high efficiency using IoT of this facility.

It also installed an "Independent power supply network Mimamori Robokun III" experimental model (**Fig. 14**) in Osaka University for demonstration testing within the framework of "Joint Research for Creating Mechanisms Regarding Disaster Prevention Monitoring and Tourism through Use of IT" with Osaka University. This system combines "**NTN** Hybrid Street
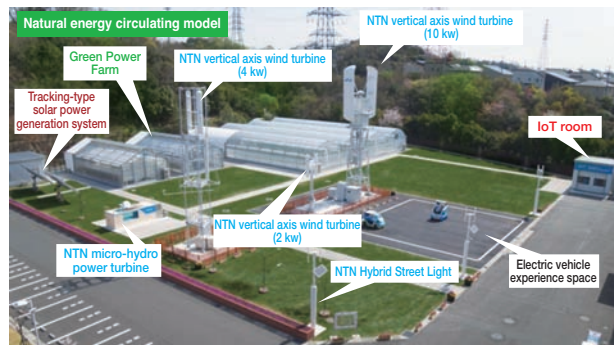

Fig. 13 Green power park

Fig. 14 Mimamori Robokun III experimental device

Light" which uses wind and solar light as the energy source for security cameras, Wi-Fi communication equipment and emergency power supply providing a monitoring function for local children and communication means in the case of a disaster (**Fig. 15**). We are conducting connectivity experiments between this experimental model and "Disaster Relief Map," verification of power generation/storage amount, operational experiment of Wi-Fi communication equipment and experiments on automatic connection in case of communication shutdown. We plan on using the know-how of communication and signal processing obtained in these experiments as element technologies of bearing abnormality diagnosis of the future.
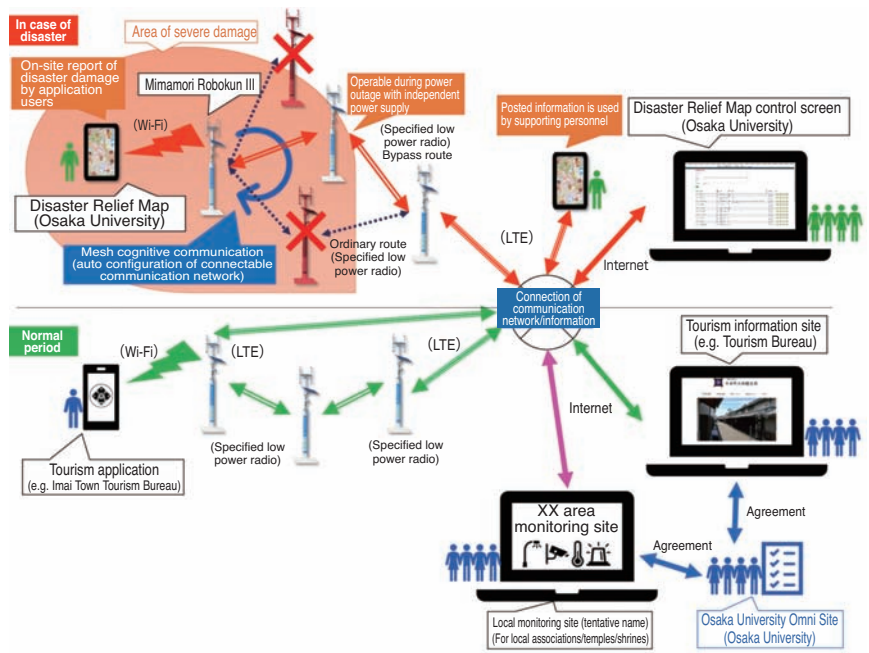
Fig. 15 Creation of mechanisms regarding disaster prevention, monitoring, and tourism through use of IT

5. Conclusion

A great number of rolling bearings are integrated in applications, not only in manufacturing, but also in various devices related to people's everyday life such as clothing, food, living and transportation. They are the optimum elements for data collection of IoT when sensors are incorporated in them. To this end, challenges regarding reduction of sensor size, securing power supply and communication means must be solved. **NTN** is committed to do its best for solving these challenges through IoT for preserving the natural environment, increasing people's living standards and improving security/safety.

References
1) P. C. Evans and M. Annunziata: Industrial Internet - Pushing the Boundaries of Minds and Machines -, GE Reports Japan (2012)
2) Yoshitsugu Kimura: Measurement and life evaluation in topology, Tribology Workshop, 29th Conference, Preprint (2018) 1.
3) Hiroyoshi Ito, Takeshi Koike: Bearing with Integral Revolution Sensor, NTN TECHNICAL REVIEW No.69 (2001) 108.
4) Takeshi Koike, Tomomi Ishikawa, Hiroyoshi Ito, Noriyoshi Mizutani: Improvement of Magnetic Flux Leakage Durability of Integrated Sensor Bearings, NTN TECHNICAL REVIEW No.71 (2003) 74.
5) Shoji Itomi, Hiroyoshi Ito, NTN Sensor Units for Construction Machinery, NTN TECHNICAL REVIEW No.76 (2008) 121.
6) Hiroyoshi Ito, Toru Takahashi, Pascal Desbiolles, Cytil. Peterschmitt, Shintarou Ueno, "High Resolution Sensor Bearing with an Index Signal",
NTN TECHNICAL REVIEW No. 78 (2010) 76.
7) Kentaro Nishikawa, Toru Takahashi, Christophie Duret: Hub Bearing with an Integrated High-Resokution Rotation Sensor, NTN TECHNICAL REVIEW No.81 (2013) 52.
8) Takashi Koike, Yasuyuki Fukushima, Yusuke Shibuya: High Resolution Absolute Angle Sensor Applicable for Detecting Absolute Angle of Robot Joints, Machine Design Vol. 62 No. 3 (2018) 55.
9) Hiroki Mano: IoT Deployment of Rolling Bearings, Machine Design Vol. 62 No. 2 (2018) 46.
10) Toru Takahashi, Michio Hori: Technical Trends on Bearing and Condition Monitoring System in Wind Turbine, Tribologist Vol. 62 No. 11 (2017) 691.
11) Akitoshi Takeuchi, Takashi Haseba, Hiroshi Ikeda: Application of Condition Monitoring System for Wind Turbines, NTN TECHNICAL REVIEW No.80 (2012) 15.
12) Natsuhiko Mori: Green Energy Business and Green Power Park, NTN TECHNICAL REVIEW No.84 (2016) 14.
13) https://www.ntn.co.jp/japan/news/press/news 201700086.html

Photo of author

Masaki EGAMI

Senior Executive Officer, R&D

[New Product]

Development of "i-WRIST™" Wrist Joint Module

Keisuke KAZUNO*   **Hiroshi ISOBE***
Jun MIDOUMAE*   **Yuuki SHIMURA***
Masayuki OHARA*

NTN has developed the angle control equipment applying a parallel link mechanism which is a type of constant velocity joint. In order to expand this equipment for appearance inspection application, we expanded the movable bending angle range from 45° to 90° and developed a wrist joint module which can be positioned toward any posture in all hemispherical directions at high speed. We changed the name from the conventional "Parallel Link High Speed Angle Control Equipment" to "i-WRIST™" and started mass production.

1. Introduction

Industrial robots are rapidly being deployed globally due to the strong demand for automation and labor saving aimed at improving productivity in manufacturing. For example, vertical multi-joint robots are widely used in severe manufacturing environments, such as handling of heavy objects and welding/painting lines. In addition, horizontal multi-joint robots and parallel link robots are also widely used in industrial applications which require high-speed handling and transportation of food.

On the other hand, a workforce shortage is one of the issues facing Japan, due to a decreasing birthrate and aging population [8]. Particularly, there is a serious labor shortage in work processes requiring skill sets and companies are employing robots in processes which have been traditionally handled by workers.

Since the announcement of the angle control unit using the proprietary parallel link mechanism in 2012, **NTN** has been exploring the use of robots in grease and cleaning applications which were not well handled by the conventional robots due to the requirement of fine-tuned and quick angular movement. Recently, we are also extending their use to visual inspection for automotive parts and electric/electronic parts which have been depending on skilled workers to respond to the new demands.

In this article, we introduce features, system configuration, setup method for operation patterns, and applications of the "i-WRIST™" utilizing its 90° bending angle, which **NTN** developed for visual inspection.

2. Configuration and features of i-WRIST™

Fig. 1 shows an overview of i-WRIST™.i-WRIST™ is a wrist joint module consisting of a proprietary parallel link mechanism and drive mechanism that controls its orientation and synchronously controls three motors to provide two degrees of freedom of attitude positioning (bending angle θ and revolving angle ϕ) to the top end. The following shows its features.

(1) High-speed operation
Fast operation of 0.1s/point or less* has been achieved on fine-tuned attitude change.
(2) Wide operating angle range
Maximum bending angle of 90°, revolving angle of 360° x n (unlimited)
(3) Smooth operation in all directions
No singular point in operation angle range with spherical link mechanism
(4) Placing end effector within internal space of link mechanism
High-speed operation is achieved by reducing the

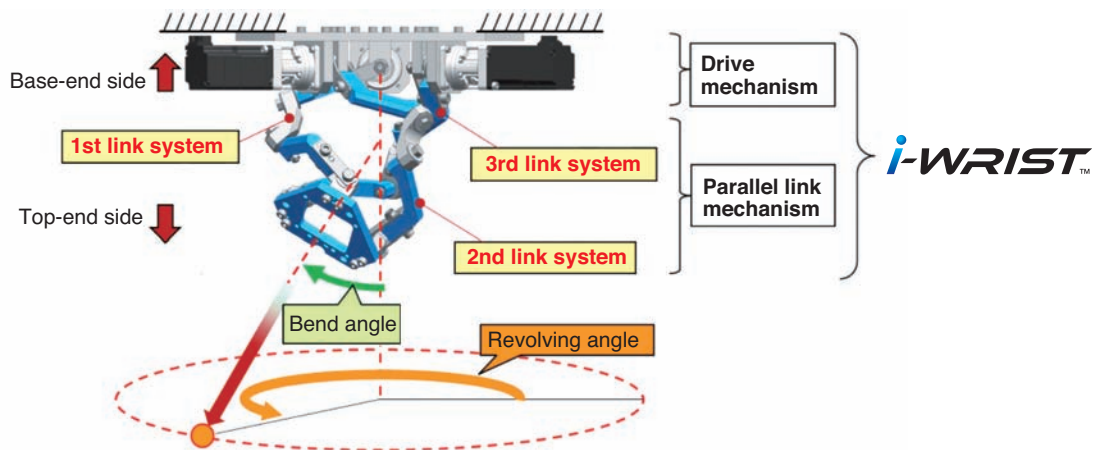*Industrial Machinery Division

Fig. 1 Schematic of i-WRIST™

moment of inertia. Cabling is placed through the internal space to avoid twisting the cables when revolving operation is repeated.

* Speed of positioning operation against points on 7 x 7 matrix of 10 mm intervals

3. System configuration example

i-WRIST™ can be used in a configuration that combines a linear motion actuator and Rz stage, as shown in **Fig. 2**. **Fig. 3** shows the configuration of the control system. An (1) i-WRIST™, (2) a proprietary controller and a (3) proprietary console (enclosed in red line) are provided as standard offering by **NTN**. Servo drivers and a linear motion actuator, etc. which are enclosed in blue line are the parts which models and series (specification) are specified by **NTN**. The parts in black lines are selected by the customer.
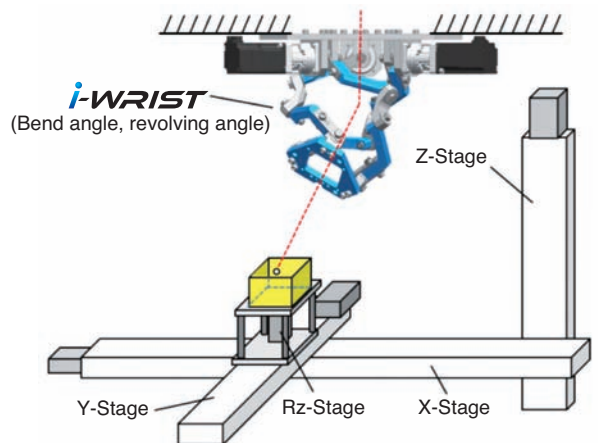
(1) i-WRIST™
Wrist joint module with three reducer motors.
(2) Proprietary controller
Installed software works not only for standalone i-WRIST™ but also in a system configuration of i-WRIST™ with linear motion actuator (XYZ axis) and Rz Stage (**Fig. 3**).
(3) Proprietary console
Used to teach operation of i-WRIST™ and linear motion actuator.

Fig. 2 Configuration example
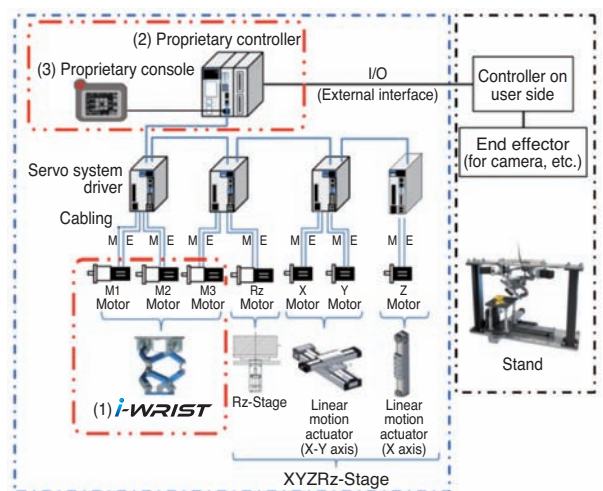
Fig. 3 Control system configuration

4. Key specifications

4.1 i-WRIST™

Fig. 4 shows the picture of i-WRIST™ outer view with a bending angle of 90˚, which was most recently developed, and Table 1 shows its key specifications. Angular contact ball bearings are used in each rotating pair in order to allow high-speed operation and appropriate pre-load is applied to ensure rigidity of i-WRIST™. The increase in moment of inertia due to installation of end effectors could be reduced by placing them within the internal space of the parallel link mechanism.
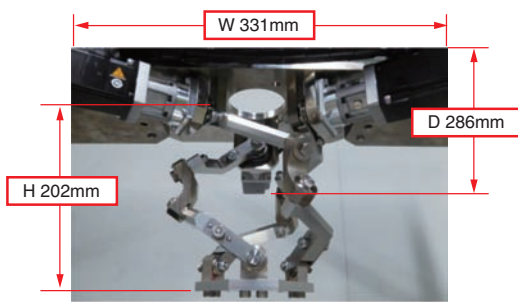
(a) Attitude with bend angle 0˚
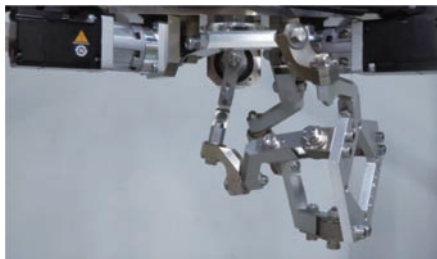
(b)Attitude with bend angle 90˚

Fig. 4 External view of i-WRIST™

Table 1 Specification of i-WRIST™

Item	Specification
Size	W331×D286×H202 mm
Weight	5.4 kg
Degree of freedom	2
Operating angle range	Bend angle: 90˚
	Revolving angle: $360˚×n$ (unlimited)
Repeated positioning accuracy	±0.05˚ or less
Portable mass (permissible moment of inertia)	1.0 kg （0.025 kgm²）
Motor output	50 W

4.2 Proprietary controller

Table 2 shows the key specifications of the proprietary controller. It uses commercial hardware with proprietary software developed by NTN. It does not require any special knowledge and allows for intuitive operation to perform complex calculations such as coordinate conversion.

Table 2 Specification of proprietary controller

Item	Specification
Size	W65×D110×H130 mm
Auxiliary unit	I/O unit (input: 32 points, output: 32 points)
Rated voltage	DC24V±20%
Items to be controlled	i-WRIST™, X-Stage, Y-Stage, Z-Stage, Rz-Stage

4.3 Proprietary console

Table 3 shows the key specifications of the proprietary console. It is a handheld device that uses commercial hardware with console screens developed by NTN.

The proprietary console is able to set not only the i-WRIST™ configuration, but also operating conditions and operating patterns of the linear motion actuator and rotating mechanism (Rz axis) shown in Fig. 3 (Control system configuration). In addition, its ability to register multiple operating patterns allows for an easy exchange of setup or tools.

Table 3 Specification of proprietary console

Item	Specification
Outer dimension	W224×L174×H107 mm
Display device	Color
Display size	W115.2×L86.4 mm
Weight	0.96 kg or less
Rated voltage	DC24V±20%
Registrable operating patterns	50 patterns (100 points max. can be registered for each operating pattern)

5. Setting of operating patterns

Typically, special knowledge is required to operate robots; however, the proprietary controller simply performs the points registered as sequential operating patterns. Therefore, operating patterns can be easily set without the need for special knowledge.

5.1 Teaching

Teaching methods vary depending on the coordinate system being used. They are broadly categorized into "base coordinate system" which is based on the entire system and "work coordinate system" which is based on the work.

5.1.1 Base coordinate system

Fig. 5 (a) shows the conceptual diagram of the base coordinate system. In this method, the job buttons on the proprietary console screen shown in Fig. 6 are used to move the X-Stage, Y-Stage, Z-Stage, i-WRIST™, Rz-Stage to the desired positions and

angles to register those positions and attitudes (Sx, Sy, Sz, θ, ϕ and Rz). This does not require an understanding of the coordinate system to set the operating patterns.

5.1.2 Work coordinate system

Fig. 5 (b) shows the conceptual diagram of the work coordinate system. In this method, the actual working position (XYZ coordinates) and working direction (θ' and ϕ') on the work to be operated are specified.

The proprietary controller automatically calculates the attitude of i-WRIST™ and linear motion actuator if the distance from the top end of i-WRIST™ to the work position of the end effector and the positions of

base coordinate system and work coordinate system are preset on the proprietary console. Therefore, the teaching process can be performed efficiently.

The position coordinates of work points and work direction can be edited while the coordinates on the 3D model of the work (work coordinates) are confirmed on the PC screen by the developed point data editing software as shown in **Fig. 7**. The edited software can be written on the proprietary console in a batch process. The operating pattern data of the proprietary console can also be stored in the PC as backup data.
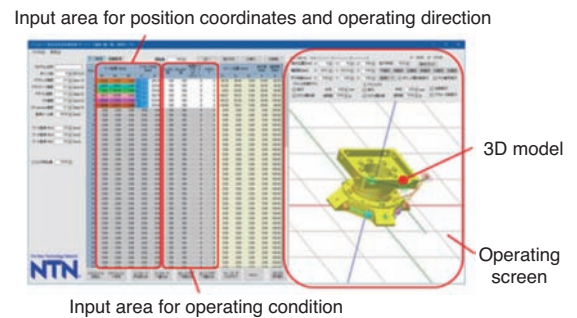
Fig. 7 Point data edit software

5.2. Other functions

As shown in **Table 4**, not only commands for each actuator position and angle can be input, but the following conditions can also be set.

(1) Operation mode

PTP (point to point) operation, which registers the point for operation to stop, and CP (continuous path), which allows continuous and synchronous movement of i-WRIST™ and other components (linear motion actuator, etc.), can be set.

(2) JOB code

The JOB code is the number (0-63) to be output to the user side controller. When JOB codes are set for each position, the user side controller can determine the operation at each point. The user can define, for example, "take a picture with camera when JOB code is '1', and do nothing when it is '2'."

(a) Base coordinate system

(b) Work coordinate system

Fig. 5 Conceptual diagram of the coordinate system

Fig. 6 Operation screen of proprietary console

Table 4 Other function

No.	Position/angle						(1) Operation mode	(2) JOB code	(3) Speed ratio
	Stage coordinates			i-WRIST™		Rz-Stage			
	Sx	Sy	Sz	θ	ϕ	Rz			
1	50	10	30	90	45	0	0	0	1
2	200	150	100	45	150	90	0	0	1
3	100	140	80	90	90	−90	0	0	1
4	150	150	100	90	180	0	0	0	1
5	50	100	90	45	45	180	0	0	1

(3) Speed ratio

This function reduces the speed of movement to the set point. For example, this can be used when vibration needs to be controlled on only a few points among many to conduct secure operation. The desired stable operation can be achieved without significant increase of overall tact time.

6. Evaluation test

In this section, we describe the basic performance test of i-WRIST™ and its results.

6.1 Repeated positioning accuracy

Fig. 8 shows the measuring device of repeated positioning accuracy.

A high-precision inclination sensor is installed on the top end of i-WRIST™ which measures inclination angles around two axes to calculate unidirectional repeated positioning accuracy from its sensor output signal.

As shown in **Fig. 9**, nine typical attitudes were defined as the measurement points of i-WRIST™ and 30 cycles of measurement were conducted. The unidirectional repeated positioning accuracy was defined as the variation $\pm 3\sigma$ around the average of these measurement results. An example of the result is shown in **Table 5**. It was revealed that the repeated positioning accuracy was within ±0.05˚, as set in the specification.
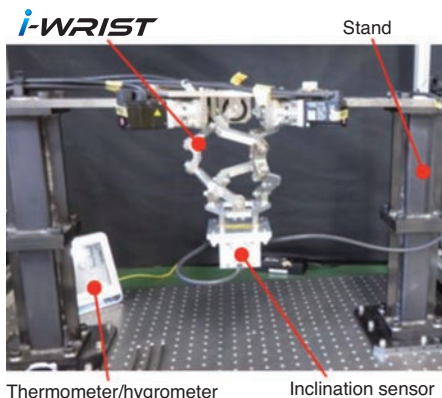
Fig. 8 Measuring device of repeated positioning accuracy
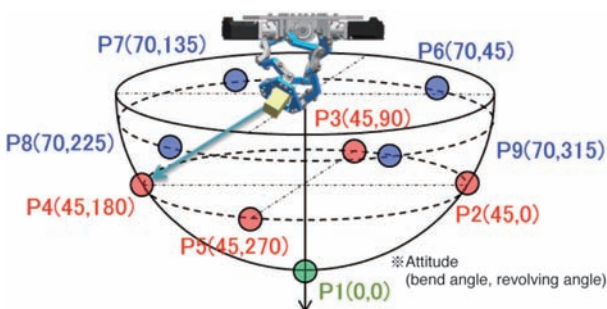
Fig. 9 Measuring posture of repeated positioning accuracy

Table 5 Measurement results of repeated positioning accuracy

Point	Repeated positioning accuracy [˚]
P1	±0.008
P2	±0.007
P3	±0.006
P4	±0.010
P5	±0.005
P6	±0.009
P7	±0.003
P8	±0.009
P9	±0.006

The measurement method and condition were based on JIS B 8432 (Manipulating Industrial Robots – Performance Criteria And Related Test Methods).

6.2 Reliability test

A continuous operation of i-WRIST™ was conducted for a target run time of 2 years (5000 hours) assuming its use in the production line of an automotive factory. As a result, the repeated positioning accuracy was still within ±0.05˚ after the continuous operation without any sign of abnormality in appearance. The continuous operation was conducted without any maintenance work, such as greasing.

7. Deployment for visual inspection application

Fig. 10 shows some of the applications where we have deployed i-WRIST™ so far. Among them, we have focused our development on the visual inspection as the demand for automated operation is rapidly increasing.

Most of the current visual inspections are conducted by workers, holding the work by hand and moving them around in various directions. **Fig. 11** shows an example of prototype visual inspection system configuration, which **NTN** created to automate this process.

In this configuration, XYA and Rz (rotational axis) stages are used to move the work and at the same time, the attitude of camera and light mounted on the i-WRIST™ are changed. Inspection directly from the side is possible because the maximum bending angle is expanded to 90˚. Also, the addition of Rz-Stage, which rotates the work, shortened the stroke of XY Stages to make the entire device more compact.

Table 6 shows the main specifications of this prototype. Although it may vary depending on the shape and size of the work and processing speed of the image processing system, the device is able to inspect 60 points of the work with $\phi 100 \times 100$ mm (height) in about 8 seconds.
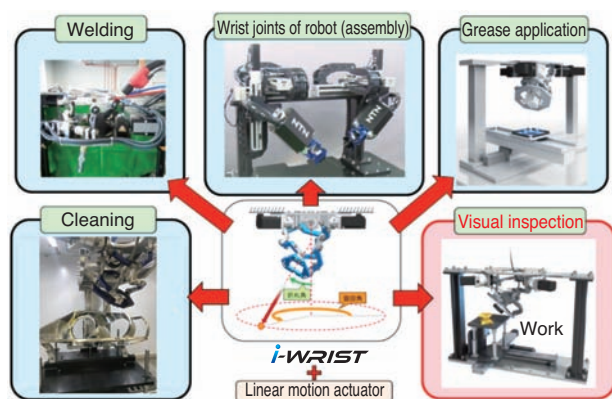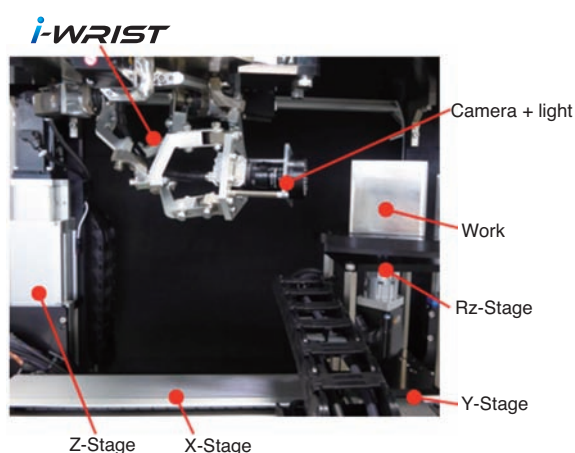
Fig. 10 Application examples of i-WRIST™

Fig. 11 Configuration example of appearance inspection equipment

Table 6 Specification of prototype model

Item	Specification
Size	W800×D850×H2000 mm
Size of the work to be inspected	ϕ Approx. ϕ100 × 100 mm (H)
Tact time (for ref. only)	Approx. 8 sec/60 points

8. Summary

Since the development of the angle control unit using the proprietary parallel link mechanism in 2012, **NTN** has been expanding its use in grease and cleaning applications, while refining the product technology. Now, we have developed i-WRIST™ for visual inspection to further take advantage of its capabilities.

As we move forward, since the labor population decreases, the demand for automating processes such as visual inspection, which have been dependent on people, is expected to grow rapidly. We are poised to continue developing robotic products to contribute to automation and manpower saving, and to further improve productivity and quality in manufacturing for the betterment of the society.

References
1) Keisuke Sone, Hiroshi Isobe, Koji Yamada, Wide Angle Active Link Equipment, NTN TECHINICAL REVIEW No. 71 (2003) 70-73.
2) Hiroshi Isobe, Yukihiro Nishio, Parallel Link High Speed Angle Control Equipment (PHACE), NTN TECHNICAL REVIEW, No. 80, (2012) 42-47.
3) Hiroshi Isobe, Yukihiro Nishio, Keisuke Sone, Hiroyuki Yamada, Yoshio Fujikawa, Parallel Link High Speed Angle Control Equipment, Proceedings of the Japan Society for Precision Engineering Spring Meeting in 2013, (2013) 809-810.
4) Hiroshi Isobe, Yukihiro Nishio, Seigo Sakata, Naoya Konagai and Hiroyuki Yamada, Parallel Link High Speed Angle Control Equipment - Implementation on Grease Application Equipment -, Proceedings of the Japan Society for Precision Engineering Spring Meeting in 2014, (2014) 1087-1088.
5) Naoya Konagai, Hiroshi Isobe, Seigo Sakata, Kenzou Nose, Hiroyuki Yamada and Yoshio Fujikawa, Parallel Link High Speed Angle Control Equipment, Proceedings of the Japan Society for Precision Engineering Spring Meeting in 2015, (2015) 605-606.
6) Kenzou Nose, Hiroshi Isobe, Seigo Sakata, Naoki Marui, Naoya Konagai: Parallel Link High Speed Angle Control Equipment - Enhancement of Performance by Improvement, Proceedings of the Japan Society for Precision Engineering Spring Meeting in 2016, (2016) 483-484.
7) Kenzou Nose, Hiroshi Isobe, Seigo Sakata, Parallel Link High Speed Angle Control Equipment, NTN TECHNICAL REVIEW, No. 84, (2016) 96-101.
8) Japan Robot Association, Need to Know This! Basic Knowledge for Utilizing Robots

Photo of authors

| Keisuke KAZUNO | Hiroshi ISOBE | Jun MIDOUMAE | Yuuki SHIMURA | Masayuki OHARA |
| Industrial Machinery Division | Industrial Machinery Division | Industrial Machinery Division | Industrial Machinery Division | Industrial Machinery Division |

Application of i-WRIST™ to the Robot Wrist Joint

Kenzou NOSE* **Seigo SAKATA***
Naoki MARUI* **Naohiko SATOU***

While the working population is decreasing, in the industrial field, robots come into use for operation of hand work by human, and to work in cooperation with human there. In such case, the robots are required to perform delicate hand work in a safe manner and at a sufficient speed.

This report introduces the application of i-WRIST™ (Parallel Link High Speed Angle Control Equipment) that has proven in a grease dispensing and external inspection to a wrist actuator of robot arm.

1. Introduction

Industrial robots have been making a significant contribution to factory automation in manufacturing by increasing productivity and production volume. In manufacturing facilities, production line efficiency has been pursued though the deployment of robots, special-purpose machinery and workers. However, due to a shortage in the labor population, the demand for automating refined manual operations, which has been traditionally difficult with conventional robots, is increasing.

NTN adopted its proprietary parallel link mechanism to develop a compact "i-WRIST™" (previously known as Parallel Link High Speed Angle Control Equipment [1)-5)]) which has a wider operating range with two degrees of freedom for fast and highly accurate angular positioning, and is actively pursuing the development of broader applications in a configuration with a linear motion actuator. In this article, we describe the application of i-WRIST™ to actuator for robot wrist joints.

2. Overview of parallel link mechanism

2.1 Basic configuration

Fig. 1 shows a conceptual diagram of the parallel link mechanism (hereafter, link mechanism) of i-WRIST™. The link mechanism takes three rows of link systems, which consist of a base-end side arm, central link and top-end side arm, (the 1st - 3rd in **Fig. 1**) placed parallel between the base-end part (which serves as

the base) and top-end part (which is used to install the end effector), making each link system joint a turning pair. The structure of this unit has pre-loaded angular contact ball bearings for the turning pair to reduce friction and to eliminate the gap in the joints.

The attitude of the top-end part is defined by the bend angle θ, which is the inclination angle between the central axis of the base-end part and central axis of the top-end part, and the revolving angle ϕ around the central axis of the top-end part looked at from the central axis of the base-end part.

The attitude of the top-end part (θ and ϕ) is determined by fixing the attitude of two base-end side arms in each link system. i-WRIST™ uses synchronous control of three motors to improve repeated positioning accuracy and rigidity.
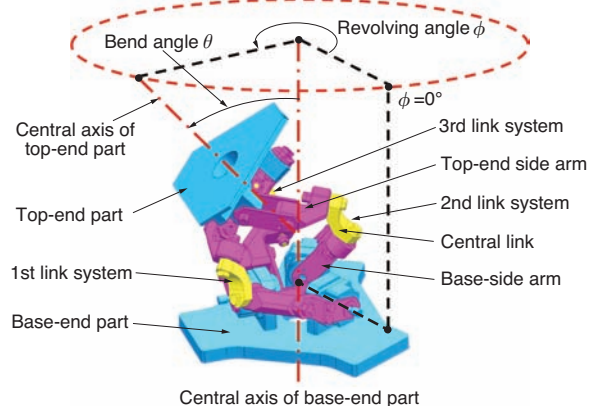

Fig. 1 Conceptual diagram of i-WRIST™ mechanism

*New Product Development R&D Center

2.2. Features

The following are the main features of the link mechanism when it is applied to actuators for robot joints.

(1) Wide operating range

It has a very wide operating range with a maximum bend angle θ of 90° and revolving angle ϕ of 360°×n (unlimited), which allows for a wide range of approaching options to the subject from different angles.

(2) High-speed/highly accurate operation

Fast and highly accurate movement, particularly for small attitude changes compared to multi-joint robots.

(3) Lightweight/compact operable parts

Positioning accuracy is improved in high speed operation by reducing weight and moment of inertia of operable parts through shifting the driving parts to the base-end side. This also makes the link mechanism more compact, which is desirable for avoiding interference of the apparatus even when the operable range is broad.

(4) No singularity in operating range

Teaching can be done relatively easily because there is no need to care for singularity.

(5) Easy handling of cables and tubes

Cables and tubes for hands and grippers to be installed at the top-end part can be run through the internal space of the link mechanism, which allows them to be easily handled. In addition, cables will not be twisted even with continuous rotation in one direction.

2.3 Comparison with other types of robots

Table 1 shows a comparison of the robot combining i-WRIST™ and linear motion actuator with general vertical multi-joint robots and parallel link robots.

Fig. 2 shows the wrist joint (3-axis of top end) of a general vertical multi-joint robot.

The vertical multi-joint robot (**Table 1B**) has advantages such as larger operating range and heavier transferable load; however, reducing the tact time for small movement is difficult because of the large movement of multiple joints that results from even a small attitude change. Since the wrist joint of the vertical multi-joint robot consists of three rotational joints(revolving axis, bend axis and rotational axis), and the revolving axis needs to be moved a greater
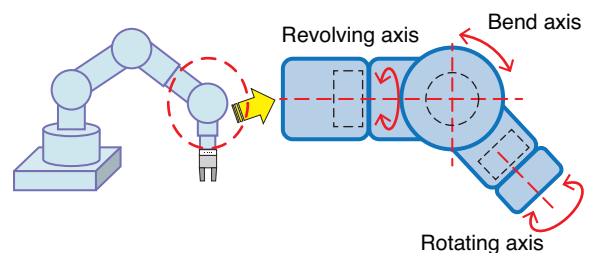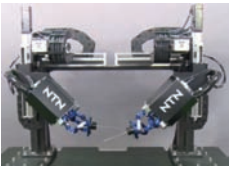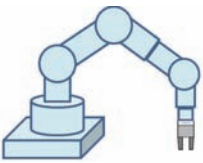

Fig. 2 Wrist joint of ordinary vertical articulated robot

Table. 1 Comparison of other type robot

Structure / Features	A **i-WRIST™** **+** **Linear motion actuator**	B **Vertical multi-joint robot**	C **Parallel link robot**
Strong area	Non-contact work, assembling of small objects	Welding, transfer	Transfer (pick and place)
Advantage	· High speed positioning with small change of attitude · No singularity in operating range · Cables can be run through link internal space (Cables not twisted even when revolving operation is repeated)	· Wide operating range · Heavier transferable load · Smaller footprint when not in use (robot arm can be folded)	· Faster parallel movement
Challenges	· Certain footprint is required even when not in use · Lighter transferable load	· Slower positioning speed with small change of attitude (depending on attitude) · Singularity in the range (special knowledge and experience needed for teaching)	· Larger equipment size relative to operating range · Certain footprint is required even when not in use

distance even for a small attitude change of the top end, smooth and quick motion is not its strong point. Therefore, it is not suitable for applications requiring fast and detailed assembling operation.

In addition, due to singularities in the operating range, operators with special knowledge and experience are required for teaching. Furthermore, robots with powerful and high-speed operation, other than collaborative robots, require fencing around the entire operational range for safety, which results in a larger required footprint.

General parallel link robots (**Table 1C**) are used mainly for pick and place applications due to their fast and parallel operation. The size of the entire equipment including driving mechanism and required footprint are large compared to the operating range.

Therefore, these robots do not usually fit in the existing space replacing workers for assembly work.

The robot proposed by **NTN** which combines the i-WRIST™ and a linear motion actuator (**Table 1A**) provides fast positioning speed and small overall movement for a small change of attitude. The i-WRIST™ is characterized by smooth and quick movement in any direction as its compact and lightweight parallel link mechanism at the top end has two degrees of freedom. Compared to the wrist joint of a vertical multi-joint robot which requires large movement of the revolving axis closer to the base for positioning, the i-WRIST™ is able to perform fast operation in all directions, which allows a shortening of tact time compared with the wrist joint of a vertical multi-joint robot. The vertical multi-joint robot's operating axes are serially configured; therefore, when the joint closer to the base (revolving axis of the wrist joint) needs to be moved a greater distance, the moment of inertia will be large preventing fast movement. On the other hand, i-WRIST™ can achieve high-speed and smooth movement because the moment of inertia is reduced by the compact parallel link mechanism. In addition, as the required space for installation is relatively small, it is considered to be a good fit for automating the process previously operated by workers.

3. Deployment for robot wrist joints

3.1 Actuator for wrist joints

We have made a prototype actuator (hereafter, actuator) for the robot wrist joint [6]. **Table 2** shows the main specifications of this prototype.

The actuator shown in **Fig. 3** is made by reducing the size of i-WRIST™ in the radial direction for lighter weight and adding one degree of freedom for rotating the overall i-WRIST™. A concentric reducing mechanism is used for the rotating mechanism for rotating the overall i-WRIST™, so it is called the gear-drive type (hereafter, GD type).

In addition, the maximum bend angle of the link mechanism is 90°. Together with the revolving angle ϕ of the i-WRIST™ and rotating angle θz of the rotating mechanism, the rotation of the rotating mechanism can be converted to rotation around the rotating angle of the top-end part, equiangularly, in any bend angle.

Fig. 4 shows the structure of the revolving pairs serving as connections between the base end part and base end arm. The base end arm is connected to the output axis of the reducer unit installed on the base
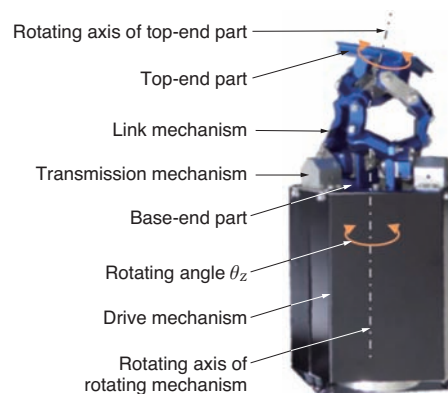

Rotating axis of top-end part
Top-end part
Link mechanism
Transmission mechanism
Base-end part
Rotating angle θz
Drive mechanism
Rotating axis of rotating mechanism

Fig. 3 Wrist joint actuator featurung i-WRIST™ (with gear drive)

Table. 2 Specification of wrist joint actuator with GD

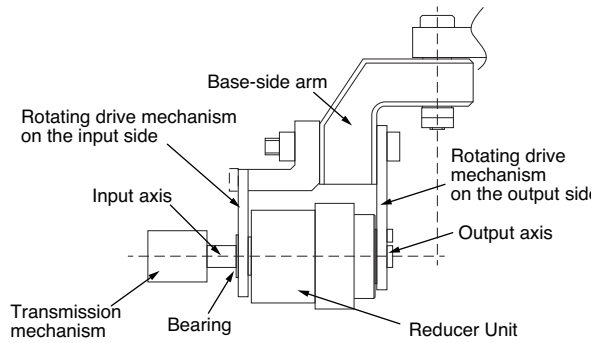| Item	Specification
Size (outer diameter×height)	ϕ145×278 mm (overall) ϕ102×115 mm (link)
Weight	3 kg
Degree of freedom	3
Operating angle range	Bend angle: 90° Revolving angle: 360°×n (unlimited) Rotating angle: 360° (-175° to 175°)
Repeated positioning accuracy	±0.05° or less
Transferable load (weight)	0.5 kg
Motor output	30 W×3 (link) 50 W×1 (rotating mechanism)

Fig. 4 Revolute pairs serving as connections between proximal end side link hubs and proximal end link member

Fig. 5 Wrist joint actuator with belt drive

end part through the output side rotation drive. The rotation of the attitude control motor transmitted to the input axis of the reducer unit through the transmitter mechanism, such as gears and belts, is reduced by the reducer unit and transmitted to the base end arm through the rotation drive of the output side. The input rotation drive fixed on the base end arm is rotatably connected to the input axis of the reducer unit through the bearings. As such, the actuator a compact configuration while improving the supportive rigidity of the base end arm by incorporating the reducer unit within the base end arm structure which supports both ends of the rotational axis of the base end arm. In addition, the impact of backlash within the transmission mechanism can be reduced by placing the transmission mechanism on the input side of the reducer unit.

The GD type rotating mechanism has an advantage in placing the reducing mechanism of high reduction in compact configuration. However, since the motor for controlling angular rotation is positioned so that the rotating axis of the rotating mechanism is concentric with the central axis of the base end part, the drive mechanism does not have internal space. Therefore, the benefit of running the cables and tubes through the internal space of the link mechanism is not attainable.

On the other hand, the BD type, which uses a belt drive, places the motor of the rotating mechanism through the belt offset from the center of the rotating mechanism and therefore, can provide a large internal space. **Fig. 5** shows the structure of the BD type. The BD type uses the belt for the link mechanism, as well, which allows the motor for attitude control to be positioned offset in parallel to the input axis of the reducer unit so that the height of the link mechanism is reduced. In addition, the ability of running cables for the motor for attitude control of the link mechanism through the internal space of the drive mechanism makes cabling work very easy and broadens the operating range of the rotation angle.
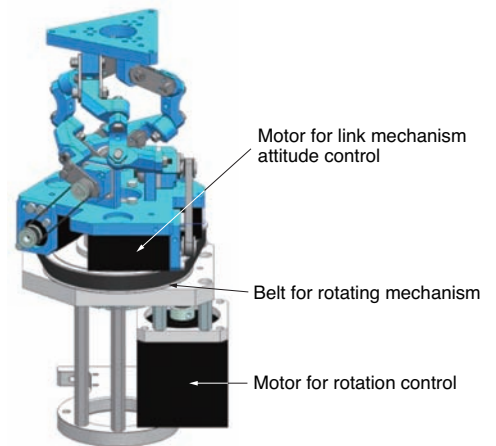
3.2 Linear motion dual-arm robot

Fig. 6 shows a linear motion dual-arm robot, which is configured with two sets of the combination of this actuator and a linear motion actuator with orthogonal axes (XYZ stage). In order to automate the existing manual work, the actuators are inclined at 45° toward center relative to vertical axis (Z axis) to facilitate collaborative work of the two arms. This linear motion dual-arm robot controls the attitude and position of the end effector with this actuator and the XYZ stage, respectively. It is able to perform various works by operating XYZ movement maintaining the attitude (asynchronous operation), and through synchronous movement of this actuator and the XYZ stage (synchronous operation).

The asynchronous operation allows for the approach attitude to be determined by controlling the attitude of the grabbed work with this actuator, then transfer it horizontally with the XYZ stage, which is
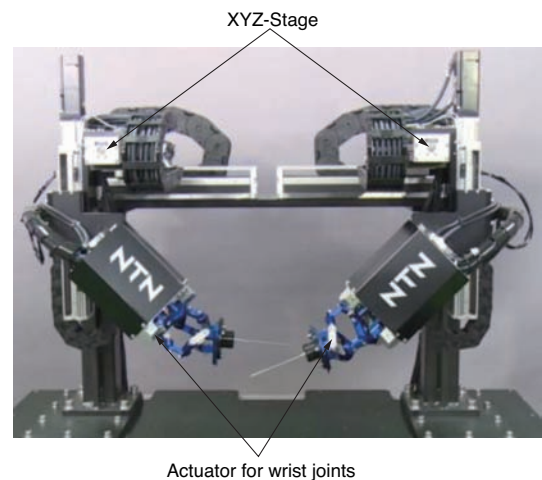

Fig. 6 Liner motion type dual arm robot featuring i-WRIST™

easily predictable by the operator when teaching. Therefore, it is suitable for assembly work. **Fig. 7** shows operation of insertion/removal of shaft. The operation consists of insertion and removal of the shafts through holes in different angles, which is performed by determining the attitude of shafts toward the holes by this actuator and inserting/removing the shafts in linear motion with the XYZ stage.

The synchronous operation facilitates refined motion of the top end of the end effector. **Fig. 8** shows placing of seals on a curved surface and **Fig. 9** shows attaching/removal of O-rings, as some examples of the applications. In these examples, 3D tracing motion on a curved or plane surface, which has been difficult to automate, is achieved by the coordinated trajectory control with this actuator and the XYZ stage, in a combination of the parallel link mechanism and linear motion actuator.

As shown in these examples, **NTN** is currently pursuing application of i-WRIST™ to robot wrist joints for use in assembly tasks.

O-ring

Fig. 9 Operation for installing and removing O-ring

4. Conclusion

We have made a an actuator prototype for a robot wrist joint based on the proprietary parallel link of two degrees of freedom with addition of one rotational degree of freedom, which achieves shape and motion close to the human wrist joint. In addition, we have built a prototype of a linear motion dual-arm robot that combines this actuator and a 3-axis linear actuator and are pursuing the development of robots which can achieve refined manual work by taking advantage of the smooth and fast operation unique to the i-WRIST™, verifying differences from vertical multi-joint robots and parallel link robots.

As we move forward, we will explore further downsizing this actuator and the entire system and pursue collaborative work with human workers by adding features such as a collision detection function. We are poised to contribute to the evolution of automation/robotics in manufacturing, to enable replacement of manual work, such as assembly of small parts, which has been difficult with conventional robots.

Hand (air chuck)

Work (shaft)

Work (hole)

Fig. 7 Operation for inserting and removing shaft

Curved surface
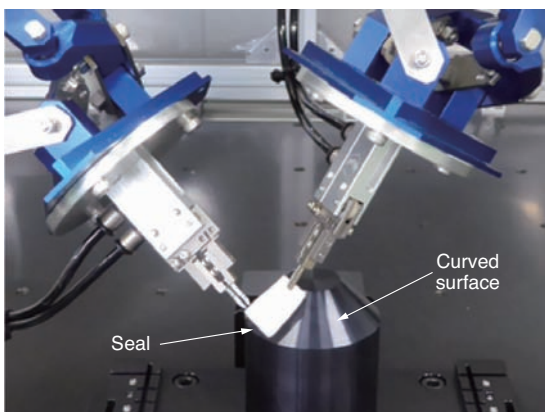
Seal

Fig. 8 Operation for put a seal on a curved surface

References

1) Hiroshi Isobe, Yukihiro Nishio, Parallel Link High Speed Angle Control Equipment (PHACE), NTN TECHNICAL REVIEW, No. 80, (1988) 42-47.

2) Hiroshi Isobe, Yukihiro Nishio, Keisuke Sone, Hiroyuki Yamada, Yoshio Fujikawa: Parallel Link High Speed Angle Control Equipment, Proceedings of the Japan Society for Precision Engineering Spring Meeting in 2013, (2013), 809-81.

3) Hiroshi Isobe, Yukihiro Nishio, Seigo Sakata, Naoya Konagai and Hiroyuki Yamada, Parallel Link High Speed Angle Control Equipment - Implementation on Grease Application Equipment - , Proceedings of the Japan Society for Precision Engineering Spring Meeting in 2014, (2014) 1087-1088.

4) Naoya Konagai, Hiroshi Isobe, Seigo Sakata, Kenzou Nose, Hiroyuki Yamada and Yoshio Fujikawa, Parallel Link High Speed Angle Control Equipment, Proceedings of the Japan Society for Precision Engineering Spring Meeting in 2015, (2015) 605-606.

5) Kenzou Nose, Hiroshi Isobe, Seigo Sakata, Naoki Marui, Naoya Konagai: Parallel Link High Speed Angle Control Equipment - Enhancement of Performance by Improvement, Proceedings of the Japan Society for Precision Engineering Spring Meeting in 2016, (2016) 483-484.

6) Kenzou Nose, Hiroshi Isobe, Seigo Sakata, Naoki Marui, Yuuki Shimura: Parallel Link High Speed Angle Control Equipment - Application to Wrist Joint Actuator for Robots, Proceedings of the Japan Society for Precision Engineering Spring Meeting in 2017, (2017) 761-762.

Photo of authors

Kenzou NOSE
New Product Development
R&D Center

Seigo SAKATA
New Product Development
R&D Center

Naoki MARUI
New Product Development
R&D Center

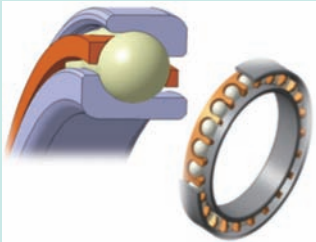**Naohiko Satou**
New Product Development
R&D Center

[Technical Article]

Technical Trend and Features of the Bearing for Robot

Makoto OEBISU*   **Hiromichi KOKUMAI***

Yasuyoshi HAYASHI*   **Masato TSUJIHASHI***

Recently, the robotics market has become very active, and demand is expanding each and every day.
Various types of mechanical equipment, such as reduction gears, are incorporated into robotics, and many bearings are used. **NTN** manufactures a wide variety of bearings for robotics applications, and in this section, the features of bearings used for robotics will be explained based on the technical trends in the industry.

1. Introduction

Robots can be broadly classified into industrial robots, field robots and service robots (**Fig. 1**).

Industrial robots are used in many manufacturing factories including automobiles and electrical equipment with demand in relatively simple and repetitive tasks; however, the demand is shifting to a more advanced and automated production process. Japan has a competitive edge in industrial robots and is expected to advance development leveraging its strength. Field robots are engaged in outdoor activities such as on farmland, in the sea and at disaster sites; therefore, robots which perform well at such sites are expected to be developed. Service robots are used in an environment where interaction with people is required, such as at home, at the workplace, and in

activities including welfare, healthcare and nursing care. Recently, it is expected that these robots will be rapidly introduced and used in a broader area to increase productivity in the service industry, secure workforce for healthcare/nursing care services, etc.

Robotics is an area that will be adopted globally, as the machines perform tasks in place of human workers, where future growth is highly expected. **NTN** produces many bearings for robots. In this article, we describe the technical trend of bearings for industrial robots, in particular, their application area and features.

2. Market needs of industrial robot

Industrial robots are required to have not only basic features such as to grab objects at a predetermined position and accurately work on them, but also (1) superior cost performance, (2) accuracy and performance suitable for the required work, easy teaching and correction (accuracy and operability), (3) small and light bodies with small footprints (compact form factor), and (4) contribution for high availability of production line (reliability and maintainability), in order to be broadly deployed in various industrial fields.

In the industry, the demand for automation by adoption of robots is recently increasing in order to deal with the labor shortage in the production lines and to realize stable product quality. The demand for robots in assembly and transfer processes is increasing, for example, from the capital investment in electronics industry due to growing demand of smart
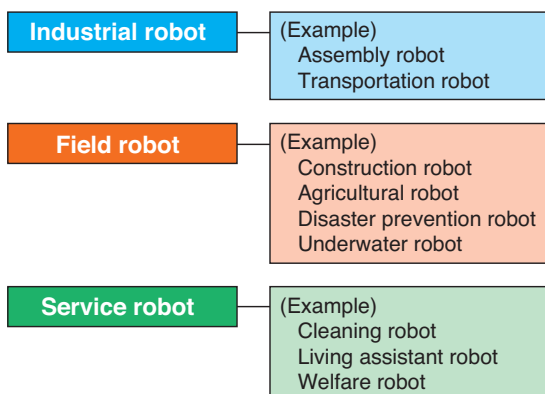
Industrial robot	(Example) Assembly robot Transportation robot
Field robot	(Example) Construction robot Agricultural robot Disaster prevention robot Underwater robot
Service robot	(Example) Cleaning robot Living assistant robot Welfare robot

Fig. 1 Classification of robot

---

*Application Engineering Dept., Industrial Machinery Division

phones, automotive related industry and IoT (Internet of Things). In addition, the demand for collaborative robots which work with human workers, is also a growing trend and expands the market size for industrial robots. Based on these trends, the requirements for industrial robots such as (1) increase of productivity by reducing tact time, (2) refined workability with improved positioning accuracy and repeatability during work transfers by increasing rigidity of robots, (3) securing work space by reducing the size and footprint of robots and (4) improved maintainability by increasing maintenance intervals, are increasing as the market needs. **Table 1** shows the market trend of the recent performance requirements for industrial robots.

Industrial robots are equipped with reducers and gas balancers where bearings are used in moving parts. Based on the aforementioned trends, bearings are required to be smaller in size and higher in rigidity with high-load capacity and long operating life.

Table. 1 Market trend of industrial robot

Required performance	Recent market needs
Cost performance (robot productivity)	· Reduction of tact time
High accuracy and operability (precise work)	· High positioning accuracy · Increased repeatability
Space saving (securing work space)	· Compactness
High reliability and maintainability	· Longer maintenance intervals

3. Structure of industrial robots and areas bearings are used

3.1. Structure of industrial robots

The typical industrial robot is the vertical multi-joint robot which moves like a human from the shoulder to the wrist, among many types (**Fig. 2**).

When a robot is operated with heavy objects, each joint drive requires large torque; therefore, reducers are used to amplify output torque of servomotors. A large robot, in particular, is equipped with balancers which produce balance power against the gravity load to complement servomotor power and contribute to energy saving.

3.2. Reducers for industrial robot and areas bearings are used

As robots of different sizes are emerging in recent years, large and small reducers are used accordingly. In this article, we describe (1) eccentric differential
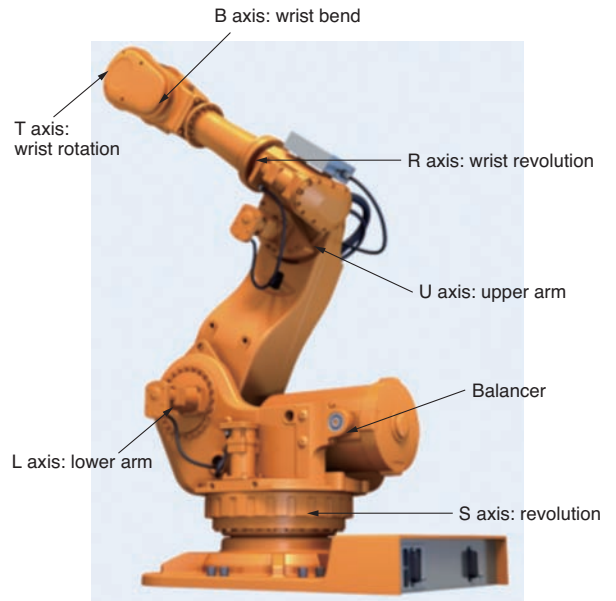

Fig. 2 6 axis articulated robot

reducer for large robots and (2) strain wave gearing reducer for small robots as examples of applications where bearings are used.

(1) Eccentric differential reducer

An example of eccentric differential reducers is Nabtesco Corporation's precision reduction gears RV. **Fig. 3** shows the structure of the precision reduction gears RV. This reducer consists of the 1st stage reducer made of a spur gear and the 2nd stage eccentric oscillating reducer with a pin gear mechanism. When the crankshaft rotates, the RV gear moves eccentrically. It rotates in the opposite direction of the input rotation by the difference of number of gears with the internal gear, which is taken out as the output. This mechanism is lightweight and has high rigidity with high tolerance to overload due to the high number of simultaneously engaged gears which also provides low backlash and low vibration with smooth and accurate torque transmission.

This reducer is equipped with needle roller bearings in the eccentric portion of the crankshaft and tapered roller bearings in the journal portion. Each bearing is required to have high rigidity and high load carrying capacity. For the main bearings, thin section type angular contact ball bearings are used in pairs which are required to have high rigidity (moment rigidity) in order to ensure positioning accuracy, which is an important property of a robot.
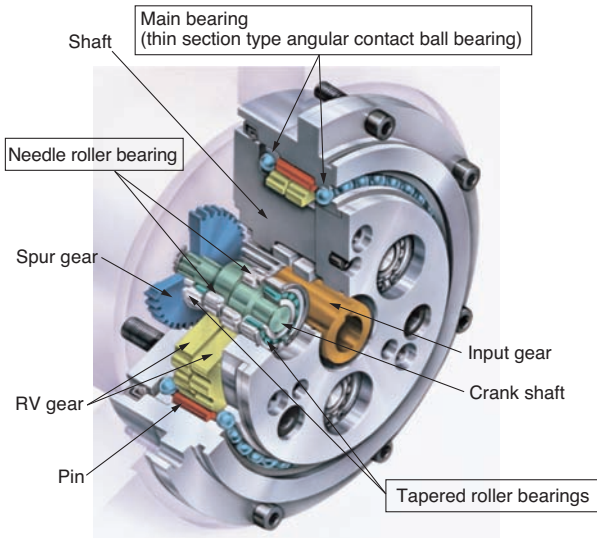
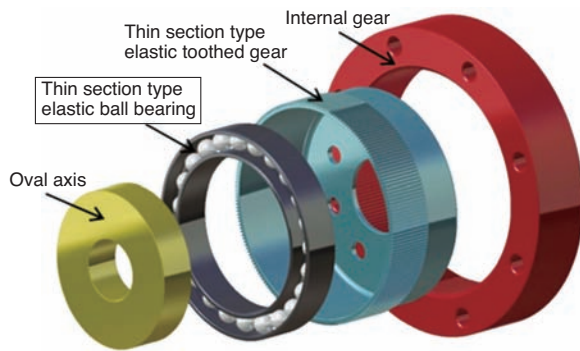**Fig. 3** Structure of precision reduction gears RV [1]

Fig. 4 Structure of strain wave gearing

Fig. 5 Operating principle

(2) Strain wave gearing reducer

The strain wave gearing reducer is mainly used as the small reducer mechanism (outer diameter of 100 mm or less). **Fig. 4** shows the schematic diagram of its structure. It consists of a thin section type elastic toothed gear made of a thin, elastic metal ring with gear cutting, it incorporates an oval shaft where thin, elastic ball bearings are inserted and the elastic toothed gear is in contact with the thick, rigid internal gear at the major axis. This provides a unique reducing mechanism cleverly utilizing the elastic deformation. The operating principle is shown in **Fig. 5**. If the internal gear is fixed while the oval shaft rotates clockwise once, the thin section type elastic gear rotates counterclockwise by the difference of the number of gears between the thin section type elastic gear and the internal gear (e.g. thin section type elastic gear has two teeth less) which is extracted as the output. **Fig. 5** shows the status where the oval shaft rotated half circle and the thin section type elastic gear moved counterclockwise by one tooth. This reducer has concentric and simple structure with compact form factor and provides a significant reduction ratio of 1/30 to 1/320. Since both teeth are simultaneously engaged like wedges, providing great contact ratio without backlash, the reducer is characterized by averaged gear errors, high angle transmission accuracy, and large torque capacity.

Stress amplitude of tension and compression is repeatedly applied to the outer ring's outer diameter surface of the thin section type elastic ball bearing, while internally engaging reaction force due to torque transmission is applied in addition to preload due to deformation of the oval part. It is important to provide
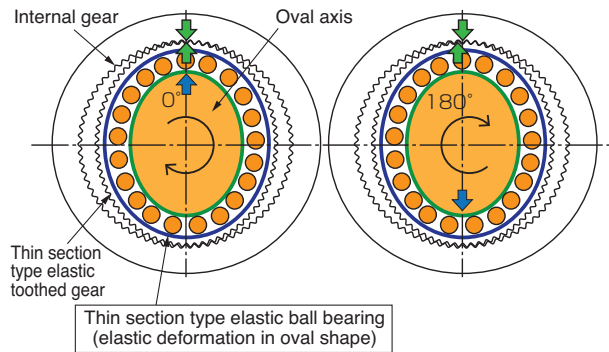
both fatigue strength against cracking of outer ring and rolling contact fatigue life when designing thin section type ball bearings. Furthermore, consideration is required for the angled shape, surface roughness, residual stress of the surface, etc. in addition to selecting the optimum thickness and thermal treatment specification so that the raceway can tolerate high stress amplitude.

3.3. Balancer for industrial robots and areas bearings are used

Fig. 6 shows an example of the balancer structure for robots. This device is applied to complement the power of the servo motor when the robot arm is extended and contracted for energy saving. Recently, the balancer has moved from coil type to gas type for compactness and high load capacity. In addition, longer maintenance interval is required for high availability.

Self-aligning roller bearings may be used for the rod cylinder support area of this balancer, considering ease of incorporation. For this purpose, it is necessary to select bearings considering abnormal wear and fretting damage, in addition to large load carrying capacity, as it is difficult to form an oil film because of large load and small oscillating angle.
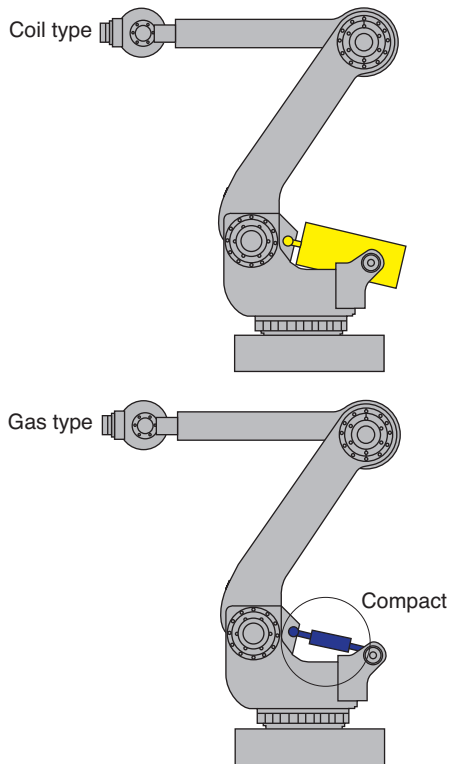
Fig. 6 Structure of balancer

4. Technical trends and characteristics of the bearings for industrial robots

4.1. Technical trends of the bearings for industrial robots

As mentioned above, the main use of the bearings for industrial robots is for reducers and balancers. These bearings are required to have "compactness," "high rigidity," "high load carrying capacity" and "long life." Particularly, compactness of bearings is important; however, that means downsizing of rolling elements due to reduction of cross section, which translates into reduction of rigidity, load carrying capacity and operating life. Namely, the compactness and high rigidity, high load carrying capacity and long operating life are in a trade-off relation, so it is important for bearings to achieve compactness without reduction of rigidity, load carrying capacity, and operating life. **Table 2** shows the requirements for bearings for industrial robots.

For reducers of robots, while high rigidity, high output torque and high efficiency are required, compactness tends to be required, as well. Angular contact ball bearings for main shafts are required to maintain rigidity and long life, while thin section type is also required. The needle roller bearings for crankshafts are required to pursue space saving within their type, as well as high rigidity and high load

carrying capacity. Balancers for robots are required to have high reliability in addition to compactness, while self-aligning roller bearings for rod cylinder support are required to have long life. **NTN** is conducting R&D for various bearings following the recent technology trend to meet the market demand.

Table. 2 Required performance of bearing for industrial robot

Areas where bearings are applied		Required performance
Reducer for robot	Main shaft	・Compact (thin section type) ・High rigidity ・Long life
	Crank shaft	・Compact (space saving) ・High rigidity ・High-load capacity ・Long life
Balancer for robots (rod cylinder support)		・High-load capacity ・Long life

4.2 Compact angular contact ball bearings

NTN designs, manufactures and promotes compact thin section type angular contact ball bearings for main shafts of precision reduction gears.

Fig. 7 shows a comparison of cross section with the 79-Series standard type (the outer diameter of the bearings is uniformly designed). The thin section type angular contact ball bearings achieved approx. 30% reduction on the radial direction , approx. 25% reduction on the axial direction in size and approx. 55% reduction of weight.

For this reduction, thinning of the raceway is indispensable; however, the resulting deformation of the raceway (distortion and curve) becomes a challenge. **NTN** achieved volume production of thin section type angular contact ball bearings by establishing machining technology including optimization of thermal processing conditions for controlling deformation (**Fig. 8**).
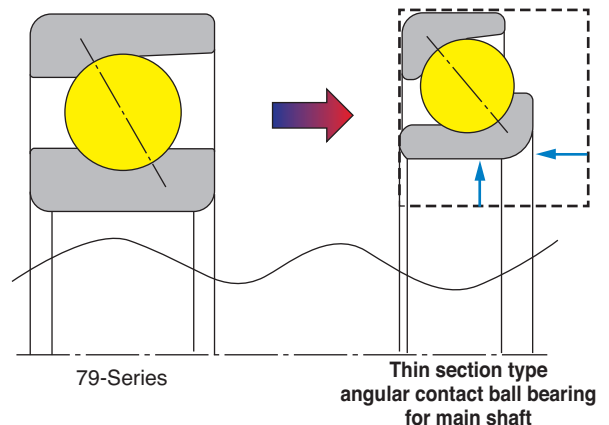

79-Series

Thin section type angular contact ball bearing for main shaft

Fig. 7 Cross-view comparison of Ultra thin angular contact ball bearing

Fig. 8 Ultra thin angular contact ball bearing

With regard to rigidity (moment rigidity) and operating life (rolling fatigue life) which are in a trade-off relation with reduction, optimal design technology has been established by increasing the distance to the action point of bearings in order to increase the moment rigidity and reducing the contact stress inside bearings to avoid reduction of operating life. **Fig. 9** shows the relation between the moment rigidity ratio and operating life ratio against the preload ratio. It reveals that the rolling fatigue life of the thin section type angular contact ball bearings is equivalent to the 79-Series standard type and the moment rigidity is increased by approx. 40% even if they are smaller in size compared to the 79-Series standard type.
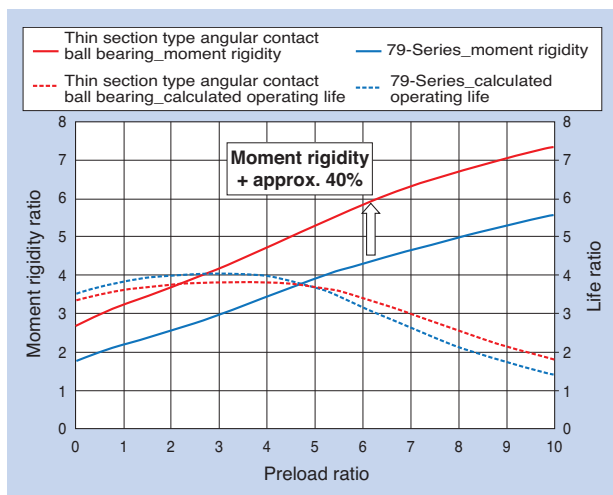
Fig. 9 Moment stiffness and lifetime ratio at loading preload

4.3 High rigidity and high-load capacity of needle roller bearings

NTN is deploying high-rigidity and high-load capacity needle roller bearings (HWT (J) Type) in the market for cranks of precision reducers.

Table 3 shows a comparison between HWT (J) Type and standard type (PK Type). The major feature of the HWT (J) Type is that it enabled increasing number of rollers compared with the PK Type, by eliminating the columns on the inner diameter side of the cage, to achieve high rigidity, high-load capacity and long operating life (**Table 4**).

Furthermore, the roller surface is carbonitrided, strengthening tolerance against damage to the surface due to foreign objects penetrated into lubricating oil or oil film shortage on the raceway, contributing to improvement in reliability and bearing operating life.

Table. 3 High load capacity needle roller bearing

Standard type	High-load capacity type	
PK Type (Machined cage)	HWT Type (Machined cage)	HWTJ Type (Pressed cage)
Limited number of rollers due to columns on the inner diameter side	More rollers can be placed as there are no columns on the inner diameter side	

Table. 4 Comparison of performance for PK type [2]

Item	Comparison
Number of rollers	＋20-30%
Basic static load rating	＋20-35%
Basic dynamic load rating	＋15-25%
Rolling fatigue life	×1.5-2
Rigidity	＋15-25%

4.4 Long operating life for self-aligning roller bearing

NTN deploys "ULTAGE" Series "EA Type" as the self-aligning roller bearings for rod cylinder support of robot balancers in the market.

The "EA Type" has improved the load carrying capacity (basic dynamic load capacity) by max. 65% (**Fig. 10**), achieving top level performance (**Fig. 11**).

In addition, the "ULTAGE" Series features sealed type (WA Type) with seals on both sides (**Fig. 12**) in its line-up, as well, which allows enclosing special grease with superior wear resistance and fretting resistance, contributing to improvement of maintainability and bearing life.
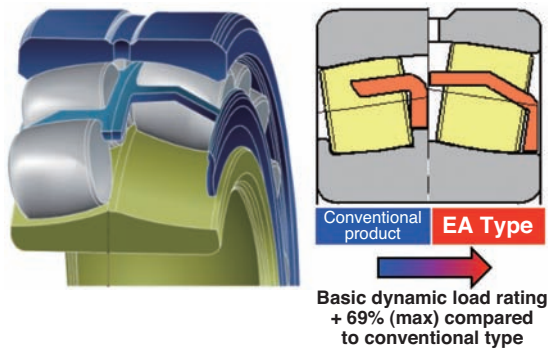
Conventional product / EA Type

Basic dynamic load rating
+ 69% (max) compared
to conventional type

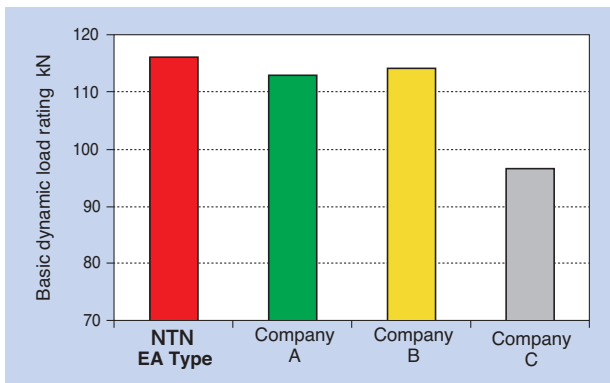Fig. 10 ULTAGE Spherical roller bearing (Type EA) [3]
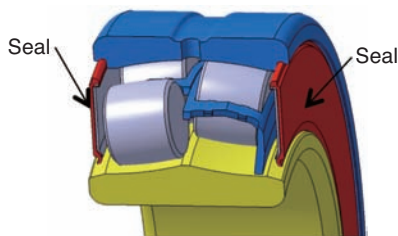

Fig. 11 Comparison of load capacity

Fig. 12 ULTAGE Spherical roller bearing [4]

5. Summary

NTN produces many bearings for robots. In this article, we described the technical trends and features of bearings for industrial robots.

It is expected that the robot demand will grow along with rapid development of the service fields, and robots are expected to work closely with humans.

NTN is poised to continue contributing to the development of robots by product development and improvement of bearings for robots.

References
1) Naptesco Corporation, Nabtesco Catalogue, Precision Reducer RV CAT 180420, (2018) Cover
2) Katsufumi Abe, New High-Capacity HWTJ Type Pressed Cage and Needle Roller Assemblies, NTN TECHNICAL REVIEW, No.71, (2003) 52-55.
3) Yukihisa Tsumori, New Spherical Roller Bearings "ULTAGE" Series Type EA and EM, NTN TECHNICAL REVIEW, No.77, (2009) 78-82.
4) NTN Corp. Sealed Self-Aligning Roller Bearing (ULTAGE WA Type), NTN TECHNICAL REVIEW, No.79, (2011) 138.

Photo of authors

Makoto OEBISU

Industrial Machinery Division
Application Engineering Dept.

Hiromichi KOKUMAI

Industrial Machinery Division
Application Engineering Dept.

Yasuyoshi HAYASHI

Industrial Machinery Division
Application Engineering Dept.

Masato TSUJIHASHI

Industrial Machinery Division
Application Engineering Dept.

Application of Condition Monitoring System for wind turbines

Makoto MIYAZAKI*
Wataru HATAKEYAMA*

NTN has developed Condition Monitoring System using sensing technology and vibration diagnosis technology, and provides information services dedicated to the maintenance of wind turbines. This article introduces some of the diagnostic methods used in the CMS and results obtained in validation tests, and gives a perspective of CMS for wind turbines.

1. Introduction

1.1. Background

According to the report from Global Wind Energy Council (GWEC2017) [1], the installed capacity of wind turbines in 2017 was 529.1 GW, an increase of 10.6% from the previous year and it is expected that the trend will continue in the coming years. There are fewer places onshore appropriate for wind turbines; therefore, development of higher efficiency wind turbines suitable for areas of low wind speed and offshore wind turbines are accelerated. In addition, selling price of electric power continues to decrease as the deployment of the wind turbine business expands, which dictates further reduction of maintenance cost and increase of availability of wind turbine facilities. Therefore, advanced maintenance with constant monitoring of facility conditions and operation to prevent prolonged shutdown due to failures are required.

1.2 Overview of CMS

The conventional, periodic measurement of vibration and abnormal noise, and analysis of grease and lubricating oil have been conducted as condition monitoring of wind turbines. However, from safety concerns, it is difficult to check for vibration and abnormal noise during operation, as it is not possible to work on the equipment during operation. Therefore, inspection is mainly conducted during outage, which may delay the detection of symptoms of failure. When unscheduled repair becomes necessary, repair parts may not be readily available for outages causing prolonged shutdown resulting in lost revenue.

By monitoring measurement data from sensors installed in the equipment in operation, it will be easier to detect symptoms of failures. Therefore, a condition monitoring system (CMS) which aims for online condition monitoring and diagnosis from the measurement data sent from the sensors is required. By using CMS, the condition monitoring can be conducted remotely to save maintenance costs. In addition, time for taking precautionary measures can be secured by detecting failed parts early, resulting in improved availability. Furthermore, by detecting early warning signs, scheduled maintenance can be conducted at an optimum time, for efficient equipment operation without significant loss of power.

NTN developed CMS taking advantage of the accumulated sensing and vibration diagnosis technology and marketing it under the name of Wind Doctor ™ (**Fig. 1**) [2], [3].

In this article, we describe the data analysis method using Wind Doctor ™ and some examples of its application.

Fig. 1 Data acquisition module [2] [3]

---

*Robotics Sensing Engineering, Industrial Machinery Division

2. Configuration of CMS and analysis method

2.1. System configuration

Fig. 2 shows the system configuration of Wind Doctor [TM 4)]. The data collection system periodically measures the equipment using the sensors installed on the measured equipment and saves the measured data to the server on the Internet. Various sensors such as for vibration, displacement and temperature, can be used as the measurement sensor. The data management software manages the measured data in the database on the server and issues an alert when an anomaly is detected. The condition monitoring software is a graphical user interface (GUI) containing a communication function with the server. It not only provides ability to visually inspect the monitored equipment but also analysis of the measured data through filtering, envelope processing, and frequency analysis, etc.

2.2 Monitoring/analysis method

In order to monitor changes and trends in equipment, it is desirable to measure the data while the equipment is running. However, for wind turbines which deal with nature, the operating environment such as wind speed and direction constantly change. Wind Doctor [TM] records the operating conditions together with sensor signals to reduce the impact of different operating conditions, extracting measured data under similar conditions and using them for diagnosis of the equipment status [4)].

When an abnormal condition is determined by diagnosis, frequency analysis of vibration data is conducted to estimate the cause of the abnormal condition. However, when the rotating speed around the axis drastically changes due to change of wind speed and direction, the accuracy of frequency analysis will decrease and cause of the abnormal condition may not be easily estimated. The analysis tool of the Wind Doctor [TM] condition monitoring software includes a function to correct the variation of the rotational speed around the axis in order to prevent deterioration of the analysis accuracy. **Fig. 3** shows the frequency spectrum before and after the correction. The frequency spectrum after the correction **(b)** has much clearer peaks compared to that of the frequency spectrum before the correction **(a)**, enabling more accurate analysis.
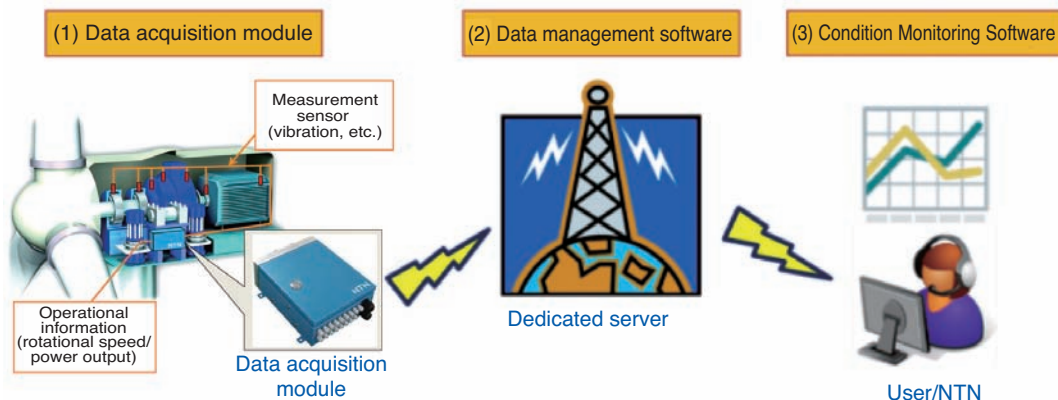

Fig. 2 System configuration of Wind Doctor [TM 4)]

(a) Frequency spectrum before correction

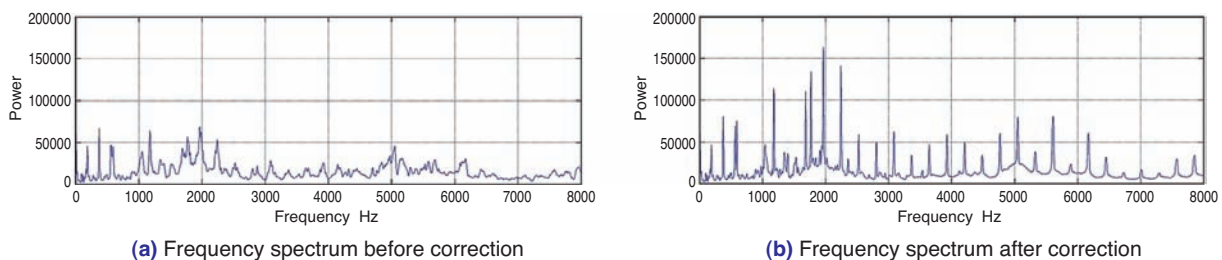**(b)** Frequency spectrum after correction

Fig. 3 Frequency spectrum. (a) Raw data, (b) Corrected data

3. Examples of recent applications

NTN has been participating in Research and Development of High Level Application of Wind Turbine Technology (Research and Development of Smart Maintenance Technology) conducted by NEDO (New Energy and Industrial Technology Development Organization) together with the University of Tokyo, etc. conducting demonstration tests on how to use CMS in the maintenance of wind turbines throughout Japan by installing Wind Doctor ™, in order to increase availability of wind turbines in Japan. The following shows some examples of the measured data.

3.1 Case study of damage on the generator bearing

Fig. 4 shows the data acquired from the vibration sensor installed on the generator drive shaft. The horizontal axis of the graph indicates dates and the vertical axis indicates vibration RMS values, which show the level of vibration. The graph was made by extracting measured data while the wind turbine was operating at 85% or more of the rated rotational speed.

The vibration RMS value started to increase a month before the measurement point A and exceeded the caution threshold at the point A. **Fig. 5** shows the envelope spectrum of the measured data at point A. The envelope spectrum is the result of frequency

analysis of the envelope curve of the filtered vibration waveform, and used for analyzing vibration components due to damage. In the envelope spectrum at the point A, we could observe the peak of the rolling element damage frequency ($2 fb$), which is the frequency of the contact of a point of the rolling element with the inner and outer ring, and the sideband at both sides of the peak, which is the modulated component of the rolling element rotation frequency ($2 fb \pm fc$). From this property, it was estimated that there was a damage to the rolling element of the bearing and the generator vibration increased due to that damage.

In the envelope spectrum at the point B (**Fig. 6**), which is the point where the vibration further increased from the point A, we could observe the peaks of inner ring damage frequency (fi) and outer ring damage frequency (fo) in addition to the rolling element damage frequency ($2 fb$). Therefore, it was estimated that the damage progressed to the raceways of the inner and outer ring in addition to the rolling element.

At point B, the facility verified the equipment status and recognized that abnormal noise occurred. The facility replaced the bearing and investigated the removed bearing by disassembling it. Damage due to stray current corrosion was observed on the raceways of the inner and outer rings of the bearing (**Fig. 7**) [5].
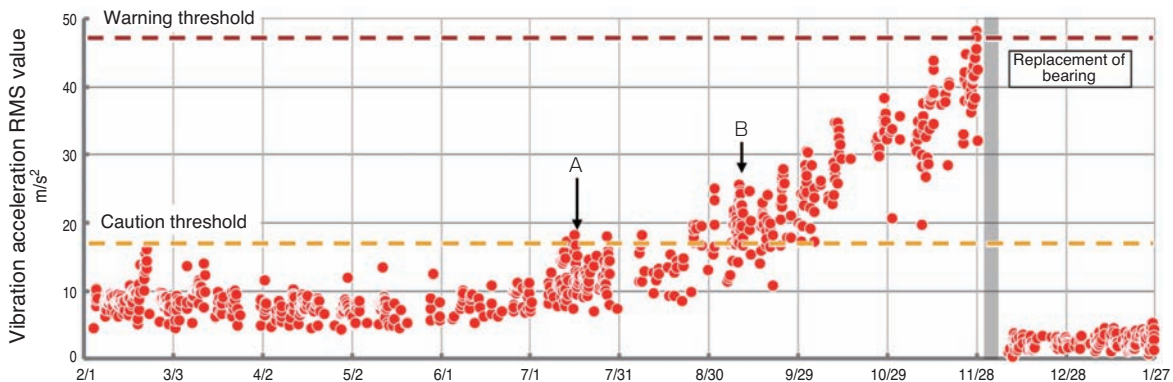

Fig. 4 Trend graph of RMS value at generator drive end
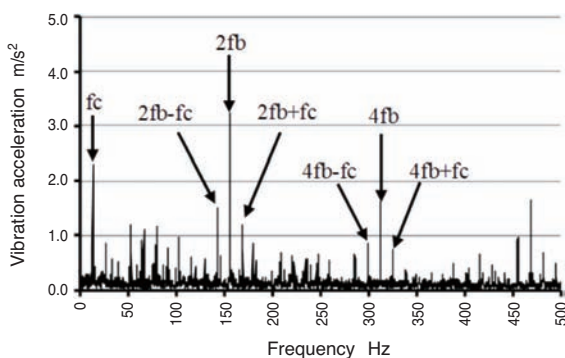
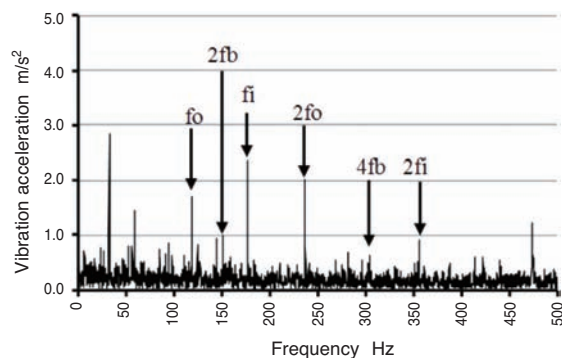

Fig. 5 Envelope spectrum at A
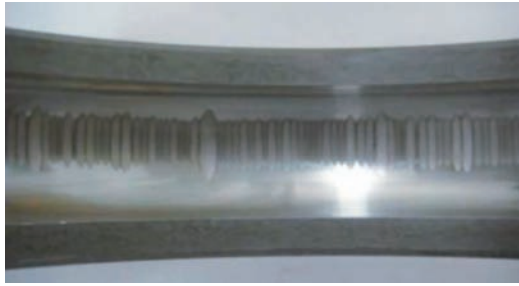

Fig. 6 Envelope spectrum at B

Fig. 7 Outer raceway failure of electrical pitting [5]

In this case, use of the CMS could detect the symptom of the failure 2 months before the facility recognized the anomaly at the site. Therefore, when the facility received the report, it could prepare for the replacement of the bearing with ample time before the winter season started when the strong wind was expected, and avoided outage during the most desirable time of power generation.

3.2 Case study of damage on the gearbox bearing

Fig. 8 shows the trend graph of RMS values obtained from the vibration sensor installed on the gearbox planetary. The graph was made by extracting measured data while the wind turbine was operating at 85% or more of the rated rotational speed.

In the envelope spectrum of the point C (**Fig. 9**), which is immediately after the installation of the CMS,

the peak of the inner ring damage frequency (f_i) of medium speed shaft bearing and sideband of the modulated components of the medium speed shaft rotation frequency ($f_i \pm f_r$, $2f_i \pm f_r$) on both sides of the peak were observed; therefore, it was estimated the existence of damage at the inner ring of the bearing immediately after installation of the CMS. However, since the vibration RMS value was at relatively low level, they decided to continue observing it, determining tentative caution threshold based on the data in the first month.

After the installation of the CMS, the vibration RMS value maintained similar level; however, the vibration RMS value started to climb up at the point D, 6 months after the installation, and exceeded the caution threshold at point E. The envelope spectrum at point E (**Fig. 10**) showed the inner ring defect frequency (f_i) and the sideband of its modulated components ($f_i \pm f_r$) more pronounced than point C; therefore, it was estimated that the damage from the inner ring of the bearing had progressed.

They reported the progress of the damage on the inner ring of the bearing at point E to the facility. Then, the facility replaced the bearing. The raceway of the removed bearing inner ring showed multiple axial cracks, as well as flaking, possibly originating from the cracks (**Fig. 11**) [5].
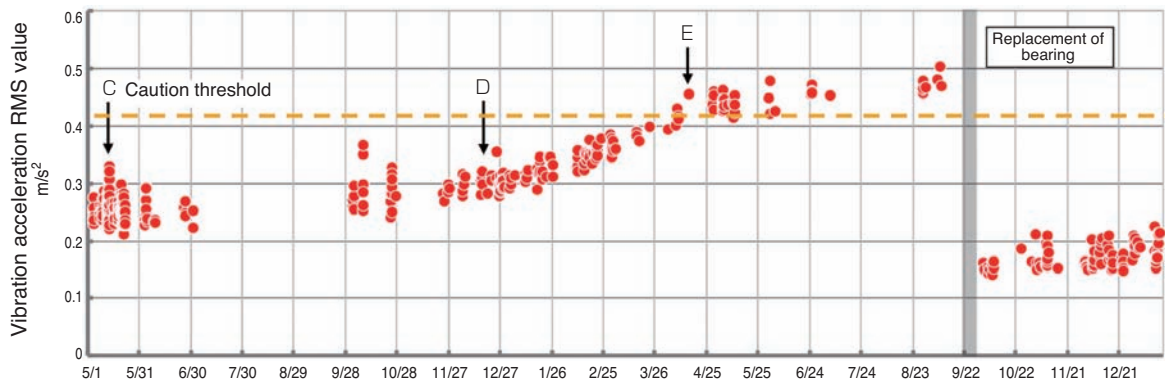

Fig. 8 Trend graph of RMS value at gearbox planetary
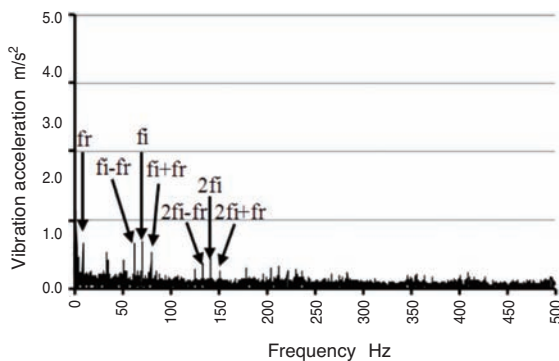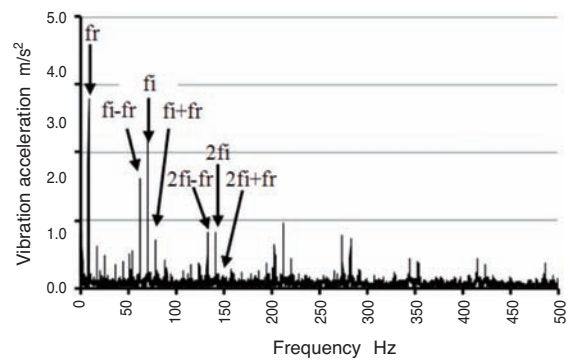

Fig. 9 Envelope spectrum at C

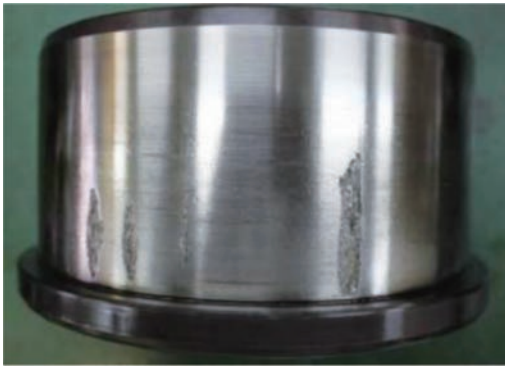**Fig. 10** Envelope spectrum at E

Fig. 11 Inner raceway failure [5]

In this case, the symptom of damage was discovered by the initial diagnosis after installation and accurately detected the progress of the damage by continuous monitoring. The facility received the analysis result from the CMS and could plan adequate preparation and replacement of the bearing at the best time.

4. Challenges ahead

In order to minimize the outage due to repair work and reduce the loss of power and maintenance cost, the prediction technology to appropriately determine the limit of the component operating life and plan the required repair work at the right time will be critical. However, the challenge for the wind turbines is the difficulty to accurately predict the remaining life since the process to the failure is quite different for each case due to varied operating environments such as wind conditions. In addition, for low-speed rotation parts such as the main bearing, the progress of damage is so slow that a long observation time is required in order to collect sufficient data in the process to failure.

It is important to continue data collection and analysis on the actual wind turbines and improve the anomaly detection technology of slow-rotating parts in order to achieve accurate prediction of the remaining life.

5. Conclusion

In this article, we described the methods for data analysis using the CMS and introduced some examples of application of Wind Doctor ™, which we have experienced in the R&D activities of NEDO's Smart Maintenance Technology project.

We will promote advancement of the CMS technology so that it can contribute to the reduction of maintenance cost and improvement of the equipment availability for wind turbine business.

References
1) GLOBAL WIND ENERGY COUNCIL，GLOBAL WIND Report 2017，(2018)．
2) Takeuchi, Haseba, Ikeda: Application of Condition Monitoring System for Wind Turbines, NTN TECHNICAL REVIEW No.80 (2012) 15-18.
3) Hashizume, Takkeuchi, Tanaka, Development of Condition Monitoring System, NTN TECHNICAL REVIEW No. 82, (2014) 74-77.
4) Wataru Hatakeyama, The Recent Applications of the Condition Monitoring Systems for Wind Turbines, THE TRIBOLOGY No. 356, (2017) 38-41.
5) NEDO, FY2017 Final Report "Research and Development of Natural Energy Technologies Based on Wind Power, Etc. / Research and Development of Advanced Applied Technologies / Research and Development of Smart Maintenance Technologies (Analysis) (Risk Analysis, etc.) (2008)

Photo of authors

Makoto MIYAZAKI

Industrial Machinery Division
Robotics Sensing Engineering

Wataru HATAKEYAMA

Industrial Machinery Division
Robotics Sensing Engineering

[New Product]

Development of Multi Track Magnetic Ring for High Accuracy Absolute Angle Detection

Takashi KOIKE*   **Yasuyuki FUKUSHIMA***
Yusuke SHIBUYA*   **Hiroyoshi ITOU****

As the introduction of industrial robots progresses, more accurate work is required. Therefore, it is necessary to detect the angle of each joint of the robot arm with high accuracy. **NTN** has developed a "Multi-track magnetic ring" that can realize absolute angle detection with high accuracy at low cost by applying our precise magnetization technology.

1. Introduction

The recent trend of IoT (Internet of Things), which is to connect "things" to the Internet, is expanding to robotic applications. In developing countries such as China, adoption of industrial robots is increasing due to the rise in labor costs, global price competition, and requirement for product quality. In Japan, labor shortages due to a decreasing birthrate and aging population has become a serious problem. This issue is raising expectations for not only industrial robots in manufacturing, but also for service robots in medical, nursing/welfare, logistics, and security fields [1].

Japan has provided many industrial robots and their components to the world such as reducers, servo motors, and various sensors. Recent development of industrial robots enabling more complex and advanced operation with artificial intelligence (AI) requires advanced components with high functionality. For precision work, positioning accuracy of the tip of the robot arm requires highly accurate detection of joint angles.

NTN has developed "Multi-track Magnetic Ring" for highly accurate angle detection, applying its precise magnetization technology [2].

2. Angle detection methods

In general, angle detection devices (hereafter, angle sensors) are broadly categorized as shown in **Fig. 1**, depending on the detecting methods and output methods. For detecting methods, there are optical methods and magnetic methods. The former detects the light from a light emitting device transmitted through the slit plate or reflected by the reflection plate using a photoreceiver. The latter detects the change of angle by the change of direction and magnitude of the magnetic field. For output methods, there are the incremental method and absolute method. The former repetitively outputs a signal corresponding to the change of angle so that the relative angle can be detected. The latter outputs the current angle information so the absolute angle can be determined. For robots, angle sensors using the absolute method are more suitable since it requires no initialization. For the multijoint robot, which has made remarkable progress in recent years, angle sensors with high resolution and accuracy are required. The servo motor widely used for this application integrates an optical angle sensor (rotary encoder) and a motor with superior properties for these requirements.
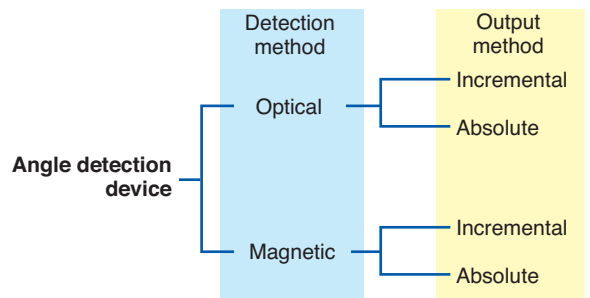
Fig. 1 Classification of angle sensor

---

*New Product Development R&D Center
**Robotics Sensing Engineering, Industrial Machinery Division

3. Magnetic angle sensor

The magnetic angle sensor of the absolute method is configured as shown in **Fig. 2**, with a pair of N- and S- pole permanent magnets attached to the rotational axis and a magnetic sensor placed against the pair on the fixed side on the coaxial direction. For the magnetic sensor, hall element and MR (Magneto resistance) element are used.

In general, this configuration of using permanent magnet and magnetic sensor is inferior to the optical angle sensor (rotary encoder) in resolution and accuracy. However, it is less expensive and less susceptible to environment such as oil, dirt, and dust. Its application to robots will greatly expand if resolution and accuracy are improved.
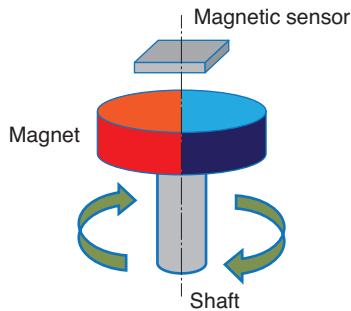
Fig. 2 Angle detection of magnetic absolute method

4. Development of rotation/angle sensors

NTN implemented volume production of "bearings with rotational sensors" for industrial machinery which can detect both speed and direction of rotation with the incremental method. This method uses a multipole (N/S poles) magnetized ring and magnetic sensor IC to deep groove ball bearings [3-4].

NTN also developed "bearings with high resolution rotational sensors" which have higher resolution than "bearings with rotational sensors" by installing a multipole (N/S poles) magnetized ring and magnetic sensor IC with multiple hall elements to deep groove ball bearings. These bearings can provide a maximum of 40 times of incremental output by multiplying the N/S pole pairs by 40 inside the magnetic sensor. Furthermore, **NTN** also developed "bearings with high resolution rotational sensor of origin signal output type" which can also output origin signals by using a specially patterned N/S multipole magnetized ring [5].

NTN developed and commercialized "angle sensor units" of the absolute method for construction machinery [6], which incorporate a permanent magnet and magnet sensor IC facing each other in axial direction within the cast iron or die cast aluminum housing. The sensor technology developed in detection of rotational speed of hub bearings for automotive use [7-8] is used in broad applications such as rotational speed control of servo motors, angle detection of steering, etc. However, the technology is yet to be applied in robot joints, which require angle detection of high accuracy.

NTN also newly developed the "multi-track magnetic ring" which can detect the absolute angle of rotational shaft with high resolution and accuracy by combining the dedicated magnetic sensor IC (refer to Section 5.2) with the magnetic rotational sensor technology it has developed.

5. About multi-track magnetic ring

5.1 Overview

Fig. 3 (a) shows the appearance of the developed "multi-track magnetic ring."

The multi-track magnetic ring consists of a core metal made of press formed steel sheet and rubber magnetic material. The rubber material is kneaded magnetic material, vulcanized and attached on the outer periphery of the core metal. Two magnetic tracks are formed on the outer diameter periphery of the rubber magnetic material, and as shown in **Fig. 3 (b)** and **(c)**. The main track is magnetized with 64 N/S pole pairs, and the sub track is magnetized with 63 pole pairs.

In addition to the multiple magnetic ring of "radial magnetized type," shown in **Fig. 3**, multi-track magnetic ring of "axial magnetized type" was also developed as shown in **Fig. 4**. **Table 1** shows the key specification.
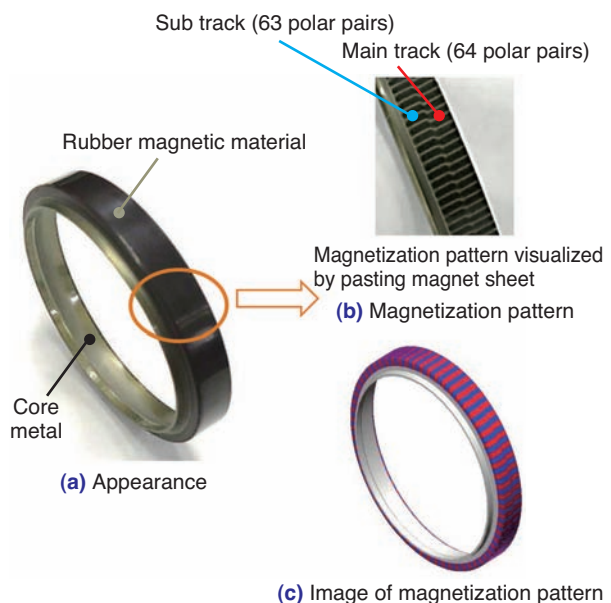

Sub track (63 polar pairs)
Main track (64 polar pairs)

Rubber magnetic material

Magnetization pattern visualized by pasting magnet sheet

(b) Magnetization pattern

Core metal

(a) Appearance

(c) Image of magnetization pattern

Fig. 3 Multi Track Magnetic Ring-radial type

Core metal
Rubber magnetic material
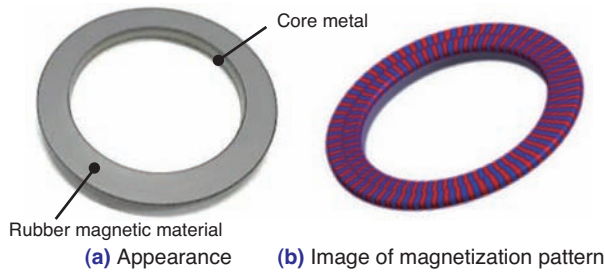**(a)** Appearance **(b)** Image of magnetization pattern
Fig. 4 Multi Track Magnetic Ring-axial type

Table 1 Main specification for Multi Track Magnetic Ring

Item \ Part number	MTR64	MTA64
Magnetized type	Radial	Axial
OD (mm)	ϕ51.5	ϕ56
ID (mm)	ϕ44	ϕ41
Width (mm)	8.2	4.0
Weight (g)	10.7	9.8
Number of magnetized polar pairs	64/63 polar pairs (Main track: 128 poles, sub track: 126 poles)	
Magnet	Rubber magnet	
Core metal	SPCC (rolled steel plate) thickness 0.6 mm	
Operating temperature range (°C)	-40 to $+110$	

5.2 Principle of absolute angle detection and resolution

Fig. 5 shows the principle of absolute angle detection by multi-track magnetic ring. The magnetic sensor IC placed against the multi-track magnetic ring integrates two detectors facing each magnetic track (detector 1 and detector 2) and absolute angle calculation unit. The iC-Haus GmbH's IC (iC-MU) can also be used [9].

The multi-track magnetic ring shown in **Table 1** obtains output signal with the cycle corresponding to

64 magnetized polar pairs from detector 1 and 63 magnetized polar pairs from detector 2. It can also detect the absolute angle by using the fact that their phase difference changes from 0° to 360° with one rotation. Therefore, it can detect which polar pair position it is in the magnetic track of 64 polar pairs. In addition, this magnetic sensor can provide multiplication of 12 bits by accurately reading the magnetic intensity between the magnetic poles. It is possible to divide the angle information of one polar pair into 2^{12}. Considering 64 polar pairs (2^6), it can output angle information of 18 bits (resolution of approx. 0.0014°) [6]. Depending on the parameter setting of the magnetic sensor IC, it is possible to output a maximum of 20 bits (resolution of approx. 0.00034°).

In order to achieve such high resolution, **NTN** is developing proprietary magnetizing technology and controlling the width of each magnetic pole of the multi-track magnetic ring very accurately.

5.3 Features
1) High resolution/high accuracy
As mentioned above, it can output angle information of maximum of 20 bits (resolution of approx. 0.00034°).

Fig. 6 indicates an example of measurement of angle error from the angle sensor combining the multi-track magnetic ring and the magnetic IC sensor described in Section 5.2. This example has an ideal alignment with the least possible installation errors, achieving the angle error of ±0.025°.

2) Hollow structure = Lightweight and compactness
Since its structure is hollow and its diameter is large, it is possible to run cables inside when it is applied to the joints of robots. This will contribute to the compactness and lightweight for robots.
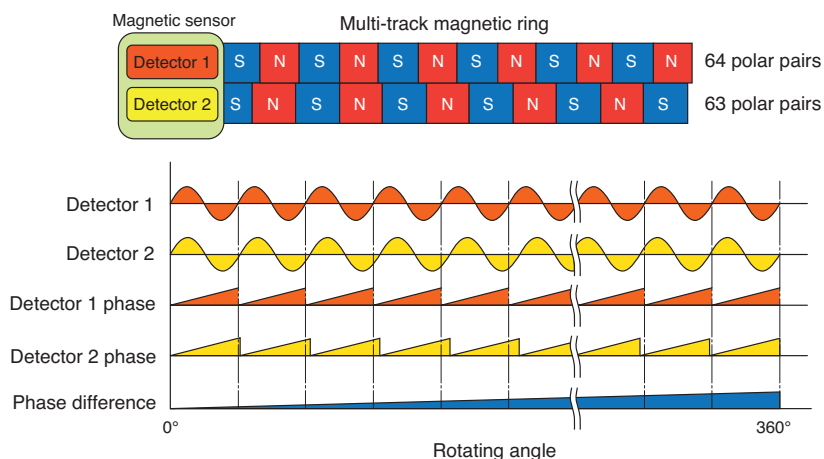

Fig. 5 Absolute angle detection principle

Fig. 7 shows an image of the application of multi-track magnetic ring and magnetic sensor IC to the joints of robots.

A multi-track magnetic ring is fixed on the output stage of the reducer and a printed circuit board implemented with the magnetic sensor IC is installed in the facing position to the magnetic track.

Since the multi-track magnetic ring is fixed on the rotational shaft by press fitting, the installation requires little space contributing small form factor of the joints. The adoption of multi-track magnetic ring is more advantageous than the conventional rotary encoder in terms of installation space. Its compactness will contribute to the increased degree of freedom for designing robots with many rotational axes.

3) Environmental resistance

Environmental resistance of magnetic property of the multi-track magnetic ring is superior to the optical method. It protects against vibration, high temperature, dirt and dust, oil mist, etc. enabling its application in an environment where optical encoders cannot be used.

6. Application for torque sensors

The developed multi-track magnetic ring assumes application for torque sensors in addition to the aforementioned absolute angle detection for robot joints.

High resolution angle detection of 18 to 20 bits can be achieved by using the multi-track magnetic ring. Therefore, torque can be detected by placing multi-track magnetic rings and magnetic IC sensors on both ends of the torsion bar and calculating the torsion amount of the torsion bar from the difference of output angles of each magnetic sensor IC.

Fig. 8 shows an example of the multi-track magnetic ring installed on the actual robot. The multi-track magnetic ring of 64/63 magnetized polar pairs is installed in each joint of the 7-axis robot arm (TOROBO ARM) developed by Tokyo Robotics, Inc. and used for detection of absolute angle and torque. This design was adopted because it achieves a high degree of freedom thanks to the hollow large diameter of the multi-track magnetic ring and accuracy of angle detection.
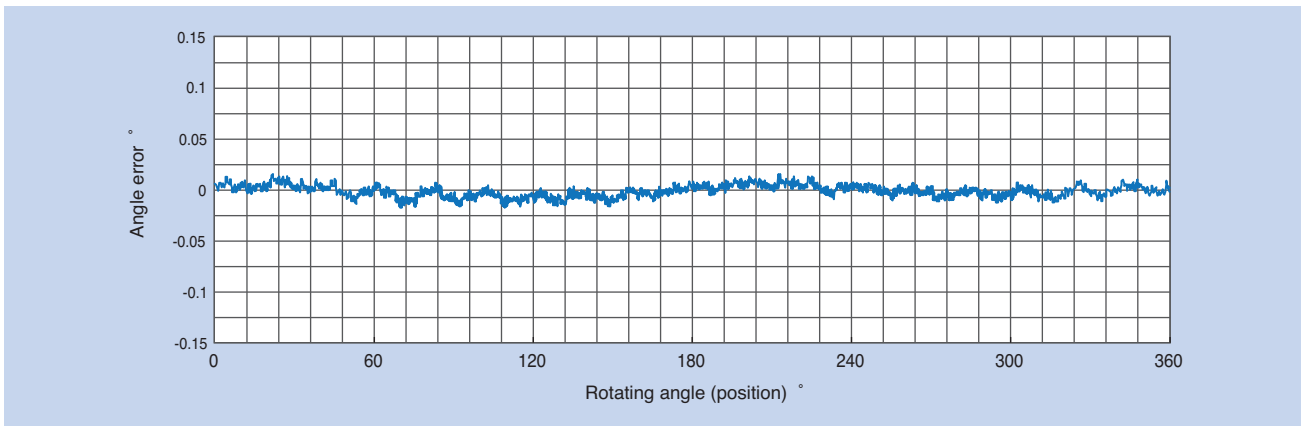

Fig. 6 Angular accuracy measurement result when combining the Multi Track Magnetic Ring and dedicated magnetic sensor IC
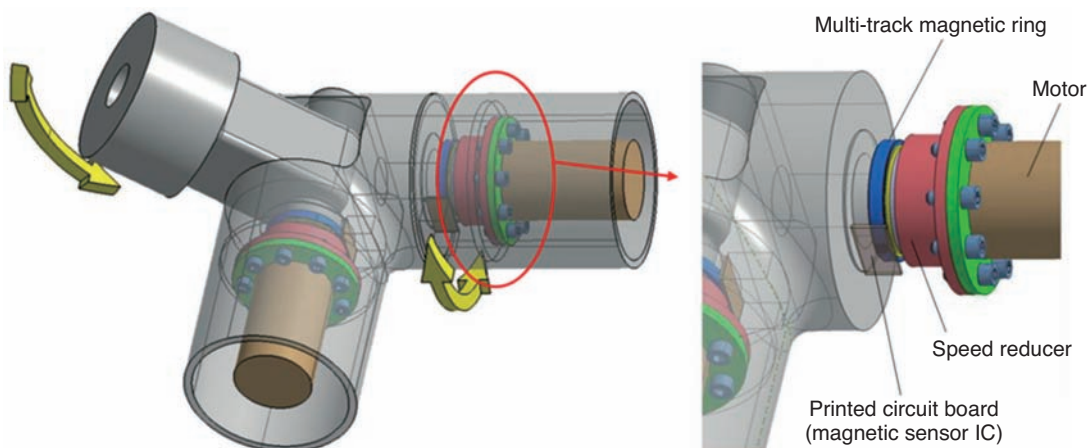

Fig. 7 Application example of the Multi Track Magnetic Ring to robot joint

Fig. 8 Application example of the Multi Track Magnetic Ring
(Source: Tokyo Robotics, Inc.)

7. Future development

There are two types of multi-track magnetic rings developed this time: 64/63 polar pair radial magnetized type and axial magnetized type. From now on, development will continue on the smaller diameter type with fewer polar pairs of 32/31 magnetized polar pairs.

In order to respond to the market demand for improved design degree of freedom and various robotic applications, we will continue developing products with higher resolution and accuracy that have a lighter and thinner form factor.

References
1) New Energy and Industrial Technology Development Organization (NEDO): NEDO Robot White Paper (2014).
2) Koike, Fukushima, Shibuya: High Resolution Absolute Angle Sensor Applicable for Detecting Absolute Angle of Robot Joints, Machine Design Vol. 62 No. 3 (2018) 55.
3) Ito, Koike: Bearing with Integral Revolution Sensor, NTN TECHNICAL REVIEW No.69 (2001) 108-116.
4) Koike, Ishikawa, Ito, Mizutani: Improvement of Magnetic Flux Leakage Durability of Integrated Sensor Bearings, NTN TECHNICAL REVIEW No.71 (2003) 74-79.
5) Ito, Takahashi, Pascal Desbiolles, Cyril Peterschmitt, Shintarou Ueno, High Resolution Sensor Bearing with an Index Signal, NTN TECHNICAL REVIEW No. 78 (2010) 70-76.
6) Itomi, Ito, NTN Sensor Units for Construction Machinery, NTN TECHNICAL REVIEW No.76 (2008) 118-125.
7) Pascal DESBIOLLES, Achim FRIZ, Development of High Resolution Sensor Element MPS40S and Dual Track Magnetic Encoder for Rotational Speed and Position Measurement, NTN TECHNICAL REVIEW No. 75, (2007) 36-41.
8) Nishikawa, Takahashi, Christophie Duret: Hub Bearing with an Integrated High-Resokution Rotation Sensor, NTN TECHNICAL REVIEW No.81 (2013) 52-57.
9) iC-Haus GmbH，iC-MU off-axis nonius encoder with integrated hall sensors

Photo of authors

Takashi KOIKE

New Product Development
R&D Center

Yasuyuki FUKUSHIMA

New Product Development
R&D Center

Yusuke SHIBUYA

New Product Development
R&D Center

Hiroyoshi ITOU

Industrial Machinery Division
Robotics Sensing Engineering

[**New Product**]

Development of Sensor Integrated Bearing Unit for Machine Tool Spindles

Shohei HASHIZUME*   **Yasuyuki FUKUSHIMA****
Yusuke SHIBUYA**   **Yohei YAMAMOTO*****

Recently, machine tools are required not only high speed, high rigidity and super precision, but also condition monitoring function and the "Connected Industries" related technology strongly for higher reliability. To realize the above mentioned machine tools, **NTN** has developed the "Sensor Integrated Bearing Unit for Machine Tool Spindles" to detect the various conditions like temperature, heat flux and vibration from the bearings. The unit has the various sensors inside the outer spacer beside the bearings. This report introduces the features, mechanism and performance of the unit.

1. Introduction

Machine tools support manufacturing in different industries including automotive, aircraft, medicine and IT, and their requirements are increasingly diversified. In recent years, various machine tools with new functionality and concepts such as multifunction numerical control and built-in condition monitoring capability have been developed [1], [2].

Recent machine tools, in particular, are required to contribute to unmanned or labor saving operation and improved productivity by using advanced condition monitoring and control technologies as well as IoT, in view of labor shortages due to a decreasing birthrate and aging population. Therefore, early detection of anomalies in main spindles and their supporting bearings in machine tools is highly desirable in order to prevent unexpected damage and the resulting production downtime required for main spindle replacement.

We have newly developed this "sensor integrated bearing unit for machine tool spindles" as a functional product to solve the above mentioned challenges. This unit, applicable to lathes and machining centers shown in **Fig. 1**, integrates various sensors into the outer ring spacer to enable condition monitoring of nearby bearing raceway surfaces. The following sections introduce the features, configuration and evaluation results of this bearing unit.
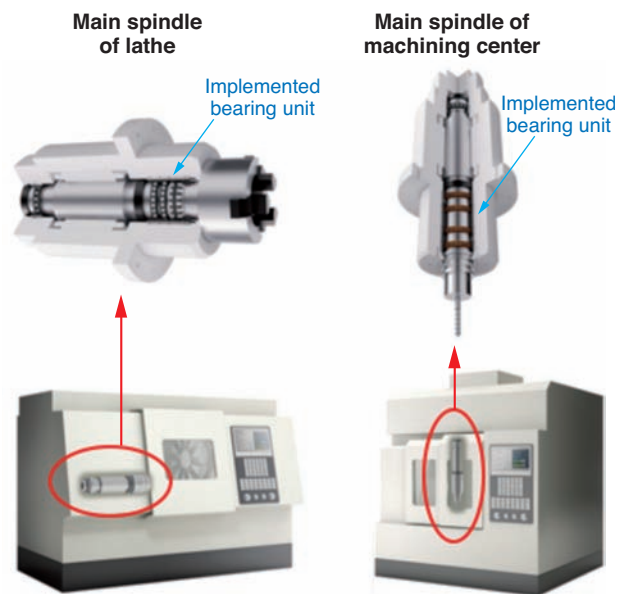
Main spindle of lathe

Main spindle of machining center

Implemented bearing unit

Implemented bearing unit

Fig. 1 Machine tools and spindles
(Left : Lathe, Right : Machining center)

2. Damage modes of bearing units for machine tool spindles and features of the developed product

Bearing units for machine tool spindles are used with lighter loads compared with other bearings for industrial machines. Therefore, they rarely experience flaking [3] due to material fatigue, but the main damage

---

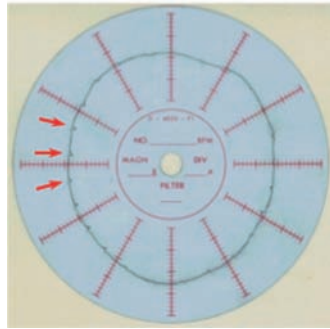*Application Engineering Dept., Industrial Machinery Division
**New Product Development R&D Center
***Product Design Department, Industrial Machinery Division
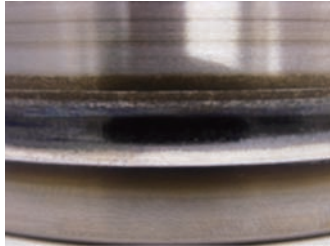
(a) Surface roughness, peeling and burnout due to poor lubrication
The photo shows burn-out of angular contact ball bearings (inner ring raceway surface)
Burn-out due to shortage of air oil supply

(b) Indentation due to collision of the main spindle and workpiece
The photo shows ball pitch indentation produced on the inner raceway surface of angular contact ball bearing (roundness measurement result; indicated by arrows)

Fig. 2 Damage example of machine tool spindle bearing

modes are "(a) surface roughness, peeling, and burnout due to poor lubrication" and "(b) indentation due to spindle collision with the workpiece" (**Fig. 2**).

The developed bearing unit incorporates various sensors in the outer ring spacer adjacent to the bearings. This enables early detection of anomalies compared to conventional measurement on the outer surface of the main spindle. In addition, a heat flow sensor is newly incorporated to improve responsiveness. Damage mode "(a) surface roughness, peeling and burnout" can be detected by temperature sensors, heat flow sensors and vibration sensors, and damage mode "(b) indentation" can be detected by vibration sensors (**Table 1**).

Table 1 Major damage mode of machine tool spindle bearings and measurement items

	Temperature	Heat flow	Vibration
(a) Detection of surface roughness, peeling and burnout due to poor lubrication	○	○	○
(b) Detection of indentation due to collision of the main spindle and workpiece	—	—	○

3. Structure of the sensor integrated bearing unit

Fig. 3 shows the structure of this bearing unit. Three types of sensors are integrated in the outer ring spacer that is inserted between two back-to-back (DB) angular contact ball bearings. The following sections describe those sensors.
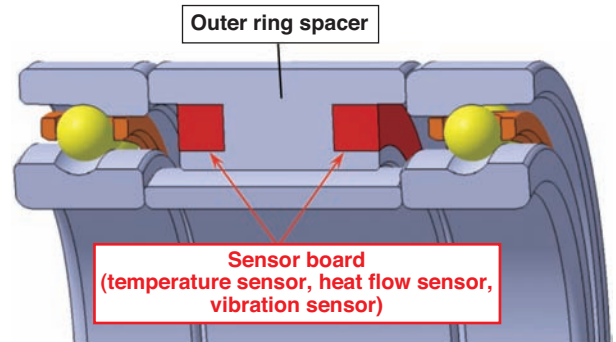
Fig. 3 The sensor integrated bearing unit

[Temperature sensor]

This sensor detects heat produced within the bearings due to rotation and the spindle's cutting load. Sensors for measuring bearing temperature during operation are usually installed on the housing's outer surface due to ease of installation; however, since a cooling path exists between the bearings and the housing's outer surface, the measured temperature becomes lower than the bearing temperature. In addition, measuring temperature at the housing means that it takes time to detect a rise in temperature when the bearing is suddenly heated, due to the large heat capacity of housing. Therefore, it is difficult to quickly determine a sudden heat-up of the bearings. This bearing unit can measure the temperature of the bearings more accurately compared with measurement on the outer surface of the housing, as it measures the temperature at the outer ring spacer adjacent to the bearings.

[Heat flow sensor]

As the spindle rotates, there will be a difference in temperature between the inner and outer rings (hereafter, inner/outer ring temperature difference) of the bearing unit for spindles. The main reason for this is the difference of heat dissipation between the inner and outer rings. The inner ring with less dissipation shows higher temperature than the outer ring. The inner/outer ring temperature difference becomes larger as the bearing rotates at higher speeds, increasing preload within the bearings and contact surface pressure on the rolling surfaces. In addition,

the inner/outer ring temperature difference also increases when operating with damage and burnout caused by poor lubrication within the bearings. The heat flow sensor adopted in this development catches minor changes better than an ordinary temperature sensor and measures the heat flux going from the inner ring with higher temperature to the outer ring, and is used for anomaly detection due to the inner/outer ring temperature difference.

[Vibration sensor]

Used for anomaly detection of both damage mode "**Table 1 (a)** surface roughness, peeling and burnout damage" and damage mode "**Table 1 (b)** indentation." In general, for measuring vibration of bearings in operation, a vibrometer is installed on the outer surface of the housing, for ease of installation, similar to the aforementioned temperature sensor. However, since vibration of the bearing in operation is measured through the housing, the measured vibration levels are reduced from those at the bearing. Therefore, detection is not possible until an anomaly progresses to a sufficiently high level of vibration. The developed bearing unit, on the other hand, integrates the vibration sensor into the outer ring spacer adjacent to bearings, which makes it possible for the sensor to detect small vibrations at the initial stage of anomaly with good sensitivity.

4. Performance evaluation test

4.1 Test conditions, tester configuration

Fig. 4 shows configuration of the tester, modeled after a machine tool main spindle. Condition detection performance was evaluated by integrating the developed bearing unit. Test conditions are shown in **Table 2**. The test unit, comprised of an ultra-high speed angular contact ball bearing with ceramic balls (HSE Type), was operated under the test conditions. Bearings were arranged in a double-row back-to-back configuration (DB) as is common for machine tool

Table 2 Conditions of functional tests

Test bearing	ϕ70×ϕ110×20 Equivalent to 5S-2LA-HSE014 (Ultra high speed angular contact ball bearing with ceramic balls)
Preload method	Fixed position preload (preload of 750N after incorporation)
Rotational speed	0〜16,000min^{-1}
Lubrication method	Air oil lubrication
Supply oil amount	0.03mL/10min
Lubricating oil	ISO VG32
Lubricating air flow	30NL/min
Outer cylinder cooling	Yes, controlled to room temperature
Attitude of axis	Horizontal axis

spindles. In addition to the integrated sensors within the developed bearing unit, sensors were also installed at the conventional measurement positions on the outer surface of the housing for comparison purposes. For correlation purposes, the temperature of the bearing outer ring outer diameter surface was also measured (**Fig. 4**).

[Sensor integrated bearing unit]
(1) Temperature sensor ▲
(2) Heat flow sensor ●
(3) Vibration sensor ■
[General measurement method]
(4) Temperature on the outer surface of housing (thermocouple) ▲
(5) Vibration on the outer surface of housing ■
(6) Temperature on the bearing outer ring outer diameter surface ▲ (thermocouple)
(7) Temperature on the bearing inner ring inner diameter surface ▲ (thermocouple)

Fig. 4 Test spindles, measurement items and points

4.2 Test results

Outputs of the various sensors in the bearing unit are shown in **Fig. 5** for the performance test described in **Table 2** and **Fig. 4**. It was verified that all the sensors performed well from the low speed range to the ultra-high speed range (d_{mn} value: 1.44 million).

Measurements from the developed bearing unit and the conventional measurement method described in Section 4.1 were also compared. **Fig. 6** and **Fig. 7** show the temperature and vibration measurement results. It was verified that readings from the temperature sensor integrated into the developed bearing unit outer ring spacer were closer to the temperature at the bearing outer ring outer diameter surface than the readings from the outer surface of the main spindle housing. It was also verified that the unit provided higher readings for vibration than measurements from the outer surface of the housing.

In addition, comparisons were also made for an acceleration/deceleration test where the rotational speed was changed at certain cycles. **Fig. 8** and
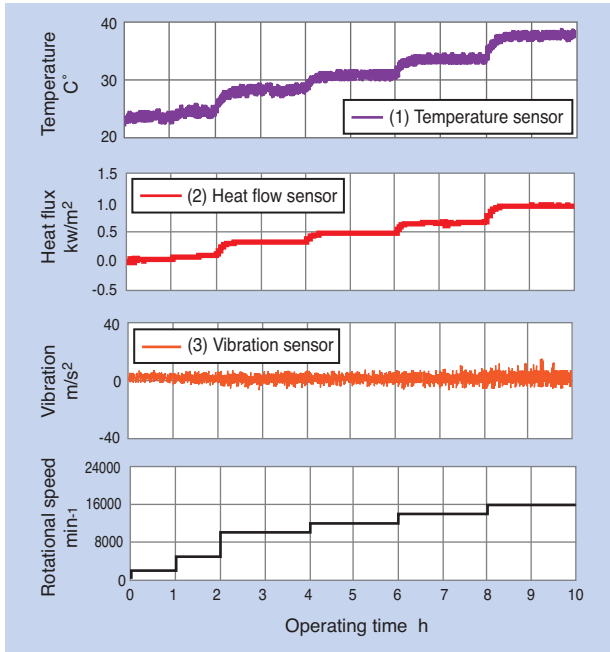
Fig. 5 Fundamental test result[※1]

Fig. 6 Temperature measurement result[※1]
(measurement point comparison)

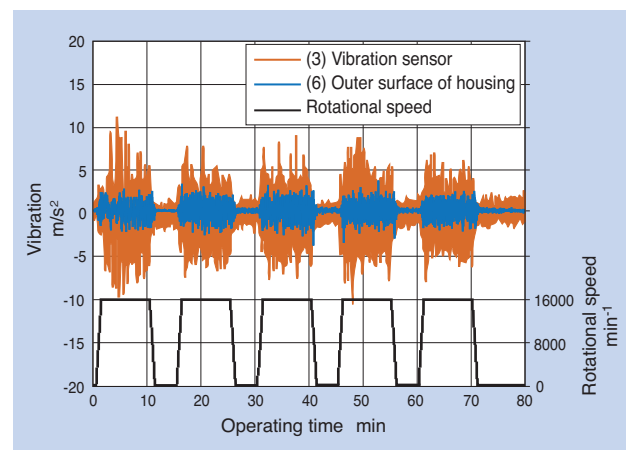**Fig. 7** Vibration measurement result[※1]
(measurement point comparison)

Fig. 9 show the temperature and vibration measurement results. It was verified, in the acceleration/deceleration test also, that readings from the temperature sensor integrated into developed bearing unit outer ring spacer were closer to temperature readings at the bearing outer ring outer diameter surface than the readings from the outer surface of the main spindle housing. The vibration sensor also gave higher readings than the measurements taken on the outer surface of the housing.

Fig. 10 shows the heat flow sensor outputs during the acceleration/deceleration test. The heat flow sensor has good responsiveness versus acceleration/deceleration of the rotational speed and the resulting change of inner/outer ring temperature difference, and improves the accuracy of anomaly detection as well. The inner/outer ring temperature difference is defined as the difference in temperature between the bearing inner ring bore surface and the outer ring outer diameter surface.
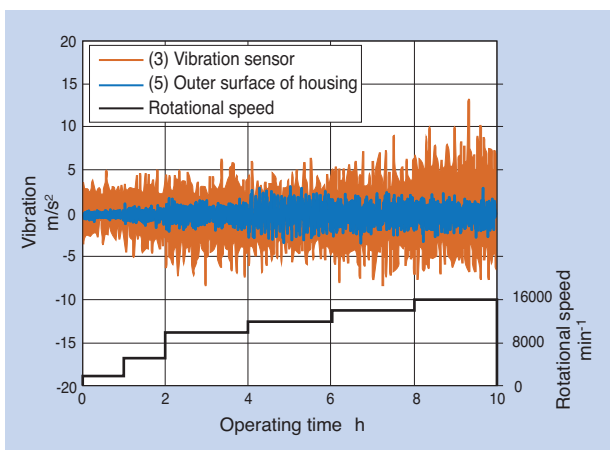
Fig. 8 Temperature measurement result in the frequent cycle test[※1] (measurement point comparison)

Fig. 9 Vibration measurement result in the frequent cycle test[※1] (measurement point comparison)

※1 Refer to **Fig.4** for measurement positions for each item.
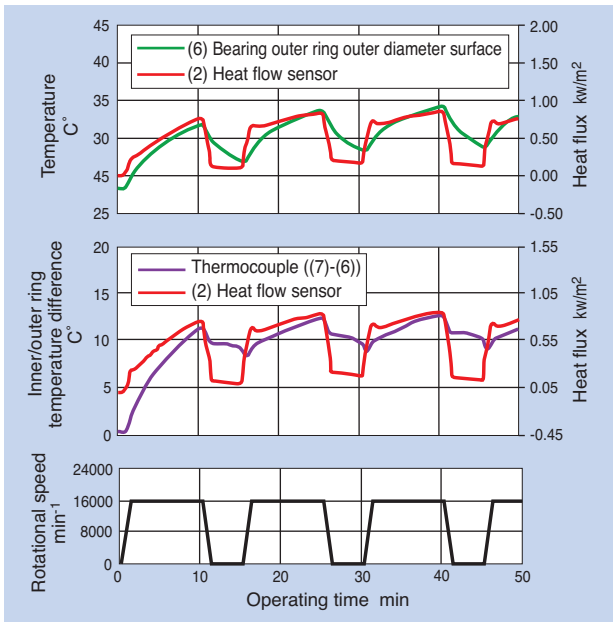
Fig. 10 Measurement result in the frequent cycle test ※1
(heat flux, temperature and temperature deference between IR and OR)

4.3 Bearing burn-out simulation test

Bearing burn-out was simulated in order to test symptom detection for this damage mode. **Table 3** shows the test conditions. The tester shown in **Fig. 4** was used, in a manner similar to the basic performance evaluation test and the acceleration/deceleration test. In this test, only a very small amount of lubricating oil was injected into the bearing when the main spindle was assembled in order to cause the test bearing to burn out easily. In addition, a limiter was set to automatically stop the tester when the motor becomes overloaded due to burn-out of the test bearing.

Fig. 11 shows the relationship between heat flux and temperature, as well as inner/outer ring temperature difference and vibration. The point in time when motor overload was detected is shown by the blue dotted line in **Fig. 11**. The test results revealed that the heat flux shows an increase of output earlier than temperature, inner/outer ring temperature difference and vibration; therefore, it is considered that this measurement is more effective for early detection of burn-out symptoms.

In **Fig. 11**, the reason why the vibration value increased even after the tester automatically stopped after detection of overload is because the motor and the main spindle continued rotating by inertia under the burn-out condition.

4.4 Bearing indentation test

In order to test anomaly detection of indentations on the raceway surface produced by spindle collision to

Table 3 Conditions of the bearing seizure test

| Test bearing	ϕ70×ϕ110×20 Equivalent to 5S-2LA-HSE014 (Ultra-high speed angular contact ball bearing with ceramic balls)
Pressurization method	Fixed position preload (preload of 750N after incorporation)
Rotational speed	Constant at 18,000min^{-1}
Lubrication method	A few drops of lubricating oil were injected when the main spindle was assembled (no lubrication during the operation)
Outer cylinder cooling	Yes, controlled to room temperature
Attitude of axis	Horizontal axis
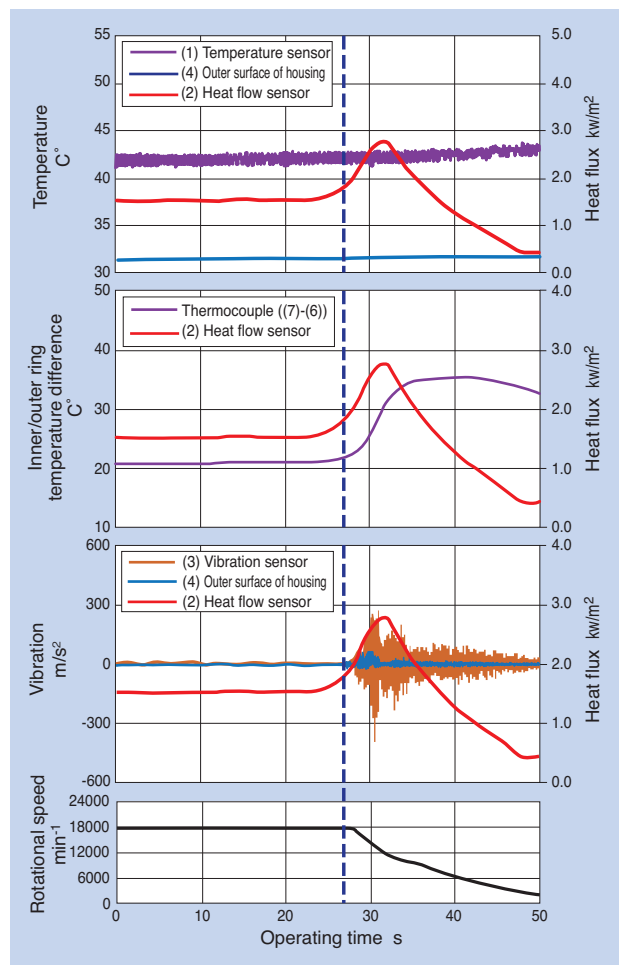
Fig. 11 Measurement result in the seizure test ※1
(heat flux, temperature and temperature deference between IR and OR, vibration)

the workpiece using a vibration sensor, a simulated indentation was made on the bearing raceway surface, and a test was conducted. **Table 4** shows the test conditions. The tester in **Fig. 4** was used in a manner similar to the basic performance evaluation test and the acceleration/deceleration test. **Fig. 12** shows the simulated indentation made on the bearing raceway surface.

Calculated values of bearing forced vibration frequencies during operation at 1,800 min^{-1} are shown

in **Table 5**. **Fig. 13** shows the vibration output frequency analysis results for the developed bearing unit and the conventional measurement method described in Section 4.1 [4]. The test result revealed that both the vibration sensor of the developed unit and the measurements taken at the main spindle housing outer surface detected the frequency caused by the damage on the outer ring when the indentation depth is 60 μm.

On the other hand, since indentations produced by spindle collision with the workpiece vary from several μm to several tens of μm in field applications, we will continue performing tests with varied depths and sizes of indentation.

Table 4 Conditions of the running test of dent bearing

Test bearing	ϕ70×ϕ110×20 Equivalent to 5S-2LA-HSE014 (Ultra-high speed angular contact ball bearing with ceramic balls)
Pressurization method	Fixed position preload (preload of 750N after incorporation)
Rotational speed	1,800min⁻¹
Simulated indentation	One location on the outer ring raceway
	Depth of 60 µm (1.5mm×3.8mm)

3D image of indented bearing

Enlarged photo of indented bearing
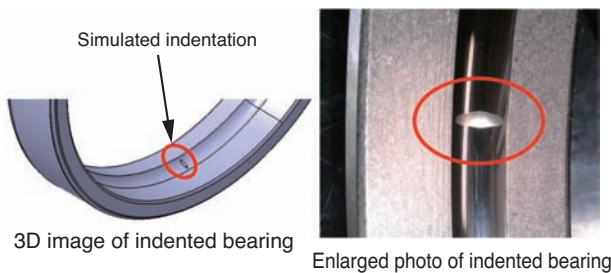
Fig. 12 Dent on the bearing raceways

Table 5 Calculation result of bearing frequency in 1800min⁻¹

	1st order	2nd order	3rd order	4th order	5th order
Number of rolling elements passed against the outer ring (Hz)	341	682	1023	1364	1705
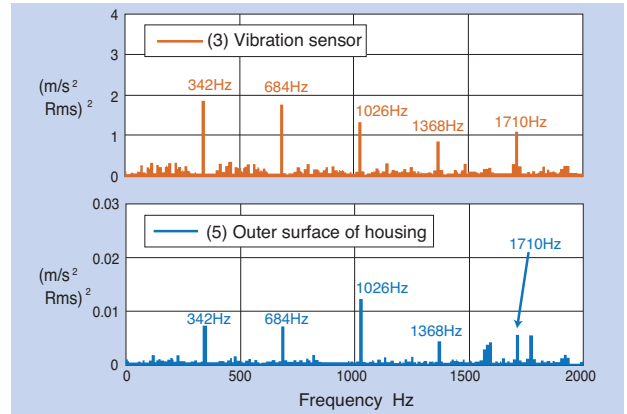
Fig. 13 Vibration frequency analysis of dent bearing[※1]

5. Summary

Due to diversified market needs and changes in social structure, machine tools are required to evolve with further enhancement of condition monitoring functionality and support of IoT. In order to respond to these needs, we have newly developed this "sensor integrated bearing unit for machine tool spindles."

With this development, we have achieved highly sensitive condition detection compared with the conventional measurement on the main spindle outer surface. In addition, the responsiveness of condition monitoring was improved by adopting heat flow sensors.

We will continue to refine this development for further improvement of performance and commercialization. In addition, we will work on the detection of other conditions such as load, as well as enhancement of condition monitoring functionality.

References
1) Naoki Matsumori, Keiichi Ueda: Technical Trend of the Precision Bearings for Machine Tools, NTN TECHNICAL REVIEW, No. 84 (2016) 40.
2) Keiichi Ueda: Technical Trend of the Precision Bearings for Machine Tools, Bearing & Motion-Tech, September 2016 issue No. 002, 33.
3) NTN Catalog: Rolling Bearings, Catalog, A-17.
4) Keisuke Hashizume, Akitoshi Takkeuchi, Yuzuru Tanaka: Development of Condition Monitoring System, NTN TECHNICAL REVIEW No. 82, (2014) 74.

Photo of authors

Shouhei HASHIZUME
Industrial Machinery Division
Application Engineering Dept.

Yasuyuki FUKUSHIMA
New Product Development
R&D Center

Yusuke SHIBUYA
New Product Development
R&D Center

Yohei YAMAMOTO
Industrial Machinery Division
Product Design Dept.

[New Product]

Angular Contact Ball Bearings for High-Speed and Heavy-Cutting Machine Tools

Jin TAKEGAHANA[*]   **Mineo KOYAMA**[*]
Kouji JINNO[**]   **Yuya TANAKA**[**]

NTN has developed new angular contact ball bearings, well suitable for machine tool spindles especially taking advanced multi-tasking which is the latest trend of the manufacturing field. The bearings perform 30% higher basic load rating and higher allowable axial load through internal design optimization. Thus the bearings support the well balanced machine tools show high-speed and heavy-cutting capability. In this document, we introduce the design points and test data.

1. Introduction

Recently, requirements for higher machine tool performance are increasing in order to address the diverse needs of different industries.

The recent trends of these requirements include (1) "increase of machining and cutting of difficult-to machine material and hard material like titanium, and requirement of a more rigid main spindle to deal with them," (2) "integration and multi-functionality of machining process for higher efficiency," (3) "requirement of five-axis tool for machining complex shapes with high precision" and (4) "requirement for smaller machine tools to adapt to the size of workpiece." To cope with these trends, "one chucking for the entire process," which is to process the workpiece from heavy cutting in mid to low speed rotation of the main spindle to refined cutting in high speed rotation by one machine tool, is demanded. As a result, the bearing for the main spindle of machine tool needs to provide a high level of both high-speed capability and high rigidity, which are in a trade-off relationship (**Fig. 1**) [1].

Also, efforts for reducing non-cutting takt time are in progress to "further increase productivity," which is an important factor for machine tools; consequently, the speed of the main spindle and table feed rate of recent machine tools is increasing. In addition, recent machine tools are required to process more complex shapes. With these changes, unexpected collision events between the tools attached to the tip of the main spindle and workpieces are recently increasing.

The impact load applied to the bearings of the main spindle due to collision may produce indentation on the raceways of the bearing inner/outer rings depending on the magnitude of the load, which impedes smooth and high precision rotation of the main spindle. Therefore, bearings of the main spindle are also required to have high load resistance to prevent/mitigate occurrence of indentation. To respond to these trends and requirements, **NTN** has developed bearings for main the spindle to support high-speed rotation and heavy cutting based on the high-speed angular contact ball bearing "HSE Type."

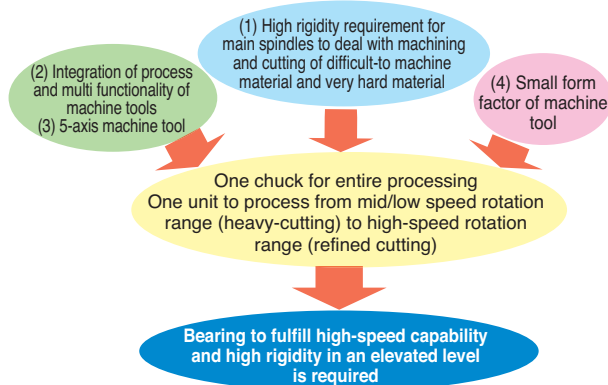In this article, we describe the features and the evaluation test results of the developed product.

Fig. 1 Technical trend of machine tools and spindle bearings [1]

---

*Application Engineering Dept., Industrial Machinery Division
**Product Design Department, Industrial Machinery Division

2. Background of development

NTN's high-speed angular contact ball bearing HSE Type adapts for broad usage from high-speed to ultra high-speed range. Consequently, many units have been adopted for main spindles of machine tools for a long time. However, machine tools are expected to evolve with even higher speed of main spindle rotation for further productivity gain. Under these circumstances, adoption of the HSE Type is expected to expand.

As another approach of productivity increase, machine tools actively incorporating integration of machining processes, multi functionality, and heavy-cutting capability are recently increasing. In these cases, d_{m}n value[※1] of the main spindle rotational speed is approximately 1.2 million and the bearings for the main spindles are required to have both high-speed capability and rigidity, which are in a trade-off relationship. Therefore, as shown in **Fig. 2**, the challenge of the bearings for main spindles is to fulfill both high-speed capability and high rigidity at an elevated level.
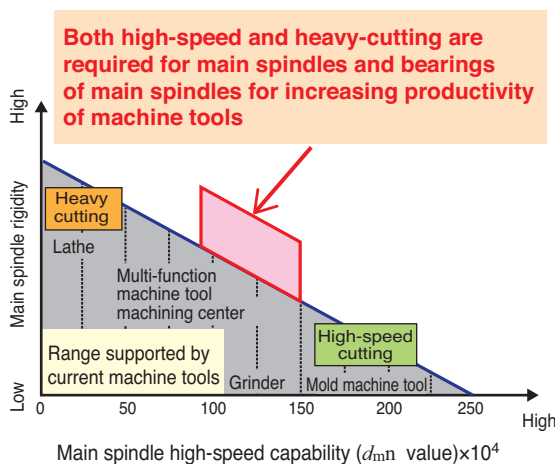
Fig. 2 New needs for main spindles and spindle bearings of machine tools

In addition, impact load (large axial load) may be applied to the main spindle and bearings of main spindles of machine tools due to unclamping load while exchanging tools during off-operation or unexpected collision of tool attached to the tip of the main spindle and the workpiece (**Fig. 3**).

When the impact load exceeds the tolerance, indentation may occur on the raceway, impeding smooth and highly precise rotation. This axial load limit is called permissible axial load (stationary) and **NTN** defines it as the load leading to any of the following [2]:

· The end of the contact ellipse produced between the rolling element and the raceway overtakes the shoulder either in the inner ring or outer ring (**Fig. 4**).
· The contact surface pressure of the raceway reaches 3,650 MPa[※2] on either the inner or outer ring.

In order to prevent/mitigate indentation, permissible axial load (stationary) needs to be increased and tolerance against collision must be enhanced.
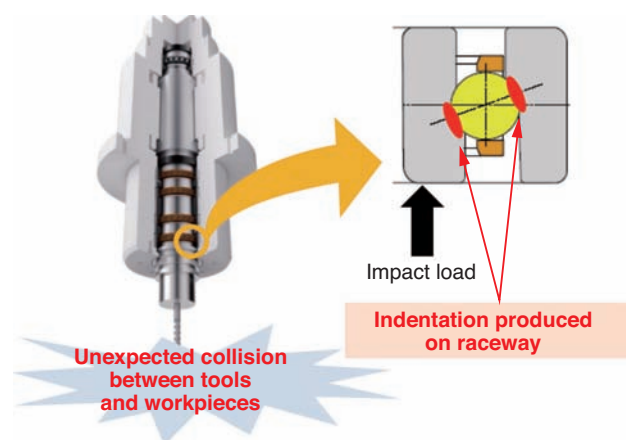

Fig. 3 Image of the unexpected collision between tool and work piece, and the resulted dent on the bearing raceways caused by the collision
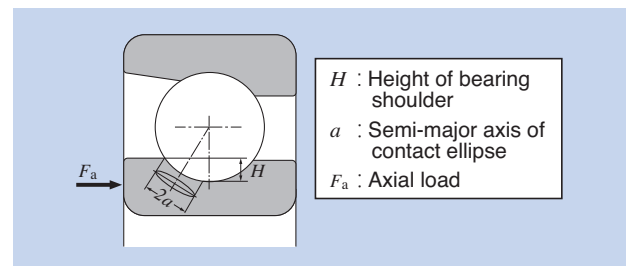

Fig. 4 Overflow of the contact ellipse from the raceway

※1 d_{m}n value expresses the rotational performance of bearings. d_{m} (diameter of rolling element (mm)) × n (rotational speed (min^{-1}))
※2 Contact surface pressure 3,650MPa is a value to produce permanent deformation of 0.00002 to 0.00005 times the rolling element diameter.

3. Features of developed product

3.1 [Support of heavy-cutting (1)] increase of load capacity

The developed product optimized the internal design such as larger rolling element diameter, in order to support heavy-cutting capability while still maintaining the high-speed capability of the aforementioned HSE Type (hereafter, conventional product) (**Fig. 5**). The developed product improved the load capacity, increasing the rated load by approx. 30% (**Fig. 6**).
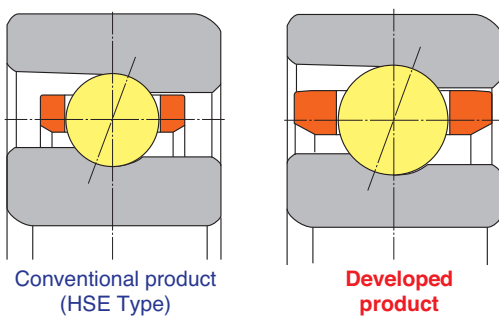

Conventional product
(HSE Type)

Developed product

Fig. 5 Conventional design and developed design
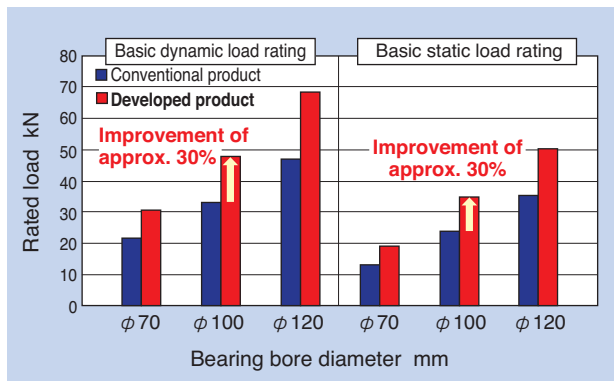
Fig. 6 Basic load rating of conventional design and developed design (ceramic balls, contact angle 20˚)

3.2 [Support of heavy-cutting (2)] improvement of cage strength

The rolling elements of rolling bearings rotate with so-called "lag-lead" which is a very small difference of relative speed due to geometrical accuracy of the bearing, installation accuracy onto shaft and housing, external load, etc. The rolling elements with relatively faster rotational speed tend to shift forward in the cage pocket (traveling direction). The rolling elements with relatively slower rotational speed tend to shift backward in the cage pocket (opposite side of the traveling direction). Consequently, the rolling elements make contact with the cage pocket to apply load on the cage.

This load varies depending on the magnitude of the "lag-lead" of rolling elements and the magnitude of the load applied to the rolling elements (hereafter, rolling element load). Since the developed product uses larger rolling elements than the conventional product, as mentioned above, the rolling element load is likely to increase. In addition, for heavy-cutting, a relatively larger machining load is applied. Therefore, a large load may be applied to the cage, as well. Therefore, an enhanced cage with larger cross section than the conventional product was adopted to increase reliability of the cage strength (**Fig. 7**).
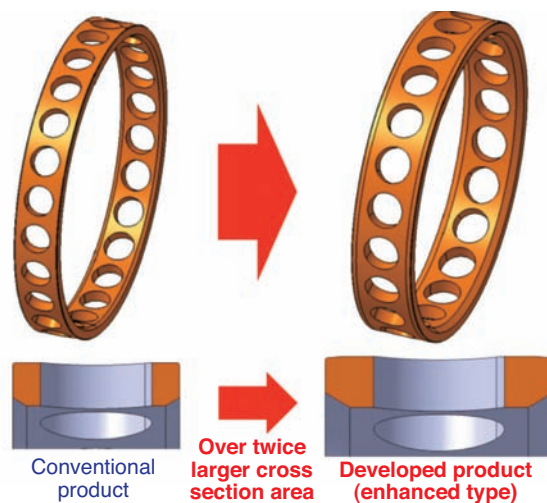

Conventional product

Over twice larger cross section area

Developed product (enhanced type)

Fig. 7 Cross section of cage
(Comparison of conventional design and developed design)

3.3 Increase of permissible axial load (stationary)

The permissible axial load (stationary) of the developed product is increased by approx. 30% compared to the conventional product by optimizing the internal design (**Fig. 8**). This will prevent/mitigate indentation on the bearing raceway surface when impact load is applied.
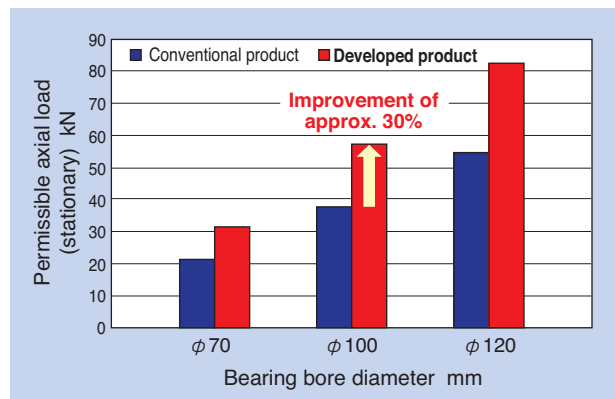

Fig. 8 Static allowable axial load
(ceramic balls, contact angle 20˚)

4. Evaluation test of developed product

4.1 Test condition

We have conducted high-speed operation tests of the developed product. The configuration of the tester is shown in **Fig. 9** and the test conditions are shown in **Table 1**.

This test used a bearing of inner ring inner diameter 70 mm, which is widely used for main spindles of the machining center. Assuming main spindles where high rigidity is required such as heavy cutting, a four-row back-to-back arrangement (DTBT) fixed position preload was used, setting 1,400 N of preload after incorporation of bearing into the main spindle, which exceeds medium preload of the conventional product. In addition, the enhanced type of **Fig. 7** was adopted for the cage of the developed product and with phenolic resin material.
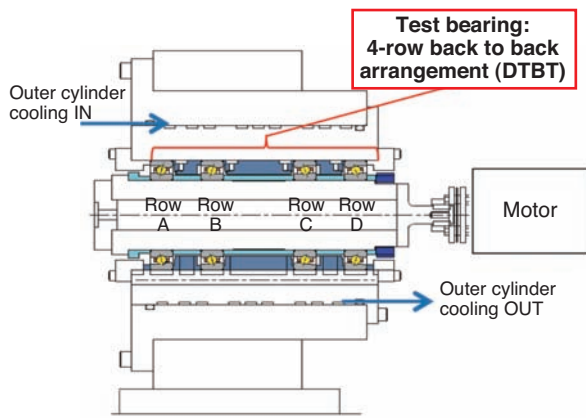
Fig. 9 High-speed running test spindle

Table 1 Test conditions

Test bearing	φ70×φ110×20×4 rows (DTBT) Equivalent to 5S-2LA-HSE014 (Ceramic ball, contact angle 20°)	
Cage specification	Conventional product	Developed product
	Phenolic resin cage	
Preload method	Fixed position preload	
Preload after incorporation	1,400N	
Rotational speed	0～18,000min^{-1}	
Lubrication method	Air oil lubrication	
Supply oil amount	0.03mL/8min	
Amount of air	35NL/min	
Lubricating oil	ISO VG32	
Outer cylinder cooling	Yes	
Attitude of axis	Horizontal axis	

4.2 Test results

Test results are shown in **Fig. 10** and **11**. The developed product shows rise of temperature similar to the conventional product while increasing the load capacity. It was verified that the operation exceeds dmn value of 1.2 million, shown in **Fig. 2**, up to d_{mn} value of 1.62 million (18,000 min^{-1}) (**Fig. 10**). It was also verified that the bearings other than row C also showed a stable rise in temperature (**Fig. 11**).
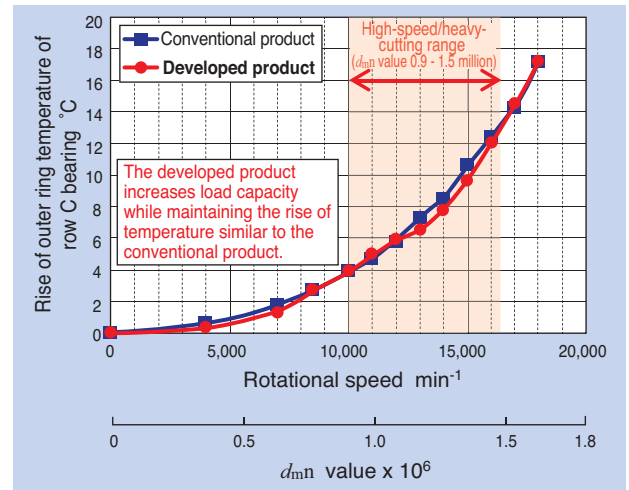

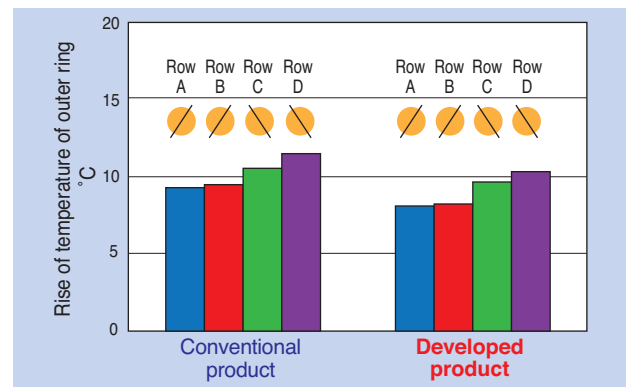**Fig. 10** High-speed running test result (C-row bearing)

Fig. 11 Outer ring temperature rise in spindle rotation speed 15,000 min^{-1}

4.3 Permissible axial load (in operation)

Based on the temperature data obtained in the aforementioned test, permissible axial load (in operation) was calculated for each bearing in the range of d_{mn} value of approximately 1.2 million. The result indicated that when d_{mn} value is 1.17 million (13,000 min^{-1}), the developed product was Fa=9.8 kN compared to the conventional product of Fa=6.8 kN, verifying that the external load applicable to the main spindle is increased by approx. 30%. In addition, similar result was obtained for d_{mn} value of 1.35 million (15,000 min^{-1}) (**Fig. 12**).
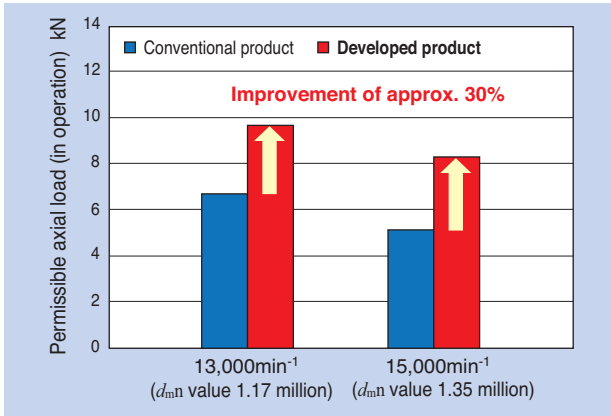
Fig. 12 Dynamic allowable axial load
(ceramic balls, contact angle 20°)

5. Application of injection molding plastic cage

5.1 Material of plastic cage

In the previous section, we verified that the developed product shows equivalent rise in temperature as the conventional product by optimization of the internal design. In this test, phenolic resin (hereafter, PF) was used for the cage. Since the phenolic resin is thermosetting, it has the advantage of higher tolerance against a rise in temperature due to high-speed rotation of the bearing. On the other hand, consideration is required for productivity and cost since it is fabricated by machining. In this section, adoption of injection molded cage, which has an advantage in productivity and cost, is also considered.

For high-speed operation of injection molded cage, research using high-melting point polyamide resin (hereafter, high melting point PA) shown in **Table 2** has been conducted [3].

Table 2 Characteristics of resin cage material

Material	Phenol (PF)	High-melting point polyamide (high-melting point PA)	Polyamide (PA)
Category	Thermosetting	Thermoplastic	
Glass transition temperature	—	158°C	58°C
Melting point	—	158°C	260°C
Production method	Cutting	Injection molding	

5.2. Evaluation test

Enhanced cage was fabricated with high-melting point PA in **Fig. 7,** and high-speed operation test of the developed product was conducted under the conditions of **Table 3**. The test conditions were the

same as **Table 1** except that the cage specification is different.

The test result revealed that the developed product with high-melting point PA cage also showed a rise in temperature similar to the conventional product. It was verified that the operation is possible, in addition to d_{mn} value of 1.2 million, shown in **Fig. 2**, up to d_{mn} value of 1.62 million (18,000 min⁻¹) (**Fig. 13**). It was also verified that the bearings other than the row C also showed a stable rise in temperature (**Fig. 14**). In this test, conventional product with ordinary polyamide resin (hereafter, PA) cage was also evaluated. The result showed an unstable rise in temperature at d_{mn}

Table 3 Test conditions

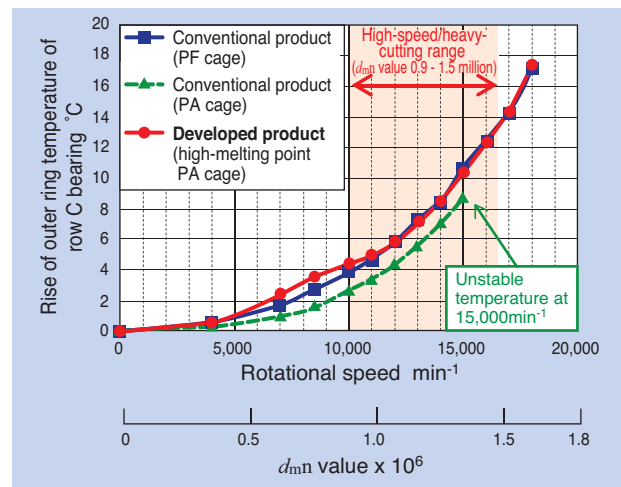| Test bearing	φ70×φ110×20×4 rows (DTBT) Equivalent to 5S-2LA-HSE014 (Ceramic ball, contact angle 20°)	
Cage specification	Conventional product	Developed product
	PF cage	High-melting point PA cage
	PA cage	

Fig. 13 High-speed running test result (C-row bearing)

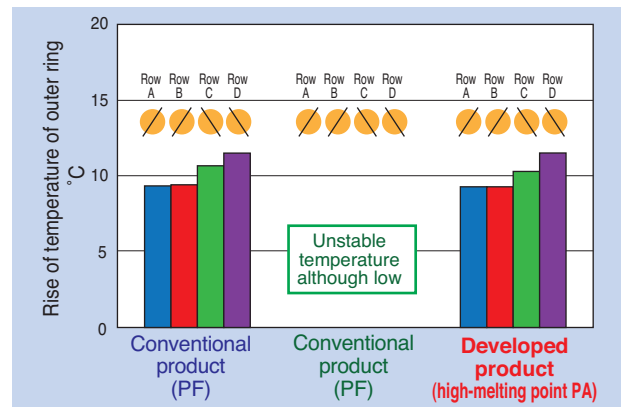**Fig. 14** Outer ring temperature rise in spindle rotation speed 15000min⁻¹

value of 1.35 million (15,000 min^{-1}) and could not support the high-speed/heavy-cutting range (d_{mn} value 0.9 - 1.5 million). We will proceed with volume production of the developed product, considering adoption of the high-melting point PA cage, as well.

6. Summary

We have developed "Angular Contact Ball Bearings for High-Speed and Heavy-Cutting Machine Tools" in order to meet new trends such as integration of machining processes and multi-functionality of machine tools. The developed product optimizes the internal design based on the conventional high-speed angular contact ball bearing "HSE Type," by increasing load capacity and permissible axial load by approx. 30% while maintaining high-speed capability. In addition, adoption of high-melting point polyamide resin (high-melting point PA) with advantageous productivity and cost was also studied for the developed product. We will also conduct performance evaluation with grease lubrication.

We are poised to continue working on the improvement of bearing performance in order to support higher functionality of machine tools.

References
1) Naoki Matsumori, Keiichi Ueda: Technical Trend of the Precision Bearings for Machine Tools, NTN TECHNICAL REVIEW, No. 84, (2016) 40.
2) NTN Catalog: Precision Rolling Bearings, CAT. No. 2260-VII/J. 16.11.03 21.
3) Atsushi Tokuda, Takumi Hayashi: Impact of Heat Resistance of Plastic Cage for High-Speed Operation of Angular Contact Ball Bearing, Japanese Society of Tribologists, Tribology Conference 2017 Fall Takamatsu

Photo of authors

Jin TAKEGAHANA	Mineo KOYAMA	Kouji JINNO	Yuya TANAKA
Industrial Machinery Division Application Engineering Dept.	Industrial Machinery Division Application Engineering Dept.	Industrial Machinery Division Product Design Dept.	Industrial Machinery Division Product Design Dept.

Machine Tool Main Spindle Bearings with Air Cooling Spacer for Grease Lubrication

Keisuke NASU*   Naoya OKAMOTO**
Yuya TANAKA**   Tomohiko OBATA***

Recently, machine tools are required multitasking for various processes and works. Though high speed and high rigidity of spindle bearings are trade-off relationship each others, they are demanded to achieve higher level performance coinstantaneously. And the application of grease lubricated spindle bearings has been increasing in the last years because of the strongly trend of the simplification of devices and systems and environmental concerning. **NTN** has been developing the application of the air cooling spacer to the grease-lubricated spindle bearings to meet the above mentioned two requirements.

1. Introduction

The required properties of main spindles vary depending on the machining needed. High rigidity and accuracy spindle are required when working difficult-to-machine material or partial processing of complex shapes. On the other hand, high-speed and highly precise rotation is required for machining molds for machine components and components used in the medical field. Therefore, demand for 5-axis machine tools with multiple machining capabilities and complex machine tools, which require bearings for main spindles, to offer both high speed and high rigidity are increasing [2].

Demand for bearings in the main spindles with grease lubrication is increasing for simplification of facilities and reduction of environmental burden. One concern of grease lubricated bearing is that heat accelerates degradation of grease thus significantly impact the lubrication life [3]. Therefore, it is critical to reduce heat during the operation of the bearings. There have been several measures taken to meet this challenge. For example, grease with superior high-speed properties, and heat resistance and optimization of internal design [4] In this development we have attempted to apply air cooling spacers to tool main spindle bearing [1] to grease lubrication as a new approach.

Machine tool main spindle bearings with air cooling spacers are the proprietary technology that **NTN** developed and is used in products with air oil lubrication.

In this article, functional evaluation of the cooling effect, in particular, when air cooling spacers are applied to grease lubrication and the arrangement for commercialization are described.

2. Structure and cooling mechanism of air oil lubrication air cooling spacer

In the following, we will describe the basic structure and cooling mechanism of the "machine tool main spindle bearings with air cooling spacers," by using actual application example..

Air nozzles are created in the outer ring spacer which is inserted between two back to back angular contact ball bearings (**Fig. 1**). These nozzles are at offset positions from the axial center and the cooling air in normal temperature injected from these nozzles goes through the space between the inner and outer spacers, as well as inside the bearings, swirling in the rotational direction of the inner ring. The cooling air removes heat from the surface of the inner ring spacer to cool it down.

  *Application Engineering Dept., Industrial Machinery Division
 **Product Design Department, Industrial Machinery Division
***Advanced Technical Research Center

As shown in the fluid analysis result of **Fig. 2**, when cooling air is injected vertically to the inner ring spacer (left figure), the cooling air immediately spreads out in the axial direction, which minimize the cooling effect. On the other hand, when the air nozzles of the cooling air are offset (right figure), the cooling air stays around the surface of the inner ring spacer longer to extend the time for the cooling air to remove heat from the inner ring spacer surface, which increases the cooling effect of the inner ring spacer.

As inner ring spacer cooled down, the adjacent bearing inner ring also cooled down. Usually, when bearings rotate, the inner ring is more heated than the outer ring. Therefore, the preload increases by the difference in thermal expansion. In this cooling technology, the difference of temperature between the bearing inner ring and outer ring can be reduced by cooling the inner ring. As a result, preload and contact surface pressure on the raceway can be reduced to achieve both high speed and high rigidity at a high level. **Table 1** and **Fig. 3** show an example of test results of the machine tool main spindle bearing with air cooling spacer [1].
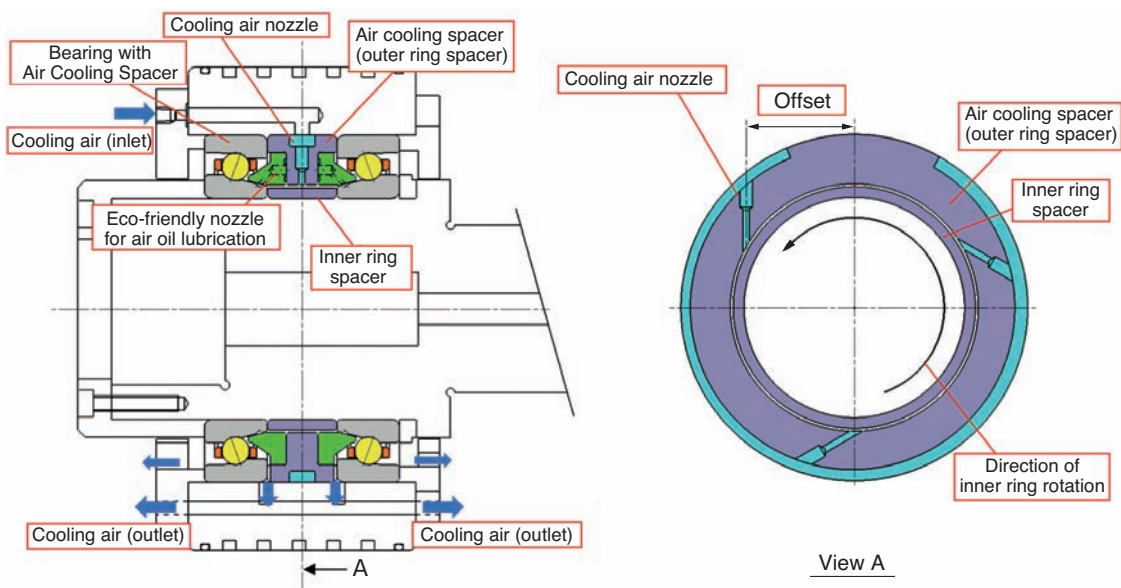
Fig. 1 Machine tool main spindle bearings with air cooling spacer (for air oil lubrication) [1]

When cooling nozzle is not offset

Cooling air collides to inner ring spacer vertically immediately after injected from air cooling nozzle and spreads to axial direction. Therefore, the cooling air only stays on the surface of the inner ring spacer for a short time, with insufficient cooling effect.

When cooling nozzle is offset

Having the air cooling nozzle in an offset position from the center of the shaft, the cooling air swirls in the inner ring radial direction and stays on the surface of the inner ring space for a long time. Therefore, the cooling air can remover more heat from the surface of the inner ring spacer, increasing the cooling effect of the inner ring spacer and inner ring.

Fig. 2 Cooling air flow between inner and outer spacers (Fluid analysis results) [1]

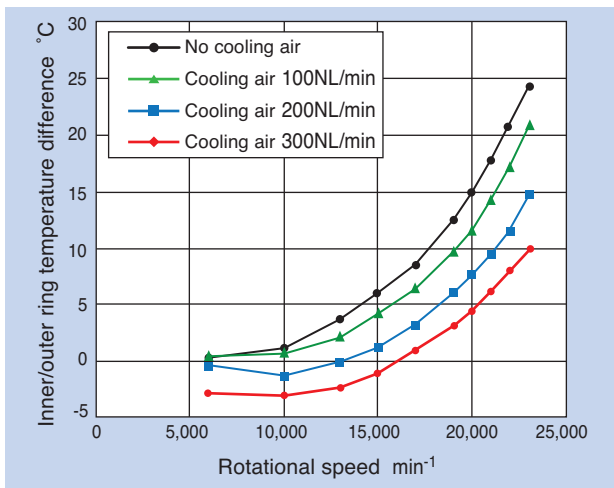**Table 1** Test conditions for high speed running test of the machine tool main spindle bearings with air cooling spacer (air oil lubrication)

Test bearing	$\phi 70 \times \phi 110 \times 20$ Equivalent to 5S-2LA-HSL014 (Eco-friendly air-oil lubrication angular contact ball bearing with ceramic balls)
Preload method	Fixed position preload (preload of 0N after incorporation)
Rotational speed	0 - 23,000min^{-1}
Lubrication method	Air oil lubrication
Supply oil amount	0.03mL/10min
Lubricating oil	ISO VG32
Lubricating air flow	30NL/min
Outer cylinder cooling	Yes, thermal tuning to room temperature (21±1℃)
Attitude of axis	Horizontal axis

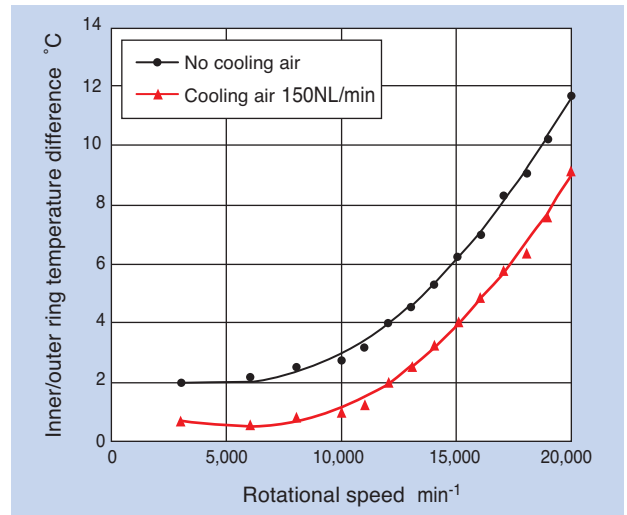**Fig. 3** Result of high speed running test of the machine tool main spindle bearings with air cooling spacer (air oil lubrication)

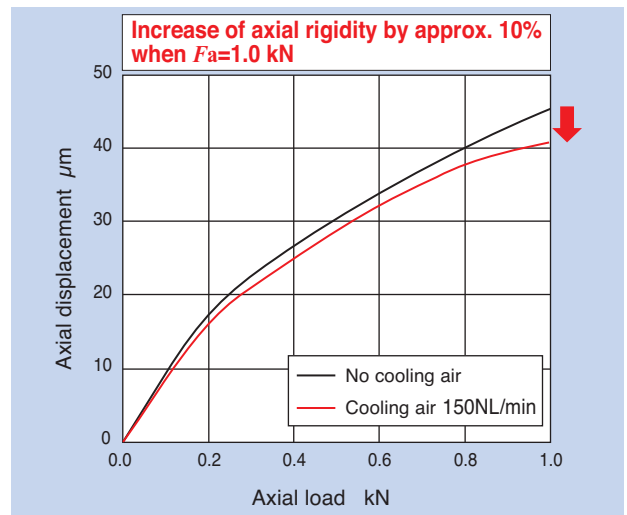From the test results in **Fig. 3**, we verified the cooling effect of the "air-oil lubrication bearings with air cooling spacers" by cooling air from low-speed to high-speed rotation, as well as the fact that the cooling effect is greater as the cooling air supply is larger.

3. Structure of grease lubrication air cooling spacer

Fig. 4 shows the structure of the "machine tool main spindle bearing with air cooling spacer" when it is applied to grease lubrication. The cooling air nozzles are formed in the outer ring spacer. It is then inserted between the back to back angular contact ball bearings with grease lubrication seals.

4. Cooling effect of grease lubrication air cooling spacer

A high-speed operation test was conducted to verify the cooling effect of the "machine tool main spindle bearing with air cooling spacer" when it is applied to grease lubrication. The test condition is shown in **Table 2** and the structure of the tester is shown in **Fig. 5**.

In this test, the upper limit of the cooling air supply was set to 150 NL/min. considering the commercialized version. The offset amount of the nozzles was set to 80% of the radius of the inner ring spacer outer diameter, based on previous test results [5].

Fig. 6 shows the test results of the high-speed operation test. It was verified that the inner/outer ring
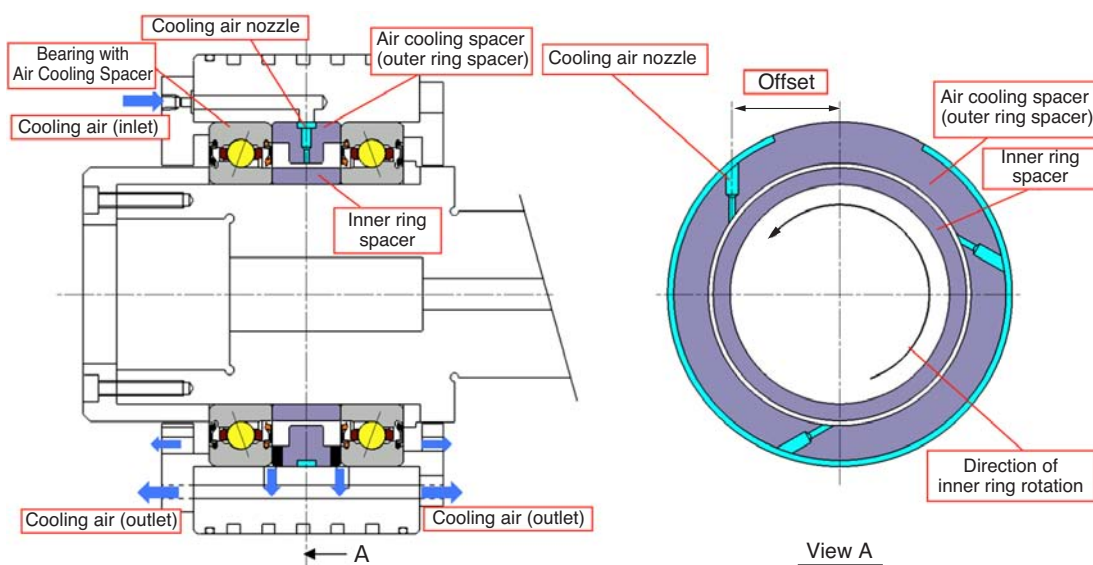
Fig. 4 Machine tool main spindle bearings with air cooling spacer (for grease lubrication)

temperature difference at 20,000 min^{-1} (d_{mn} value 1.8 million) decreases approx. 2.5°C with 150 NL/min of cooling air supply compared to no supply. Because of this decrease of inner/outer ring temperature difference, the maximum contact stress on the raceway surface at 20,000 min^{-1} can be reduced by approx. 10%. These results bring about the following effect. (1) The temperature at 18,000 min^{-1} with no cooling air supply and the temperature at 20,000 min^{-1} with supply of 150 NL/min cooling air are equivalent, which enables higher speed by approx. 10%. (2) Preload of the bearings after incorporation into the main spindle can be increased, which enables increase of main spindle axial rigidity by approx. 10% (**Fig. 7**). In addition, improvement of lubrication durability can be expected. This point will be further verified.

Fig. 6 Result of high speed running test of the machine tool main spindle bearings with air cooling spacer (grease lubrication)

Table 2 Test conditions for high speed running test of the machine tool main spindle bearings with air cooling spacer (grease lubrication)

Test bearing	ϕ70×ϕ110×20 Equivalent to 5S-2LA-BNS014LLB (High speed angular contact ball bearing with grease lubrication seals and ceramic balls)
Preload method	Fixed position preload (preload of 40N after incorporation)
Rotational speed	0～20,000min^{-1}
Lubrication method	Grease lubrication
Grease	SE-1
Outer cylinder cooling	Yes, thermal tuning to room temperature (21±1°C)
Attitude of axis	Horizontal axis

Fig. 7 Relation between cooling air amount and axial rigidity (grease lubricated air cooling spacer)

Fig. 5 Structure of test spindle (grease lubricated air cooling spacer)

5. Challenges for commercialization of grease lubrication air cooling spacer

From the results of the previous Section, it was verified that the machine tool main spindle bearing with air cooling spacer has cooling effect for grease lubrication, as well. On the other hand, by observing the bearing after the high-speed operation test, grease was found attached in the seal gap of the bearing with cooling air supply, as shown in **Fig. 8** . A small amount of grease was observed leaking from the width surface of the bearing.

In order to increase lubrication durability of the bearings, it is desirable to hold as much grease as possible inside the bearings. Therefore, it is necessary to reduce the leakage of grease from the width surface
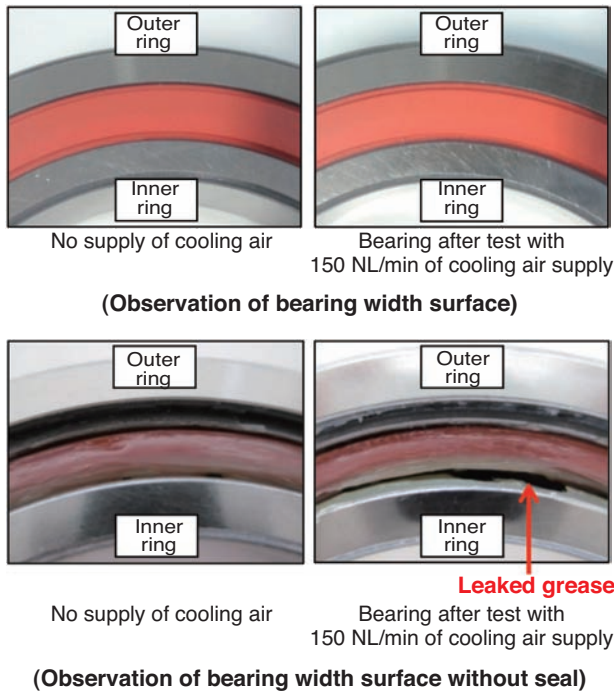
No supply of cooling air

Bearing after test with
150 NL/min of cooling air supply

(Observation of bearing width surface)

Leaked grease

No supply of cooling air

Bearing after test with
150 NL/min of cooling air supply

(Observation of bearing width surface without seal)

Fig. 8 Grease status inside the bearing
after the high speed running test

of the bearings to a minimum. A possible cause of the grease leakage was the flow of cooling air into the bearings. Thus, a change of the spacer shape was studied to let the air exhaust from the exhaust port created on the air cooling spacer, so that the air does not flow into the bearings.

The cooling air flow was simulated under the fluid analysis condition shown in **Table 3**.

Fig. 9 (a) shows the enlarged view of the standard spacer shape evaluated with **Fig. 5**. **Fig. 9 (b)** shows the result of the analysis. When cooling air is supplied to the nozzles of the standard spacer, the cooling air collides with the inner ring spacer and then spreads out to the axial direction with a fast flow rate while maintaining a fast flow rate in the radial direction. A part of the injected cooling air reaches the exhaust port placed on the outer ring spacer; however, a part flows into the bearings. It was estimated that the grease leaked, affected by the air flow into the bearings.

The cooling air flow in the axial direction can be controlled by increasing the gap between the nozzle and the inner ring spacer. By securing sufficient space at the opening of the nozzle, air can flow adhering to the inner ring, maintaining the flow rate toward the tangential direction, which is the direction of injection.

In addition, by creating a slope with large inclination on each side of the inner spacer, the air flow into the bearings can be reduced by guiding the air to the exhaust port, not in the axial direction. The inner ring

spacer was divided into two along with the introduction of the slope for ease of assembly.

The improved spacer with these changes in specification is shown in **Fig. 10 (a)**. The improved spacer is expected to provide better cooling effect as the amount and time of adhesion of air to the inner ring are increased from the standard spacer. As shown in the result of the analysis of **Fig. 10 (b)**, a smooth flow in the tangential direction of the inner ring was verified with reduction of flow into the bearings.

Table 4 shows the percentage of cooling air flown to the bearings and exhaust port, and the ratio of heat transfer between the standard spacer and the improved spacer. With the standard spacer, 50% of the supplied air flows through the bearings; however, it is reduced to approximately 10% with the improved spacer. The heat transfer also shows improvement of 50%. Improvement of cooling effect can be expected with grease lubrication, while preventing grease leakage by using the improved spacer.

Table 3 Fluid analysis conditions

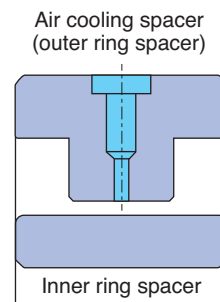| Inner ring rotational speed	$19,100 min^{-1}$
Air pressure	0.2MPa (Equivalent to 150 NL/min of air supply)
Temperature	Inner ring 50°C; other 27°C

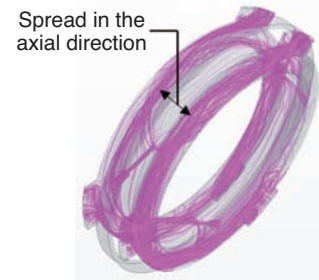**Fig. 9 (a)** Standard designed spacer shape

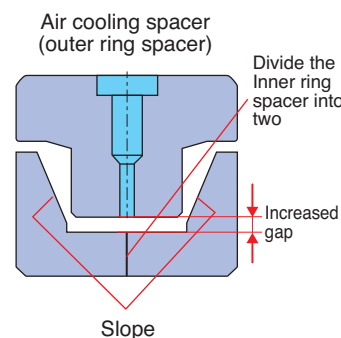**Fig. 9 (b)** Cooling air flow of Standard designed spacer (Fluid analysis results)

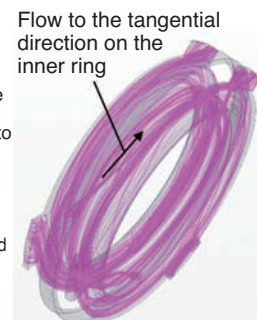**Fig. 10 (a)** Development designed spacer

Fig. 10 (b) Cooling air flow of development designed spacer (Fluid analysis results)

varies significantly and the cooling air flow can change depending on the drive methods and exhaust methods. Therefore, we will develop prototypes and continue verifying the superiority of the improved spacer.

Table 4 Fluid analysis results of standard spacer and development spacer

		Standard spacer	Improved spacer
Flow rate of the cooling air	Exhaust port	41%	87%
	Inside bearing	59%	13%
Heat transfer ratio		1	1.5

6. Summary

Demand of bearings for main spindles using grease lubrication is expected to grow for higher functionality and reduced environmental burden of machine tools. At **NTN,** we have attempted to apply the "machine tool main spindle bearing with air cooling spacer," which uses **NTN**'s proprietary air cooling technology to grease lubrication as a new approach and verified its effect. We will continue to work on improving the performance and refinement of the product, such as ensuring grease retention, toward commercialization.

References
1) Keisuke Nasu, Naoya Okamoto and Masato Yoshino: Machine Tool Main Spindle Bearings with Air Cooling Spacers, NTN TECHNICAL REVIEW, No. 84, (2016) 52.
2) Naoki Matsumori, Keiichi Ueda: Technical Trend of the Precision Bearings for Machine Tools, NTN TECHNICAL REVIEW, No. 84, (2016) 40.
3) Takayuki Kawamura: Research on the Lubrication Mechanism of Grease for High Speed Bearings, NTN TECHNICAL REVIEW, No. 76, (2008) 39, Machine Design, Vol. 60, No. 1 (Jan issue, 2016) 28.
4) NTN Catalog: Precision Rolling Bearings, CAT. No. 2260-VII/J. 16.11.03.82.
5) Yushi Onda, Kikuo Fukada, Yohei Yamamoto and Masato Yoshino: Machine Tool Main Spindle Bearings with Air Cooling Spacers, NTN TECHNICAL REVIEW, No. 82, (2014) 38.

Photo of authors

Keisuke NASU

Industrial Machinery Division
Application Engineering Dept.

Naoya OKAMOTO

Industrial Machinery Division
Product Design Dept.

Yuya TANAKA

Industrial Machinery Division
Product Design Dept.

Tomohiko OBATA

Advanced Technical
Research Center

[New Product]

ULTAGE Precision Standard Angular Contact Ball Bearing, 72U Series

Takayuki KITANO
Youhei YAMAMOTO

NTN has developed the new ULTAGE precision standard angular contact ball bearing, the 72U series for productivity improvement and energy reducing consumption of industrial machinery with a focus on machine tool. The newly developed bearing has adopted the new phenol resin cage. We introduce the design points and results of the above mentioned tests of the "NTN's ULTAGE precision standard angular contact ball bearing 72U series" that have created a new epoch in the areas of load resistance, high-speed and lubrication performance in this paper.

1. Introduction

Recently, further increases in productivity and reductions in energy consumption are demanded in industrial fields including machine tools, in view of social challenges such as the reduction of the labor pool due to decreasing birthrates and aging population, and environmental issues. To respond to these demands, higher output and higher efficiency are required.

Bearings are one of the key components of industrial machines, often referred to as "essential and indispensable in the industry." Many bearings are used in the rotational parts of machinery affecting heat dissipation, efficiency and output; therefore, improvement in performance of the bearings is the key to achieving improvement in performance of machinery.

Angular contact ball bearings have higher load carrying capacity and rigidity than deep grove ball bearings, and are used in many machines in broad industry fields.

NTN has increased performance of angular contact ball bearings of the "70" and "79" dimension series, which are broadly used as bearings for machine tool main spindles, and is already marketing them as 70U/79U Series in the line-up of high functional products under the name of "ULTAGE"[1 2]. Based on this successful outcome and the market trend, we have newly developed the 72U Series, which is the high-function angular contact ball bearing in the dimension series "72."

2. Features of developed product

The precision standard type angular contact ball bearings are superior in load carrying capacity and rigidity compared with the angular contact ball bearings of special high-speed specification, which use rolling elements of smaller diameter [3]; however, their application was limited to lower speed.

In this development, the goal was set to expand the application range and further increase the load carrying capacity while ensuring both rigidity and high-speed capability, which are in a trade-off relationship, by reviewing the internal design of the 72 Series -- which intrinsically has a larger load carrying capacity and higher rigidity than the 70U/79U Series.

2.1 Load resistance

The newly developed product, 72U Series, achieved approximately 1.1 times greater basic dynamic load rating, approximately 1.2 times greater basic static load rating and approximately 1.3 times longer basic rating life compared to the conventional product (**Fig. 1** and **Fig. 2**).

*Product Design Department, Industrial Machinery Division

※1 ULTAGE is a name created from the combination of "ultimate," and "stage," signifying performance in any applications expressing NTN's idea of exploring the ultimate performance of precision bearings [1].

For machine tool main spindles and bearings, impact load (large axial load) may be applied due to unclamping load while exchanging tools during off-operation or unexpected collision of tool attached to the tip of the main spindle and the workpiece.

When the impact load exceeds the design limit, indentation may occur on the raceway, impeding smooth and highly precise rotation. This axial load limit is called permissible axial load (stationary) and **NTN** defines it as the load leading to any of the following [4].

· The end of the contact ellipse produced between the rolling element and the raceway reaches the shoulder of either the inner ring or outer ring raceway. (**Fig. 3**).

· The contact surface pressure of the raceway reaches 3,650 MPa[※2] on either the inner or outer ring.

※2 Contact surface pressure 3,650MPa is a value to produce permanent deformation of 0.00002 to 0.00005 times the rolling element diameter.

H : Height of bearing shoulder
a : Semi-major axis of contact ellipse
F_a : Axial load

Fig. 3 Overflow of the contact ellipse from the raceway

| Part number of bearing | 【Developed product】 7210UC 【Conventional product】 7210C (φ50mm × φ90mm ×20mm Contact angle 15° steel ball specification) |
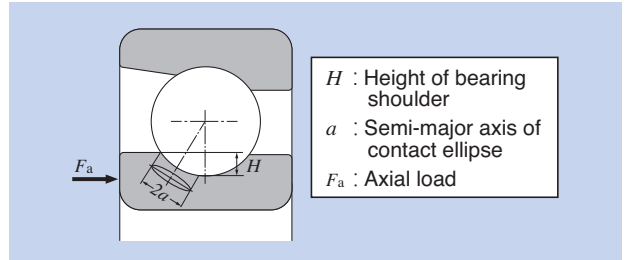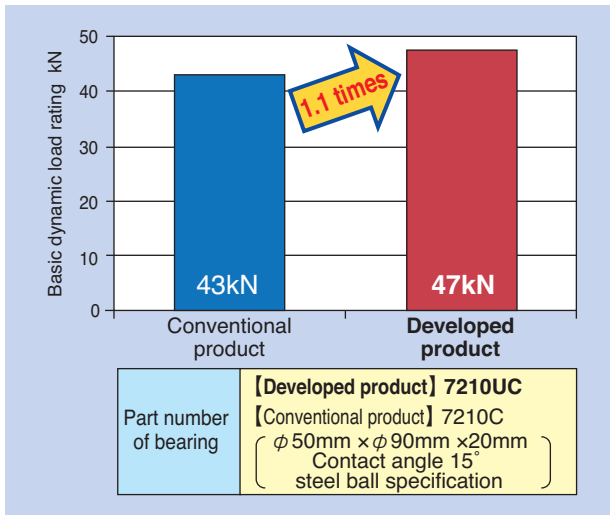
Fig. 1 (a) Basic dynamic load rating (7210C)

| Part number of bearing | 【Developed product】 7220UC 【Conventional product】 7220C (φ100mm × φ180mm ×34mm Contact angle 15° steel ball specification) |
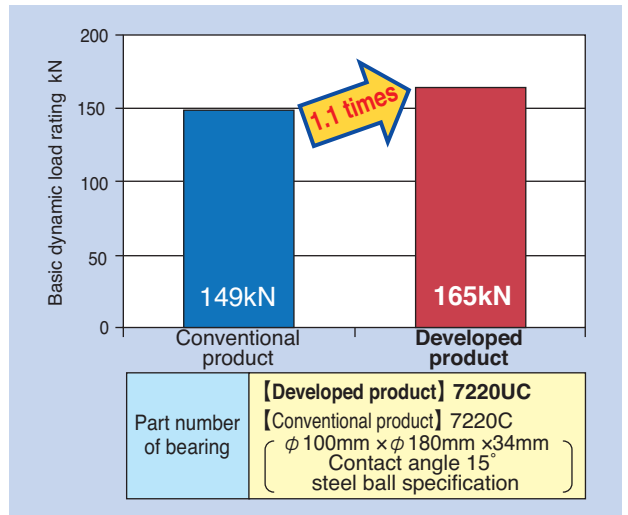
Fig. 1 (b) Basic dynamic load rating (7220C)

| Part number of bearing | 【Developed product】 7210UC 【Conventional product】 7210C (φ50mm × φ90mm ×20mm Contact angle 15° steel ball specification) |
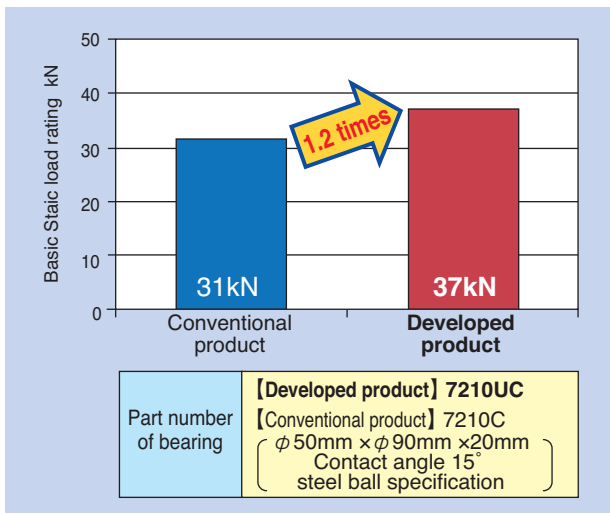
Fig. 2 (a) Basic static load rating (7210C)

| Part number of bearing | 【Developed product】】 7220UC 【Conventional product】 7220C (φ100mm × φ180mm ×34mm Contact angle 15° steel ball specification) |
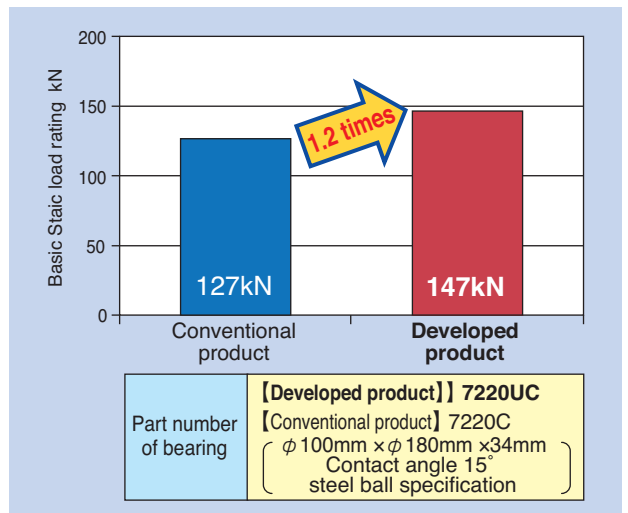
Fig. 2 (b) Basic static load rating (7220C)

The newly developed 72U Series achieved approximately 2.5 times larger permissible axial load, significantly exceeding the conventional product, by reviewing the internal design such as the size of the height of shoulder (**Fig. 4** and **5**).
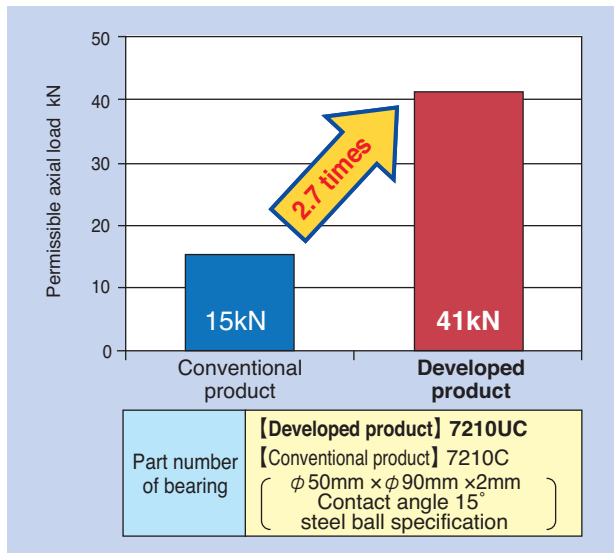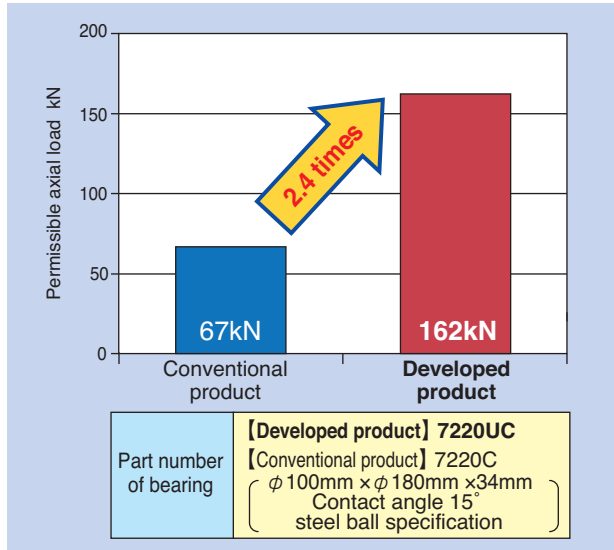

Fig. 4 Allowable axial load (7210C)

Fig. 5 Allowable axial load (7220C)

2.2 High-speed capability (lubricating capability)

For air-oil lubrication, not only the supply of lubricating oil into the bearing but also the drainage of lubricating oil out of the bearing is important. Without smooth supply and drainage, lubricating oil may remain inside the bearing without good heat transfer, resulting in a possible rise in temperature and potential seizure [5), 6)]. To maintain a stable

temperature under high speed operation, an optimum internal design of rolling elements and raceway shapes plus consideration of supply and drainage of lubricating oil are required.

When grease lubrication is used, consideration for grease deterioration due to heat (namely, grease life) is important; therefore, an internal bearing design for grease retention is required.

Even if the conventional product uses the cage made of polyamide resin, the newly developed product adopts the cage made of phenolic resin which has superior properties for high-speed operation with both air-oil lubrication and grease lubrication, and adopts a new shape designed for improved lubricating capability. The key points are described in the following section.

2.2.1 New-shape phenolic resin cage

The groove on the inner diameter surface of the new-shape phenolic resin cage (hereafter, new-shape cage) was deepened compared with the standard design to achieve the following two objectives (**Fig. 6**):
(1) Stabilize cage behavior by improving the cage so that it is actively guided to the outer ring, arranging the contact position of the rolling elements and cage pockets.
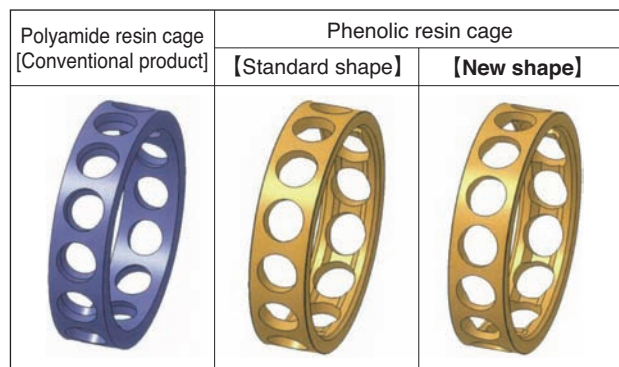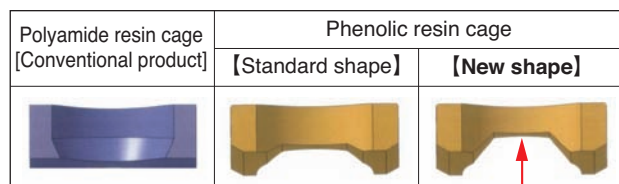(2) Extend the grease life by improving the grease retention, expanding the space for holding the grease.

Fig. 6 (a) Appearance of resin cage

Fig. 6 (b) Bore diameter shape of resin cage

Fig. 7 and **8** show the results of high-speed operation test of the cages with standard shape and new shape. It was verified that the temperature of the bearing outer ring of the new-shape cage, newly adopted this time (○ in the graph) was equivalent to or below the standard shape cage (□ in the graph), both for air-oil lubrication and grease lubrication.
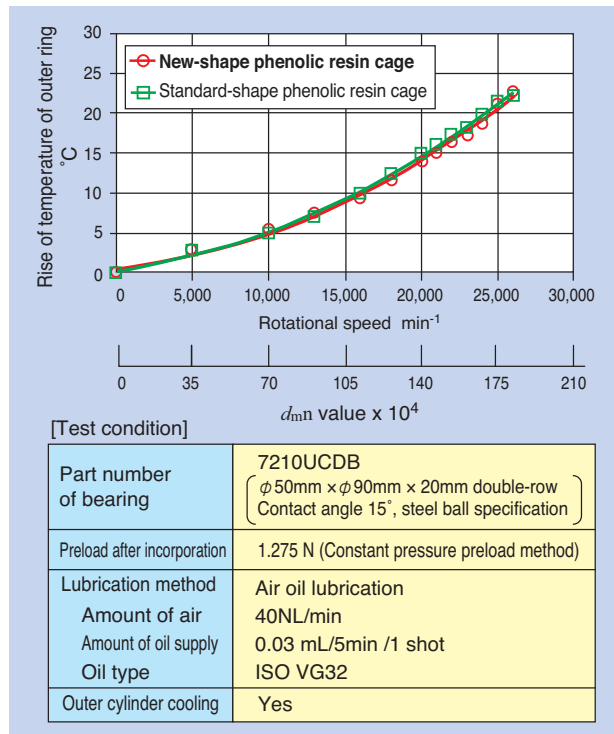

[Test condition]

Part number of bearing	7210UCDB φ50mm × φ90mm × 20mm double-row Contact angle 15˚, steel ball specification
Preload after incorporation	1.275 N (Constant pressure preload method)
Lubrication method Amount of air Amount of oil supply Oil type	Air oil lubrication 40NL/min 0.03 mL/5min /1 shot ISO VG32
Outer cylinder cooling	Yes

Fig. 7 High-speed test of standard and new cage (air-oil lubrication)

[Test condition]

Part number of bearing	7210UCDB φ50mm × φ90mm × 20mm double-row Contact angle 15˚, steel ball specification
Preload after incorporation	980 N (Constant pressure preload method)
Lubrication method Grease brand	Grease lubrication SE-1
Outer cylinder cooling	Yes
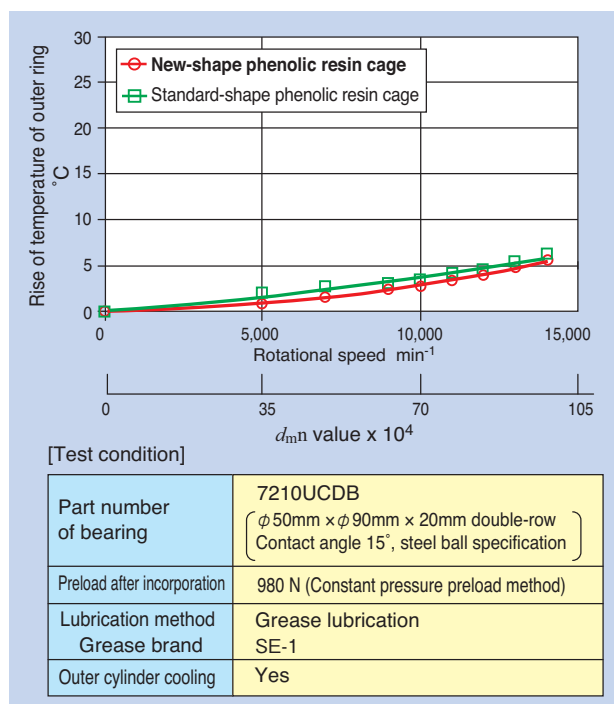
Fig. 8 High-speed test of standard and new cage (grease lubrication)

2.2.2 Modification of inner ring shape

Since the inner ring outer diameter (front side), which is the loaded side of the newly developed 72U Series, affects the permissible axial load, dimensions such as the shoulder height were reviewed. On the other hand, the inner ring outer diameter (back side), which is the anti-loaded side, was designed with lower height than the conventional product to make it easier to supply lubricating oil and grease injection between the cage and the inner ring raceway surface by combining it with the aforementioned new-shape cage. Particularly in the case of air-oil lubrication, this allows supply of lubricating oil from the slanted direction (nozzle target), which was not possible with the conventional product, reducing the restriction of size for installing a spacer with nozzle between bearings, improving the degree of freedom for designing the peripheral structure of the bearings (**Fig. 9**).
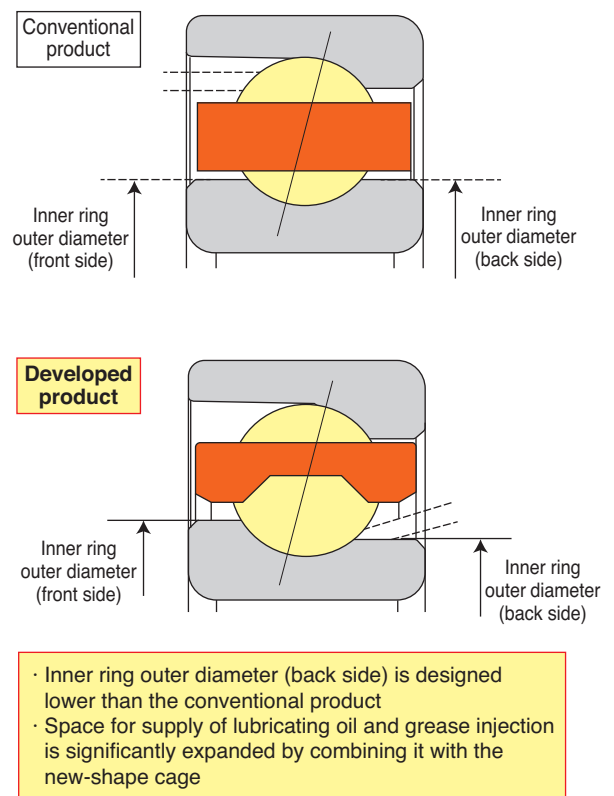

· Inner ring outer diameter (back side) is designed lower than the conventional product
· Space for supply of lubricating oil and grease injection is significantly expanded by combining it with the new-shape cage

Fig. 9 Section of ULTAGE precision standard angular contact ball bearing 72U series

2.3 Rigidity

In order to achieve both rigidity and high-speed capability of the newly developed 72U Series, which are in a trade-off relationship, we checked the impact of the internal bearing design of rolling elements and raceway shapes on rigidity, and when found to be significant, restricted the change to the minimum so that the rigidity can be maintained.

The comparison of the rigidity between the newly developed product and the conventional product is shown in **Fig. 10** and **11**. Although the rigidity of the developed product is slightly lower than the conventional product, it is almost at the same level.

Difference of displacement at F_a = 3 kN: approx. 0.8 μm

Part number of bearing	【Developed product】 7210UCDB 【Conventional product】 7210CDB ϕ50mm ×ϕ90mm × 20mm double-row Contact angle 15˚, steel ball specification
Preload after incorporation	GN preload (fixed position preload method)
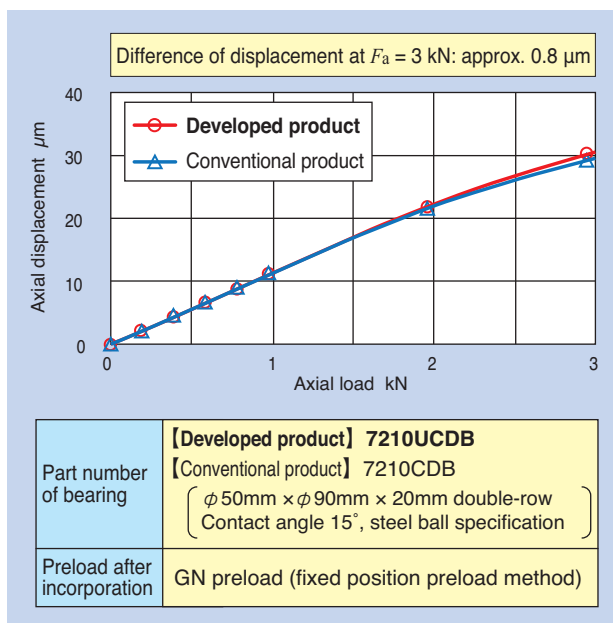
Fig. 10 Axial rigidity (7210CDB)

Difference of displacement at F_a = 5 kN: approx. 0.4 μm

Part number of bearing	【Developed product】 7220UCDB 【Conventional product】 77220CDB ϕ100mm ×ϕ180mm ×34mm double-row Contact angle 15˚, steel ball specification
Preload after incorporation	GN preload (fixed position preload method)
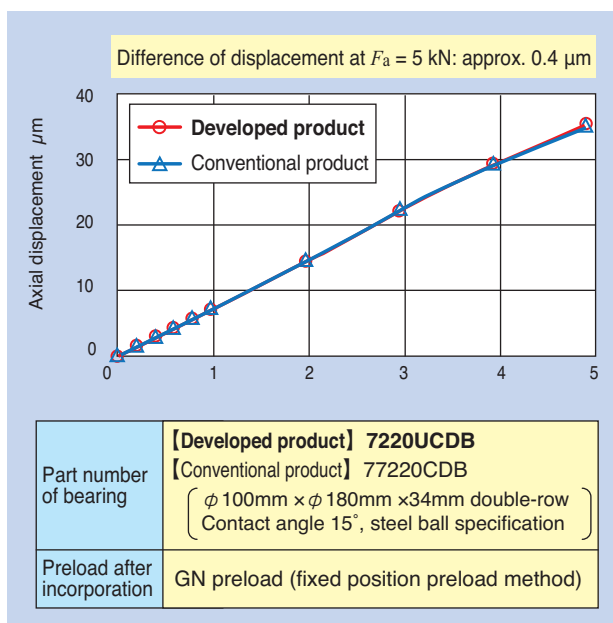
Fig. 11 Axial rigidity (7220CDB)

3. Operation test results

The operation test results under a constant pressure preload of the newly developed 72U Series and the conventional product are shown in **Fig. 12** and **13**. It was verified that the temperature of the bearing outer ring of the developed product (○ in the graph) was equivalent to or below the conventional product (△ in the graph), both for air-oil lubrication and grease lubrication.

This developed product achieved improvement of load carrying capacity and permissible axial load. On the other hand, rigidity of this developed product is maintained at the same level as the conventional product, and by combining with the aforementioned new-shape cage, high-speed capability is also maintained at the stable temperature similar to or below that of the conventional product, achieving approximately 1.6 times larger d_{mn} value[※3] of 1.8 million for air-oil lubrication and approximately 1.1 times larger d_{mn} value of 1 million (both with contact angle of 15˚ and use of steel balls).

※3 d_{mn} value expresses the rotational performance of bearings. d_m (diameter of rolling element (mm) x n (rotational speed (min⁻¹))
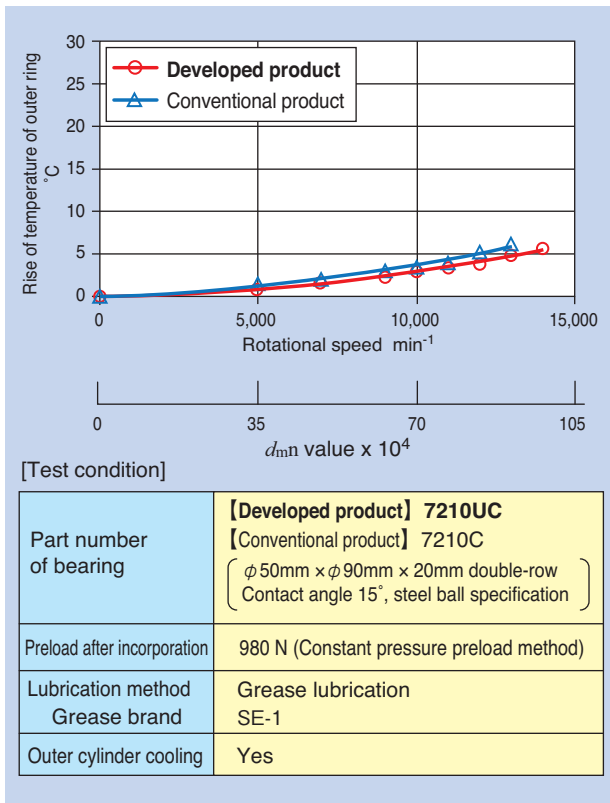

[Test condition]

Part number of bearing	【Developed product】 7210UCDB 【Conventional product】 7210CDB ϕ50mm ×ϕ90mm × 20mm double-row Contact angle 15˚, steel ball specification
Preload after incorporation	1,275 N (Constant pressure preload method)
Lubrication method Amount of air	Air oil lubrication 40NL/min
Amount of oil supply Oil type	0.03 mL/5min /1 shot ISO VG32
Outer cylinder cooling	Yes

Fig. 12 Running test (air-oil lubrication)

[Test condition]

Part number of bearing	【Developed product】 **7210UC** 【Conventional product】 7210C （φ50mm × φ90mm × 20mm double-row Contact angle 15°, steel ball specification）
Preload after incorporation	980 N (Constant pressure preload method)
Lubrication method Grease brand	Grease lubrication SE-1
Outer cylinder cooling	Yes

Fig. 13 Running test (grease lubrication)

4. Series configuration

The configuration of the newly developed 72U Series is shown in **Table 1**. The inner diameter of the bearings is configured from 10 to 130 mm with three contact angles (15°, 25° and 30°). We also added ceramic balls in addition to steel balls for rolling elements.

Table. 1 ULTAGE precision standard angular contact ball bearing 72U series

Steel ball specification	Contact angle 15°	72XXUC
	Contact angle 25°	72XXUAD
	Contact angle 30°	72XXU（A）
Ceramic ball specification	Contact angle 15°	5S-72XXUC
	Contact angle 25°	5S-72XXUAD
	Contact angle 30°	5S-72XXU（A）

Supported bearing size: inner diameter from 10 to 130 mm
(common to both specifications)

5. Summary

The newly developed ULTAGE Precision Standard Angular Contact Ball Bearing 72U Series achieved improved load resistance and equivalent or better high-speed capability compared to the conventional products, while maintaining rigidity.

The developed product is one of the precision bearings that satisfies the market requirement for machine tools and other industrial machines with ongoing requirements for higher functionality.

We are poised to work on the improvement of the existing Series including the Standard Series and development of new Series for our precision angular contact ball bearings.

References
1) Hiroshi Takiuchi and Futoshi Kosugi, "ULTAGE" Series Precision Bearings for Machine Tools, NTN TECHNICAL REVIEW, No. 72, (2004) 26 page.
2) Keiichi Ueda, ULTAGE Standard Angular Contact Ball Bearings, 79U/70U type, NTN TECHNICAL REVIEW, No. 72 (2004) 30 page.
3) Hiroshi Tako and Yasutsugu Tanaka: Technical Trend of Machine Tool Bearings, NTN TECHNICAL REVIEW, No. 78, (2010) 8 page.
4) NTN Catalog: Precision Rolling Bearings, CAT. No. 2260-VII/J. 16.11.03, (2016) 21 page.
5) Keiichi Ueda, Technical Trend of the Bearings for Machine Tools, Eco-friendly Technologies, THE TRIBOLOGY No. 188, (2003, 4) 19 page.
6) Keiichi Ueda, Technical Trend of the Precision Bearings for Machine Tools, NTN TECHNICAL REVIEW, No. 84, (2016) 40 page.

Photo of authors

Takayuki KITANO
Industrial Machinery Division
Product Design Dept.

Yohei YAMAMOTO
Industrial Machinery Division
Product Design Dept.

[New Product]

Plastics Sliding Sheet Used Slide Guide of Machine Tools
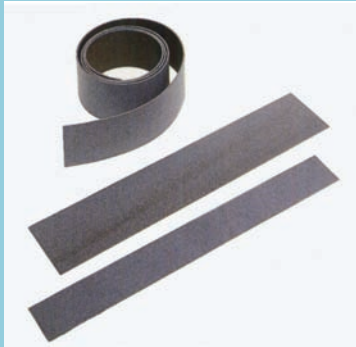
Takuya ISHII*   Satoru FUKUZAWA*   Norikazu MUNEDA*

Machine tools are required to operate at high speed, high precision. The models of using plastics sliding sheet in guide are increasing. When cutting resistance is high, the models are superior in processing precision by low vibration. Low friction properties and wear resistance are required to plastics sliding sheet. In this report, characteristic of sliding sheet formed from PTFE and special filler is introduced.

1. Introduction

Machine tools process workpieces using relative motion between the tools and workpieces; therefore, performance of the guideway which moves either the tool or workpiece has a significant impact on processing accuracy. There are two types of guideways, rolling type and sliding type, which are selected depending on the use. The rolling type, such as a linear guide, moves tools or workpieces with rollers. The sliding type either uses lubricating oil on the guideway for sliding between two metal surfaces or uses a plastic sliding sheet adhered to one of the metal surfaces for sliding between the other metal surface. For the sliding sheet material, polytetra fluoroethylene (PTFE) is used for its low friction and high anti-galling properties. The properties of the plastic sliding sheet play a critical role since the sliding surface is in mixed lubrication condition.

In this article, we describe the sliding sheet for machine tool guideways made of BEAREE FL3307, which is PTFE blended with special filler material, for improved friction wear properties under the mixed lubrication condition.

2. Characteristics of various guide types [1)]

Table 1 shows the features of different guide types. The rolling guide type has low friction resistance and is capable of moving tools or workpieces at high speed without causing stick slip; therefore, it provides high processing accuracy. However, since the area of contact is small due to line contact of the rollers, rigidity is low and vibration may occur under heavy load. Therefore, it is not suitable for processing objects with high cutting resistance.

The sliding guide type has a large area of contact due to plane contact leading to a high rigidity; therefore, it is suitable for processing objects with high cutting resistance. By using a plastic sliding sheet on the guideway, a high vibration damping property can be achieved and stick slip can be largely prevented compared to sliding between two metal materials. In addition, seizure can be avoided even under poor lubrication conditions.

Fig. 1 shows an overview diagram of the machine tool sliding guide type. Recently, as the cases of processing

Table 1 Characteristic of guide type in machine tools

Item	Sliding guide type		Rolling guide type (Linear guide)
	Plastic sliding	Metal sliding	
Rigidity	○	○	△
Vibration damping properties	◎	○	△
Friction resistance	○	△	◎
Stick slip	○	△	◎

◎：Excellent   ○：Good   △：Fair

Moving part to fix tools or workpieces

Guideway
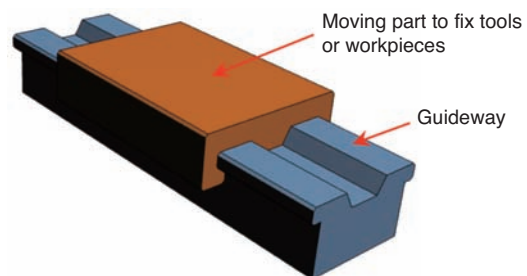
Fig. 1 Slide guide type of machining tools

*Precision Plastic Engineering Dept. Composite Material Product Division

difficult-to-cut materials, such as carbon fiber reinforced plastics, are increasing, machine tool models with sliding guideways using plastic sliding sheets are becoming more popular due to their superior processing accuracy with low vibration even when the cutting resistance is high.

3. Performance required for plastic sliding sheet

In the sliding guideway type, oil grooves are created on the guideway to facilitate the formation of a lubricating film. In addition, scraping is also applied on the surface to create a uniform contact condition with micro dimples of several tens of μ m [2]. **Fig. 2** shows the surface conditions before and after scraping on a BEAREE FL3307 plastic sliding sheet. Scraping is done by hand by skilled technicians. The plastic sliding sheet has an advantage over metal material for easy scraping.

The micro dimples on the guideway created by scraping increases lubricating oil retention and stabilizes friction resistance to a low level. When the plastic sliding sheet wears out or is deformed by the load, the dimples on the sliding surface are reduced which increases the friction resistance; therefore, the plastic sliding sheet requires good wear and compression creep resistance.

For machine tools, high speed transfer of tools or workpieces is required in order to reduce machining cycle time. Therefore, it is desirable for plastic sliding sheets to have low starting static wear coefficient and dynamic friction coefficient, as well as low contact pressure and speed dependency [3].

Before scraping   After scraping
Fig. 2 Hand scraper surface of plastics sliding sheet

4. Features and manufacturing process of PTFE plastic sliding sheet

PTFE has low friction coefficient, high non-adhesive properties, and a high heat tolerance up to a continuous operating temperature is 260˚C. It also has excellent chemical and weathering resistance enabling its use on the guideway, which is in contact with lubricating oil and coolant for a long time. PTFE alone, however, has poor friction and compression creep resistance and a large linear expansion coefficient; therefore, fillers such as glass fiber, carbon fiber, bronze powder, graphite, etc. are blended into the material. The friction/wear properties change depending on the fillers and blend ratio. It is important to choose the right filler and blend ratio for the specific use.

Fig. 3 shows the manufacturing process of sliding sheets for machine tool guideways. As PTFE has high melt viscosity preventing injection molding, a plastic sheet of 0.8 to 1.5 mm thickness is manufactured by skiving the material from a compression molding. Skiving is a manufacturing process to obtain sheets from the mold material by slicing it with a blade while rotating the mold material.

Since PTFE has high non-adhesive properties and cannot be adhered as is, the surface is chemically etched by treatment liquid so that it can be adhered. **NTN** has prepared an adhesive dedicated for adhering the plastic sheet on the guideways made of cast iron, etc. which has resistance against lubricating oil and coolant. The tensile shear strength of cast iron and BEAREE FL3307 plastic sliding sheet using this adhesive is 6 MPa and has a sufficient safety factor against frictional shear of 0.06 MPa calculated from the used contact pressure and friction coefficient (when contact pressure is 1 MPa and friction coefficient is 0.06).

Compression molding

Skiving
Width 300mm, length 30m
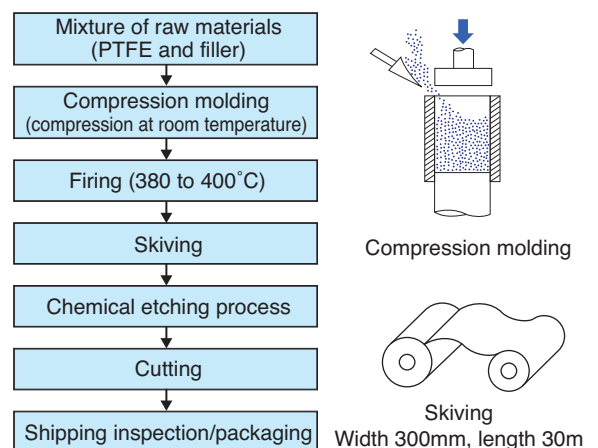
Fig. 3 Manufacturing process of plastics sliding sheet

5. Performance of NTN plastic sliding sheet

A comparison of the performance of 3 types of plastic sliding sheets (BEAREE FL3307 (hereafter, **NTN** product), glass fiber (GF) blended PTFE (hereafter, Comparison Product A) and carbon fiber (CF) and bronze powder blended PTFE (hereafter, Comparison Product B)) was performed. **Table 2** shows the comparison of performance.

NTN product has higher tensile strength and elongation with superior friction wear properties and compression creep properties. Details of the test method and results of the friction wear and compression creep properties are described below.

Table 2 Comparison of features plastics sliding sheets

	Item	NTN product	Comparison product A	Comparison product B
	Sheet material	BEAREE FL3307	GF blended PTFE	CF and bronze powder blended PTFE
Physical properties	Tensile strength	20MPa	15MPa	13MPa
	Elongation	220%	200%	180%
Friction properties	Static friction property	○	△	△
	Contact pressure dependency of dynamic friction coefficient	○	△	△
	Speed dependency of dynamic friction coefficient	○	○	△
	Compression creep properties	○	△	△

○：Good △：Fair

5.1 Friction wear test method

The reciprocating motion tester shown in **Fig. 4**, which simulates the guideway of machine tools, was used for the friction wear test. A vertical load was applied to a metal block test piece, which has the plastic sliding sheet adhered to it, and the metal mating material was set in reciprocating motion. The plastic sliding sheet was not scraped but oil grooves were applied after adhesion. The metal mating material is meehanite cast iron with surface roughness of Ra 0.25 μm which is induction hardened and polished on the sliding direction. Lubricating oil for machine tools was applied on the sliding surface.

The friction coefficient was calculated by dividing the friction force, which was measured by the load cell attached to the mating material, by the vertical load.
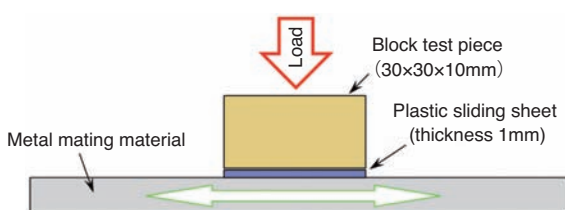
Fig. 4 Diagram of reciprocating motion test

5.2 Contact surface/speed dependency of dynamic friction coefficient

The dynamic friction coefficient was measured by changing the contact pressure and speed under the test condition shown in **Table 3**. **Fig. 5** shows the relation between the contact pressure and the dynamic friction coefficient and **Fig. 6** shows the relation between the speed and the dynamic friction coefficient.

The dynamic friction coefficient tends to decrease as the contact pressure increases. In the contact pressure dependency test, the dynamic friction coefficient of **NTN**'s product was slightly lower than the comparison products, and the dependency was small when the contact pressure was higher than 0.3 MPa. In the speed dependency test, the dynamic friction coefficient of **NTN**'s product was equivalent to or less than the comparison products with small speed dependency.

Fig. 7 and **8** are the photographs of the plastic sheet of **NTN**'s product and Comparison Product A, taken by scanning electron microscope. Fillers are exposed on the sliding surface of the plastic sheet.

Table 3 Test condition of dynamic friction

Item	Contact pressure dependency test	Speed dependency test
Contact pressure	0.1 to 1.0 MPa	0.5MPa
Speed	30m/min	10～50m/min
Stroke	±100mm	
Lubricating oil	Lubricating oil for machine tool	
Temperature	Room temperature	
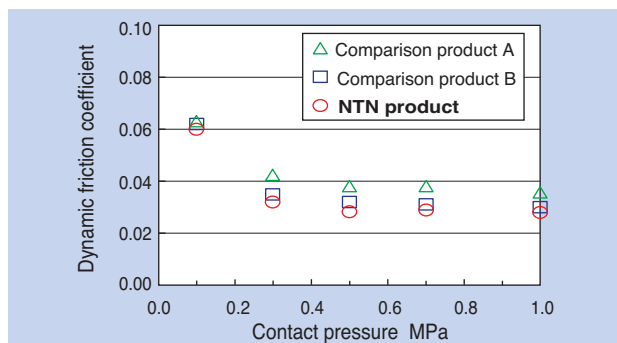
Fig. 5 Coefficient of dynamic friction versus surface pressure
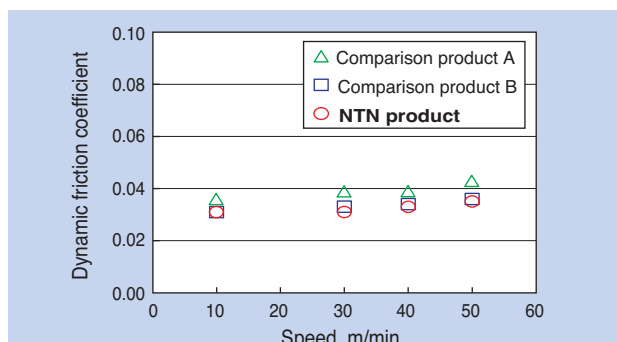
Fig. 6 Coefficient of dynamic friction versus velocity
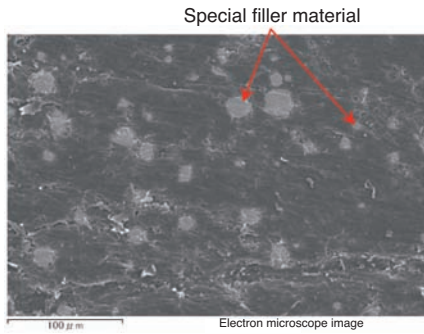
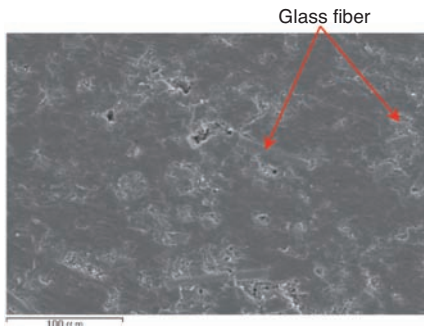Fig. 7 Surface of **NTN** plastics sliding sheet

Fig. 8 Surface of comparative-A plastics sliding sheet

In Comparison Product A, the direction of fiber filler material is random, with some only exposing the ends of the fibers. Fiber fillers are not likely to fall out when a frictional shear force is applied due to their shape; however, the friction coefficient does increase due to the resistance of the fiber end's edges. This is also true with Comparison Product B, which is blended with carbon fibers. **NTN**'s product has fillers scattered on the sliding surface; however, these fillers are not fiber-like and not anisotropic; therefore, they are unlikely to increase friction coefficient.

The sliding surface can easily form an oil film due to the oil grooves and micro dimples (from scraping); however, it is in mixed lubrication condition as the plastic sliding sheet is partially in contact with the mating metal material. When this contact becomes plane contact, lubricating oil is ejected, resulting in a higher friction coefficient. It is assumed that **NTN**'s product creates point contact at the exposed fillers; therefore, lubricating oil remains on the contact surface, resulting in a good lubrication condition and low friction coefficient.

5.3 Wear properties

Fig. 9 shows the specific wear rate of **NTN**'s product when tested for wear under the test conditions shown in **Table 4**. Specific wear rate is the volume of wear per sliding distance per load, which is calculated from the measurements before the test and after the test. The smaller the specific wear rate, the better the wear resistance.
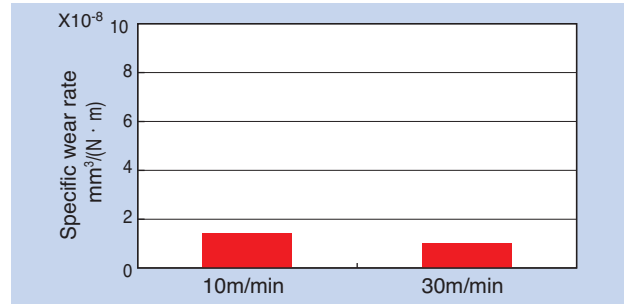
Fig. 9 Specific wear of **NTN** Plastics sliding sheet

Table 4 Wear test condition

Item	Description
Contact pressure	0.5MPa
Speed	10m/min, 30m/min
Stroke	±100mm
Lubricating oil	Lubricating oil for machine tool
Temperature	Room temperature
Time	100h

The specific wear rate of **NTN**'s product is very low at any speed and is superior in wear resistance.

6. Summary

In this article, we introduced the BEAREE FL3307 Plastic Sliding Sheet, used in the sliding guideways of machine tools. This material mix has low friction, low wear properties, and a small compression creep deformation rate, which contributes to higher speed and higher machining accuracy of machine tools.

We will continually improve our material blending technologies for lower friction/wear and develop products that meet the demands of higher functionality and energy efficiency in various fields.

References
1) Japanese Society of Tribologists: Tribology Handbook, 1st issue, Yokendo, (2001) 343.
2) Haruhisa Sakamoto: Triboloty Technology and Trends in Machine Tools, THE TRIBOLOGY No. 331, (2015) 18-20.
3) Fumio Obata: Research and Development of low sliding friction coefficient/High Chatter Resistance Sliding Linear Guide, Innovation Japan 2009---University Trade Fair, Conference No. PM-08.

Photo of authors

Takuya ISHII
Composite Material Product Division
Precision Plastics Engineering Dept

Satoru FUKUZAWA
Composite Material Product Division
Precision Plastics Engineering Dept

Norikazu MUNEDA
Composite Material Product Division
Precision Plastics Engineering Dept

Lubrication Mechanism of Low Friction Seal of Ball Bearing for Transmission

Tomohiro SUGAI[*]
Katsuaki SASAKI[**]
Takahiro WAKUDA[**]
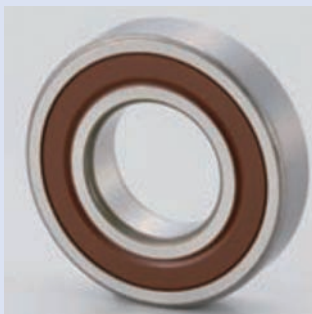
A low friction seal for use in ball bearings developed for automotive transmissions has arc-shaped (half-cylindrical shaped) micro bumps on the sliding surface of the seal lip. This generates a lubrication oil film between the seal lip and inner ring by a wedge effect in the bump area, thereby achieving low friction.

This article reports the mechanism of fluid film formation and friction resistance by soft EHL (ElastoHydrodynamic Lubrication) analysis.

1. Introduction

Contact type seals may be used in bearings for automotive transmissions to reduce the impact on bearing life caused by hard foreign objects penetrating the bearings, such as wear debris from the gears in the transmission. However, since these seals come in contact with the bearing inner ring, frictional torque during rotation may increase. Furthermore, in applications where high-speed rotation is required, such as recent EVs and HEVs, the use of contact type seals is difficult due to the restricting seal peripheral speed limits. Although further torque reduction is a requirement for bearings used in automotive transmissions, since torque reduction and sealing performance are conflicting properties, it has been difficult to achieve significant torque reduction while ensuring a high level of seal performance.

To solve this challenge, **NTN** has developed a low friction ball bearing seal for transmission applications that uses arc-shaped (half-cylindrical shaped) micro bumps in equal distance on the surface of the seal lip that slides against the bearing inner ring [1]. This seal achieves lower torque while satisfying the required bearing life, since the height of the bumps is smaller than the size of the foreign objects that affect bearing life, based on the relationship between the foreign object size in the lubricating oil and bearing operating life. Ordinary seals are considered to operate in a mixed lubrication or fluid lubrication condition [2,3]; however, since the formed oil film is very thin (less

than the magnitude of roughness), due to micro EHL (elastohydrodynamic lubrication) from the rough surface, shear resistance is large even if the seals are in a fluid lubrication condition. This new seal, on the other hand, produces a pressure gradient in the lubricating oil that flows along the circumference of the inner ring with micro bumps that are larger than the surface roughness of the seal and inner ring, to actively create oil film of lubricating oil on the sliding surface between the seal lip and bearing inner ring. This facilitates fluid lubrication, reduces the rotational torque, and improves the peripheral speed limit.

In this article, we review the investigation results of the oil film formation mechanism and friction resistance using soft EHL analysis, which provides coupled analysis of the elastic deformation of the entire seal, including bumps, and the fluid pressure of lubricating oil.

2. Soft EHL analysis

2.1 Analysis model and program

Fig. 1 shows the developed seal. The figure on the left shows the cross section of the bearing with the seal and the figure on the right shows the cut out view of the seal along the circumference. Arc-shaped (half-cylindrical shaped) micro bumps in equal distance on the seal sliding surface contact the bearing inner ring. The bumps are curved in the axial direction as well, providing point contact with the inner ring sliding surface when they are installed in the bearing as

---

[*]Advanced Technology R&D Center
[**]Automotive Bearing Engineering Dept., Automotive Business Headquarters

Arc-shaped (half-cylindrical shaped micro bumps
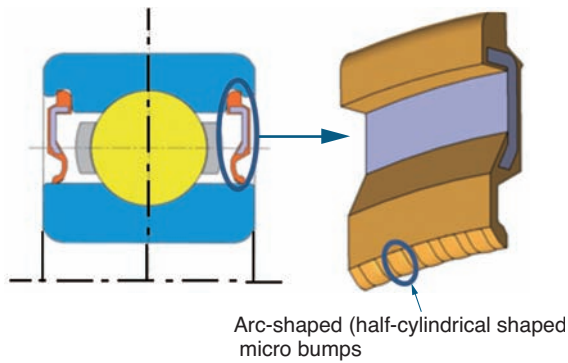
Fig. 1 Low friction seal

shown in **Fig. 2**. As shown in **Fig. 3**, at the bumps, the distance from the sliding surface gradually decreases in the circumferential direction, namely, direction of the flow, which, while rotating, produces fluid pressure in the lubricating oil on the sliding surface in a gradient, forming an oil film between the seal sliding surface and the inner ring. When enough oil film is formed on the sliding surface, it creates a fluid lubrication condition and frictional torque is expected to decrease compared with the conventional seal without these bumps. The thickness of the oil film between the seal lip and bearing inner ring, and seal frictional torque due to fluid viscosity resistance are calculated by the soft EHL analysis coupling the oil film pressure and seal deformation.

In general, when oil film analysis of rolling bearings is performed, semi-infinite elastic body approximation

Inner ring

Micro bumps

(a) Before deformation

Point contact

(b) When mounted in bearing
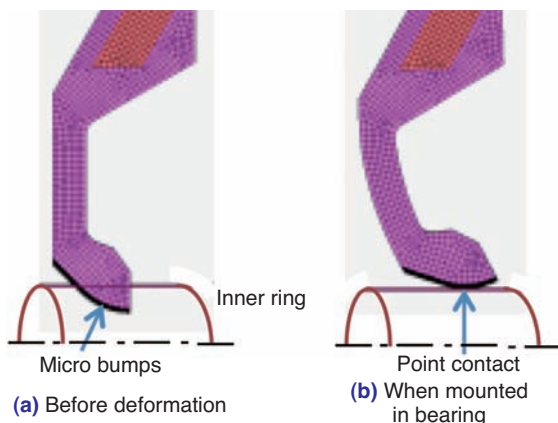
Fig. 2 Deformed shape of the seal lip mounted in bearing

Pressure distribution

Seal

Oil flow

Inner ring

Direction of rotation
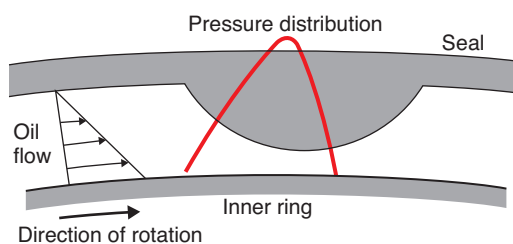
Fig. 3 Wedge action at the micro bump

is used in structure analysis for calculating shapes since the elastic deformation is small. However, when rubber seals are analyzed, semi-infinite elastic body approximation does not work as the elastic deformation is large; therefore, non-linear structure analysis is required [4]. Changes of the lubricating oil properties due to pressure are not considered, since the increase of pressure in the oil is small because the seal deforms more easily due to the increased pressure. Seal deformation, including that of the bumps, is calculated using general purpose non-linear analysis software with the finite element method, and the oil film pressure is calculated using the solution of the following Reynolds equation that describes viscous fluid motion on the lubricating surface [5].

$$\frac{\partial}{\partial x}\left(\frac{\rho h^3}{12\eta}\frac{\partial p}{\partial x}\right) + \frac{\partial}{\partial y}\left(\frac{\rho h^3}{12\eta}\frac{\partial p}{\partial y}\right) = u_0 \frac{\partial(\rho h)}{\partial x}$$

Where, x: coordinate in the flow (circumferential) direction, y: coordinate in the direction perpendicular to flow (rotational axis), ρ: density, h: oil film thickness, η: lubricating oil viscosity, p: pressure, u_0: velocity on the sliding surface. In addition, flow rate in the x direction u is a function of the coordinate in the direction of the film thickness z and can be expressed by the following equation.

$$u = -\frac{1}{2\eta}\frac{\partial p}{\partial x}z(h-z) + \left(1-\frac{z}{h}\right)u_0$$

The first term of the right side is the Poiseuille flow induced by the difference of pressure and the second term of the right side is the Couette flow induced by the motion of the wall surface. For the cavitation condition, Swift-Steiber's condition [6] was used. In addition, a periodic boundary condition was used as this is an axisymmetric problem.

By repeating structure analysis and fluid analysis, a convergent solution was obtained. Since the oil film pressure significantly changes with a small change of oil film thickness, and the seal deformation is significantly affected by a small change of pressure, convergence properties may be degraded by strong non-linearity in the coupled analysis. By appropriately controlling the relaxation amount according to the convergence condition in an iterative computation when the Reynolds equation is solved with the relaxation method [7], we have enabled calculation with good convergence properties, as shown in **Fig. 4**. The calculation was performed in the following two steps:

First step: The condition of the bearing with inner ring, outer ring and seal is calculated with structure analysis only. This is equivalent to the condition of the seal while not rotating.

Second step: Using the calculation result of the first

step as the initial condition, coupled analysis with the fluid is performed. This is equivalent to the conditions when the seal is rotating. The initial oil film thickness is set by exploring the inner ring position where the load capacity and tension force due to oil film pressure are balanced, with the seal shape as calculated in the first step (not rotating). In the first half of this step, inner ring position is returned to the predetermined position.

In the calculation of torque, a fluid lubrication condition was assumed with the seal lip sliding surface and the inner ring well separated by the oil film and only torque due to viscosity resistance of the lubricating oil considered.

along with the flow at the minimum film thickness position. Approximately 0.22 MPa of maximum pressure was observed. The minimum oil film thickness was about 1 μ m. The composite roughness

Table. 1 Properties and conditions

Seal material	Acrylic rubber
Bearing inner ring OD (mm)	64
Bump radius (mm)	1.5
Bump height (μm)	40
Number of bumps	180
Lubricating oil dynamic viscosity (40˚C) (mm²/s)	26
Rotational speed (min⁻¹)	1500
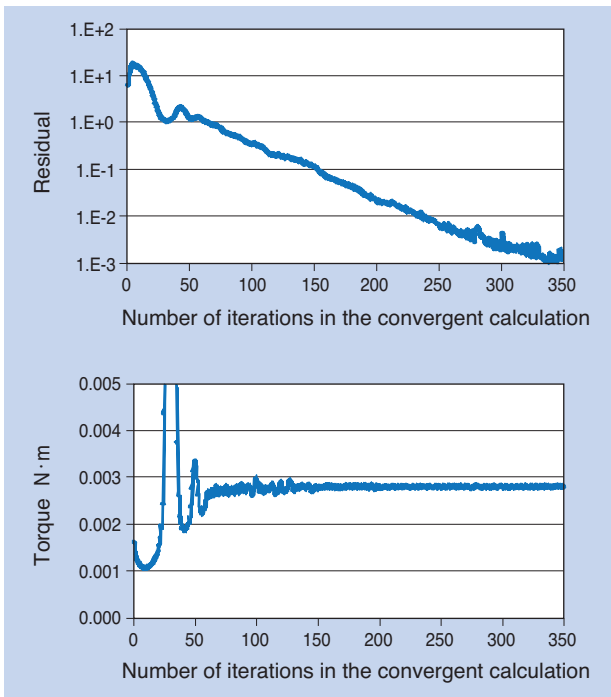
Fig. 4 Convergence of calculation
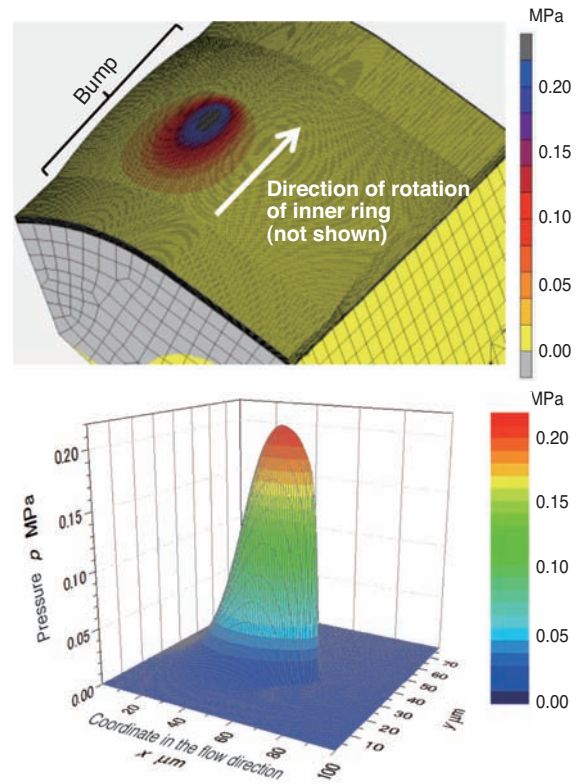
Fig. 5 Calculation result of oil film pressure distribution

2.2 Conditions and results of calculation

The properties and operating conditions of the developed seal under review are shown in **Table 1**. The rubber rigidity and lubricating oil viscosity were defined as a function of temperature considering thermal expansion of the rubber. In this article, impact from surface roughness, stress relaxation of rubber, pressure to lip seal by oil flow within the transmission, shaft run-out, etc. are not considered. **Fig. 5** and **6** show an example of the calculation results. **Fig. 5** shows oil film pressure distribution against the seal lip sliding surface, while the diagram above shows the picture of the seal lip sliding surface viewed from the inner ring side. Oil film pressure is shown at the bump. **Fig. 6** shows oil film thickness and pressure distribution
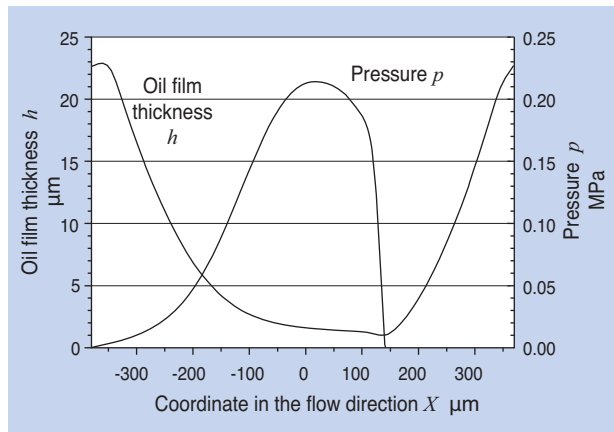
Fig. 6 Oil film thickness and pressure distribution

of sliding surface is about Rq 0.22 μm. Sufficient oil film is formed on the surface compared to the roughness, creating a fluid lubrication condition. **Fig. 7** shows the relationship between temperature and minimum film thickness. The oil film thickness is reduced as the temperature rises; however, the minimum film thickness is about 1 μm even at 150˚C, which is sufficient compared to the roughness. **Fig. 8** shows the relationship between temperature and seal torque. The indicated torque comes from two seals used in one bearing. In addition, factors making up the total torque are categorized into the following three

groups and color coded: torque caused by the Poiseuille flow at the bumps, torque caused by the Couette flow at the bumps, and torque caused by the Couette flow at the non-bump area, which is the sliding surface between the bumps. Since the increase in pressure at the non-bump area is small, torque caused by Poiseuille flow at the non-bump area is also small and not shown. The torque decreases as the temperature rises, to approximately 0.007 Nm at 120˚C. The main factor of the torque is the Couette flow at the bump area. **Fig. 9** shows the relation between the number of bumps and torque. When bumps are fewer, torque due to the Couette flow at the non-bump area increases. The reason for this is that the area of the sliding surface at the non-bump area increases and, in addition, the gap of the sliding surface of non-bump area decreases. When the sliding surface gap decreases, the shear resistance and seal torque increase. When there are fewer bumps, the distance between the bumps increases, and the sliding surface of the non-bump area undergoes elastic deformation due to the tension force, moving it closer to the inner ring sliding surface and reducing the gap between the sliding surfaces. **Fig. 10** shows a schematic diagram of the non-bump area. **Fig. 11** shows the relationship between the number of bumps and the gaps between bumps under non-operating conditions. In the figure, the gap in the area between bumps is shown as a ratio against the

Fig. 7 Relationship between temperature and minimum film thickness

Fig. 8 Relationship between temperature and seal torque
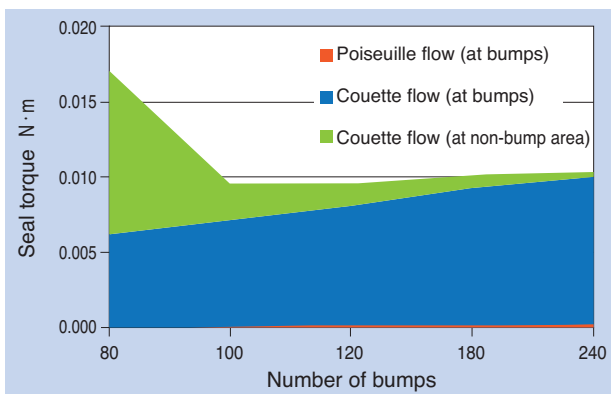
Fig. 9 Relationship between number of bumps and seal torque
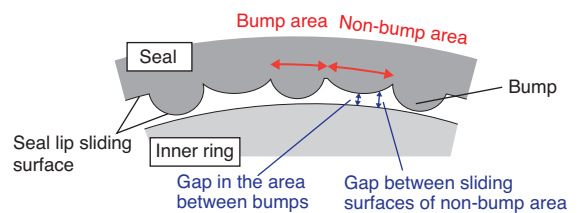
Fig. 10 Schematic drawing of elastic deformation of non-bump area
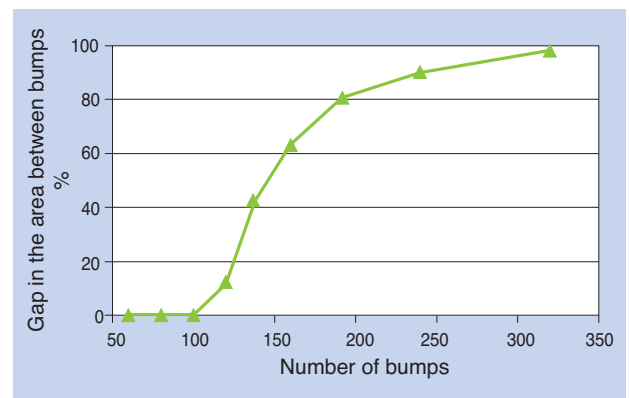
Fig. 11 Relationship between number of bumps and gaps in the middle between bumps under non-operating condition

height of the bumps. In this study, when the number of bumps is around 100 or less, the gap in the area between bumps becomes 0, which means that the sliding surface of the non-bump area comes in contact with the inner ring. However, during operation, an oil film is formed by the pressure gradient created when the non-bump area is close to the inner ring, resulting in no direct contact between the surfaces.

When the number of bumps increases, torque due to the Couette flow at the bump area increases. The more bumps, the lower the tension force per bump; therefore, the minimum film thickness of the bump area increases and the torque increases, because the total area of sliding surface of the bumps increases. Under the conditions of this study, the lowest torque result occurred when the number of bumps was around 100.

3. Verification test

3.1 Oil film thickness

The oil film thickness at the seal bump area was measured using the infrared microspectroscopic method. The infrared spectroscopic method is a method of structural analysis and quantification of substances that uses infrared rays applied to the test pieces and analyzes the spectrum obtained from transmitted or reflected light. When infrared rays are transmitted through substances, light in a certain frequency range is absorbed by the substance and the intensity of light through the substance is weakened. The intensity of light through the substance and the light path length are correlated. **Fig. 12** shows the schematic diagram of the measurement device. Since acrylic rubber absorbs infrared rays, 0.3 μm of gold is vacuum deposited on the surface of the acrylic rubber so that the light is reflected on the rubber surface. The test piece, which simulates a seal bump, is pushed into the rotational sapphire disc and infrared rays are irradiated to the disc from the opposite side. Oil film thickness can be estimated by measuring the intensity
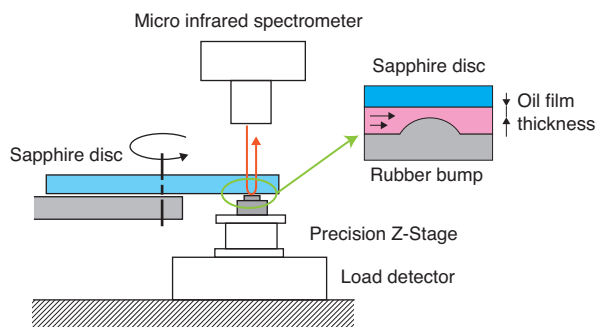
of light reflected on the bump surface, after it is transmitted through the oil film. The pressure of the rubber bump to the disc is controlled by the Z-stage. In this experiment, the pressure and speed are set as parameters.

The measurement results and calculation results from the soft EHL analysis are compared in **Fig. 13**. Both results show the same trend and approximate magnitude, verifying an oil film thickness of around 1 μm. However, the measured value is larger than the analysis results in the range where the oil film is thinner. The reason for this difference may be the impact from the measuring range and vibration of the sapphire disc surface. The analysis shows the minimum film thickness; however, the measurement result is the average of a 30 x 30 μm area; therefore, the measurement value of the oil film thickness may have been larger. Also, there was approximately 0.35 μm of disc surface vibration due to the rotation, which may have resulted in a larger measurement value of oil film thickness.
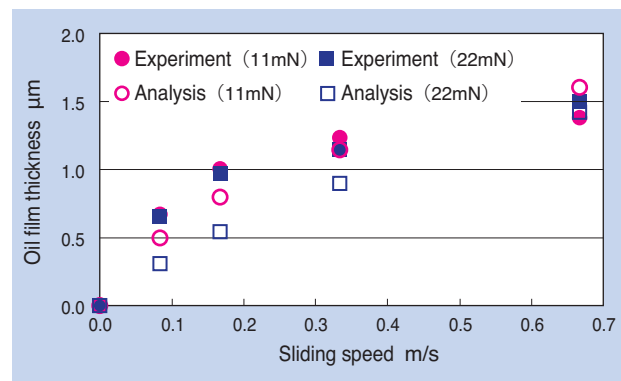
Fig. 13 Comparison of experimental results with analysis ones of film thickness

3.2 Bearing torque

The bearing torque was measured by installing the developed seal on a bearing designed for use in a transmission. The specification of the seal and the test conditions were the same as shown in **Table 1**. The lubricating method was an oil bath with the upper surface of the lowest rolling element at the oil level. In addition, 754 N of radial load was applied to the bearing. This measurement result and measurement results of bearings using the conventional contact type seal and non-contact type seal without bumps are shown in **Fig. 14**.

When compared to the bearing using the conventional contact type seals (without bumps), the torque of the new seal with bumps is reduced by 80% or more. Conventional contact type seals are considered to operate in mixed lubrication or fluid

Fig. 12 Schematic drawing oil film thickness measuring device

lubrication conditions, including solid contact; however, since the formed oil film is very thin due to micro EHL (elastohydrodynamic lubrication) from the rough surface, shear resistance is large even if the seal is in a fluid lubrication condition. On the other hand, the developed seal forms sufficient oil film at the bumps creating a fluid lubrication condition, which is assumed to be the one of the contributing factors for the reduction of friction torque. In addition, as shown in **Fig. 9**, when the number of bumps is not too small, since the torque at the non-bump area due to the Couette flow is small compared to the torque due to the Couette flow at the bumps, the distance of sliding surfaces in the developed seal is increased, which should also contribute to the reduction of friction torque.

The increase of torque compared to a bearing with the conventional non-contact type seal is around 0.01 Nm. Since the seal torque of non-contact type seal is estimated to be very small, the seal torque of the developed seal is estimated as around 0.01 Nm, which is equivalent to the calculation results shown in **Fig. 8** and **9**.
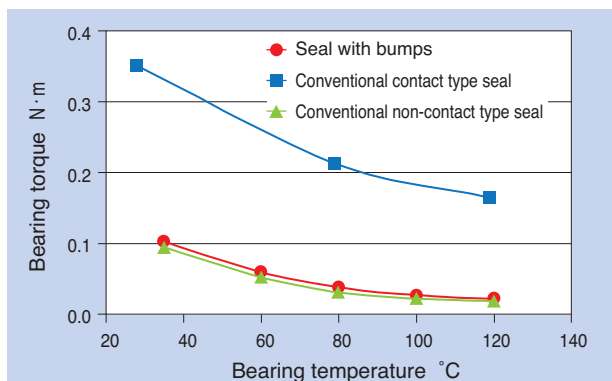
Fig. 14 Experimental results of bearing torque

4. Conclusion

We have developed an oil film analysis program for investigating the mechanism of oil film formation and friction resistance of a newly developed seal. This seal generates oil formation between the sliding surfaces of the seal lip and bearing inner ring due to the arc-shaped (half-cylindrical shaped) micro bumps set in equal distances on the seal lip toward the bearing inner ring sliding surface. Within the range of conditions evaluated in this article, the developed seal facilitated oil film formation due to the fluid lubrication effect of the bumps and produced lower torque than conventional contact type seals.

Although not mentioned in this article, interference, bump height, and variation of rubber properties also impact bearing torque. With the developed program, it is possible to predict torque of the newly developed seal and optimize the specification of the bumps.

References
1) Sasaki, Wakuda, Sugai, Ultra-low Friction Sealed Ball Bearing for Transmission, NTN TECHNICAL REVIEW, No.85,(2017) 62-66.
2) Mizuta, Research on clarification of lubrication mechanism of oil seal for rotational body and reduction of friction, Doctoral Dissertation (2013)
3) Kaneta, Sealing Theory, Tribologist, Vol. 43, No. 2, (1998), 125-130
4) Kaneta, Analysis of Soft EHL, Tribologist, Vol. 38, No. 10, (1993), 890-894.
5) Yamamoto, Kaneta, Tribology, Rikogakusha (2007)
6) Nakahara, Fluid Film Behavior, Journal of Japan Society of Lubrication Engineers, Vol. 26, No. 3 (1981), 146-152
7) C.H.VENNER, A.A.LUBRECHT, MULTILEVEL METHODS IN LUBRICATION, ELSEVIER, (2000)

Photo of authors

Tomohiro SUGAI
Advanced Technology
R&D Center

Katsuaki SASAKI
Automotive Business Headquarters
Automotive Bearing Engineering Dept.

Takahiro WAKUDA
Automotive Business Headquarters
Automotive Bearing Engineering Dept.

Hub Bearing with Steering Function that Improves Vehicle Dynamic Performance

Norio ISHIHARA*   Hirokazu OOBA*   Atsushi ITOU*
Mitsunori ISHIBASHI**   Makoto YAMAKADO**   Yoshio KANO**
Masato ABE**

NTN has developed a hub bearing with a next generation steering function capable of improving the motion performance of the vehicle by incorporating the steering angle adjustment mechanism in the hub bearing.

In this developed product, it is possible to independently correct and steer the left and right wheels according to the driving situation of the driver, but in this report we report on the result of the implementation in the mode to synchronize the left and right.

1. Introduction

We are developing "Hub Bearing with Steering-Assist Function (hereafter, sHUB)" which integrates hub bearings and steering angle adjustment mechanism. As shown in **Fig. 1**, it can be installed in the conventional front wheel steering and suspension system to independently correct the steering of each wheel with a command signal from the controller based on the vehicle information.

sHUB is a system intended to improve vehicle linear stability and fuel efficiency, as well as to improve vehicle cornering stability and risk avoidance in emergencies such as slippage. The system also has potential for applications in future autonomous vehicles for risk avoidance behavior.

We have studied a simulation of the vehicle with sHUB and verified that this system would improve vehicle responsiveness against yaw rate and lateral acceleration.

The specification for sHUB was determined based on this analysis result and a prototype unit was created. The prototype (for right wheel) is shown in **Fig. 2**.

We have conducted an engine bench test of the prototype and verified that the basic performance satisfies the target values. In addition, we have verified effect of this control law with an actual vehicle test.

This article reports these test results.
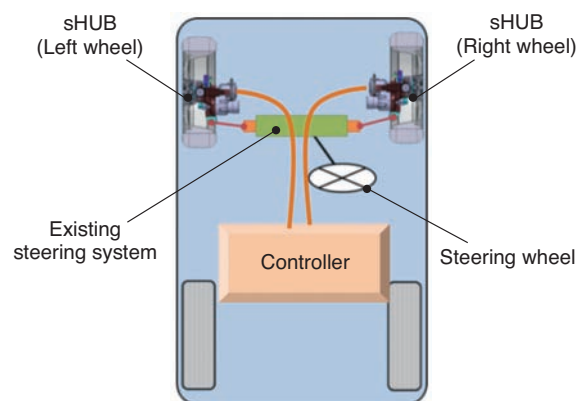
Fig. 1 Image of Vehicle with sHUBs
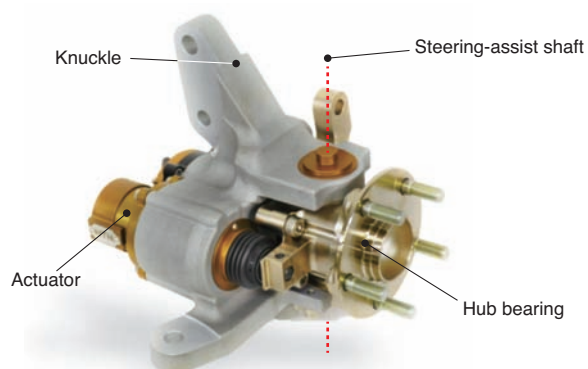
Fig. 2 Prototype of sHUB

---

 *New Product Development R&D Center
**Department of Vehicle System Engineering, Kanagawa Institute of Technology

2. Vehicle motion control law

2.1 Vehicle motion control with front wheel steering

An improved version of the Matlab/Simulink ® Vehicle Motion Simulation Model [1] developed at the Yamakado/Kano Laboratory of Kanagawa Institute of Technology was applied to the vehicle model with sHUBs installed in both front wheels. With this model, the potential for improvement of motion performance was verified. In addition, this simulation model was used to study the best control parameter settings.

This simulation model can reproduce change of vehicle attitude since it takes into consideration the anti-dive and anti-squat effect with the suspension link mechanism against longitudinal and lateral force to the tires [2], [3], [4].

2.2 Control for improving steering responsiveness

The following shows the control law to improve the responsiveness of vehicle yaw rate and lateral acceleration against the driver's steering action. The symbols are defined as follows:

n : Steering gear ratio
V : Vehicle speed
I : Vehicle yaw inertia moment
l : Wheel base
l_r : Distance between the vehicle center of gravity and rear wheel shaft
K_r : Tire cornering power per rear wheel
$\beta(s)$: Laplace transformation of lateral slip angle β of vehicle center of gravity
$r(s)$: Laplace transformation of yaw rate r
$\delta(s)$: Laplace transformation of front wheel tire angle δ
$\delta_h(s)$: Laplace transformation of steering angle δ_h
$\ddot{y}(s)$: Laplace transformation of lateral acceleration $\tilde{y}$
ω_n : Natural frequency of vehicle response against steering action
ζ : Damping ratio of vehicle response against steering action

$G_\delta{}^\beta(0)$, $G_\delta{}^r(0)$, $G_\delta{}^{\ddot{y}}(0)$: Vehicle response parameters against steering action

$$\frac{\delta}{\delta_h}(s)$$

$$= \frac{1}{n} \left[\frac{\dfrac{1+\dfrac{2\zeta}{\omega_n}s+\dfrac{1}{\omega_n{}^2}s^2}{1+\dfrac{2\zeta(1+\alpha_1)}{\omega_n(1+\alpha_2)}s+\dfrac{1}{\omega_n{}^2(1+\alpha_2)^2}s^2} \times}{} \frac{1+\left(\alpha_3\dfrac{l_r}{V_{\beta=0}}+(1-\alpha_3)\dfrac{l_r}{V}\right)s+\dfrac{I}{2lK_r}s^2}{1+\dfrac{l_r}{V}s+\dfrac{l}{2lK_r}s^2} \right] \quad (1)$$

$$\beta(s) = G_\delta{}^\beta(0)\frac{1+T_\beta s}{1+\dfrac{2\zeta s}{\omega_n}+\dfrac{s^2}{\omega_n{}^2}}\frac{\delta}{\delta_h}(s)\delta_h(s) \quad (2)$$

$$r(s) = G_\delta{}^r(0)\frac{1+T_r s}{1+\dfrac{2\zeta s}{\omega_n}+\dfrac{s^2}{\omega_n{}^2}}\frac{\delta}{\delta_h}(s)\delta_h(s) \quad (3)$$

$$\ddot{y}(s) = G_\delta{}^{\ddot{y}}(0)\frac{1+\dfrac{l_r}{V}s+\dfrac{I}{2lK_r}s^2}{1+\dfrac{2\zeta s}{\omega_n}+\dfrac{s^2}{\omega_n{}^2}}\frac{\delta}{\delta_h}(s)\delta_h(s) \quad (4)$$

Equation (1) is the control law to determine vehicle tire angle to improve responsiveness of vehicle yaw rate and lateral acceleration. The sHUB corrective steering angle is the difference between this angle and the tire steering angle with the driver's steering action. By substituting this control law to equations (2), (3) and (4), and adjusting the parameters α_1, α_2 and α_3, responsiveness against lateral slip angle β, yaw rate r and lateral acceleration $\ddot{y}$ can be improved. Parameters α_1, α_2 and α_3 are the values corresponding to damping ratio ζ, natural frequency ω_n and lateral acceleration $\ddot{y}$, respectively. This simulation can reproduce the basic vehicle motion well, such that the vehicle motion performance (responsiveness to yaw rate and lateral acceleration) against steering degrades as the driver's steering speed or lateral acceleration increases.

The actual simulation was conducted with a two-wheel model (wheels on both sides are controlled with the same angle) and the impact of the parameters α_1, α_2 and α_3 on the steering responsiveness was investigated. The parameters were studied based on the results [5].

Fig. 3 shows the results of the analysis when a lane change (approximately 4.0 m of width) was made with steering action of 0.5 Hz sinusoidal wave.

The values determined by the above study were used for the control parameters α_1, α_2 and α_3 of sHUB. From the top, **(a)** angle of steering wheel, **(b)** front wheel steering angle, **(c)** operating angle speed of sHUB, **(d)** vehicle yaw rate and **(e)** vehicle lateral acceleration are shown. In these graphs, the red line indicates the case when corrective steering was made by sHUB and the blue line indicates the case without correction. In both cases, the same angle of steering wheel was used.

From the analysis result of the front wheel steering angle, it was revealed that sHUB increased the tire steering angle at the beginning of the corrective steering and controlled the corrective steering angle to be zero at the beginning of returning the steering wheel. The sHUB steering angle corresponds to the

difference between the red line of the front wheel steering angle (vehicle with sHUB) and the blue line (ordinary vehicle) shown in **Fig. 3 (b)**.

With this control, it was verified that responsiveness improved, as faster rising of yaw rate and lateral acceleration and smaller phase lag of yaw rate and lateral acceleration were observed against the driver's steering action.

In addition, we have studied the target of sHUB required for improving responsiveness to vehicle yaw rate and lateral acceleration based on the result of analysis conducted with varying speed and lateral acceleration within the range of ordinary operation. **Table 1** shows the study results. Improvement of vehicle responsiveness can be expected when satisfying the performance of maximum steering angle of ±3 deg and maximum angular speed of 10 deg/s.
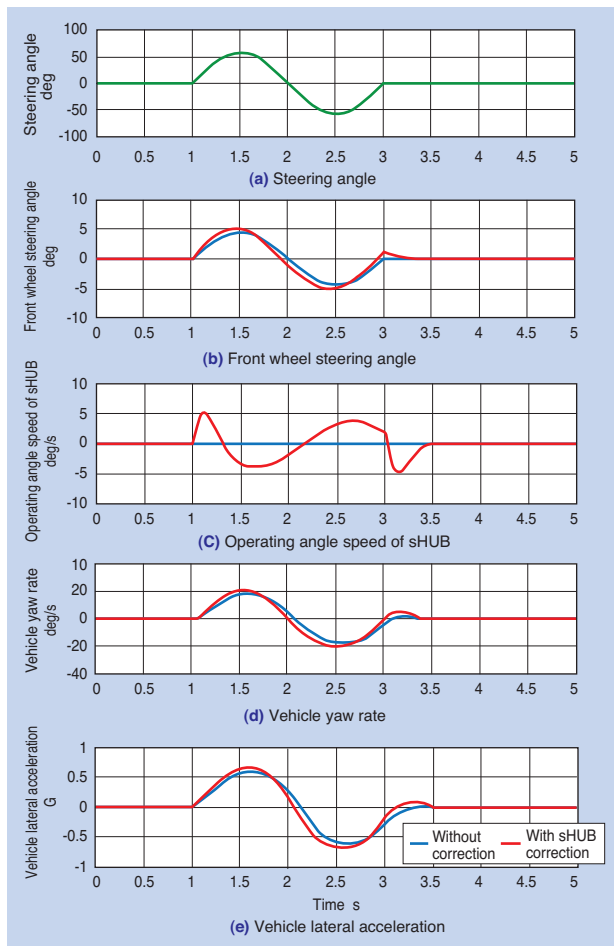
Fig. 3 Simulation Results

Table. 1 Target Spec of sHUB

Item	Values
Maximum steering angle	±3 deg
Maximum steering angular speed	10 deg/s

3. Structure of sHUB

3.1. Components

Fig. 4 shows the components of sHUB. sHUB consists of hub bearing, knuckle and actuator. The roles of the respective components are described as follows:

· **Hub bearing** : rotary support of tire; rotary support of steering-assist shaft against knuckle
· **Knuckle** : connection with vehicle suspension
· **Actuator** : fixed to knuckle and steers hub bearing
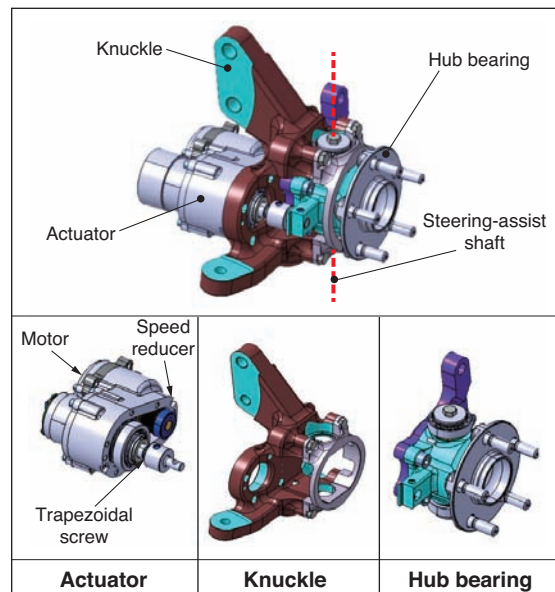
Fig. 4 Components of sHUB

The motor of the actuator is controlled by the controller with vehicle speed and steering wheel angle as the input conditions. The rotary motion of the motor is transmitted to the trapezoidal screw nut through a reducer and converted to linear motion. The linear motion part of the trapezoidal screw drives the end of the arm installed on the hub bearing, which steers the tire around the steering shaft.

The reverse input from the tire is blocked by the self-lock mechanism of this trapezoidal screw. Therefore, power consumption of the motor can be saved. (It's unclear what is trying to be communicated here, please expand as necessary.)

3.2 sHUB specification

The specifications of the prototype that satisfies the targets of **Table 1** and installable without changing the steering geometry of the test vehicle are shown in **Table 2**. The weight was set to 13.8 kg, which adds 5 kg or less to the standard components (knuckle and hub bearing) of the original vehicle.

Table. 2 Specifications of sHUB Prototype

Item	Values
Maximum steering torque	350 Nm
Supply voltage	24 V
Maximum steering angle	±3.5 deg
Maximum steering angular speed	16 deg/s
Weight	13.8 kg

4. Bench test result

4.1 Property test equipment

Fig. 5 shows the configuration of the test equipment. The prototype knuckle was fixed to the test equipment and load was applied to a point at the flange edge 120 mm away from the steering shaft by the air cylinder to simulate the reaction force from tire.

The actual load on the flange was measured by a load cell while sHUB was in operation.
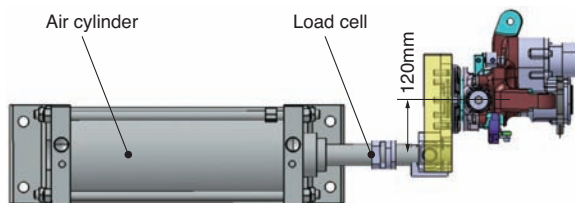
Fig. 5 Test equipment of sHUB

4.2 Relationship between the motor command value and steering angle

Fig. 6 shows the relation between the motor command value and steering angle. The steering angle is the angle of the hub flange surface actually measured.

It was verified that this prototype operated linearly with respect to the command value.

Since the tire is fixed to the hub flange surface with bolts, the angle of the hub flange surface and the angle of tire are the same.

4.3 Response speed

While the steering torque is applied (load applied at 120 mm from the shaft by the air cylinder) to the hub bearing, the command value shown in **Fig. 7** (broken line) was given to the controller to drive the sHUB to steer and the response speed was obtained. The response speed was defined as the maximum rising speed of the sHUB steering angle (**Fig. 7** : solid line). **Fig. 8** shows the steering maximum angular speed of sHUB against the load torque.

When the steering torque increases, the maximum angular speed decreases; however, we could verify the angular speed to satisfy the objective. (Please clarify this last sentence.)
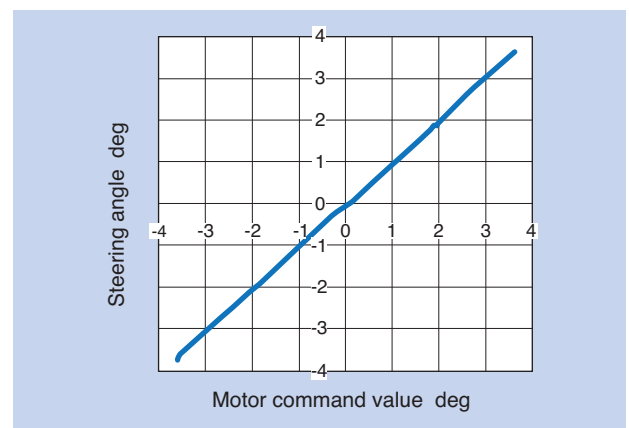
Fig. 6 Relationship between Motor Command Value and Steering Angle
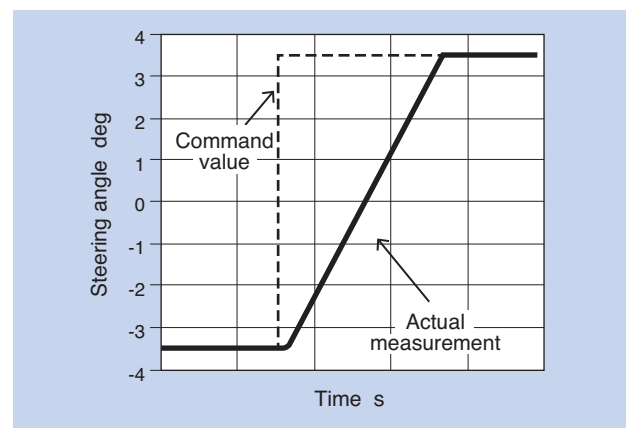
Fig. 7 Input Value and Steering Angle
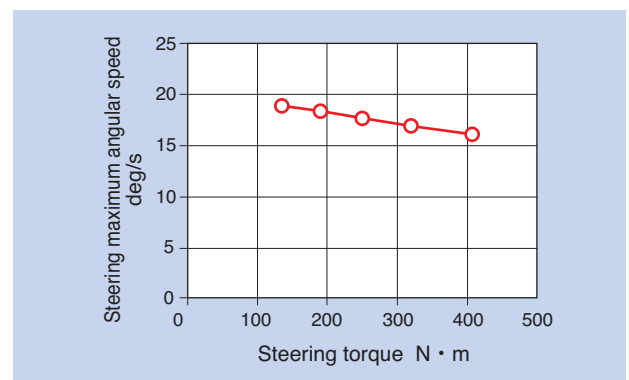
Fig. 8 Maximum Angular Speed on Steering Torque

5. Actual vehicle test results

5.1 Parameter setting

The values of the parameters α_1, α_2 and α_3 were determined by the sensitivity evaluation results from the single lane change test and the slalom running test of the test vehicle with sHUB.

5.2 Response test

The system was installed on the test vehicle to verify the mechanical responsiveness of sHUB against the command value.

The test vehicle traveled on the single lane change course shown in **Fig. 9** at a speed of 80 km/h. The road surface was asphalt (dry).

Fig. 10 shows the command value to sHUB for single lane change with the black line and the actual corrected steering angle with the red line. **Fig. 10 (a)** shows the data of the entire test and **(b)** shows the enlarged view of the area indicated by the broken line in **(a)** As shown in **(b)**, there was a delay of around 20 ms max.; however, it was insignificant in the driving test.
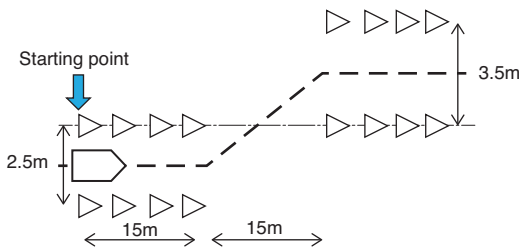
Fig. 9 Course Layout for Single Lane Change

(a) Full test data

(b) Enlarged view of portion
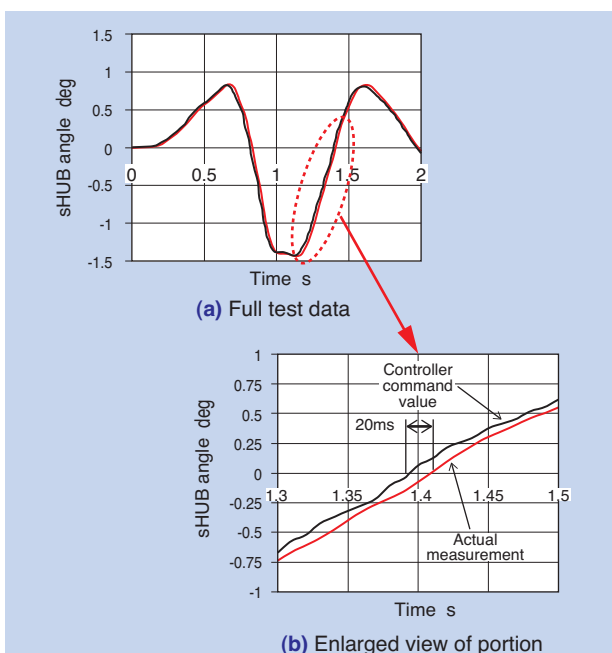
Fig. 10 Mechanical Response Motion for Single Lane Change

5.3 Steering transient response test

In order to verify the improvement of the vehicle responsiveness with the sHUB controlled by this control law, a "pulse steering input" test was conducted according to "Transient Response Test Procedures for Passenger Cars (JASO Z110:2003)." [6] Due to limitations in the test site space, the test conditions were set at a vehicle speed of 80 km/h and pulse width of 0.5 s.**Fig. 11** shows the operating procedure of the steering wheel. The triangular wave is the input through the driver's steering action.

The analysis results of frequency response of yaw rate **(a)** and lateral acceleration **(b)** against the steering wheel angle are shown in **Fig. 12**, from the data obtained in this test. The red line indicates the result with corrective steering by sHUB and the blue line is the result with no correction. The tests were conducted three times each and similar results were obtained.

By using this control, the vehicle performance was increased as the peak value increased and the phase lag improved, both for yaw rate and lateral acceleration, in the steering wheel angle frequency range (0.5 to 2.0Hz) used in ordinary driving. Therefore, the driver feels better vehicle responsiveness against the steering action and better overall maneuverability.
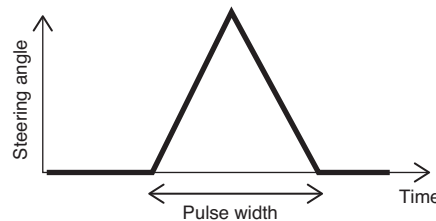
Fig. 11 Input Steering Condition

(a) Yaw rate   **(b)** Lateral acceleration
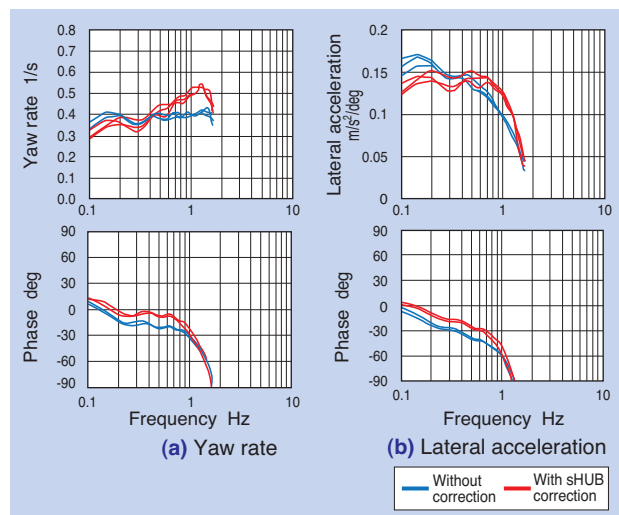
Fig. 12 Transient Response Characteristic

5.4 Single lane change driving test

A single lane change test was conducted to evaluate the vehicle driving limit performance (behavior, responsiveness, convergence performance, etc.). The course layout was the same as **Fig. 9**.

The vehicle entered the starting point at a speed of 80 km/h to run with no acceleration after passing the starting point. **Fig. 13** shows the result of this test. The red line indicates the case when the correction was made for the tire angle by sHUB and the blue line indicates the case without correction. There was no difference in the vehicle speed depending on the correction.

When corrective steering was made by sHUB, the steering action of the driver was smaller overall, and the driver's corrective steering amount after lane change was smaller as well. Therefore, it must have been easier for the driver to maneuver the vehicle, with intuitive operation.
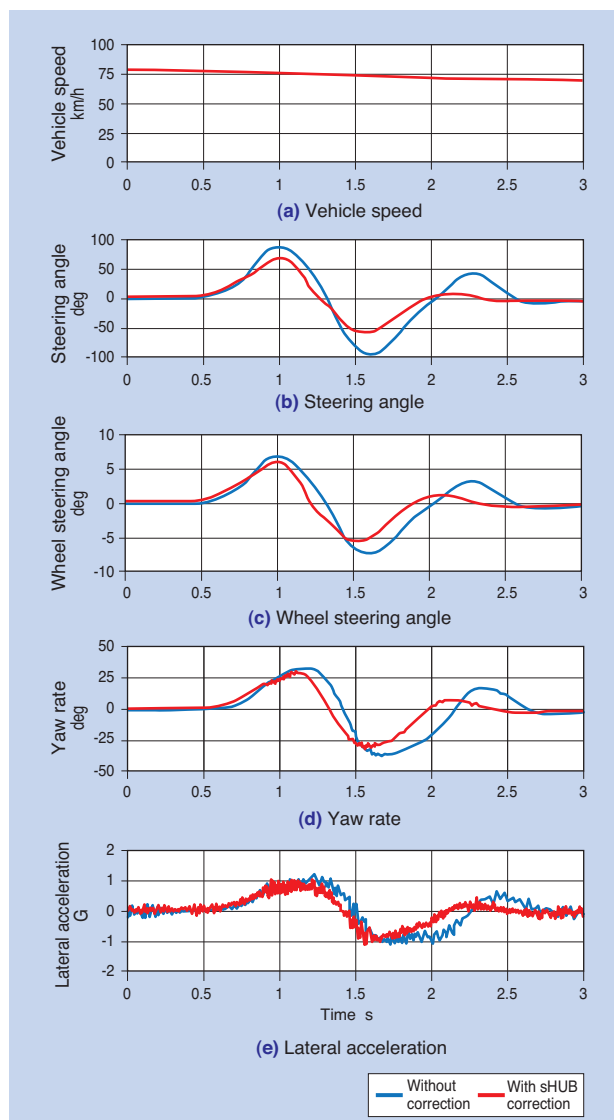
The delay of peak for the vehicle yaw rate and lateral acceleration against the driver's steering action was also small with improved responsiveness.

Fig. 14 shows the driving trajectory of this test. The corrective steering by sHUB prevented over steering when the driver returned the steering wheel while driving.
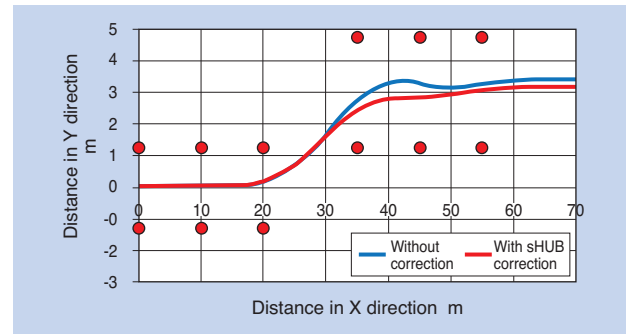
Fig. 14 Vehicular Swept Path

5.5 Slalom driving test

A slalom driving test was conducted to verify the driving stability.

Fig. 15 shows the course layout of this test. In this test, the vehicle entered the starting point at a speed of 50 km/h.

Fig. 16 and **17** show the change of yaw rate and lateral acceleration against the steering angle. The red line indicates the case when the corrective steering was made by sHUB and the blue line indicates the case without correction.

Controlling the sHUB allows smaller steering wheel action and improved linearity of yaw rate and lateral acceleration, with which the driver can drive the vehicle with ease.
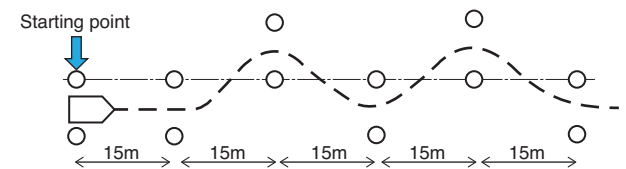
Fig. 15 Course Layout for Slalom
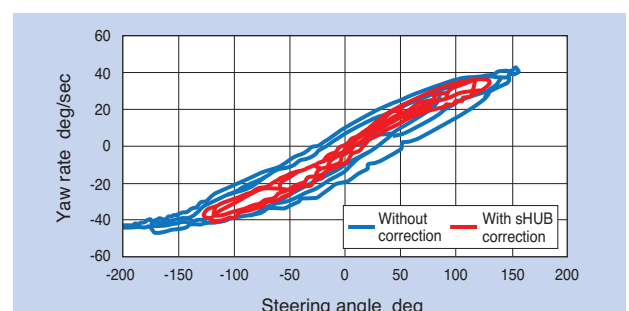
Fig. 16 Relationship between Steering Angle and Yaw Rate

Fig. 13 Test Result

-89-
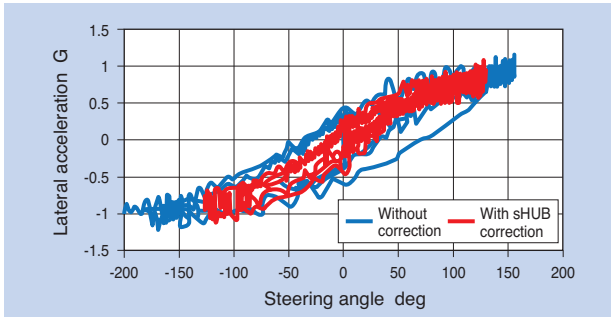
Fig. 17 Relationship between Steering Angle and GY

6. Conclusion

We have developed a hub module with steering-assist function (sHUB) which is installed in both sides of the front wheels to improve driver maneuverability. With appropriate corrective steering of both wheels according to traveling conditions, improvement of the vehicle motion performance was achieved.

With vehicle motion simulation, the responsiveness of steering was improved and the control law for realizing the ideal vehicle behavior was established. From the above simulation result, the target specification for the sHUB was determined, a bench test using a prototype was conducted and performance to satisfy the target specification was verified.

Improvement of vehicle motion performance with the above control law was verified by installing the sHUB in the test vehicle.

On an ongoing basis, we will continue studying the control law to independently control each sHUB on the right/left wheel and verify its effect with an actual vehicle test.

Additional note:

This article is a transcript of the translation of the original paper "Hub Bearing with Integrated Active Front Steering Function that Improves Vehicle Dynamic Performance" into Japanese from the Proceedings for the Spring Meeting of Society of Automotive Engineers of Japan, 2018 No. 58-18 20185263.

References
1) Takuma Sekiya, "Hub Bearing with Integrated Active Front Steering Function that Improves Vehicle Dynamic Performance," Kanagawa Institute of Technology, Graduation Thesis 16YKN02, (2016)
2) Katsuyoshi Miyamoto, "A study on fundamental vehicle specifications and handling characteristics," Kanagawa Institute of Technology, Graduation Thesis 12ABE05, (2012)
3) Takuma Sekiya, Rio Tanaka, Makoto Yamakado, Yoshio Kano, Masato Abe, "A Study on Vehicle Handling Dynamics using a Simple Description Type of Three Dimensional Vehicle Model", Proceedings for the Fall Meeting in 2017, 20176253, (2017), p1365-1369.
4) Katsuyoshi Miyamoto, Hiroyuki Matsumoto, Isao Kuwayama, Yoshio Kano, Masato Abe, "Effect of Vehicle Fundamental Specifications on Steering Characteristics Relying on Tire Cornering Characteristics (Second Report)" Proceedings of the Society of Automotive Engineers of Japan Annual Congress, 2014, 2014753, No.122-14, (2017), p1-4.
5) Masato Abe, "Automotive Vehicle Dynamics," (2nd Edition), Tokyo Denki University Press (2012)
6) JASO Z110, 2003 "Automotive Standard: Transient Response Test Procedures for Passenger Cars"

Photo of authors

Norio ISHIHARA
New Product Development R&D Center

Hirokazu OOBA
New Product Development R&D Center

Atsushi ITOU
New Product Development R&D Center

Mitsunori ISHIBASHI
Kanagawa Institute of Technology
Department of Vehicle System Engineering

Makoto YAMAKADO
Kanagawa Institute of Technology
Department of Vehicle System Engineering

Yoshio KANO
Kanagawa Institute of Technology
Department of Vehicle System Engineering

Masato ABE
Kanagawa Institute of Technology
Department of Vehicle System Engineering

[**New Product**]

"Tapered Roller Bearings" with Early Failure Detection Sensor

Naota YAMAMOTO*   Hiroshi UCHIMURA   Shota TOHO***

In this paper, we introduce "Tapered Roller Bearings" with early failure detection sensor, which can detect flaking that may occur on bearings during operation. Continuous use of bearings with flaking failure leads to a risk of damage to peripheral components such as the shaft and housing due to abnormal bearing rotation. Furthermore, such flaking might also cause secondary damage such as damage to gear parts when flaking debris from bearings is dispersed and becomes stuck in the gears. Therefore, when flaking occurs on bearings, it is best to stop operation promptly. However, until now, it was difficult to detect flaking on bearings because it was undetectable due to the vibrations or noise of the entire machine. The developed product utilizes a magnetic sensor for the tapered roller bearing, with its own split type filter seal structure. Therefore the developed product can detect failure and prevent flaking debris from flowing out of the bearings.

1. Introduction

With regard to bearings used in construction machinery applications with oil lubrication, early detection of damage (flaking) is one strategy for reducing the life cycle cost (LCC) in addition to the usual approach of increasing life and reliability of the bearing itself. Flaking is a phenomenon wherein the rolling surfaces of a bearing exfoliate in scales, propagating to the entire rolling surface (**Fig. 1**) with continued operation and inducing noise and vibration that prevents smooth rotation. In addition, if flaking fragments circulate within the machine, other mechanical components, such as gears, may be damaged. Therefore, it is critical to detect early signs of flaking and its progress in order to reduce LCC.

In this article, we describe a "tapered roller bearing with early failure detection function" (hereafter, developed product) as a solution to this challenge.

Fig. 1 Inner ring of tapered roller bearing which flaking had spread

2. Structure and features

The developed product consists of a tapered roller bearing, which is widely used under heavy load conditions, including those in construction machinery, and a "seal ring with filter" (hereafter, seal ring) with integrated magnetic metal sensor (**Fig. 2**). The seal ring prevents flaking fragments from migrating outside the bearing while maintaining lubricating oil for circulation. In addition, the integrated magnetic metal sensor can provide early detection of flaking.
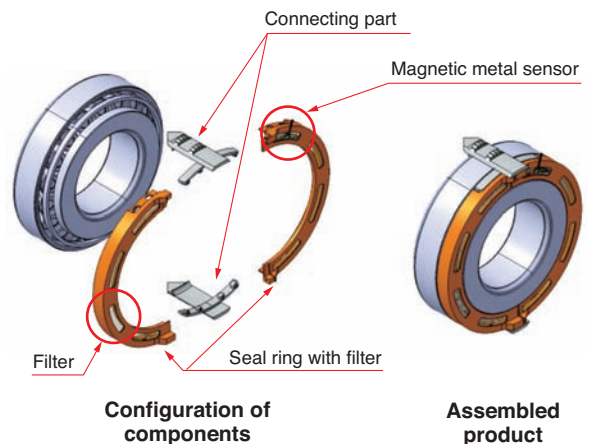

Connecting part
Magnetic metal sensor
Filter
Seal ring with filter

Configuration of components   **Assembled product**

Fig. 2 "Tapered Roller Bearings" with early failure detection sensor

*Application Engineering Dept., Industrial Business Headquarters
**Product Design Department, Industrial Business Headquarters

2.1 Magnetic metal sensor

The developed product uses a magnetic metal sensor to detect flaking. **Fig. 3** shows a circuit diagram for the sensor. Two permanent magnets are placed on the circuit board and when a flaking fragment passes through the space between them, the output voltage drops.
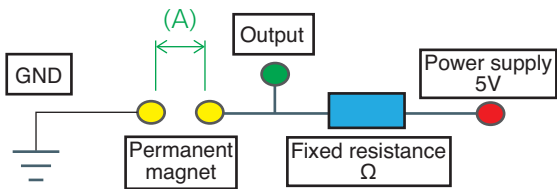
Fig. 3 Sensor circuit diagram

In this method, the distance (A) between the two permanent magnets in **Fig. 3** affects the sensitivity for the detection of flaking fragments. The greater the distance is, the lower the detection sensitivity becomes. On the other hand, when the distance (A) is too small, the system detects wear debris smaller than the flaking fragments; therefore the detection accuracy of flaking fragments degrades (**Fig. 4**). The developed product optimized the distance (A) to increase the detection accuracy of flaking fragments.
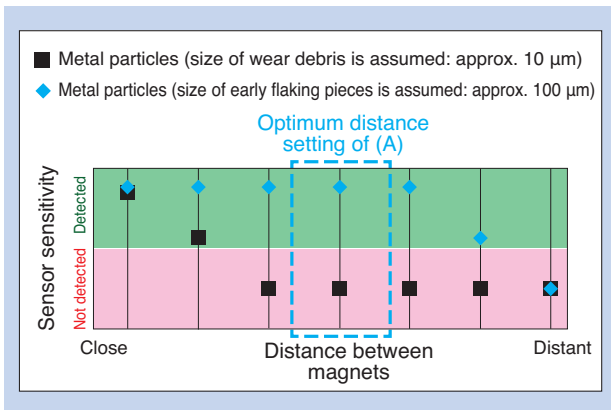
Fig. 4 Magnet distance and sensor sensitivity

2.2 Seal ring with filter

In applications with circulating lubrication, bearings and other mechanical components such as gears are often lubricated together. In these cases, when flaking occurs, the flaking fragments are dispersed within the machine together with the lubricating oil and may damage other mechanical components. Therefore, a seal ring with the following specifications was made to prevent the spread of flaking fragments from the bearing.

· Make the gap between the seal ring and inner ring smaller (**Fig. 5**※1).
· Provide multiple magnets, as well as pockets to hold the captured flaking fragments in the seal ring.
· Provide multiple filters to maintain ease of oil circulation (**Fig. 6**).

Fig. 7 shows how a flaking fragment is captured by the seal ring.
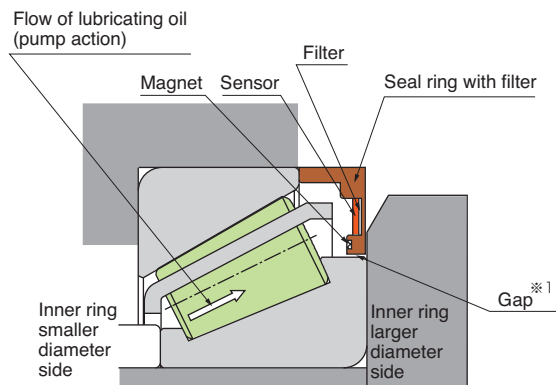
Fig. 5 Cross sectional view of developed product
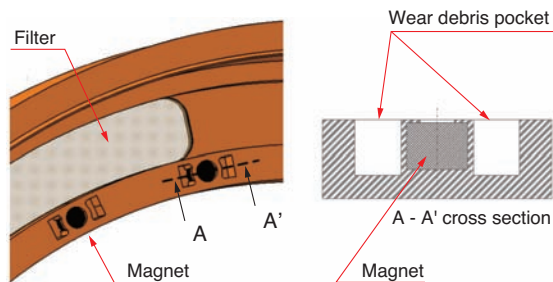
Fig. 6 Filter and built-in magnet
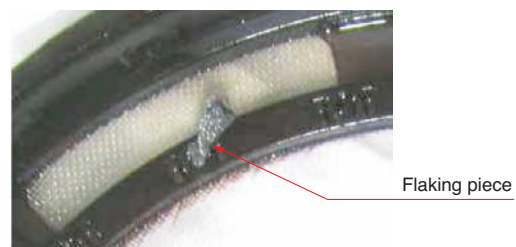
Fig. 7 Magnet with flaking pieces

The seal ring is a split type design consisting of two semi-circular components, as shown in **Fig. 2**, for ease of assembly into the target machine. Two different styles, type-A and type-B, with differing connection methods (**Fig. 8**) are used. When the tapered roller bearing and seal ring are inserted into the housing together, type-A is used, where a connecting part is inserted in the groove of the inner diameter of the housing [1]. When the seal ring is fixed to the shoulder or end part of the housing, type-B is used. In either case, the seal ring is fixed to the housing, and even when creeping (phenomenon wherein the outer ring rotates during operation) occurs the sensor cables do not become disconnected.

usually used in environments with high external vibration; therefore, the threshold of vibration is often set at 2 to 3 times higher than the level at stable operation, so that those external vibrations are not detected as a failure. In these settings, a rise such as that in **Fig. 11** is not identified as a failure, and the machine will continue to operate after flaking occurs, which may induce further propagation of flaking and cause damage to other machine elements.

Therefore, the developed product is verified to be more effective for early detection of flaking than the ordinary method of detecting abnormalities in the vibration signature.

Fig. 8 Types of connected parts
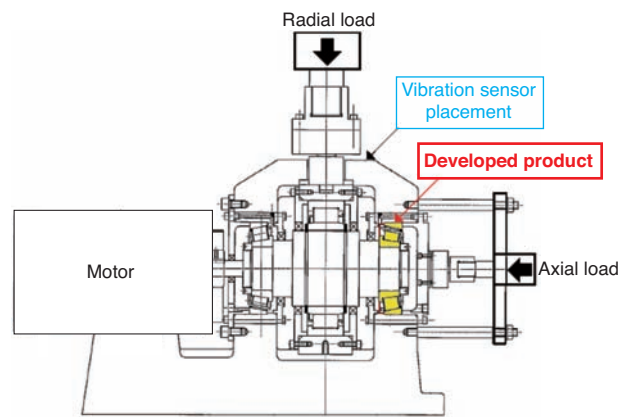
Fig. 9 Test equipment

3. Performance test results

3.1 Detection performance of flaking fragments

The evaluation test shown in **Fig. 9** and **Table 1** was conducted to verify the detection performance of flaking fragments. In order to promote flaking, an indentation was applied to the rolling contact surface of a rolling element before the test (**Fig. 10**).

Fig. 11 shows the test results. Since a voltage drop of the magnetic metal sensor output was observed 102 hours after the beginning of the test, the test equipment was shut down and the bearing was inspected. Flaking on the rolling contact surface of a rolling element was verified (**Fig. 12**).

In this test, we also conducted measurement using an accelerometer on the outer surface of the housing, which is an ordinary failure detection method, and made a comparison with the measurement using the magnetic metal sensor. As a result, the accelerometer on the outer surface of the housing also detected the change of vibration 102 hours after the beginning of the test, in like manner to the magnetic metal sensor. However, in construction machinery, which is the main application of the developed product, bearings are

Table. 1 Test Condition

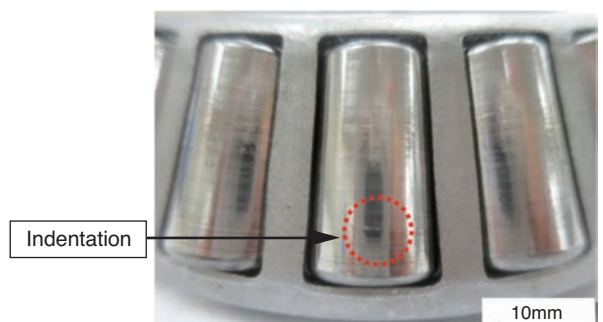| Bearing Inner diameter x outer diameter x width	Tapered roller bearings $\phi 65 \times \phi 130 \times 37$ mm
Rotational speed	2,000min^{-1}
Lubricating oil	Turbine oil (VG46)
Lubrication method	Circulating lubrication
Radial load	12.5kN
Axial load	100kN
Maximum contact surface pressure	2,070MPa

Fig. 10 Test bearing before the test

Fig. 11 Test result

Flaking   10mm

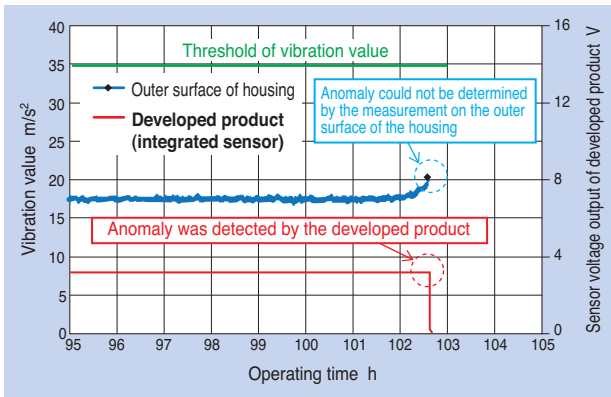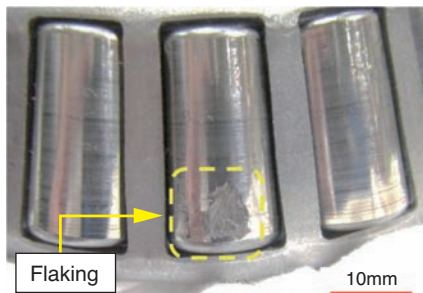**Fig. 12** Test bearing after the test

3.2 Capture performance of flaking fragments

In construction machinery, the developed product may continue to operate even after flaking is detected. Therefore, seal rings are required to capture the flaking fragments to prevent damage to other machine elements. After the test in Section 3.1, we resumed the evaluation test shown in **Table 1** by re-installing the test bearing into the test equipment shown in **Fig. 9**.

The result was that the motor indicated overload 13 hours after the beginning of the test, and the test equipment was turned off so that the bearing could be inspected. It was verified that the flaking had propagated on the rolling contact surface of the rolling elements (**Fig. 13**). We also observed a significant number of flaking fragments in the seal ring, verifying the effect of the developed product for preventing the flaking fragments from spreading outside of the bearing (**Fig. 14**).

10mm

Fig. 13 Test bearing after the continuous test
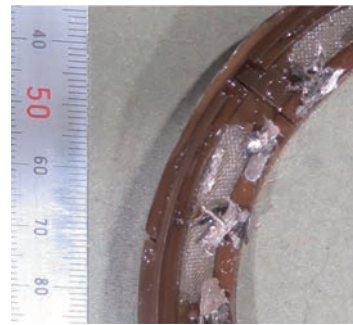
Fig. 14 Test bearing after the continuous test

4. Development of additional functionality

In addition to the flaking detection introduced in this article, other types of condition monitoring, such as bearing temperature and vibration, are also being performed. In the case of the bearing temperature and vibration, measurements are often conducted at the outer surface of the housing due to the restriction of sensor placement; therefore, sufficient sensitivity or reliability may not be available because of the distance from the bearings.

In addition, measurement of shaft rotational speed is also performed for controlling machine output. However, early failure may occur due to the severe external environment when sensors are attached to the machine exterior.

Therefore, the addition of temperature and rotational speed sensors to this development product was studied (**Fig. 15**).
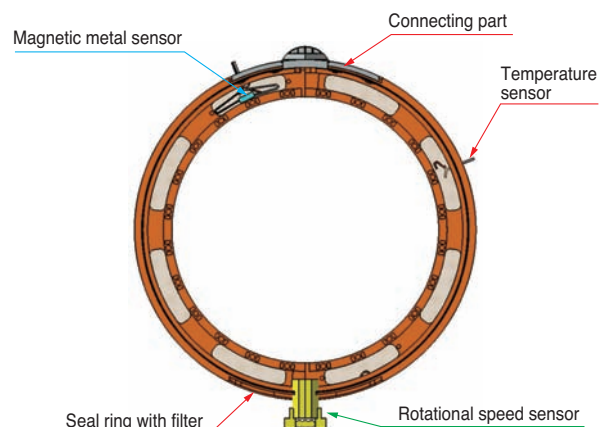

Fig. 15 Prototype image

4.1 Results of the temperature sensor test

A temperature sensor was installed in the seal ring and temperature of the lubricating oil circulating within the bearing was measured. For comparison purposes, the temperature was also measured at the outer surface of the outer ring of the bearing.

Fig. 16 shows the temperature measurement result during the flaking fragment capture performance test of Section 3.2, until the test equipment was turned off.

This test determined that the temperature sensor installed in the seal ring indicated about 5°C of difference at 2 hours after the beginning of the test compared with the measurement at the outer surface of the outer ring; however, the difference shrank to less than 2°C after 8 hours, which was almost equivalent.
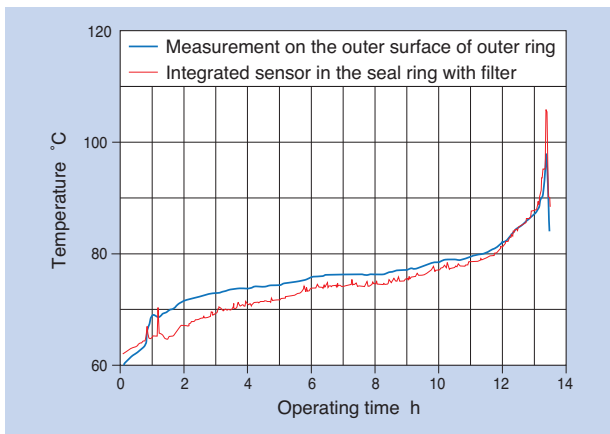

Fig. 16 Temperature rise test result

4.2 Results from the rotational speed sensor test

A rotational speed sensor capable of operating in lubricating oil [2] was installed inside of the seal ring to measure rotational speed of the cage. The rotational speed of the cage and that of the main spindle were correlated, and it was verified that the converted value of the measured cage rotational speed matched the spindle rotational speed of the test equipment (Fig. 17).

In the future this sensor is expected to be implemented in the developed product as a rotational speed sensor for use in lubricating oil.
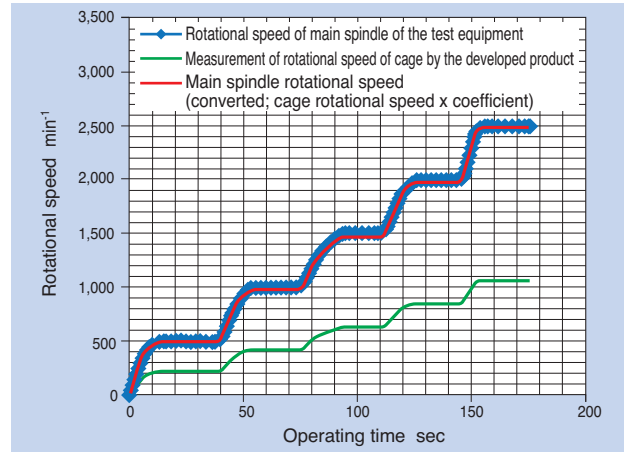
Fig. 17 Rotational speed instrumentation result

5. Conclusion

This article introduced the structure and features of the developed product, "tapered roller bearing with early failure detection function."

This developed product is expected to detect the early stages of bearing damage (flaking), as well as prevent secondary damage to peripheral components due to the spread of flaking fragments, thereby reducing life cycle costs. In addition, it can also incorporate various sensors for multi-sensing and IoT applications.

We are committed to continue the development of products with high added value.

References
1) Naota Yamamoto, Hiroshi Uchimura, Shota Toho: Tapered Roller Bearing with an early failure detection function, Hydraulics & Pneumatics (2017) 19-23
2) Kenichiro Naito, Naota Yamamoto, Katsunori Sone: Market Trend and High-Functionality of Wheel Bearings for Off-Highway Truck, NTN TECHNICAL REVIEW, No.80 (2012) 78-82.

Photo of authors

Naota YAMAMOTO
Industrial Business Headquarters
Application Engineering Dept.

Hiroshi UCHIMURA
Industrial Business Headquarters
Product Design Dept.

Shota TOHO
Industrial Business Headquarters
Product Design Dept.

Asymmetrical Spherical Roller Bearings for Wind Turbine Main Shafts

Kazumasa SEKO
*Takashi YAMAMOTO**

Wind turbine main shaft bearings are subjected to axial loading caused by wind loads. The use of spherical roller bearings for such applications results in one row being subjected to larger loads as compared to the opposite row. Additionally, spherical roller bearings have a characteristic of rolling and sliding due to inherent internal geometry. These conditions, combined with insufficient lubrication at the roller/raceway contact, lead to wear at the outer raceway surface. As a result damage might occur particularly in the outer ring raceway surface.

NTN has developed "Asymmetrical Spherical Roller Bearings" for wind turbine main shafts that have an asymmetrical design utilizing different length rollers and a different contact angle between internal left and right roller rows in order to address these issues.

1. Introduction

Wind power generation has evolved globally into a clean energy with little impact on environment and no CO_2 emissions.

According to an announcement from Global Wind Energy Council (GWEC), the installed capacity of wind turbines at the end of 2017 was 540 GW, an increase of over 5 times from the previous 10 years. In addition, according to GWEC's market prediction, the increase will continue at the pace of approximately 9% to 10% a year (**Fig. 1**).

Previously, adoption of wind turbines has been promoted by national policy such as Feed-in Tariff (FIT). However, Europe and the U.S. are promoting wind turbines to become a profitable energy source without subsidies so that it can compete against thermal or hydroelectric power generation, by gradually reducing subsidies.

Wind turbine manufacturers are now engaged in full development of off-shore turbines for improving power generation efficiency and equipment availability, as well as a countermeasure against a reduction in the number of sites adequate for on-shore wind turbines.

The construction costs of off-shore turbines are significantly higher compared to on-shore models; as a result, the power generation capacity per facility is larger, in some cases up to 12 MW.

On the other hand, much higher reliability is required for bearings for larger and off-shore wind turbines since the replacement cost is significant once failures are found.
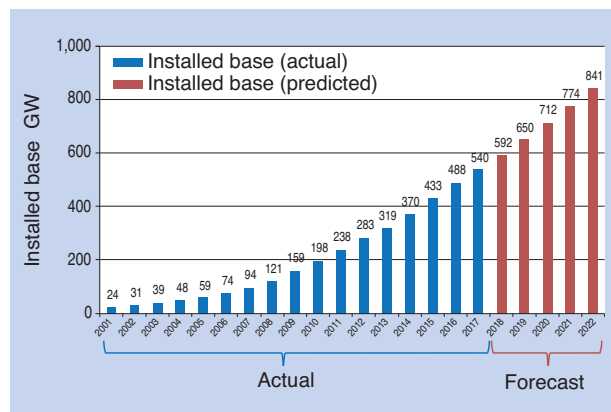

Fig. 1 Global cumulative installed wind capacity [1]

2. Structure of wind turbines

2.1 Location where bearings are used

Wind turbines come in different types such as horizontal axis and vertical axis. We will introduce you to the representative type for large commercial use:the three-blade (wing) horizontal axis type.

Fig. 2 shows the nacelle portion of the induction generator, which is the mainstream design for on-

---

*Application Engineering Dept., Industrial Business Headquarters
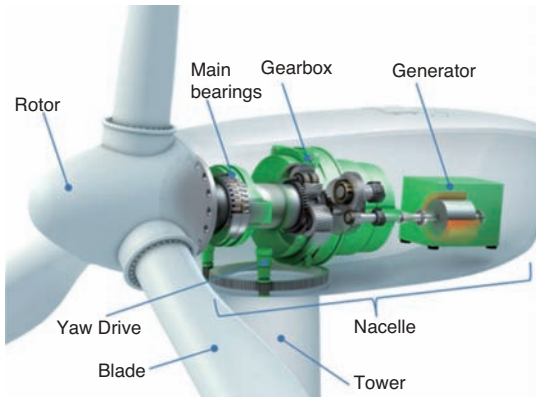**Product Design Department, Industrial Business Headquarters
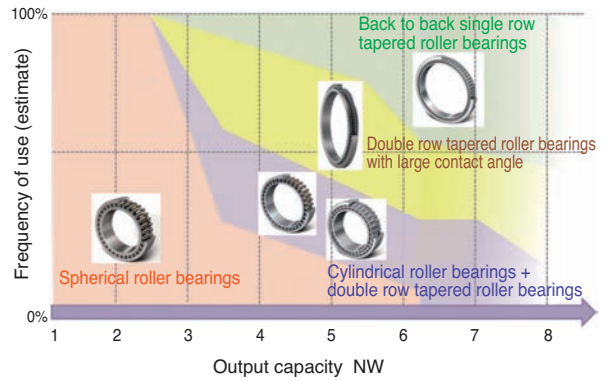
Fig. 2 Internal structure of wind turbine

Fig. 3 Relationship between generation capacity and type of main shaft bearings [2)]

shore turbines with around 2 MW of output. Receiving wind energy, the blades enable the rotor to rotate; the rotational speed is increased by the gearbox, which is converted to electric energy by the induction generator.

Bearings are used to support the rotor shaft, within the gearbox and generator, as well as to allow pitch control of each blade, yaw control of the tower top and within the reducer which drives them. Approximately 20 to 30 bearings are used per wind turbine.

2.2. Type of main bearings

Main bearings that support rotor shafts have become larger and larger over the years. Off-shore wind turbines use bearings of extremely large size, over 2m of outer diameter, which are not used in regular industrial machines. In addition, different types of bearings are used depending on the power capacity. In wind turbines of around 2 MW of generation capacity, spherical roller bearings are often used as they have high load capacity and superior allowable capability toward mounting errors.

On the other hand, for models with over 2 MW of capacity, bearing types used in them are varied such as back-to-back single row tapered roller bearings, double row tapered roller bearings with large contact angle, combination of cylindrical roller bearings and double-row tapered roller bearings, etc., depending on the structure and power generation methods of different wind turbine manufacturers. In the case of off-shore models with over 5 MW of capacity, tapered roller bearings are more frequently used because of their advantage of contact angle and moment load carrying capacity. **Fig. 3** shows the relationship between generating capacity and type of main bearings.

3. Cases of damage and countermeasures

3.1 Technical challenges that the market faces

As mentioned before, high reliability is required for bearings of wind turbines; however, there are cases where main bearings fail before the theoretical calculated operating life. Demand for long operating life is high, especially for spherical roller bearings, which are the current mainstream model widely used for main bearings of wind turbines with around 2 MW of generating capacity.

For main bearings of wind turbines, in addition to radial load applied vertically from the weight of the rotor and blade, unidirectional axial load is applied horizontally from the wind; therefore, larger load is applied to the rear row (away from the blades) compared with the front row (near the blades) in upwind model[※1] turbines, which is the current mainstream model (**Fig. 4**).
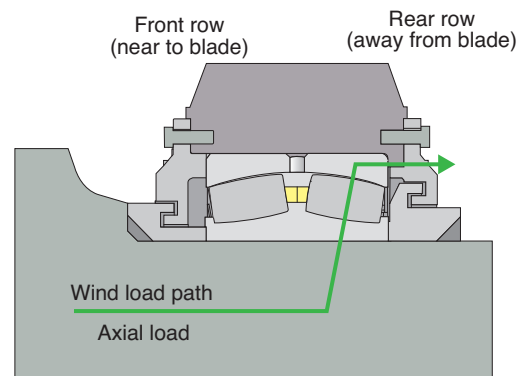

Fig. 4 Loading condition of SRB for main shaft bearings

※1 Upwind type: wind turbine with the rotor to receive the wind positioned in the upwind side.

In addition, due to the metal contact between the raceway surface and the rollers from rolling and sliding, typical of spherical roller bearings[※2] (**Fig. 5**), and poor lubrication (insufficient oil film), stepped wear may propagate on the surface of the raceway from the points with a high PV value[※3]. Due to this phenomenon, stress concentration on the rolling-only points, where no wear occurs, may cause flaking and cracking, especially on the rear row outer ring where high load is applied (**Fig. 6**, **Fig. 7 (a) - (c)**). While uniform load is applied about the entire raceway of the rotating inner ring, load is concentrated within a certain load zone of the fixed outer ring; therefore, when the load is repeatedly applied, damage may occur.
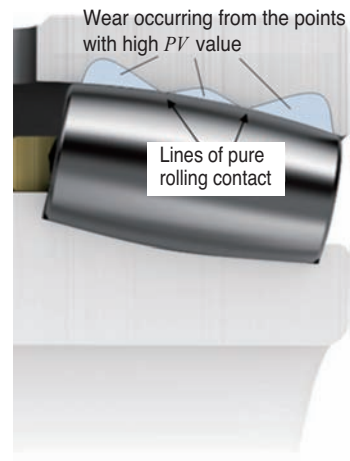
(a) Area of wear occurrence

(b) Area of stress concentration occurrence

(c) Area of flaking occurrence

Fig. 7 Mechanism of flaking on non-slip line
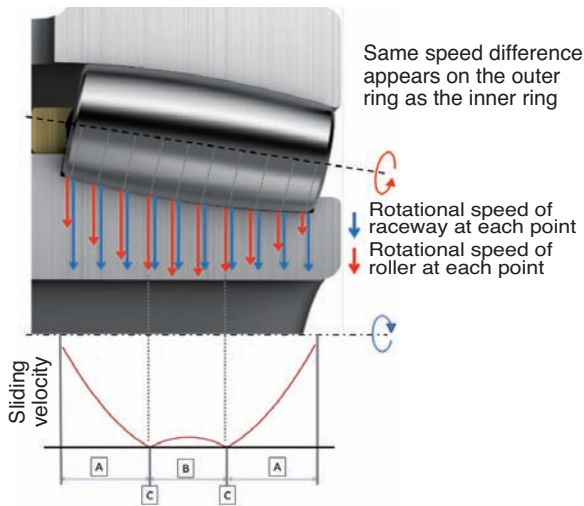
A：Roller rotational speed < raceway rotational speed
B：Roller rotational speed > raceway rotational speed
C：Roller rotational speed = raceway rotational speed

Fig. 5 Image of rolling and sliding in SRB

Flaking at lines of pure rolling contact

Fig. 6 Flaking on non-slip line

※2 Rolling and sliding: sliding due to the difference of rotational speed between the roller and raceway.
※3 PV value: product of contact pressure (P) and rolling and sliding velocity (V).

3.2 Countermeasure by asymmetric design

NTN has reviewed the design of rollers for use under the conditions typical to wind turbines to improve operating life and wear resistance and developed "Asymmetrical Spherical Roller Bearings (hereafter, developed product) as a measure to counteract the aforementioned damage. Specifically, the developed product adopts a smaller contact angle for the front row and larger contact angle for the rear row, as well as longer rollers for the rear row and shorter rollers for the front row to efficiently carry uniaxial wind loading at the rear row and to actively accept radial loading at the front row. With this change, the load can be appropriately shared by the rollers of the front and rear rows (**Fig. 8**) [3), 4)].
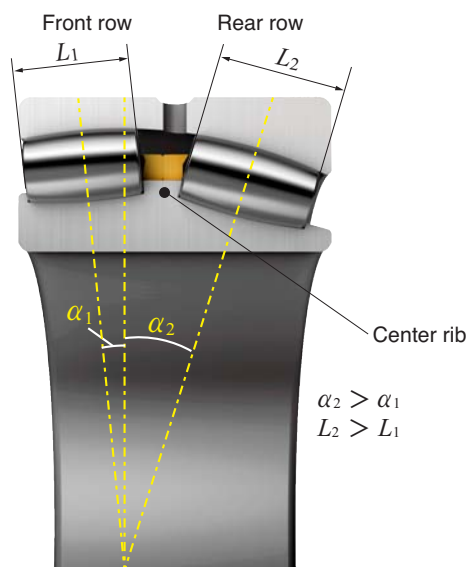
Fig. 8 Cross section of Asymmetrical SRB

This developed product can be designed within the same dimensions as the conventional product; therefore, it can replace existing conventional product in the operating wind turbines to enable longer operating life and prevent early failure, contributing to the reduction of maintenance cost. The developed product has around 2.5 times the calculated operating life of the conventional product and achieves around 30% reduction of PV value, which is an indicator for wear, under the typical environment conditions of the wind turbine main bearings (**Fig. 9** and **10**).

Alternately, the design allows approximately 10% reduction in bore diameter for a bearing with equivalent life as the conventional product, resulting in approximately 30% less weight. For example, the operating life of the conventional product of 240/600B (ϕ 600× ϕ 870×width 272) and that of the developed

product of 240/530B (ϕ 530× ϕ 780×width 250) are the same. By adopting this developed product when wind turbines are newly designed, bearings can be downsized, contributing to compact and lightweight wind turbines overall (**Fig. 11**).

The developed product has a center rib on the inner ring so that the roller position is supported at three points, namely, the inner ring raceway, outer ring raceway and the inner ring center rib (**Fig. 8**). This prevents skew[※4] of rollers to reduce sliding between the raceway and the rollers.
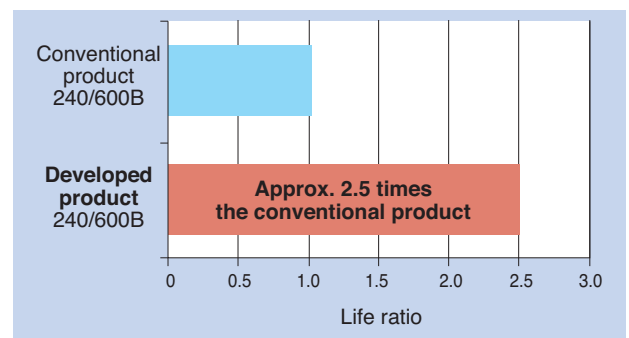
Fig. 9 Comparison result of calculation life of conventional SRB and asymmetrical SRB
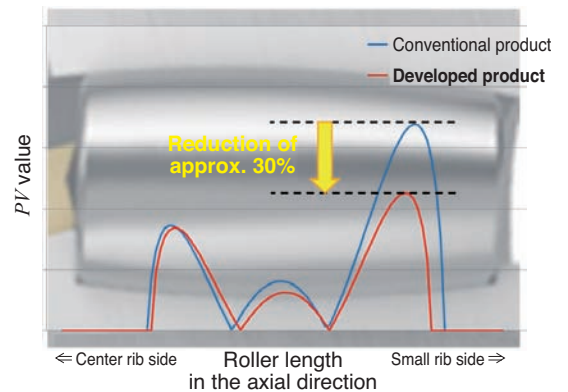
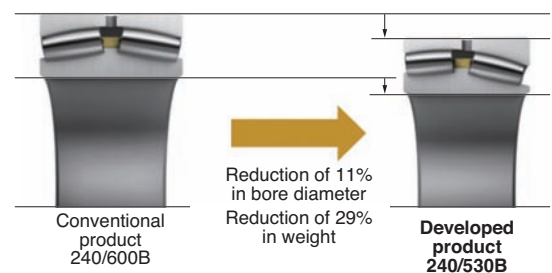**Fig. 10** Comparison result of PV value on rear side row of conventional SRB and asymmetrical SRB

Fig. 11 Example of design for down sizing

※4 Skew: roller inclination over its normal axis of rotation in roller bearings.

4. Evaluation of the bearings of the actual size

Fig. 12 and **Table 1** shows the test equipment and test conditions, respectively. The load was assumed to be a combination of radial load and axial load averaged from bearing loading of actual wind turbines. The test was conducted by measuring the operating temperature under three discrete rotational speeds which occur within actual wind turbines.
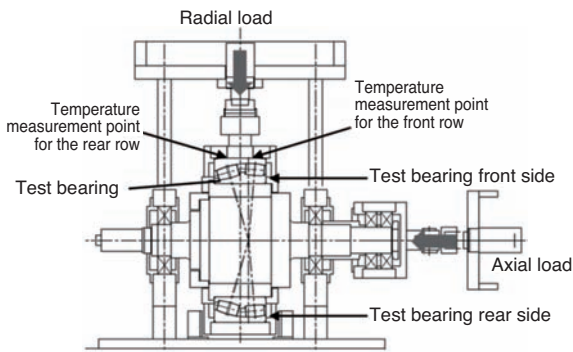
Fig. 13 shows the test results and the calculation results of the rolling element load distribution of each bearing. By comparing the test results, it was revealed that the rise of temperature of the rear row of the developed product was 2 to 3℃ lower than the conventional product, and the difference in temperature between the front row and rear row was also smaller. From this result, we can conclude that the developed product efficiently distributes the load to each row compared with the conventional product under the average load conditions of wind turbines, as shown in the calculation results of the rolling element load distribution.

Fig. 12 Testing machine for actual size bearings test

Table. 1 Test condition of actual size bearing test

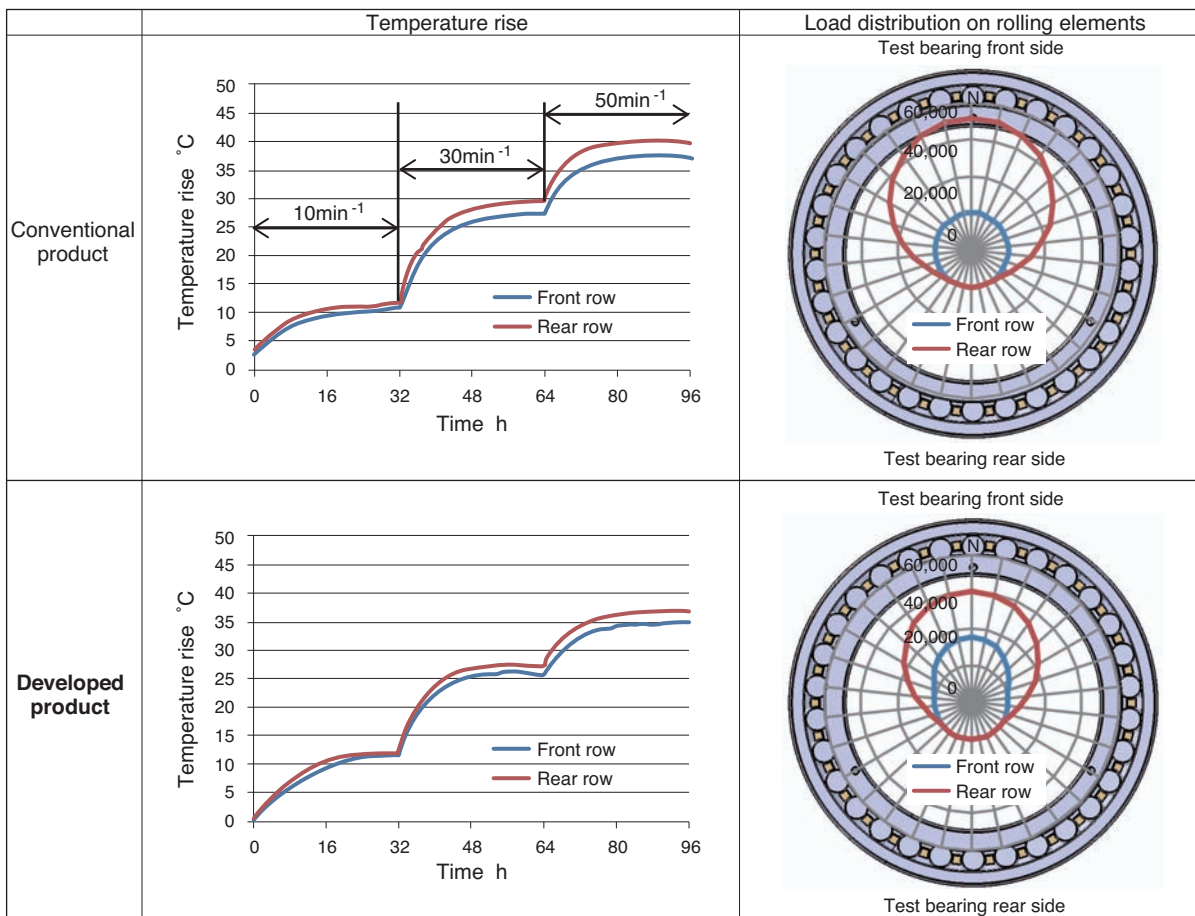| Test bearing		Conventional product	Developed product
Bearing size (mm)		ID 600 x OD 870 x W 272	
Bearing design		Standard	Asymmetric
Rotational speed (min^{-1})		10, 30, 50 (step-up)	
Test duration (h)		32 at each rotational speed	
Load (kN)	Radial	392 (0.06C_r)	
	Axial	115	

Fig. 13 Test result and calculation result of load duration distribution with actual size bearings

5. Summary

With spherical roller bearings used for main bearings of wind turbines, flaking and cracking may occur due to wear on the outer ring raceway of the rear row. This damage may be a result of rolling and sliding movement typical of these types of the bearings and poor lubrication, as well as unidirectional axial wind load applied to the rear row.

NTN developed "Asymmetrical Spherical Roller Bearings" for wind turbine main shafts which have different lengths and contact angles for the rollers of different rows. The following are features of the developed product.

· **Asymmetric design with different lengths and contact angles for rollers of different rows.**
· **Improved calculated life of approx. 2.5 times (compared with the conventional product)***
· **30% reduced PV value (compared with the conventional product) for improved wear resistance***
· **Design that allows bearings with equivalent life as the conventional product with approx. 10% less bore diameter and approx. 30% less weight**

* Calculated under average fatigue load applied to the wind turbine main bearings assumed by **NTN**.

References
1) GWEC, GLOBAL WIND STATISTIC 2017, (February, 2018), pp 3.
2) Michio Hori, Natsumi Itou, Makoto Shizunai, Toru Takahashi, Technical Trends of Bearings for Wind Turbines, Japan Wind Energy Association, Special Issue for the 40th Anniversary, Vol. No. 123 (November, 2017), pp 454.
3) Kazumasa Seko, NTN New Products, Introduction of "Asymmetric Spherical Roller Bearings" for Wind Turbine Main Shafts, Clean Energy, Vol. 307, (Feb, 2018), pp 67.
4) Kazumasa Seko, Development of "Asymmetric Spherical Roller Bearings" for Wind Turbine Main Shafts, THE TRIBOLOGY, No. 368, (Apr, 2018), pp 16.

Photo of authors

Kazumasa SEKO

Industrial Business Headquarters
Application Engineering Dept.

Takashi YAMAMOTO

Industrial Business Headquarters
Product Design Dept.

Grid Connectable NTN Micro Hydro Turbine

Takashi ITOU*   kanta KIMURA*   Yasunari KANAMURA*

  Demand of renewable energy such as hydroelectric power generation is increasing rapidly from rise of global warming and the interest to the energy mix. **NTN** already commercialized the **NTN** Micro hydro Turbine which is used in existing agricultural canal and industrial canal and makes electric power available in the place where the no power system exists. **NTN** develops Grid Connectable **NTN** Micro hydro Turbine. This paper introduces the features and the structure of the developed products .

1. Introduction

   The energy issue is a global challenge that we have to deal with to achieve a sustainable society. Some of the key initiatives include reduction of greenhouse gas emissions related to recent climate change, energy saving for phasing out fossil fuel dependency, and diversifying energy sources by promoting use of renewable energy. **Fig. 1** shows the actual power mix before the Great East Japan Earthquake and the prediction for FY2030. Renewable energy, in particular, is assumed to more than double from the actual ratio before the Great East Japan Earthquake, indicating high expectations [1].

Fig. 1 The power supply construction in FY2030

   Securing the emergency power supply in case of natural disasters is also a great challenge. Although standby generators are being installed for emergency power sources, storage of fuel is another challenge. Renewable energy does not require storage of fuel and can be used as an emergency power source. **NTN** has productized a Green Power Station, which stores power from photovoltaic power generation and wind power generation into batteries and is used for lighting at night or as an emergency power source.

   Hydraulic power generation is a stable power source with little variance compared to photovoltaic or wind power generation. **NTN** has developed and productized the "**NTN** Micro Hydro Turbine" which uses the energy of running water in waterways [2]. **NTN** Micro Hydro Turbine is an independent power source which assumes private consumption by storing generated power in batteries for supply in the areas without good power infrastructure or as an emergency power source in case of disasters.

   On the other hand, feed-in tariffs (FIT) started in July 2012 to promote renewable energy in Japan. FIT is a program to require power companies to purchase power generated by renewable energy at a fixed price. Introduction of this program facilitates recovery of capital investment; therefore, installed bases of photovoltaic power generation is significantly growing.
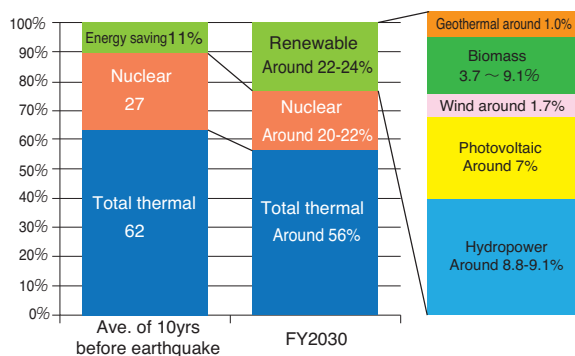
---

*Engineering Dept. Green Energy Products Division

NTN's own market research revealed that there was strong demand for hydraulic power generation of the grid connectable type, so that the generated power can be sold, taking advantage of FIT. In addition, since the purchase price for hydraulic power generation of less than 200 kW is more profitable than 200 kW or more, as shown in **Table 1**, adoption of hydraulic power generation of less than 200 kW will be likely to grow [3].

In this article, we describe the structure and features of "Grid Connectable **NTN** Micro Hydro Turbine" that **NTN** has developed which allows sale of generated power.

Table. 1 FIT price of hydro turbine

	1,000 kW or more and less than 5,000kW	200kW or more and less than 1,000kW	Less than 200kW
FY2017 FY2018 FY2019 FY2020	24 yen + tax	29 yen + tax	34 yen + tax
Purchase period	20 years		

2. Grid connection

Grid connection means that power generation facilities such as photovoltaic power generation and hydraulic power generation are connected to power transmission lines or power distribution lines of utility companies, as shown in **Fig. 2**. By connecting power generation facilities to the grid, the generated power can be sold to the utility companies.
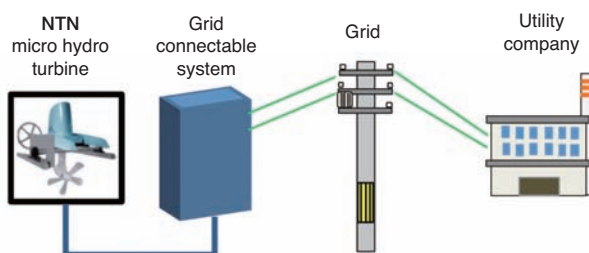

Fig. 2 Image of grid connection

3. Structure of Grid Connectable NTN Micro Hydro Turbine

Fig. 3. shows the outer view of **NTN** micro hydro turbine, **Table 2** shows the specification and **Fig. 4** shows the configuration of Grid Connectable **NTN** Micro Hydro Turbine.

The AC power generated by **NTN** micro hydro turbine is converted to DC power by the controller and input to the power conditioner.

The power conditioner is a device to convert the DC power to AC power and transmit it to the grid. The controller and the power conditioner are collectively called the grid connectable system, which enables power generated by the **NTN** micro hydro turbine to be efficiently transmitted to the grid and sold to the utility company.

Fig. 3 NTN Micro Hydro Turbine

Table. 2 Specification of **NTN** Micro Hydro Turbine

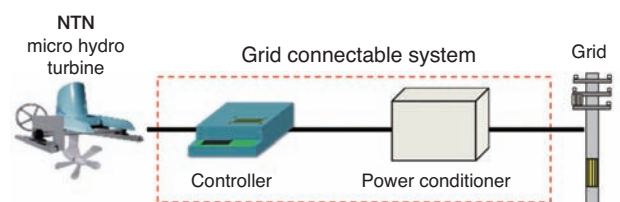| Hydro turbine blade diameter mm	Output kW	Rated flow rate m/s	Recommended waterway exceeding (mm)
600	0.4	2	Width : 700 Depth : 700
900	1.0	2	Width : 1,000 Depth : 1,000
1,300	2.0	2	Width : 1,400 Depth : 1,400

Fig. 4 System configuration of Grid Connectable **NTN** Micro Hydro Turbine

4. Functions of the components of the grid connectable system

(1) Controller

The controller consists of rectifying circuitry which rectifies the power generated by the generator and control circuitry which controls the Grid Connectable **NTN** Micro Hydro Turbine. The controller has the following functions:

1) Converts (rectifies) the AC power generated by the generator to DC power and inputs it to the power conditioner.
2) Monitors the generated power and rotational speed of the generator.
3) Controls the rotational speed of the hydro turbine blades in order to push out foreign objects entangled in the blades [2].

(2) Power conditioner

The power conditioner is a device to convert the DC power converted by the controller to AC power, which is transmittable to the grid, and transmit it to the grid. In the grid connectable system of "Grid Connectable **NTN** Micro Hydro Turbine," the maximum power point tracking (MPPT) is adopted for the control of maximizing power generation.

5. Power generation control of Grid Connectable NTN Micro Hydro Turbine

MPPT is a control to automatically maximize power generation.

By applying MPPT to power generation control for hydraulic power generation, the load to the generator is changed to control the rotational speed of the turbine blades, while measuring generated power, for the speed to obtain the maximum power generation. The Grid Connectable **NTN** Micro Hydro Turbine has models for 0.4 kW, 1 kW and 2 kW of power generation and the standard implementation of MPPT for systems with less than 2 kW power generation is the first in the industry. MPPT implementation in the Grid Connectable **NTN** Micro Hydro Turbine has the following benefits:

· Eliminates the need for measuring the width, water level, and flow rate of the waterway to which the system is to be installed and adjusting the controller to the result, achieving a significant reduction in installation time and cost.
· Enables maximization of power generation, even when the water level or flow rate changes in the waterway.

The following is the control process of MPPT (**Fig. 5**):

(1) Reduce the rotational speed of the turbine blades from N1 to N2 to increase the power output from P1 to P2.
(2) Reduce the rotational speed of the turbine blades from N2 to N3 to increase the power output from P2 to P3.
(3) When the rotational speed of the turbine blades decreases from N3 to N4, power output changes from P3 to P4.
(4) As the power output decreases to P4, the rotational speed is increased back to N3.
(5) When the rotational speed of the turbine blades increases from N3 to N2, power output changes from P3 to P2.
(6) As the power output decreases to P2, the rotational speed is decreased back to N3.

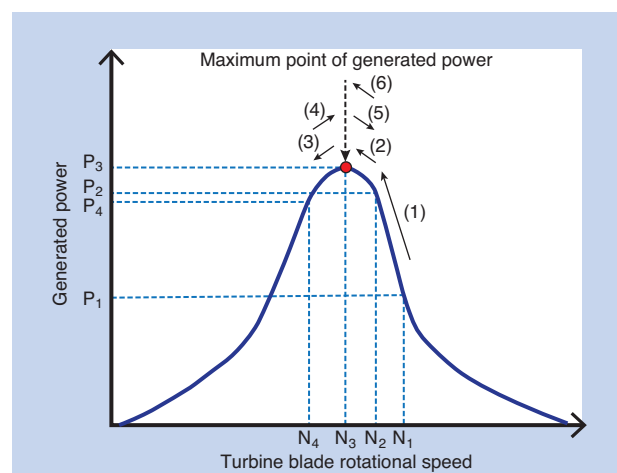By repeating this process, generated power is maximized.

Fig. 5 Control Method of MPPT

However, when MPPT was applied to hydraulic power generation, there were cases where the maximum power generation could not be attained by the following:

When the flow rate and water level of the waterway changed abruptly in a short time and deviated from the maximum power point of MPPT, the control could not follow the change and the load to the generator continued to increase causing a shortage of turbine blade torque driven by the water flow and reduction of turbine blade rotational speed. This phenomenon occurs when, in **Fig. 6** "Rotation speed of blades vs. torque characteristic diagram," the operating condition, which is usually at point (1), moves to the stall region such as point (2), causing reduction of rotational speed and torque of turbine blades, resulting in lower power generation.

The Grid Connectable **NTN** Micro Hydro Turbine compares and controls the turbine blade rotational speed and generated power at all times so that maximum power is attainable and the operating conditions never move into the stall region.

The problem has been resolved by incorporating control to detect the deviation of the operating point and drive the MPPT to return to the maximum power point, even when the conditions move into the stall region.
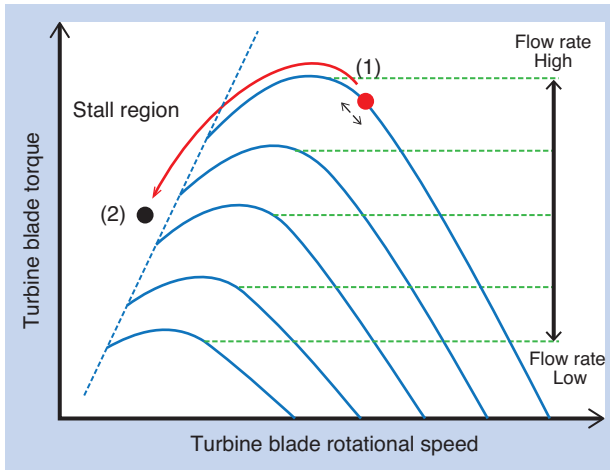

Fig. 6 Rotation speed of propeller vs torque characteristic diagram

6. Demonstration test in the actual waterway

The demonstration test of the developed grid connectable system was conducted to evaluate performance. The configuration of the demonstration test is shown in **Fig. 7** and the test condition is shown in **Table 3**. The demonstration test verified the tracking performance of the maximum power generation by MPPT of power conditioner. The waterway used for the demonstration test did not have enough water and a portion of the turbine blades was out of water.

First, the maximum power generation of the waterway under the demonstration test was verified by connecting the electronic load to the controller output, as shown in **Fig. 8 (a)**, changing the generated voltage (proportional to the rotational speed of the turbine blades) and measuring the generated power. The results are shown in **Fig. 9**. The maximum generated power was 749 W.

Next, the power conditioner was connected, as shown in **Fig. 8 (b)** for the measurement. In this demonstration test, simulated power supply load was used to simulate the condition of grid connection.

Fig. 10 shows the results of the generated power. The generated power was 738 W on average, which

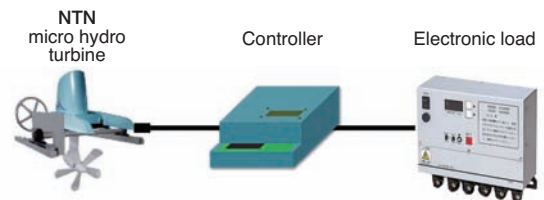means it has tracked the maximum power generation well.

Fig. 7 Field test

Table. 3 Test condition

Item	Condition
Hydro turbine blade diameter	ϕ900
Water depth	670 mm
Flow rate in the demonstration test	2.0 m/s

(a) When electronic load is connected

(b) When power conditioner is connected
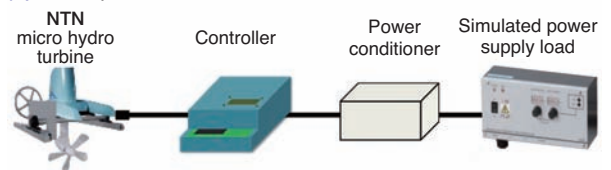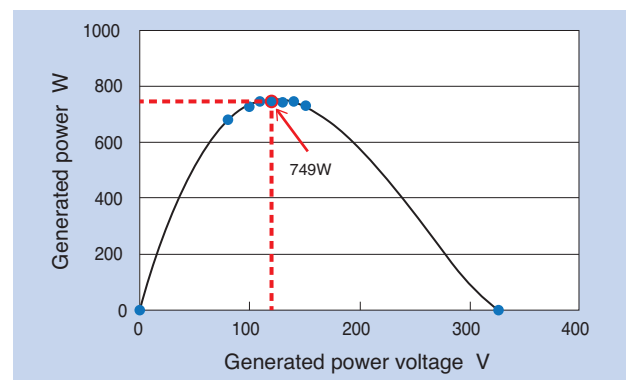

Fig. 8 Test lig layout of field test
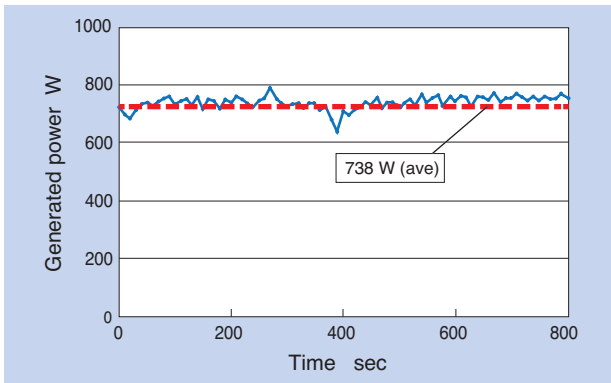

Fig. 9 Result of field test

Fig. 10 Result of field test
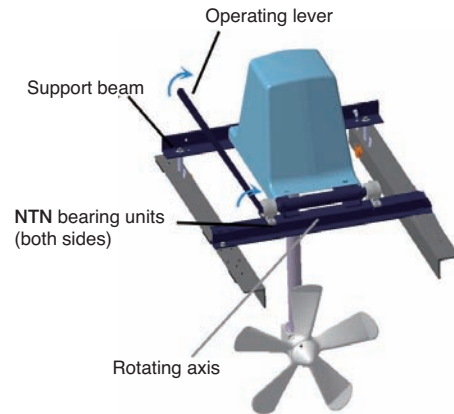
738 W (ave)

Fig. 13 Lever type

7. Mechanism for easy operation "Easy Lifter"

When waterways are swollen by heavy rain from typhoons, etc, driftwood and debris may damage the hydro turbines. This should be avoided. If turbine blades can be lifted above water level, they can be more safely operated. **NTN** micro hydro turbine can be equipped with a mechanism, "Easy Lifter," to temporarily lift the turbine blades from the water in emergency.

In addition, this mechanism can also be used to safely and easily lift the blades without requiring heavy machinery such as cranes for periodic maintenance, allowing time and cost reduction for maintenance and inspection tasks. **Fig. 11** shows the condition of normal operation and **Fig. 12** shows how the blades are lifted up.

There are two ways for operating "Easy Lifter." **Fig. 13** shows the lever type, where the turbine connected to the rotational shaft is manually operated by a lever pivoting at the **NTN** bearing unit, and **Fig. 14** shows the worm gear type where electric motors can be mounted.
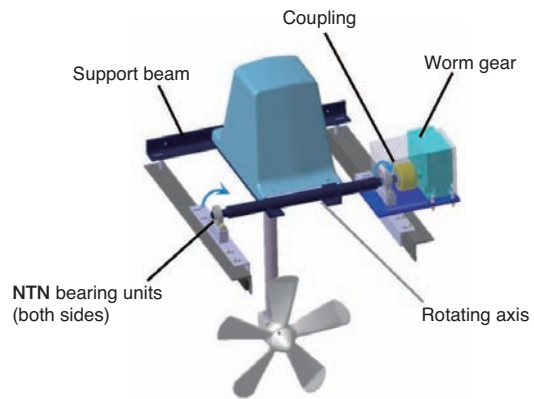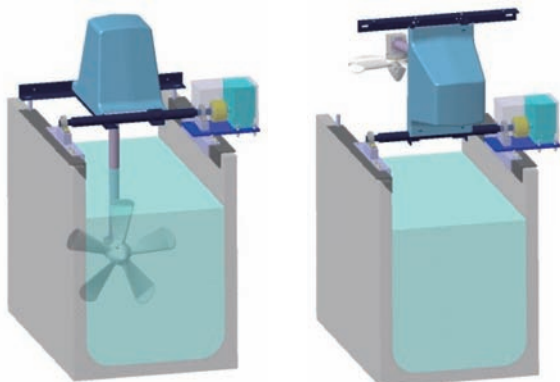

Fig. 11 Normal operation   **Fig. 12** After lifting up blade unit

Fig. 14 Worm gear type

8. Conclusion

In this article, we have described the functions and features of "Grid Connectable **NTN** Micro Hydro Turbine" which allows the sale of electric power generated by **NTN** micro turbine, configuration and performance of the controller and power conditioner of **NTN**'s highly efficient and proprietary grid connectable system, and "Easy Lifter", which allows temporary lifting of the turbine blades from the water.

The market for hydraulic power generation using agricultural waterways, etc. is expected to grow with high demand for hydraulic power generation system with shorter recovery of capital investment and ease of operation. We will continue to work toward higher efficiency and respond to the needs for broader adoption of micro hydro turbines.

NTN is also working on fulfilling related products using natural energy, including photovoltaic and wind power generation for diversification of energy sources and achievement of a sustainable society.

For example, the demand and application area are expanding for **NTN** Hybrid Street Light [4], which was

launched in 2016. **NTN** Hybrid Street Light has been adopted, as an independent power source and structure for the application "Disaster Relief Map," the largest disaster rescue/prevention map in Japan developed by Osaka University and "Mimamori Robokun III," Wi-Fi communication infrastructure equipped with a monitoring camera developed by the "National Activity Support Network for Local Municipalities," a non-profit organization [5]. "Mimamori Robokun III" is equipped with a monitoring camera and Wi-Fi equipment as a standard, as well as a LED light, and requires stable power supply even in an environment not favorable for wind or daylight conditions. Therefore, a higher power capacity version of the hybrid street light was newly introduced at the Green Power Station.

We will continue proposing locally produced and consumed energy through development and marketing of products that use natural energy in order to achieve a low-carbon society. In addition, we will contribute to the safety and security of local communities by demand stimulation at the local governments and local community associations.

References
1) Ministry of Economy, Trade and Industry: Long-term Energy Supply and Demand Outlook and related materials
2) Tomoya Kawai, Hiroki Mukai, Tomomi Gotou, Micro Hydro Turbine, NTN TECHNICAL REVIEW, No. 84, (2016) 29.
3) Ministry of Economy, Trade and Industry home page: "Nattoku! Renewable Energy"
4) NTN news on new products, "NTN Launches Extremely Silent Hybrid Street Lights," https://www.ntnglobal.com/en/news/new_products/news201600059.html
5) NTN news on new products, NTN Participates in "Joint Research for Creating Mechanisms Regarding Disaster Prevention Monitoring and Tourism through Use of IT," https://.ntnglobal.com/en/news/press/news 201700089.html

Photo of authors

Takashi ITOU

Green Energy Products Division
Engineering Dept.

Kanta KIMURA

Green Energy Products Division
Engineering Dept.

Yasunari KANAMURA

Green Energy Products Division
Engineering Dept.

Award Winning Products

ULTAGE[※1] Tapered Roller Bearing for Automotive Application

Takashi KAWAI   Yasuhito FUJIKAKE   Takanori ISHIKAWA   Susumu MIYAIRI

1. Introduction

"ULTAGE* Tapered Roller Bearing for Automotive Application" [1] realizing the world's highest standard of high load capacity and high-speed rotational performance received the Automotive Components Award of the 2017 "CHO" MONODZUKURI Innovative Parts and Components Award sponsored by MONODZUKURI Nippon Conference and Nikkan Kogyo Shimbun, Ltd.

In order to obtain the longest possible bearing life based on theory, a "new optimizing design technology for internal design of bearings" was build and "proprietary roller processing technology" was established as original technology.
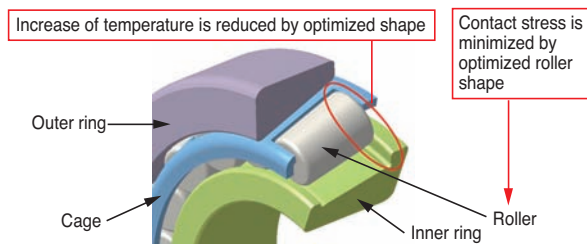

Increase of temperature is reduced by optimized shape

Contact stress is minimized by optimized roller shape

Outer ring

Cage

Roller

Inner ring

Fig. 1 Structure of ULTAGE Tapered Roller Bearing for Automotive Application

2. Structure

Fig. 1 shows the overall structure of ULTAGE Tapered Roller Bearing for Automotive Application.

3. Features

The following shows the characteristics of ULTAGE Tapered Roller Bearing for Automotive Application in comparison with conventional tapered roller bearings [2]:

(1) The world's highest load capacity:
Basic dynamic load rating - 1.3 times
(2) Long operating life (compared with the basic rating life):
Standard type (bearing steel; standard quenching) - 2.5 times or more
High-functionality type (FA process) - 3.8 times or more

(3) World-class high speed rotational performance:
Permissible rotational speed – improved by approx. 10%
(4) Allowable inclination angle (magnitude of misalignment):
Allowable inclination angle - Up to 4 times

Fig. 2 shows an example of calculation of contact stress distribution at axial cross section of raceway. With ULTAGE Tapered Roller Bearing for Automotive Application, adoption of special crowning leads to improvement of bearing operating life by minimizing the overall contact stress distribution while suppressing excessive pressure at the end of the contact area (edge load).
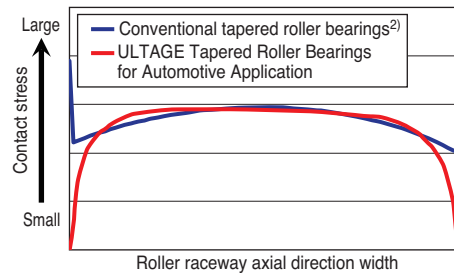

Large

Small

Contact stress

— Conventional tapered roller bearings[2]
— ULTAGE Tapered Roller Bearings for Automotive Application

Roller raceway axial direction width

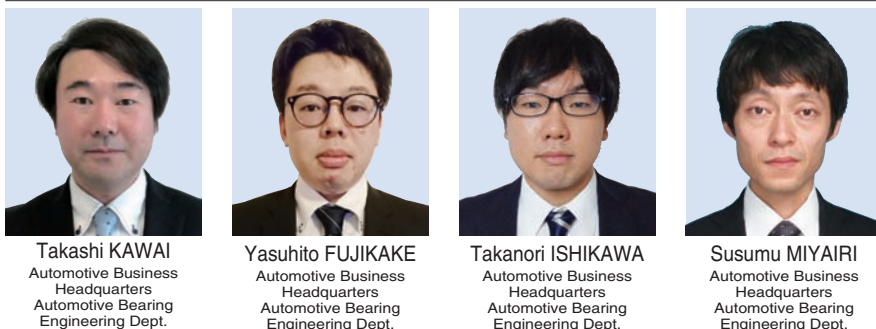**Fig. 2** Contact stress distribution on raceway

4. Summary

While the operating conditions of tapered roller bearings for automotive application are becoming increasingly severe, requirements for smaller size and longer operating life are increasing. We want to introduce our ULTAGE Tapered Roller Bearings for Automotive Application into a broad market to meet those requirements and contribute to vehicle fuel economy.

References
1) Yasuhito Fujikake, Takanori Ishikawa, Susumu Miyairi: ULTAGE Tapered Roller Bearing for Automotive Application, NTN TECHNICAL REVIEW, No. 85, (2017) 51-55.
2) NTN, Roller Bearings, Overview Catalog, CAT. No. 2202 - VII/J.

Photo of authors

Takashi KAWAI
Automotive Business Headquarters
Automotive Bearing Engineering Dept.

Yasuhito FUJIKAKE
Automotive Business Headquarters
Automotive Bearing Engineering Dept.

Takanori ISHIKAWA
Automotive Business Headquarters
Automotive Bearing Engineering Dept.

Susumu MIYAIRI
Automotive Business Headquarters
Automotive Bearing Engineering Dept.

※1 ULTAGE[TM] is a name created from the combination of "ultimate," signifying refinement, and "stage," signifying **NTN**'s intention that this series of products be employed in diverse applications and is the general name for **NTN**'s new generation of bearings that are noted for their industry-leading performance.

**Society of Materials Science, Japan,
"51st Symposium on X-ray Studies on Mechanical Behavior of Materials, the Best Presentation Award"**

Effect of Residual Stress on Peeling of Rolling Bearings

Naoya KAMURA   **Takumi FUJITA**   **Toshihiko SASAKI**

1. Introduction

This study revealed that rolling contact fatigue is a phenomenon that involves not only the change of residual stress, half width and retained austenite, but also crystal orientation. This was demonstrated by investigating the progression of rolling contact fatigue that results in peeling damage using X-ray residual stress measurement with a two-dimensional detector [1], [2].

The presentation of this study at the " 51st Symposium on X-ray Studies on Mechanical Behavior of Materials", sponsored by The Society of Materials Science, Japan received the "Best Presentation Award" which is presented to selected young researchers. In this report, an overview of this presentation is presented.

2. Overview

The rolling contact fatigue test was conducted under lean lubrication conditions, using a two-roller testing machine. The surfaces of the specimens were measured with an X-ray diffraction ring analysis system using a two-dimensional detector. The residual stress measurement, retained austenite measurement and crystal orientation was investigated using triaxial stress analysis theory. For the specimens, standard heat treated SUJ2 and carbonitrided bearing steels were used, and the change of X-ray analysis values due to rolling contact fatigue of these specimens was investigated. **Fig. 1** shows an example of X-ray diffraction ring obtained from the test.

Fig. 2 shows the change of the parameter S/S_0, which indicates progression of crystal orientation. The test revealed that the carbonitrided specimen delays the progression of crystal orientation compared with the standard heat treated specimen. It is assumed that the retained austenite and solid solution element (mainly nitrogen) are affecting this result.

3. Future development

The estimation of rolling contact fatigue using X-ray analysis is an important technology to facilitate prediction of failure and quick evaluation of rolling contact fatigue of rolling bearings. We will continue to advance this study on an ongoing basis.

(a) Before testing   **(b)** 10^6 cycles
Fig. 1 Diffraction rings before and after testing

Fig. 2 Relationships between progress of crystal orientation S/S_0 and the number of loading cycles

S_0 : Standard deviation of intensity distribution of diffraction ring before testing.

S : Standard deviation of intensity distribution of diffraction ring while testing.

References
1) Naoya Kamura, Takumi Fujita and Toshihiko Sasaki: Effect of residual stress on peeling of rolling bearings (2nd report), Proceedings of the 51st Symposium on X-Ray Studies on Mechanical Behaviour of Materials, (2017) 109-112.
2) Naoya Kamura, Takumi Fujita and Toshihiko Sasaki: Evaluation of Rolling Contact Fatigue by X-ray Diffraction Ring, NTN TECHNICAL REVIEW, No. 83, (2015) 67-74.
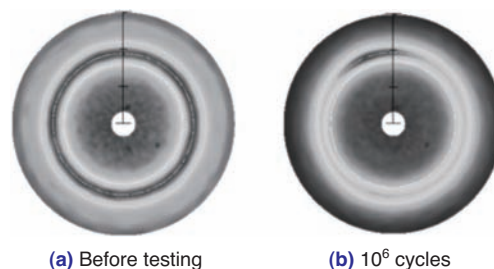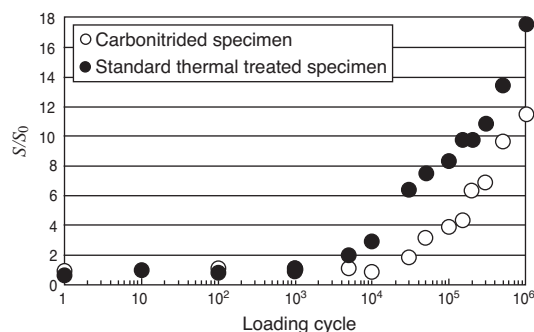
Photo of authors

Naoya KAMURA
Advanced Technology
Headquarters

Takumi FUJITA
Advanced Technology
Headquarters

Toshihiko SASAKI
Faculty of Human Sciences,
Kanazawa University

"Japanese Society of Tribologists 2017 Best Paper Award"

Rolling Contact Fatigue of Thrust Ball Bearing under Low Lambda Condition

Takumi FUJITA   Naoya HASEGAWA   Naoya KAMURA   Toshihiko SASAKI

1. Introduction

The subject paper [1] submitted to the "Tribologist", the journal of the Japanese Society of Tribologists, was awarded the best paper for FY2017. An overview of this paper is as follows:

2. Overview

Various factors that can affect the rolling contact fatigue life under lean lubrication conditions, or low lambda conditions, were examined. These testing conditions were based on the results of rolling contact fatigue life tests of thrust ball bearings under low lambda conditions. The difference between the calculated operating life and actual life was investigated by systematically changing the surface roughness, load and rolling speed of the rolling elements and raceway (**Fig.1**). The difference between the calculated operating life and actual life was also reviewed based on the difference in surface roughness, or fitting, data before and after the test and the examination results of peeling damage [2].

As a result, two types of surface initiated exfoliation were discovered. In this paper, exfoliation of smaller particles close to the size of the width of the rolling trajectory is called flaking, and exfoliation of larger particles is called peeling. The generation of these two types of exfoliation is determined by the initial surface roughness of the rolling elements and raceway and fitting condition. It was also found that the fitting behavior is dependent upon the operating conditions, and the load on the rolling elements determines the exfoliation type. The exfoliation type of photos 1 through 9 in **Fig.1** is flaking, and that of photos 10 through 12 is peeling.

It is **NTN**'s claim that the exfoliation that changes depending on the operating conditions should also be considered in the estimation of rolling contact fatigue life of rolling element bearings under low lambda conditions. This assertion, based on the findings detailed in this report, is not reflected in the conventional ISO or JIS fatigue life estimation formulas. Based on the results of this study, the following should be the next subject of ongoing research for rolling contact fatigue life estimation of rolling element bearings under low lambda conditions:
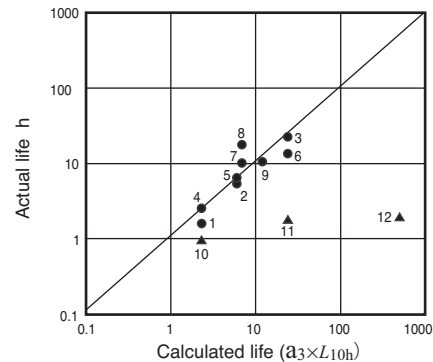

Fig. 1 Correlation diagram between calculated life ($a_3 \times L_{10h}$) and estimated life from experimental results.

(1) Estimation of fitting based on lubrication conditions and rolling element material
(2) Estimation of surface roughness and load distribution of lubricating oil while considering the effect of fitting
(3) Estimation of internal stress under true contact point considering the result of (2) and residual stress
(4) Establishing the relationship between stress (3) and operating life (S-N diagram)

3. Future development

Research of a rolling bearing life estimation method under low lambda conditions is an important research subject that can determine the reliability of rolling bearings. The continued use of low viscosity lubricating oil used to meet the industry requirement of higher efficiency of machinery necessitates this research. **NTN** will continue to study the subjects discussed in this paper in order to contribute to the improvement of the reliability of our rolling bearings.

References
1) Takumi Fujita, Naoya Hasegawa, Naoya Kamura, Toshihiko Sasaki: Rolling Contact Fatigue Life of Thrust Ball Bearing under Low Lambda Condition, Tribologist, 60, 11 (2015) 741-751.
2) Takumi Fujita, Naoya Hasegawa, Naoya Kamura, Toshihiko Sasaki: Rolling Contact Fatigue Life of Thrust Ball Bearing under Low Lambda Condition, NTN TECHNICAL REVIEW, No. 84, (2016) 85-95.

Photo of authors

Takumi FUJITA
Advanced Technology
Headquarters

Naoya HASEGAWA
Advanced Technology
Headquarters

Naoya KAMURA
Advanced Technology
Headquarters

Toshihiko SASAKI
Faculty of Human Sciences,
Kanazawa University

Short Type Sealed Journal Bearing Unit for Rolling Stock

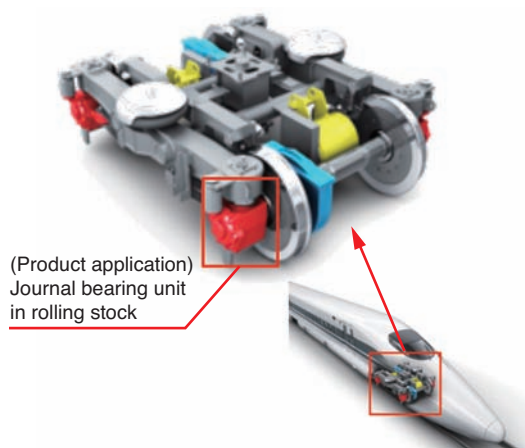## Featuring secure sealing and short axial length of journal bearing units

Inner ring — Cage

Roller

Outer ring

Newly developed oil seal placed within the bearing width
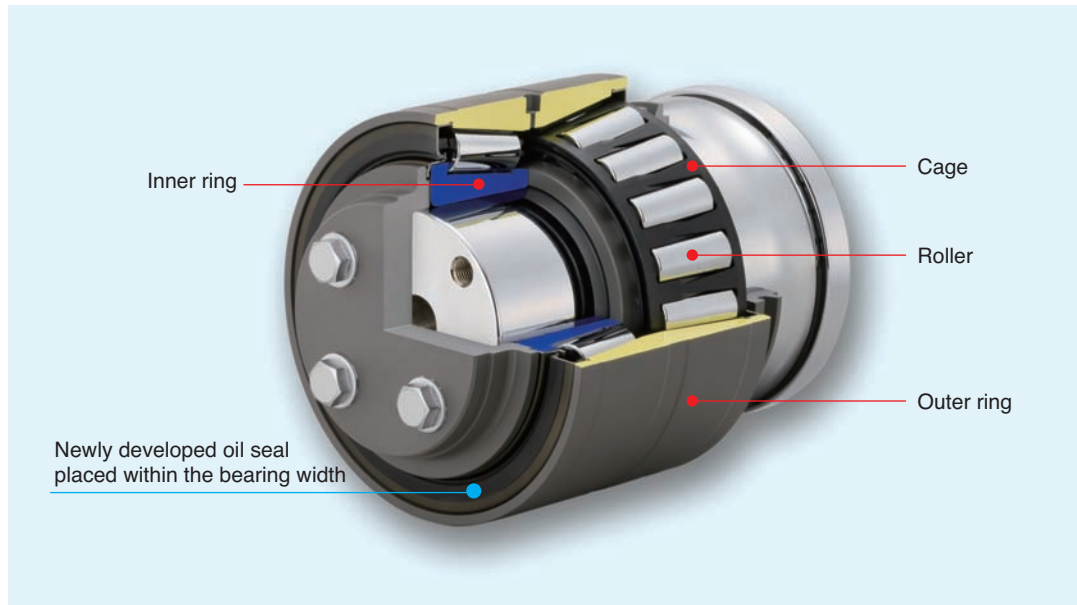
Features

(1) Approximately 15% shorter axial length and 30% reduced journal deflection, contributes to improved journal bearing durability

(2) Rated load capacity, high-speed rotational performance and grease sealing performance equivalent to conventional products
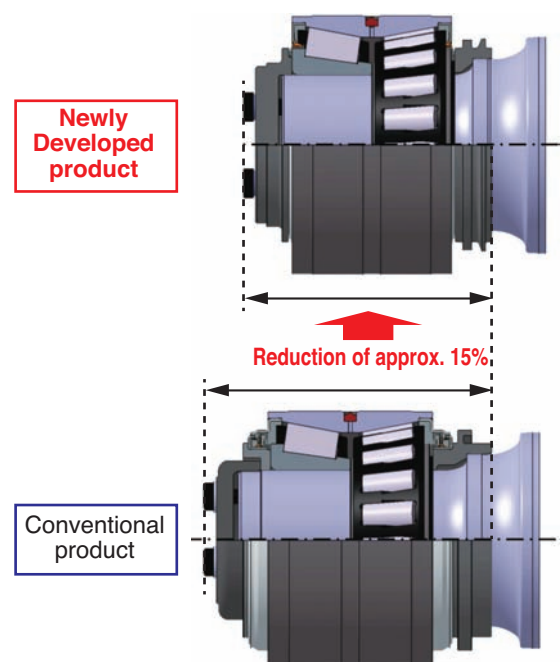
Applications

● Journal bearing for rolling stock

(Product application) Journal bearing unit in rolling stock

Structure

Placing the newly developed oil seal within the journal bearing width allows secure sealing and short axial length of journal bearing units.

Newly Developed product

Reduction of approx. 15%

Conventional product

Compact Plunging Type Constant Velocity Joint for Propeller Shafts (HEDJ-P)

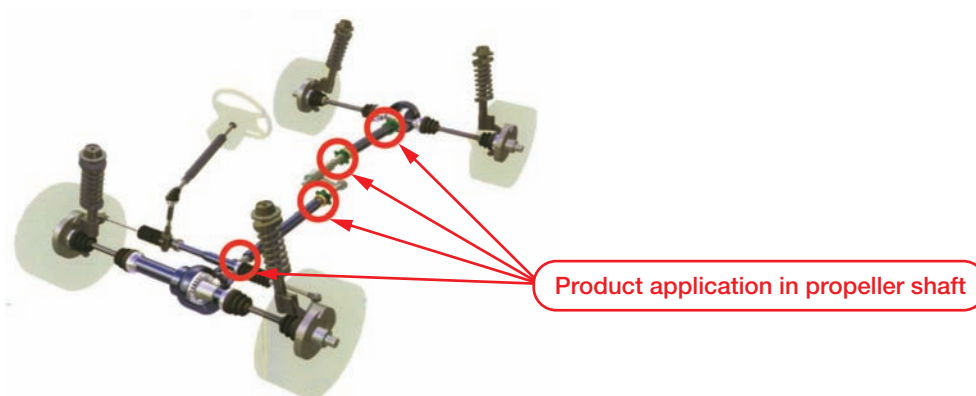**Plunging type constant velocity joint for propeller shafts provides compact and lightweight design**
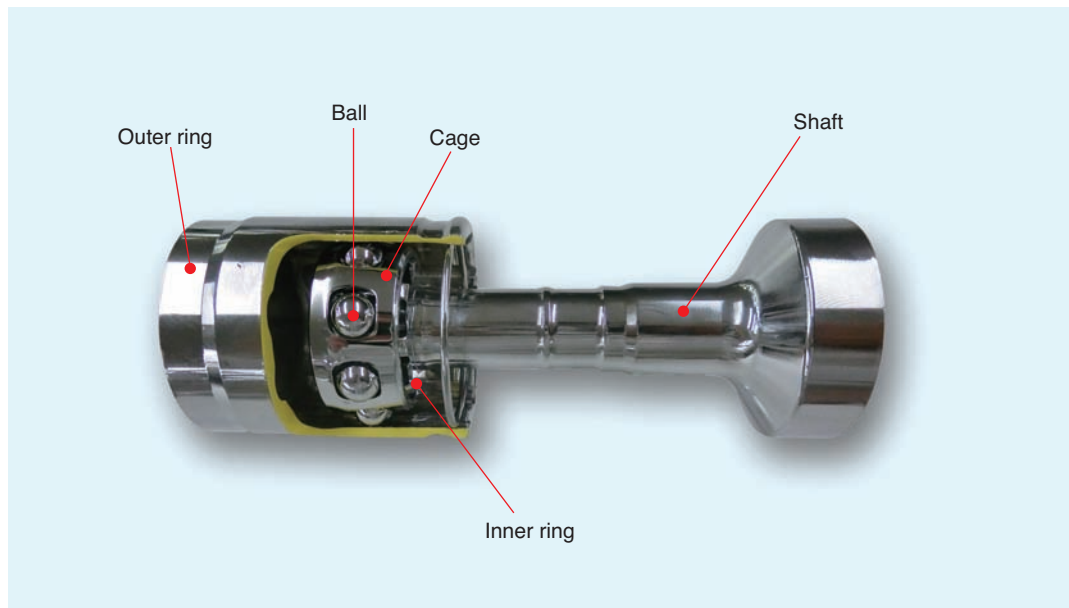
Features

- **Weight: 17% reduction**
  (compared with conventional products)
- **Outer ring outer diameter: 6% reduction**
  (compared with conventional products)
- **Strength and durability:**
  equivalent to the conventional products

Structure

Compact and lightweight design achieved by focused development on the most critical functions of constant velocity joint for propeller shafts.
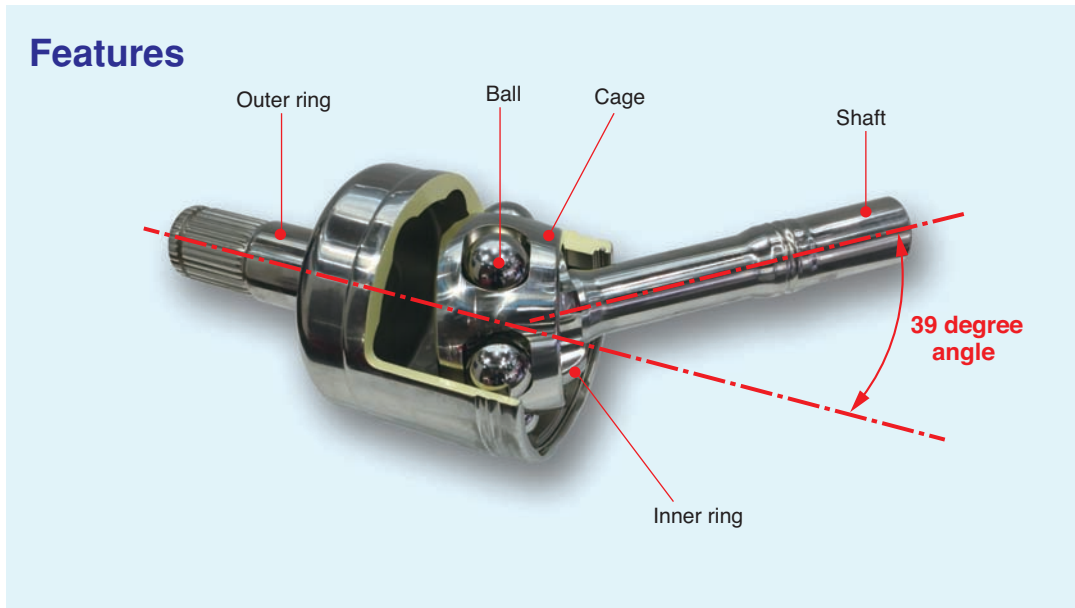
Applications

- Constant velocity joint for Propeller Shafts

Ultra High Angle DOJ (DOJ-W) for Multipurpose Off-road Vehicles※

Plunging constant velocity joint with a maximum operating angle of 39 degrees

Features

Outer ring　Ball　Cage　Shaft

39 degree angle

Inner ring

Features

- **Maximum operating angle: 39 degrees**
  (conventional product is 30.5 degrees)

- **Strength and durability:**
  equivalent to the conventional products

- **Outer ring outer diameter:**
  minimum increase in outer diameter dimension
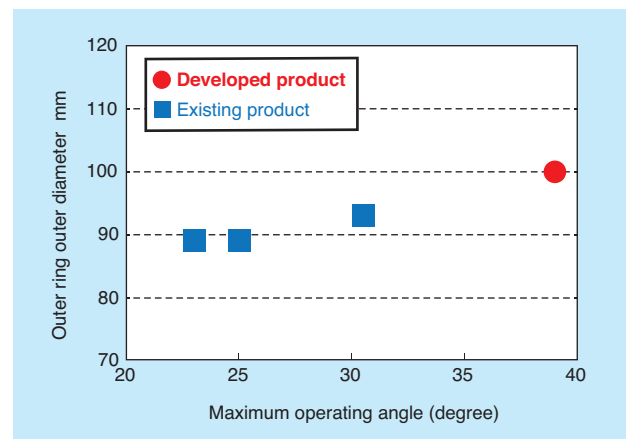 **of less than 8% over compact design**

Applications

- Drive shafts for multipurpose off-road vehicles

Product application in off-highway vehicle

Maximum operating angle and outer ring outer diameter

- ● **Developed product**
- ■ Existing product

Outer ring outer diameter mm

Maximum operating angle (degree)

※Generic name for 4-wheel buggy vehicles with round steering wheels which are gaining popularity mainly in the U.S.A. for a wide range of applications from business to leisure. It is also referred to as SSV (Side by Side Vehicle), UTV (Utility Task Vehicle) or ROV (Recreational Off highway Vehicle).